

**Utilising Reverse Hydrology to  
quantify and improve the  
spatio-temporal information content of  
catchment rainfall estimates for flood  
modelling**

*Ann Kretzschmar BSc, MSc, PGCE, MSc*

Lancaster Environment Centre, Lancaster University

This thesis is submitted in fulfilment of the regulations for the degree of

Doctor of Philosophy

July 2017

## Abstract

### **Utilising Reverse Hydrology to quantify and improve the spatio-temporal information content of catchment rainfall estimates for flood modelling**

Ann Kretzschmar *BSc, MSc, PGCE, MSc*, Lancaster Environment Centre, Lancaster University, July 2017

Reverse Hydrology is a term describing methods for estimating rainfall from streamflow. The method presented here is based on combining inversion of a causal rainfall-runoff model with regularisation. This novel method, termed *RegDer*, combines a continuous-time transfer function model with regularised derivative estimates and is compared with an alternative method for direct inversion of a discrete-time transfer function using sub-hourly data from two catchments with contrasting rainfall and catchment storage characteristics. It has been demonstrated to recover the prominent features of the observed rainfall enabling it to generate a streamflow hydrograph indistinguishable from the observed catchment outflow. The loss of temporal resolution of the resultant rainfall series is the price paid for the numerical stability of the *RegDer* method, however this does not affect its ability to capture the dynamics required for streamflow generation. The inferred rainfall series was initially interpreted as an estimate of catchment rainfall but was later more precisely described as the rainfall necessary for generating streamflow – Discharge Generating Rainfall (DGR). The spatial aspect of the method was investigated using data from a densely gauged catchment. Frequency domain aspects of *RegDer* dual interpretation as a composite spectral decomposition method are analysed and discussed in the context of catchment data. Potential applications and developments of the approach include in-filling and extending rainfall records, reducing uncertainty in both gauged and ungauged catchments by improving rainfall estimates, assessing and refining rain gauge networks and re-evaluating areal rainfall estimation.

## Declaration

### Published papers

- 1) Kretzschmar, A., Tych, W and Chappell, N. A. (2014) *Reversing hydrology: Estimation of sub-hourly rainfall time-series from streamflow*. Environmental Modelling & Software 60: 290-301.
- 2) Kretzschmar, A., Tych, W., Chappell, N. A., Beven, K. J., (2015) *Reversing hydrology: quantifying the temporal aggregation effect of catchment rainfall estimation using sub-hourly data*, Hydrology Research, 47 (3) 630-645
- 3) Kretzschmar, A., Tych, W., Chappell, N., Beven, K., (2016) *What Really Happens at the End of the Rainbow? – Paying the Price for Reducing Uncertainty (Using Reverse Hydrology Models)*, Procedia Engineering, Volume 154, Pages 1333-1340, ISSN 1877-7058

### Unpublished Chapters

- 1) **Chapter 7** - Implications of spatio-temporal sampling of a rainfall field when generating a streamflow hydrograph: An investigation of Discharge Generating Rainfall using Reverse Hydrology
- 2) **Chapter 8** - Extending and filling the gap in a rainfall record using Reverse Hydrology and Spectral Decomposition

In the initial stages (leading up to paper 1), I was responsible, with support from WT, for jointly developing and improving the draft core method supplied by WT, followed by independent testing and evaluation. I also developed a usable library of related Matlab functions.

Leading up to paper 2, I was responsible for developing and extending, with WT methodological and technical support, the testing regime involving spectral analysis and adding to the Matlab routine library.

I developed GIS techniques required for spatial analysis leading to paper 3 and beyond (chapter 7) and combined these with the necessary Matlab analysis routines, thus producing a full spatio-temporal analysis system.

For chapter 7, I extended the methodology to spatially distributed data and developed a testing regime that resulted in the definition of the concept of Discharge Generating Rainfall. I presented this work at HIC 2016 and EGU 2017.

By expanding the ideas presented in chapter 7, I developed the idea for extending a rainfall record based on Discharge Generating Rainfall and spectral decomposition. KJB and WT provided supporting expertise.

At all stages, WT provided methodological and also technical support, and NAC and KJB provided hydrology support, giving feedback and advice on the application, hydrological interpretation and uncertainty implications.

Signed:

Wlodek Tych

Nick Chappell

Keith Beven

## Acknowledgements

Where do I start? After some of the best years of my life there are so many people who have helped, supported and influenced me. Seven years ago, when I took the decision to give up my job and move to Lancaster, I never dreamt of all the incredible experiences I would have.

This thesis is dedicated to my family: my parents, Win and Teddy Hope who are no longer with me, but I hope would have been proud of my achievements, and my children, Alex and Caitlin (and their respective partners Catherine and Dave), who probably thought I was just a bit crazy going back to University at the ripe old age of 54. I hope they are just a little bit proud of their old Mum now. Of course, I must not forget my cats, Mollie and Midge, who have kept me company through many long days and nights whilst writing this thesis. Sadly, Midge passed away before it was completed but Mollie has proved a very able deputy.

My thanks for never-ending patience, generosity and support go to Wlodek Tych, my long-suffering supervisor, without whose encouragement and enthusiasm I would never started this project never mind finished it! Of course, I have had support and advice from many others not least my other supervisors Nick Chappell, who took me out in the field on several occasions so I would know what real hydrology was about rather than just sitting at a computer playing with numbers, and Keith Beven, who had enough faith in me to fund me as part of the NERC Credible Consortium: both have given me huge amounts of very valuable support and advice.

I have worked alongside Mike Entwistle, David Ainsworth and Chris Holroyd in EBP; with Steven Owens and many others in ISS setting up Moodle (we won an award for the best student work team); with Christine, Olga and Mandy in ISS training; with Duncan Whyatt, Roger Timmis and Marie-Angelis Solaro Garcia and more recently on a modelling project with Rebecca Killick and Suzi Ilic. To all these people and many more, I would like to say ‘thank you’, your friendliness, advice and support has helped me through. Then, of course, there are all the staff in LEC for whom I have demonstrated over the years – I learnt a lot from them and, I hope, have given something

back in the way of support to the students: the high points being the Carrock Fell fieldcourse, the Slapton Leys fieldcourse, teaching 1<sup>st</sup> year tutorials and giving a lecture to part one students in Faraday – good preparation for EGU!

I have made many new friends, particularly the members of the Mature Students Society, the Hiking Club and Lancaster University Brass Band. Special thanks must go to Rachel Gristwood who kindly took on the unenviable task of checking and formatting my references and to Ethan Wallace for proof reading. Some who have played their part in keeping me sane(ish) include Sue Brayshaw, Sandra Giddings, Katie Ross, Fe Mukwamba-Sendall, Josh Sendall, Julie Sproule and Prusaanth Kumar as well as old friends from my time in Basingstoke who have been following my progress and cheering me along on those bad days. Then there are the members of B46 LEC3 – Sue Brayshaw (again), Ceri Davies, Tamsin Blayney, Laura Deeprise, Becca Burns, Natalie Swann, Runmei Wang, Ethan Wallace and many others, too numerous to mention, who have passed through over the years.

I have had such great experiences during my time in LEC. I achieved a long-held ambition to take part in University Challenge; played in 4 Unibrass contests; travelled around the country attending various meetings as part of the Credible Consortium, met some amazing people and made many new friends; attended the BHS conference in 2014, winning the prize for the best poster by a ‘young’ hydrologist(!); travelled to South Korea to present at HIC2016 and to Vienna to present at EGU 2017 (in an enormously scary lecture hall!). It has been a wonderful few years and I really do not want it to stop – at least once I have caught up on my sleep! I really hope I am able to continue making use of my work and the experience I have gained. I am too young to retire!

A big thank you must go to all the sources of funding that have enabled me have these fantastic experiences: The Peel Trust, Lancaster University Alumni Association, NERC Credible Consortium [Consortium on Risk in the Environment: Diagnostics, Integration, Benchmarking, Learning and Elicitation (CREDIBLE)] grant number: NE/J017299/1, the British Hydrological Society, LU Faculty of Science and Technology, Grad College and the Maths Forsees Network. I would also like to thank Mary Ockenden for the collection and quality assurance of rainfall and streamflow

data for the Blind Beck catchment (NERC award NER/S/A/2006/14326), Jamal Mohd Hanapi and Johnny Larenus for the collection of rainfall and streamflow data for the Baru catchment and Paul McKenna for its quality assurance (NERC award GR3/9439).

And finally I must thank JRR Tolkein, Peter Jackson and Howard Shore – I have lost count of the number of times I have listened to ‘*the Lord of the Rings*’ Symphony whilst writing this thesis!

*Ann Kretzschmar, Galgate, July 2017*

## Project outputs

### *Papers*

- 1) Kretzschmar, A., Tych, W and Chappell, N. A. (2014) Reversing hydrology: Estimation of sub-hourly rainfall time-series from streamflow. *Environmental Modelling & Software* 60: 290-301, <https://doi.org/10.1016/j.envsoft.2014.06.017>
- 2) Kretzschmar, A., Tych, W., Chappell, N. A., Beven, K. J., (2015) Reversing hydrology: quantifying the temporal aggregation effect of catchment rainfall estimation using sub-hourly data, *Hydrology Research*, 47 (3) 630-645; DOI: 10.2166/nh.2015.076
- 3) Kretzschmar, A., Tych, W., Chappell, N., Beven, K., (2016) What Really Happens at the End of the Rainbow? – Paying the Price for Reducing Uncertainty (Using Reverse Hydrology Models), *Procedia Engineering*, Volume 154, Pages 1333-1340, ISSN 1877-7058, <http://dx.doi.org/10.1016/j.proeng.2016.07.485>.

### *Software*

A library of Matlab functions implementing Reverse Hydrology estimation and validation has been developed throughout the project and will be made available for download on ResearchGate.

### *Conference presentations*

- 1) HIC 2016, 12th International Conference on Hydroinformatics, Song-do Conference Centre, Incheon, South Korea – Kretzschmar, A., Tych, W., Chappell, N., Beven, K., - What really happens at the end of the rainbow? – reducing uncertainty with reverse hydrology models - [https://www.researchgate.net/publication/308623125\\_Conference\\_Presentation\\_HIC\\_2016](https://www.researchgate.net/publication/308623125_Conference_Presentation_HIC_2016)
- 2) European Geosciences Union General Assembly 2017, Vienna, Austria – Kretzschmar, A., Tych, W., Beven, K., Chappell, N., - How important is the spatio-temporal structure of a rainfall field when generating a streamflow hydrograph? An investigation using Reverse Hydrology (EGU2017-11724) DOI: 10.13140/RG.2.2.21314.89288

### *Posters*

- 1) BHS Symposium 2014 – winner of best poster by an early career hydrologist (see Figure a) - [https://www.researchgate.net/publication/318529945\\_Reversing\\_Hydrology\\_Estimation\\_of\\_sub-hourly\\_time-series\\_from\\_streamflow](https://www.researchgate.net/publication/318529945_Reversing_Hydrology_Estimation_of_sub-hourly_time-series_from_streamflow)
- 2) CREDIBLE consortium wrap-up meeting September 2016

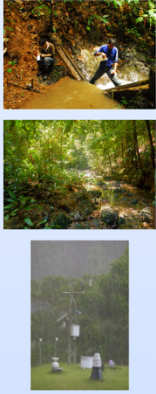


# Reversing hydrology: Estimation of sub-hourly rainfall time-series from streamflow

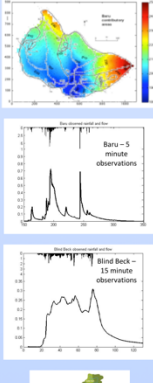
Ann Kretzschmar, Wlodek Tych, Nick Chappell, Keith Beven  
 Lancaster Environment Centre, Lancaster University, Lancaster LA1 4YQ, UK  
 Email: a.kretzschmar@lancaster.ac.uk



Baru – 0.44 km<sup>2</sup>; tropical Borneo; convective rainfall; shallow pathways



Test catchments



Blind Beck – 8.8 km<sup>2</sup>; temperate NW UK; frontal rainfall; deep pathways

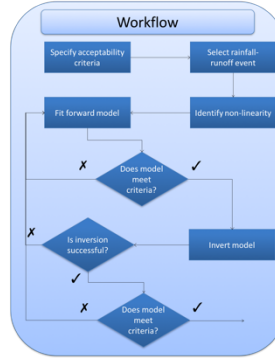


## Motivation

Development of a tool for improving estimates of catchment rainfall (key driver of catchment processes)

- Robust system modelling (works forwards and backwards)
- Capture of system dynamics using a simple model
- Evaluate information content of rainfall input data
- Ability to generate long rainfall series where only short records exist

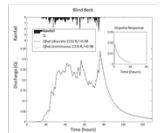
## Methodology



### Data-Based Mechanistic (DBM) modelling

- Select parsimonious models (those with the minimum number of parameters necessary to describe the system dynamics) that have a physical explanation
- Fit Transfer Function models (Young and Garnier, 2006) to sub-hourly rainfall and streamflow
- Invert acceptable models to derive a rainfall time-series
- Continuous time models inverted using a novel regularisation technique – **RegDer** (Kretzschmar et al, 2014)
- Comparison with discrete direct transfer function inverse - **InvTF** (Andrews et al, 2010)

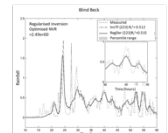
## Preliminary results



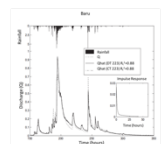
Forward model fit and catchment response

Catchment	Model Structure	R <sup>2</sup>		YIC		Inverse R <sup>2</sup>		Time Constants (hr)		Residual Variance	
		Discrete	Continuous	Discrete	Continuous	InvTF	RegDer	Fast	Slow	InvTF	RegDer
Blind Beck	[2 2 3]	0.983	0.983	-11.2	-6.71	0.512	0.515	6.35	22.10	0.055	0.055
Baru	[2 2 3]	0.879	0.878	-10.2	-8.05	-0.349	0.433	1.14	20.56	0.109	0.046

- Well-fitting forward models (98% Blind Beck; 88% Baru)
- Models with similar fit (equifinality – Beven, 2006) select lowest YIC
- Blind Beck: Both methods give similar results (inverse R<sup>2</sup>, residual variance)
- Baru: the methods produce rainfall with very different characteristics
  - **InvTF** has a high frequency component not related to the rainfall
  - **RegDer** method produces a smoothed series with dynamics faster than the time-constant
- **RegDer** shows a trade-off between numerical robustness and temporal resolution moderating the noise-amplifying inversion process



Inferred rainfall – comparison of methods



Forward model fit and catchment response

## Evaluation

Wide range of possible tests (Bennett et al., 2013) some inappropriate as normality assumed

**Numerical** - R<sup>2</sup> (Nash-Sutcliffe efficiency) – how well the variance is explained

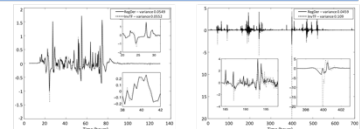
YIC (Young Information Criterion) (Young, 2001) – a measure of the balance between goodness-of-fit and number of parameters

**Graphical** - Analysis of residuals

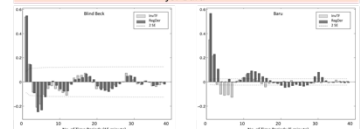
Auto-correlation structure

**Qualitative** - Visual comparison – rising limb, peaks, recessions

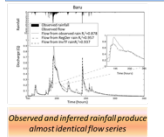
**Monte Carlo Simulations** – model uncertainty utilising covariance matrix (well-fitting models lead to narrow confidence bands)



Comparison of residuals and auto-correlation confirms the similarities between the methods for Blind Beck and differences for Baru



## Conclusions



Observed and inferred rainfall produce almost identical flow series

- Inversion by both **InvTF** and new **RegDer** methods captured the dynamics of both catchments
- **RegDer** generated sequences with less high frequency noise than **InvTF** particularly for tropical Baru
- Smoothing by **RegDer** is on a smaller scale than the dominant catchment dynamics
- Temporal detail of rainfall may not be important for modelling streamflow

### What next ...?

- Further evaluations using a range of global rainfall and flow-path regimes
- Use of decision theory to choose between models
- Use of inversion to investigate the information content of input data
- Investigation of the effect of time resolution

**Acknowledgements:**  
 Thanks go to NERC (Credible grant NE/J017299/1) and Keith Beven for funding this project to Mary Ockenden for the Blind Beck data (NERC NER/S/A/2006/14326) and to Jamal Mohd Hanapi, Johnny Laremus, Paul McKenna for the Baru data (NERC GR/9439) and last but not least to Wlodek Tych and Nick Chappell for their unstinting advice and support.

**References:**

Andrews, F., Croke, B., Jeanes, K., 2010. Robust estimation of the total unit hydro-graph. In: 2010 International Congress on Environmental Modelling and Software Modelling for Environment's Sake. Ottawa, Canada.  
 Bennett, N.D., Croke, B.F.W., Guariso, G., Guillaume, J.H.A., Hamilton, A.J., Jakeman, A.J., Marsili-Libelli, S., Newham, L.T.H., Norton, J.P., Perrin, C., Pierce, S.A., Robson, B., Seppelt, R., Voinov, A.A., Fath, B.D., Andreasson, V., 2013. Characterising performance of environmental models. Environ. Softw. 40, 1-20.  
 Beven, K., 2006. A manifesto for the equifinality thesis. J. Hydrol. 320, 18-36.  
 Kretzschmar, A., Tych, W., Chappell, N.A., 2014. Reversing hydrology: Estimation of sub-hourly rainfall time-series from streamflow. Environ. Model. Softw., 60, 290-301.  
 Young, P.C., 2001. Data-based mechanistic modelling and validation of rainfall-flow processes. In: Anderson, M.G., Bates, P.D. (Eds.), Model Validation: Perspectives in Hydrological Science. J. Wiley, Chichester, pp. 117-161.  
 Young, P., Garnier, H., 2006. Identification and estimation of continuous-time, data-based mechanistic (DBM) models for environmental systems. Environ. Model. Softw. 21 (8), 1055e1072.

Figure a - BHS Symposium 2014 - best poster by an early career hydrologist

## Abbreviations

23R	Brue 23 rain-gauge network
49F	Brue 49 rain-gauge network
ACF	Auto-correlation function
AR	Auto-regressive
ARX	Auto-regressive with exogenous variables
AV	Simple catchment average
BALANCE	A measure of over/under estimation of the sub-sample with respect to the true rainfall
BE	Benchmark
BGS	British Geological Survey
CAPTAIN	Computer-Aided Program for Time-series Analysis and Identification of Noisy Systems
CAR	Catchment average rainfall
CHASM	Catchment Hydrology and Sustainable Management
CREDIBLE	Consortium on Risk in the Environment: Diagnostics, Integration, Benchmarking, Learning and Elicitation
CT	Continuous time
DBM	Data-based mechanistic modelling
DGR	Discharge generating rainfall
DT	Discrete time
DVFC	Danum Valley Field Centre
ECAR	Event based catchment average rainfall
EGU	European Geosciences Union
ER	Effective rain
ESGR	Event based rainfall at a single gauge
f	frequency
FFT	Fast fourier transform
FIS	Fixed interval smoothing
FT	Fourier transform
GIS	Geographical Information systems
GLM	General linear model

GORE	Goodness of Rainfall Estimate - i.e. how well the sub-sample represents the true rainfall
HIC	Hydro-informatics Conference
HYREX	The Hydrological Radar Experiment programme
ICR	Inferred catchment rainfall
IER	Inferred effective rainfall
IHACRES	Identification of unit Hydrographs and Component flows from Rainfall, Evaporation and Streamflow data.
InvTF	Direct inverse transfer function
IQR	Inter-quartile range
$IR_t^2$	Inverse $R_t^2$
IRW	Integrated random walk
IRWSM	Integrated random walk with fixed interval smoothing
KF	Kalman filter
LNSE	Nash-Sutcliffe Efficiency on log transformed data
LU	Lancaster University
MAE	Mean absolute error
MCS	Monte Carlo Simulations
ML	Maximum Likelihood
N-S	Nyquist-Shannon sampling limit
NERC	Natural Environment Research Council
NRFA	National River Flow Archive
NSE	Nash-Sutcliffe efficiency
NVR	Noise Variance Ratio
OER	Observed effective rain
P	Rainfall
PBIAS	Percentage bias
$P_d$	Pathway percentage
PDF	Probability distribution function
PDIFF	Percentage difference in peaks
$P_e$	Effective or linearised rainfall
$P_{eh}$	Inferred effective or linearised rainfall
PEP	Percentage error in peak
$P_h$	Inferred catchment rainfall

$P_{obs}$	Observed rainfall
PUB	Prediction in ungauged basins
Q	Discharge
$Q_{inv}$	Flow simulated from inferred rainfall
$Q_{obs}$	Observed flow
$Q_{sim}$	Flow simulated from observed rainfall
R	Rainfall
$R^2$	Correlation coefficient
RACF	Residual auto-correlation function
RC	Runoff coefficient
<i>RegDer</i>	Regularised derivative inversion method
RIV	Refined Instrumental Variable
RMSE	Root mean square error
$R_t^2$	Nash-Sutcliffe efficiency
$R_t^2L$	Nash-Sutcliffe Efficiency on log transformed data
s	Laplace operator d/dt
SDF	Spectral density function
SFI	Slow flow index
SGR	Single gauge rainfall
SSG	steady state gain
T	periodicity
TC	time constant
TF	Transfer function
TP	Thiessen Polygon
TR	True Rain
UH	Unit Hydrograph
WY1	Water year 1 (October 1994-September 1995)
WY2	Water year 2 (October 1995-September 1996)
WY3	Water year 3 (October 1996-September 1997)
YIC	Young information criterion
$z^{-1}$	backward shift operator

# Table of Contents

<i>Abstract</i> .....	<i>i</i>
<i>Declaration</i> .....	<i>ii</i>
<i>Acknowledgements</i> .....	<i>iv</i>
<i>Project outputs</i> .....	<i>vii</i>
<i>Abbreviations</i> .....	<i>ix</i>
<i>Table of Contents</i> .....	<i>xii</i>
<i>Table of Figures</i> .....	<i>xvii</i>
<i>List of Tables</i> .....	<i>xxxi</i>
<b>Chapter 1 Introduction</b> .....	<b>1</b>
1.1. <i>Flooding and climate change</i> .....	<b>1</b>
1.2. <i>Flow generation processes and pathways</i> .....	<b>2</b>
1.3. <i>Scaling and measurement in space and time</i> .....	<b>4</b>
1.4. <i>Hydrological modelling – a brief introduction</i> .....	<b>5</b>
1.5. <i>Why reverse hydrology?</i> .....	<b>10</b>
1.6. <i>Aims and objectives</i> .....	<b>14</b>
1.7. <i>The story so far</i> .....	<b>14</b>
<b>Chapter 2 Background to methods used</b> .....	<b>17</b>
2.1. <i>Introduction</i> .....	<b>17</b>
2.2. <i>Spatial and temporal variability</i> .....	<b>17</b>
2.3. <i>Non-linearity</i> .....	<b>21</b>
2.4. <i>Data-Based Mechanistic (DBM) modelling</i> .....	<b>22</b>
2.4.1. <i>Physical interpretation</i> .....	<b>25</b>
2.5. <i>Transfer function inversion methodology</i> .....	<b>29</b>
2.5.1. <i>Regularised derivative estimate approach</i> .....	<b>30</b>
2.5.2. <i>The alternative fast compensating mode approach</i> .....	<b>31</b>
2.6. <i>Goodness of fit metrics</i> .....	<b>31</b>

2.6.1. Model selection criteria .....	31
2.6.2. Model Evaluation .....	33
2.6.3. Summary .....	37
2.7. Spectral analysis .....	37
2.8. Uncertainty .....	42
<b>Chapter 3 Test catchments and data .....</b>	<b>45</b>
3.1. Blind Beck - temperate catchment.....	45
3.2. Baru - tropical catchment.....	48
3.3. Brue, Somerset, UK .....	51
<b>Chapter 4 Reversing hydrology: estimation of sub-hourly rainfall time-series from streamflow .....</b>	<b>59</b>
Abstract .....	59
4.1. Introduction.....	59
4.2. Novel parsimonious method for input estimation using reduced order output derivatives.....	62
4.3. Estimation and implementation of regularised derivatives (RegDer method) .....	65
4.4. Comparison with the discrete-time inversion procedure (InvTF method) .....	68
4.5. First evaluation of the new RegDer methodology (including InvTF comparisons) .....	68
4.6. Choice of evaluation metrics .....	69
4.7. Data .....	70
4.7.1. Baru - tropical catchment responses.....	70
4.7.2. Blind Beck - temperate catchment response.....	70
4.8. First results and discussion.....	71
4.9. Conclusions.....	83
<b>Chapter 5 Reversing Hydrology: quantifying the temporal aggregation effect of catchment rainfall estimation using sub-hourly data .....</b>	<b>85</b>

<i>Abstract</i> .....	<b>85</b>
<i>5.1. Introduction</i> .....	<b>85</b>
<i>5.2. Application catchments</i> .....	<b>91</b>
5.2.1. Baru – tropical catchment.....	91
5.2.2. Blind Beck – temperate catchment .....	93
<i>5.3. Model formulation and physical interpretation</i> .....	<b>95</b>
<i>5.4. Continuous model formulation</i> .....	<b>98</b>
<i>5.5. Sampling frequency</i> .....	<b>100</b>
<i>5.6. Temporal aggregation of effective rainfall</i> .....	<b>100</b>
<i>5.7. Spectral Analysis</i> .....	<b>101</b>
<i>5.8. Results and discussion</i> .....	<b>102</b>
<i>5.9. Conclusions</i> .....	<b>109</b>
<b><i>Chapter 6 What really happens at the end of the rainbow? – paying the price for reducing uncertainty (using reverse hydrology models)</i></b> .....	<b>111</b>
<i>Abstract</i> .....	<b>111</b>
<i>6.1. Introduction</i> .....	<b>112</b>
<i>6.2. Methodology</i> .....	<b>113</b>
<i>6.3. Test catchment</i> .....	<b>115</b>
<i>6.4. Initial spatial analysis</i> .....	<b>116</b>
<i>6.5. Initial Results and Discussion</i> .....	<b>117</b>
<i>6.6. Conclusions</i> .....	<b>119</b>
<b><i>Chapter 7 Implications of spatio-temporal sampling of a rainfall field when generating a streamflow hydrograph: An investigation of Discharge Generating Rainfall using Reverse Hydrology</i></b> .....	<b>121</b>
<i>Abstract</i> .....	<b>121</b>
<i>7.1. Introduction</i> .....	<b>122</b>
<i>7.2. Review</i> .....	<b>123</b>

7.3. Aims of the paper .....	125
7.4. Reverse Hydrology and Discharge Generating Rainfall .....	125
7.4.1. Model selection criteria .....	128
7.5. Case study – Brue Experimental Catchment, South-west England ....	129
7.6. Annual data.....	131
7.7. The effect of aggregation on rainfall structure.....	134
7.8. Comparison of catchment average rainfall with rainfall at individual gauges .....	137
7.9. Model fitting and hydrograph generation .....	143
7.10. Rainfall variation at single gauges .....	149
7.11. Hydrographs from inferred rainfall.....	162
7.12. Inferred Discharge Generating Rainfall (DGR) .....	166
7.13. Summary and Conclusions.....	171
Appendix A1 – Best fit models to SGR.....	174
Appendix A2 – Catchment maps: distribution of time-delay and non- linearity .....	175
Appendix B – Cross-validation plots.....	178
Appendix C – Event based patterns.....	182
<b>Chapter 8.....In-filling and extending a rainfall record using Reverse Hydrology and Spectral Decomposition.....</b>	<b>187</b>
Abstract .....	187
8.1. Introduction.....	188
8.2. Review.....	188
8.3. Aim of the paper .....	190
8.4. Discharge Generating Rainfall .....	191
8.5. Data source – Brue Experimental Catchment, South-west England .....	193



<i>8.6. Model fitting and hydrograph generation.....</i>	<b>193</b>
<i>8.7. Modelling realistic rainfall series by spectral decomposition .....</i>	<b>195</b>
<i>8.8. Building the hybrid rainfall model .....</i>	<b>198</b>
<i>8.9. Multiple realisations.....</i>	<b>210</b>
<i>8.10. Gap filling.....</i>	<b>214</b>
<i>8.11. Discussion .....</i>	<b>220</b>
<i>8.12. Conclusions.....</i>	<b>223</b>
<b><i>Chapter 9 Summary and conclusions.....</i></b>	<b>226</b>
<i>9.1 Summary of key findings .....</i>	<b>226</b>
<i>9.2 Conclusions .....</i>	<b>228</b>
<i>9.3 Suggestions for further work.....</i>	<b>232</b>
<i>References .....</i>	<b>235</b>

## Table of Figures

Figure 1-1: Schematic showing the steps in model development/ selection in order of increasing approximation (adapted from Beven, 2012a) .....	9
Figure 2-1: Maps of rainfall over the Brue catchment showing the variability in time and space. The brighter the color, the higher the rainfall. The pie chart at top right shows the proportion of gauges measuring rain in the illustrated time step (more yellow - more gauges with rain) .....	18
Figure 2-2 - Block diagram of a basic first order system .....	26
Figure 2-3 - Decomposition of a second order TF into first order systems connected by different pathways .....	27
Figure 2-4 - A schematic representation of a general identity system assuming a perfect model and a perfect inverse. In the ideal case, the system input $U$ is identical to the system output $Y^*$ (adapted from Buchholz and Grünhagen, 2004) .....	28
Figure 2-5 - The low-pass filtering (damping) effect of the catchment (storage) as the high frequency rainfall signal is converted into lower frequency discharge (adapted from Smith et al., 2004) .....	39
Figure 2-6 - Definition of period and amplitude of a sinusoidal waveform .....	40
Figure 2-7 - Phase shift and vertical shift of a sinusoidal function .....	40
Figure 2-8: a) Time-series and b) frequency plots (periodogram) for the same set of rainfall and flow data. The periodogram pair shows the low-pass filtering effect of the catchment on the rainfall signal. The high frequency attenuation strength is illustrated in this double-logarithmic scaled graph .....	41
Figure 3-1 - Location and topography of the 8.8 km <sup>2</sup> Blind Beck catchment, NW England .....	46
Figure 3-2 - Rainfall and flow in the Blind Beck catchment on 26-31st December 2007 sampled at 15 minute intervals .....	46

Figure 3-3 - a) The WISER water quality monitoring system at the main weir, Blind Beck Experimental Catchment, Cumbria, UK, b) The water-level recorder (left) and WISER water quality monitoring system (centre) at the main weir, Blind Beck Experimental Catchment, Cumbria, UK (Photos courtesy of: NA Chappell) .....	47
Figure 3-4 - Saturated area close to the Low Hall stream gauging station within the Blind Beck Experimental Catchment, Cumbria, UK (Photo courtesy of NA Chappell) .....	48
Figure 3-5 - Location of the 0.44 km <sup>2</sup> tropical Baru catchment .....	49
Figure 3-6 – 5-minute rainfall and flow data from the 0.44 km <sup>2</sup> Baru catchment (February 1996) .....	49
Figure 3-7: Images showing the character of the Baru catchment (Photos courtesy of N.A. Chappell and W. Tych) .....	50
Figure 3-8 - Brue catchment geology, location and gauge network. (Crown Copyright/database right 2016. A British Geological Survey/EDINA supplied service; National River Flow Archive, 2012) .....	52
Figure 3-9 - The Brue catchment: The weir at Lovington (NRFA, 2012) and a typical river channel near Glastonbury. Upstream rain causes levels to rise and flooding when the embankments overtop. Flooded fields near Glastonbury (Edwin Graham, <a href="http://geograph.org.uk">geograph.org.uk</a> ) .....	53
Figure 3-10 - Brue catchment showing how rain-gauges are grouped geographically for convenience. Colouring units are the Thiessen polygons .....	55
Figure 3-11 - Cumulative rainfall for groups of rain-gauges (geographical grouping – see Figure 3-10) across the Brue catchment. Variation between gauges even over a 3-year period is obvious as is the similarity between FRAN, KNOW, MOWO and GODM, all situated at the southern edge of the catchment .....	56
Figure 3-12 - Distribution of rainfall over the Brue catchment in each of the three water years studied. (Gauges are shown alphabetically). Differences in distribution over the years and seasons can be observed. The winter periods	

are characterised by frontal rainfall affecting the whole catchment, whereas summers tend to be characterised by much more localised storm events. Winters are wetter than summers (statistics shown in Table 3-4) showing that low intensity frontal rainfall actually produces more rainfall than the summer convective storms ..... 57

Figure 4-1: The use of Hammerstein-type non-linearity in the model identification (a) and inversion (b) processes where  $P$  is the observed rainfall,  $P_e$  is the effective rainfall,  $Q$  is the observed streamflow,  $P_{eh}$  is the inferred effective rainfall and  $P_h$  is the inferred rainfall with the non-linearity reapplied ..... 60

Figure 4-2: Measured and estimated streamflow for: a) Baru (at 5 minute intervals) and b) Blind Beck (at 15 minute intervals), together with the associated hyetograms and impulse responses ..... 74

Figure 4-3: Comparison of rainfall simulated using the InvTF and RegDer (NVR optimised) methods for a) Baru and b) Blind Beck. Examination of the inset confirms that the RegDer method estimates the Baru catchment rainfall better (see Table 4-2) whilst there is little difference between the methods for Blind Beck rainfall. 99% uncertainty bands generated by Monte Carlo analysis are shown and can be seen to be very narrow ..... 75

Figure 4-4: Comparison of residuals for a) Baru and b) Blind Beck for the two inversion methods showing the similarities in performance between the methods when used for Blind Beck (with a minor increase in noise for InvTF) and the differences when used for Baru (with large artefacts in InvTF) ..... 76

Figure 4-5: comparative plots of the residuals autocorrelation function (RACF) for InvTF (light grey bars) and RegDer (dark grey bars) and both catchments (Baru in (a) and Blind Beck in (b)) showing the differences between methods of inversion. In both cases, RegDer quickly attenuates whereas InvTF shows negative ACF values characterising the fast switching, noisy residuals/artefacts ..... 78

- Figure 4-6: Comparison of the estimation of peaks for the two methods showing that for Blind Beck, both methods estimate the observed peak quite well with little difference between them whilst for Baru, the InvTF method hugely underestimates the peak whilst RegDer slightly over-estimates. The metrics PDIFF and PEP were taken from Bennett et al (2013) ..... 79
- Figure 4-7: Outputs modelled from observed and modelled rainfall sequences for a) Baru and b) Blind Beck showing that the outputs (discharges) are indistinguishable over much of the figure despite the differing characteristics of the rainfall inputs ..... 82
- Figure 5-1: a) The location of the 0.44km<sup>2</sup> tropical Baru catchment in Sabah (dark grey area in bottom left map – Sabah Foundation Forest management concession), Borneo and b) the hydro- and hyetographs for the February 1996 sampled at 5 min intervals showing the flashy response of the catchment to the high intensity, spatially variable rainfall ..... 92
- Figure 5-2: a) The location of the 8.8km<sup>2</sup> temperate Blind Beck catchment in Northwest England and b) the hydro- and hyetographs for Blind Beck for the period from 26th Dec 2007 at 16:45 to 31st December 2007 at 21:45 sampled at 15 min intervals showing its response to less intense frontal rainfall and deeper hydrological pathways ..... 94
- Figure 5-3: model identification and inversion workflow where P is the observed catchment rainfall,  $P_e$  is the effective rainfall, Q is the observed streamflow,  $P_{eh}$  is the inferred effective rainfall and  $P_h$  the inferred catchment rainfall. Non-linearity is represented by the bilinear power law (Beven, 2012a, p91). The continuous time transfer function is given by  $G(s)$  where  $A(s)$  and  $B(s)$  are the denominator and numerator polynomials and the inversion process is represented by  $G^{-1}(s)$  where  $A^*(s)$  and  $B^*(s)$  refer to the symbolic denominator and numerator polynomials of the regularised inverse transfer function as in (Equation 5-4) ..... 96
- Figure 5-4: observed effective and inferred effective rainfall profiles generated using the RegDer inversion method for a) Blind Beck and b) Baru ..... 99

Figure 5-5: Comparison of aggregated sequence to the Inferred effective rainfall sequence for a) Blind Beck (sampling interval 15 mins) b) Baru (sampling interval 5 mins) at aggregations of 4, 8 12 and 24 time periods (samples) illustrating how aggregation lowers the peak and spreads the volume of rainfall over a longer time period. The inferred effective rainfall sequence is plotted for comparison ..... 104

Figure 5-6: The  $Rt^2$  and  $R$  tend to a maximum value as aggregation increases for a) Blind Beck and b) Baru. The resolution of the inferred effective rainfall is taken to be point at which the maximum is reached or very little change is apparent. For Blind Beck, this value is reached at 10 periods for both  $Rt^2$  and  $R$ . The result for Baru is not quite as clear but can be estimated to be 10 periods from  $R$  and 11 or 12 from  $Rt^2$  though  $Rt^2$  continues to increase up to 24 time periods perhaps due to higher variability of the rainfall .....105

Figure 5-7: A similar plot to Figure 5-6 with aggregation by Moving Average for a) Blind Beck and b) Baru. Rather than reaching an asymptotic level, the  $Rt^2$  and  $R$  values maximize at 9 time periods for Blind Beck and 12 time periods for Baru (determined graphically in Matlab). These values have been used as the estimates of the resolution of the inferred effective rainfall and agree well with the estimates made by resampling. Convolution term in the caption is with reference to the method of calculating the moving average ..... 106

Figure 5-8: Periodograms for a) Blind Beck and b) Baru showing the frequency structure of the effective rain, inferred effective rain and streamflow sequences. The grey area shows frequencies beyond the 6dB difference between smoothed ER and IER spectral point. Both catchments show a similarity in the frequency spectra of effective and inferred effective rainfall within the catchment system. The inferred effective rainfall spectrum is very close to that of the actual effective rainfall within a wide range of frequencies mostly covering those corresponding to the catchments' time constants. There is also a strong low pass filtering effect cutting off high frequencies with low amplitudes instead of boosting this high frequency noise ..... 107

Figure 5-9: Comparison of observed discharge and discharge generated from the Inferred Effective Rainfall for a) Blind Beck and b) Baru. The flow sequences match almost perfectly in the case of Blind Beck and very closely in the case of Baru where the peak flows are under-estimated. Note that the forward (rainfall-discharge) model fit for Blind Beck (98%) is better than for Baru (88%) (Kretzschmar et al, 2014) .....	110
Figure 6-1 – The variability in the rainfall field in space and time over the Brue catchment – brighter colours mean more rain (mm). Rainfall sampled at 15 minute intervals. The pie charts show how many gauges measure rain - the more yellow, the more gauges are measuring rainfall .....	112
Figure 6-2 - the model identification and inversion workflow showing the off-line non-linear transformation .....	114
Figure 6-3 - Brue catchment geology, location and gauge network. (Crown Copyright/database right 2016. A British Geological Survey/EDINA supplied service; National River Flow Archive, 2012) .....	116
Figure 6-4 - Comparison of modelled $R_t^2$ (green bars) with inferred, aggregated $R_t^2$ (red bars) for each individual gauge. (Crown Copyright/database right 2016. A British Geological Survey/EDINA supplied service; National River Flow Archive, 2012) .....	118
Figure 6-5 - Observed rainfall from example gauges comparing flow generated using the observed and inferred rainfall with the observed flow .....	120
Figure 7-1 - Model identification and inversion workflow showing the off-line linear transformation .....	127
Figure 7-2 - Brue catchment showing location of 23 gauges used in the study and the underlying geology. (Note that this map is also used elsewhere in a different context, so is provided here for clarity.) .....	130
Figure 7-3 - Correlation against distance between gauge pairs for the Brue catchment. As expected, correlation decreases as distance between gauges increases providing justification for removing highly correlated gauges in close geographical proximity .....	131

- Figure 7-4 - 3 years of catchment average rainfall data sampled at 15 minute intervals for the Brue catchment plotted as water years - October 1994 to September 1997. Differences between years and between seasons are evident from these plots and from the statistics shown in Table 7-1 ..... 132
- Figure 7-5 - 3 years of flow data sampled at 15 minute intervals for the Brue catchment plotted as water years - October 1994 to September 1997. Differences between years and between seasons are evident from these plots and from the statistics shown in Table 7-1 ..... 133
- Figure 7-6 - Key characteristics of the rainfall series showing the effect of increasing sampling period a) Standard deviation (mm), b) Lag-1 autocorrelation coefficient c) Skewness d) Kurtosis e) Proportion of wet time periods f) Maximum intensity (mm/hr).....136
- Figure 7-7 - Top plot - An example of rain at individual gauges (grey bars) overplotted with catchment average rain (red bars); Bottom plot - the number of gauges with rain measured at each time period. The plots give an idea of the temporal and spatial variation in rainfall and illustrate how spreading rainfall evenly over the catchment lowers the rainfall peaks. This may be the case even when all gauges have rain if some gauges have high rainfall and others low ..... 140
- Figure 7-8 - Box plots of the 4 basic statistics, maximum rainfall intensity and proportion of wet time periods for the 23 gauges across the Brue catchment sampled at 15 minute intervals. The catchment average value is shown as a black + ..... 141
- Figure 7-9a/b/c - Hyetographs (catchment average rainfall) and observed and simulated hydrographs for WY1 (using best model identified. The modelled hydrograph (red line) shows differences from the observed hydrograph (blue line). The modelled hydrograph matches both peaks and recessions well ( $Rt2=0.908$  and  $Rt2L =0.839$  although some differences are apparent highlighting the weaknesses in using  $Rt2$  as a performance measure. Peaks are visible in the modelled hydrograph that do not occur in the observed hydrograph corresponding with rainfall peaks which do not influence the hydrograph ..... 145/6/7



- Figure 7-10 - A short section of hydrograph from WY3 showing missing peaks, extra peaks and badly reproduced recessions in more detail (blue: observed flow; red: predicted flow using CAR input) ..... 148
- Figure 7-11: Cumulative rainfall for each water year. Variation in temporal patterns can be seen as changes in the shape of the CAR plot (red line). The grey lines show the cumulative rainfall measured at each gauge. The shape and range indicate how both spatial and temporal patterns vary from gauge to gauge and from year to year ..... 150
- Figure 7-12a/b/c: Total rainfall over the Brue catchment in WY1 by gauge. The Thiessen polygons are coloured according to the rainfall at the gauge. Highest rainfall is on the higher ground to the north-east and lowest close to the catchment outlet..... 151/2/3
- Figure 7-13a/b/c - Hydrographs simulated from rainfall measured at individual gauges (plotted in grey) over plotted by the observed hydrograph (blue line) for WY1. In many cases, the individual gauges over-estimate both the peak flow and the recessions. Also simulated peaks may be observed which do not occur in the observed hydrograph ..... 155/6/7
- Figure 7-14a/b/c Spatio-temporal importance of the gauges is illustrated by plotting the fit of model unique to each rainfall-runoff combination on a catchment map. The theissen polygons are coloured according to the coding listed in Table 7-4. All gauges in WY1 are coded green – good fit ( $Rt2 > 0.80$ ) with six over 0.9 so can be expected to be representative of the catchment as a whole. CAR model fit is 0.908 ..... 158/9/60
- Figure 7-15a/b/c: Hydrographs generated from inferred rainfall measured at individual gauges (grey lines) compared with observed hydrograph (red line) for Water year 1 (WY1): October 1994 - September 1995. It can be seen that the simulated hydrographs are almost exact match with the observed even where the forward hydrograph does not fit well. The inferred rainfall contains only the information required to generate the hydrograph. The part of the rainfall spectrum that has no part in generating discharge is filtered out by the model ..... 163/4/5

Figure 7-16a/b/c - Catchment average and inferred catchment average rainfall during the spring in each of the three years .....	167/8/9
Figure A2-1a WY1 – The longest time delays on permeable areas of catchment however the range is small, 24-26 15-minute time-periods .....	175
Figure A2-1b WY1 – non-linearity generally decreases towards catchment outlet, ranging from 0.55 near the outlet to 0.65 as distance and elevation increase .....	175
Figure A2-2a WY2 – Time –delay is shorter, further from the catchment outlet with 2 exceptions which lie on the permeable band. There appears to be no significant correlation with rainfall amounts (see Figure 7-12b) .....	176
Figure A2-2b WY2 – The pattern of non-linearity is the reverse of WY1 with lowest being furthest from the catchment outlet .....	176
Figure A2-3a WY3 – Time delay generally decreases towards catchment outlet – with two exceptions. Rainfall generally follows the same pattern (see Figure 7-12c) .....	177
Figure A2-3b WY3 – No distinct pattern is visible in the non-linearity. Rainfall generally decreases towards the outlet (see Figure 7-12c) occurring in much more defined bursts than in other years (see Figure 7-4) resulting in several distinct flow events unrelated to the seasons (see Figure 7-5).....	177
Figure B - 1: Cross-validation plots for WY2 and WY3 based on the model identified for WY1. The $R_t^2$ fits are acceptable in both cases indicating the model for WY1 is a reasonable average model for the whole period. In WY3 the recessions are better reproduced than by the best-fit model for WY3 (Figure 7-9) .....	179
Figure B - 2: Cross-validation plots for WY1 and WY3 based on the model identified for WY2. The $R_t^2$ fits are acceptable in both cases indicating the model for WY2 is a reasonable average model for the whole period. In WY3 the recessions are better reproduced than by the best-fit model for WY3 (Figure 7-9) .....	180
Figure B - 3: Cross-validation plots for WY1 and WY2 based on the model identified for WY3. The $R_t^2$ and $R_t^2L$ fits are acceptable in both cases	

indicating the model for WY3 is a reasonable average model for the whole period over the whole performance range even though the recessions fit poorly in WY3. (Figure 7-9) .....	181
Figure C-1 – Comparison of model fits and hydrographs generated from ECAR (which could be an average of several gauges or an estimate from one gauge) and DGR for the same gauge or gauge-set. It can be seen that although for both the summer and autumn events the catchment average generates a good approximation of the observed hydrograph, it shows some peaks not present in the observed outflow hydrograph due to rain at gauges which are included in the ECAR but having no effect on the outflow. The Autumn event does not fit at all well and it can be assumed that several gauges are supplying misinformation, that is, adding significant amounts of rain to ECAR whilst not affecting the outflow.....	184
Figure 8-1 - Model identification and inversion workflow showing the off-line linear transformation .....	192
Figure 8-2 - Brue catchment showing location of 23 gauges used in the study and the underlying geology.....	194
Figure 8-3 - Frequency plots of the DGR and the residual series CAR-DGR. DGR mirrors the flow and drops sharply at the frequency of the critical time constant of the catchment. All frequencies below the cut-off point – where the amplitude of the DGR has dropped by 6 dB – are low power and have no significant effect on discharge generation (shaded area) as these parts of the signal are filtered-off by the catchment dynamics .....	196
Figure 8-4 – Comparison of CAR and DGR for a short section of record. DGR mirrors the flow but it is also obvious that the same amount of rain does not always generate the same amount of flow – non-linearity – due probably to the state of the catchment .....	197
Figure 8-5 – The basic method for rainfall generation by spectral decomposition. Reverse hydrology is used to generate the low frequency band part of the rainfall signal related to the catchment hydrograph response (DGR), and analysis of the residuals (CAR-DGR) is used to build a model of the high	

frequency part of the rainfall spectrum with the same distribution as the modelled residual series. A digital filter is constructed based on the AR structure of the residual series. After some manipulation, the resulting rainfall sequence looks like rainfall, has a similar temporal and frequency structure to the observed rainfall ..... 198

Figure 8-6 – The rainfall construction model is based on the rainfall and flow series for WY1. Flow modelled using the best available estimate of CAR and the best-fit model is compared to the observed hydrograph.  $R_t^2$  of 0.904 suggests that the peaks and high flows are well matched but the  $R_t^2L$  is lower suggesting that recessions are slightly less well captured. This is the benchmark with which to compare the performance of the constructed rainfall series for the same period. .... 199

Figure 8-7 – Time domain plots of Discharge Generating Rainfall (DGR) (top plot), an estimate of the low frequency part of the signal. and the residual difference CAR-DGR (lower plot), an estimate of the high frequency part of the rainfall signal, for WY1 .....200

Figure 8-8 – the auto-correlation structure of the residual series, IRES. The 95% confidence limits are shown in red. In this example, 13 correlation coefficients should be included to reproduce the correlation structure..... 201

Figure 8-9: Comparison of the distributions of calibration residuals (IRES) and simulated residuals (XIRES). Left hand plot – cumulative distribution function, right hand plot – frequency histogram (slightly enlarged to show detail around 0)..... 202

Figure 8-10 – comparison of the series of simulated residuals (XIACF – blue line and blue bars) and base residuals (IRES – red line and yellow bars) shows them to have similar distributions ..... 202

Figure 8-11 – the top plot shows the series  $NR = \left( \frac{\sum CAR}{\sum DGR_T} * DGR \right) + XIACF$  (Equation 8-6a). The bottom plot compares hydrographs generated from this series with the observed hydrograph. .... 203

- Figure 8-12 – Frequency spectra of NR (new rainfall sequence) and CAR are very similar in the area of interest showing that the auto-correlation structure has been maintained ..... 205
- Figure 8-13 - Frequency spectra of CAR and NRCV. The spectra show a slight vertical shift as a result of the rescaling of the rainfall series but the frequency patterns remain unchanged ..... 205
- Figure 8-14 – Hydrograph generated from constructed rainfall series NRCV compared with the observed hydrograph. An  $R_t^2$  of 0.930 is better than the hydrograph generated from observed rainfall. The  $R_t^2L$  value confirms that fit is good over the whole flow range ..... 206
- Figure 8-15: Discharge generated from pure DGR plotted against discharge generated from a constructed rainfall series (correlation coefficient = 0.968) showing that the constructed series does generate the correct hydrograph. .... 207
- Figure 8-16 – comparison of hydrographs generated from the DGR inferred from the CAR and DGR inferred from NRCV. The fits are almost identical confirming that although the rainfall pattern is different, the discharge generating characteristics have been preserved ..... 209
- Figure 8-17 - 50 possible rainfall realisations (grey bars) compared with the observed rainfall series (red dotted bars) and the observed flow (blue line, bottom plot) and hydrograph generated from the mean of 50 realisations (light blue line in bottom plot).  $R_t^2$  between observed flow and simulated hydrograph is 0.963. Enlarged section of the plot are shown in Figure 8.18 ..... 211
- Figure 8-18 - Enlargements of two sections of Figure 8-17. The top plot shows a section where the flow is active and the bottom plot a long slow recession. Usually where flow is active, all the realisations follow similar patterns, where there is little activity and a long recession, rainfall is having little or no effect on the flow so any random amount of rainfall can be generated. The observed hydrograph is shown in blue and the hydrograph simulated from the mean of the rainfall realisations in light blue. The  $R_t^2$  values are 0.944 for the section with active flow

and 0.810 for the recession plot indicating that the process works best where there is active flow.....	212
Figure 8-19: Hydrographs simulated from 50 rainfall realisations (grey lines). The hydrograph simulated from the mean of the 50 rainfall realisations is plotted in black and the observed hydrograph in blue .....	213
Figure 8-20: $R_t^2$ values for the hydrographs plotted from each rainfall realisation (blue circles). Also shown, for comparison, are the $R_t^2$ values for hydrographs simulated from the observed rainfall and the average of the rainfall realisations .....	214
Figure 8-21 – Observed rainfall and flow time-series with a gap in the rainfall (WY1-WY3). The observed rainfall over the gap is shown for comparison with the generated rainfall .....	215
Figure 8-22: Hydrographs modelled from observed rainfall in the calibration period (top plot) and from reconstructed the rainfall model (bottom plot) .....	216
Figure 8-23 – Gap in WY2 (length 10000 time periods) in-filled by DGR generated from flow and model fitted to calibration time-series. The calibration series is effectively WY1 .....	217
Figure 8-24 - Top plot shows the observed rainfall with the in-fill over plotted. The bottom plot shows just the in-filled series .....	218
Figure 8-25 - Hyetograph of in-filled rain and the hydrograph generated from it over the gap (top plots) and the hyetograph and hydrograph for the full record with the gap filled .....	219
Figure 8-26 - Hyetograph of the observed rainfall over the 'gap' and the simulated series used to in-fill. Similar patterns of rainfall can be observed although the spread of the simulated rain is not as great as the observed .....	225



## List of Tables

Table 3-1 – 15-minute rainfall and flow statistics for 26th - 31st December 2007 in the Blind Beck catchment.....	47
Table 3-2 - Statistics of 5-minute rainfall and flow for February 1996.....	50
Table 3-3 - Statistics for the Brue catchment October 1994 - September 1997. Rainfall statistics for each rain-gauge. Gauges are grouped geographically (see Figure 3-10).....	54
Table 3-4 - Statistics of rainfall measured in mm at 15 minute intervals over the Brue catchment showing the differences between winter and summer for the 3 years studied (catchment average rainfall estimated using Thiessen polygon method). .....	58
Table 4-1: The best CT-TF models fitted to subsets of data for Blind Beck (sampled at 15 minute intervals) and Baru (sampled at 5 minute intervals). There is little difference in efficiency (Rt2) between the different models so selection was based on the lowest order model with the lowest YIC (Young, 2001). The YIC is an objective measure combining the goodness of fit with a measure of over-parameterisation. A model with a large negative YIC fits the data well with a small number of parameters.....	71
Table 4-2: Efficiency (Rt2) values for the rainfall sequences estimated by inverting the models selected for Blind Beck and Baru using the InvTF and RegDer methods of inversion.....	72
Table 4-3: Residuals analysis for Blind Beck and Baru for both inversion methods showing the similarity between the methods for Blind Beck and the differences for Baru. ....	77
Table 4-4: Efficiency (Rt2) of forward CT-TF models of streamflow based on the observed rainfall or RegDer or InvTF rainfall as inputs. ....	80
Table 4 5: Data and model output statistics (rainfall (mm)). The following abbreviations were used: Var – variance, Kurt – kurtosis, Skew- skewness, IQR – inter-quartile range, prct – percentiles. Obs refers to observed rainfall. The Wet prefix in the table rows refers to statistics calculated only for samples with non-zero rainfall (>0 for inferred). ....	83
Table 5-1: The sampling frequency (hrs) and time constants (TCq – fast and TCs - slow) are listed for each of the study catchments together with the slow flow index (SFI – the percentage of the flow taking the slow pathway), the Nyquist-Shannon safe sampling limit (hrs) and the time resolution of the inferred effective rainfall (IER)	



estimated by both resampling and moving average methods. Also shown is the frequency domain estimate of the resolution – the cut-off point beyond which the signal carries very little information (illustrated in Figure 5-8) and can be considered unimportant. Time resolution of the inferred effective rainfall sequences estimated by both resampling and moving average methods are less than the dominant (fast) mode of the catchments and considerably less than the ‘safe’ Nyquist-Shannon limit.....	103
Table 5-2: The estimated resolution of the inferred effective rainfall for Blind Beck is well within both the Nyquist limit and the safe sampling limits suggested by the Ljung (1999) and Young (2010) whereas the resolution for Baru, whilst well within the Nyquist limit, is close to the fast TCq and outside the suggested safe sampling limits of Ljung and Young. ....	103
Table 6-1 - Validation of the 23-gauge network with respect to the full 49 gauges using the BALANCE and GORE criteria.....	117
Table 7-1 – Characteristics of the rain by water year and summer/ winter season for October 1994 – September 1997.....	134
Table 7-2 - The effect of increasing sampling period from 15 mins to 24 hrs on the statistics of rainfall structure for the 3 water years studied (October 1994-September 1997).....	135
Table 7-3 - Goodness-of-fit measures for individual models for each year between observed hydrograph and hydrograph modelled from catchment average rainfall and cross-validation results for each period. All models perform reasonably well in each period when reproducing peaks (Rt2). Low flows are reproduced well for WY1 and WY2 but not for WY3 (Rt2L) .....	144
Table 7-4 - Arbitrary thresholds for goodness-of-fit levels and associated colour coding used in Figure 7-14. ....	154
Table 7-5 - Comparison of the performance of the best fit catchment average model with the range of fit to individual gauges (full listing in Table A 1).....	161
Table 7-6 - Range of Rt2 values for hydrographs generate from observed gauge rainfall and inferred gauge rainfall when compared to the observed hydrograph. In all cases use of inferred rainfall improves the hydrograph fit, usually significantly. A value of 1.000 implies perfect fit. Examination of the hydrographs shows this is not the case but the variation is in the 4th decimal place.....	166
Table A 1 - structure of best fit models identified for the observations at each of the 23 rain gauges used in the study. Model fits shown Rt2 between simulated and observed hydrographs and hydrographs simulated from inferred rainfall (DGR). Model structure is given as a triad (defined in Equation 2-2) .....	174
Table C-1 – descriptions of the three example events used to illustrate the DBM/ Reverse Hydrology method of identifying misinformative gauges. The three	

storms can be seen to have very different characteristics a) is a short-lived summer convective cell that passes mostly over the eastern side of the catchment. Storm b) is a more widespread over the catchment with the heaviest rain to the northeast. Storm c) is a widespread event with a heavier core falling mostly on the northern side of the catchment but with a few southern gauges measuring more rain .....	183
Table C-2 – Model fits for a selection of gauges for each of the example events. The hydrograph generated from ECAR for the summer event shows a good fit to the Qobs as do each of the sample gauges. The Qinv hydrograph shows an improved fit. The Qsim hydrograph for the winter event shows a slightly less good fit and one of the individual sample gauges shows less good fit. The autumn event shows a poor fit to ECAR. Two of the sample gauges show a poor fit that is only partly resolved by using the DGR .....	185
Table 8-1 – Proportion of zero rainfall periods in CAR is 0.809. Adjusting the threshold value and setting all values in NR less than the threshold to 0 allows the proportion of zero rainfall periods in the constructed sequence to be matched with CAR. (Due to the stochastic nature of the process, the exact figures will vary with every realisation) .....	204
Table 8-2 - characteristics of the series at the stages of building the rainfall model. Many of the statistics are well matched but notable exceptions are Standard deviation and maximum intensity indicating that for this particular reconstruction extreme values are not well represented.....	207
Table 8-3 - Basic statistics for the whole record - Observed rainfall, no gap and observed rainfall with a 'gap' filled. Also shown, for comparison, are the same statistics for the observed rain over the period of the 'gap' and for the constructed rain used to fill the gap.....	220
Table 8-4 - Negative DGR as a percentage of total DGR at each stage of the gap filling routine. High values may indicate that the calibration model is not a good representation of the gap in the record. ....	221

# Chapter 1 Introduction

## 1.1. Flooding and climate change

Floods are the most common and often the most destructive of natural disasters. Almost everywhere on Earth where it rains is vulnerable to flooding. Although flooding is most commonly a result of heavy rainfall, it can be caused by rivers, dam failures, changes in groundwater, inadequate drainage (sewer flooding), rapid ice-melt or coastal flooding in the form of extreme high tides and or storm surges and combinations of these (Dale, 2005). Most floods take time to evolve giving time for areas likely to be affected to be evacuated, however fast developing and flash floods are highly damaging, destructive and dangerous and leave little time for defensive measures to be taken. The consequences of flooding are aggravated by man's wish to live close to water and the building of both commercial and residential property on natural floodplains (Merz *et al.*, 2010). Due to climate change, extreme flood events are expected to occur more frequently (Huntington, 2006) and a warmer climate means that the atmosphere can carry more moisture with more energy available to generate more extreme storms. Heavy rainfall, snowfall and heatwaves have become more frequent (Royal Society, 2017) and the frequency of floods has increased (Milly *et al.*, 2002). Attributing individual events to anthropogenic warming is difficult due to natural variability, however exposure to flooding is likely to increase as the degree of warming increases (Hirabayashi *et al.*, 2013) and short-term regional variations become more extreme. It is becoming apparent that atmospheric rivers play an important role in storms and floods in the Pacific south-west US (Dettinger, 2011) whilst many of the largest winter flood events in the UK have been linked to atmospheric rivers (Lavers *et al.*, 2011) including Storm Desmond which brought record rainfall and river levels and severe disruption to the northern UK in December 2015 (JBATrust, 2016). The projected increases in extreme rainfall and associated flooding mean that accurate predictions of rainfall and streamflow will become even more important in the future. It is unlikely that flooding can be eliminated, the challenge is to manage and reduce the risk (Shaw *et al.*, 2011).

Rainfall is the key driver of flood generation processes (Nijssen and Lettenmaier, 2004) and is the major input to most hydrological models however it is highly variable in both

time and space. The total amount of rainfall over a catchment is important but so is its spatial location and intensity as it may affect localised flood risk and operational decisions such as flow releases from reservoirs (Croke, 2006) or estimation of over-bank flows. Linsley (1967) stated that, if the right data is available, streamflow hydrographs can be generated that are as accurate as the input data. Rainfall is the major input and has the greatest variability so how well the hydrograph can be simulated may be dependent on how well the variation is understood and can be defined (Xu and Singh, 1998).

Deriving the relationship between rainfall and flow is a fundamental problem (Xu and Singh, 1998) not least because many of the processes of water flow in a catchment take place underground and are difficult or impossible to measure (Beven, 2012a). Much of what is understood about these processes is inferred from point measurements which, due to variability, only provide a limited picture of what is happening (Cole and Moore, 2008). How a catchment responds varies from event to event or even within the same event due to variations in antecedent conditions and the type of storm (Chappell *et al.*, 2017b). The heterogeneity of catchment characteristics interacts with rainfall properties such as intensity, volume and storm movement resulting in different areas of the catchment generating different amounts of flow (Shankar *et al.*, 2002). Catchment characteristics may include antecedent wetness, topography, soil types and structures, regolith and rock types, channel density and human influence. Not all rainfall contributes directly to the storm hydrograph as some is lost by evaporation.

## **1.2. Flow generation processes and pathways**

The shape of a streamflow hydrograph results from the integration of all flow processes which happen upstream as a result of rainfall and, thus, it is not a localised event but a catchment-wide response. The complex interactions between catchment and rainfall characteristics result in a wide range of flow generation mechanisms. Water may take a combination of pathways through the catchment, which may vary in both time and space affecting the final hydrograph shape (Brutsaert, 2005). Stormflow generating processes may involve overland flow as a result of precipitation in excess of the infiltration capacity of the soil (Horton, 1933), however this assumes the infiltration rate to be less than the precipitation rate over the whole catchment and that stormflow

is the result of overland flow. Overland flow does not occur everywhere but is the main mechanism in impervious areas. Saturation excess runoff (Dunne and Black, 1970) is a rapid transport mechanism where soils are saturated by emerging sub-surface outflow or perched water tables. It may occur with subsurface flow, the relative importance of each being dependent on the catchment and precipitation rates. Lowdermilk (1934) and Hursh (1936) suggested that sub-surface flow could be the main storm flow generation mechanism. Later studies suggested it might be the only mechanism (Hewlett and Hibbert, 1963; Whipkey, 1965). Weyman (1970) showed that soil did not have to be completely saturated for saturation excess contributions to occur but could be a result of lower soil horizons having a reduced permeability. Sub-surface pathways include preferential flow paths through percolines (a network of old root channels, soil cracks and animal burrows - Bunting, 1961) and soil pipes (Beven and Germann, 1982) that by-pass slower mechanisms such as flow through the soil matrix. Sub-surface flow may also occur along boundaries between permeable and less permeable layers (Bonnell and Gilmour, 1978). None of these mechanisms are mutually exclusive and they may occur in different parts of the catchment at different times or in different areas during the same storm (Dunne, 1978). The original assumption was that storm runoff was due to water generated by the current event. Work using tracers (Sklash et al., 1996) revealed that some flow comes from displaced 'old' water that has previously been stored and is rapidly released during a storm event (Kirchner, 2003). This concept has importance for the understanding of hillslope hydrology, water quality variations and the ecological impact of storms.

The relationship between rainfall and flow is time dependent. At long time scales, for example, annual, the relationship may show direct correlation between rainfall and flow volumes. As the timescale under consideration shortens, the relationship becomes more complex and more non-linear in character (Skøien *et al*, 2003). A linear relationship is one in which the same amount of rainfall will always generate the same amount of flow. Under non-linearity, the relationship is more complex and it cannot be assumed that the same amount of flow will result from the same amount of rainfall. This was demonstrated by Minshall (1960) who showed how the shape of the unit hydrograph changed with different volumes of rainfall input. The causes of non-linearity in the rainfall-runoff relationship include antecedent conditions (the amount of soil moisture present, evaporation, infiltration rates, groundwater flow) and the effect of routing

within the catchment, that is, the time taken for runoff to reach the measurement point (McDonnell, 2003).

### 1.3. Scaling and measurement in space and time

The timescale of a rainfall-runoff relationship should be determined by its purpose, for instance, a monthly or annual time-step may be adequate for determining overall catchment water yield. However measurements may need to be made at a much smaller interval then aggregated in order to get accurate estimates at the required time period. This may be particularly important in small catchments or those susceptible to flash flooding. If flood peak or water quality assessment is the purpose, then small time steps are also required so that the detail can be captured (Chappell *et al*, 2017a). The effects of sparse data sampling (in both space and time) are a major source of uncertainty in rainfall-runoff relationships (Kavetski *et al*, 2011). Catchment size also has an effect with both small relatively homogeneous catchments (for example, urban areas) and large catchments over long time periods, where local variations in rainfall and runoff are smoothed out, having relatively simple rainfall-runoff relationships. More generally, intermediate size catchments measured at short time periods with intermittent rainfall and variations in catchment characteristics show complex, non-linear relationships (Shaw *et al.*, 2011).

Improvements have been made in rainfall measurement techniques, for example, rainfall radar, remote sensing or improved rain-gauge design however much reliance must still be placed on, often sparse, rain-gauge networks. Many rain-gauges only measure at a daily time-step and thus may miss the detail of individual storm events both temporally and spatially. This is especially important in small catchments or those with a fast response time. Rainfall radar can give a much better indication of the spatial distribution of rainfall than a sparse rain-gauge network but must be calibrated, often against rain-gauge measurements (Wood *et al.*, 2000). Radar can be an accurate and valuable source of rainfall data over a large area however robust radar calibration is reliant on good rainfall estimates (Moore *et al.*, 2000). Spatial resolution could be more important than temporal in large catchments (Beven, 2012a), however it has been argued that errors due to spatial variability may be much less than those from other

assumptions (Jakeman *et al.*, 1990). Whatever model is used; its predictions are only as good as the input data (Shaw *et al.*, 2011).

Thus, it can be seen that it is important to have reliable estimates of the rainfall over a catchment. It is often the case that a single rain-gauge or a sparse rain-gauge network is assumed to represent the spatially and temporally variable rainfall field. The design and density of rain-gauge networks has been the subject of research over a long period and was one of the drivers for the set-up of the Brue experimental catchment (Bell and Moore, 2000). Rain-gauges may also be subject to measurement errors, for example, under-catch (Pollock *et al.*, 2014) and can only provide a measurement of rainfall over a limited area that may or may not be representative of the rainfall over the whole catchment. The rain that falls on the catchment that becomes streamflow can be measured at the outlet. The measured streamflow contains information not just about the rainfall but the way the catchment damps the rainfall signal as it is converted to streamflow. If this information could be extracted, it might be possible to improve rainfall forecasts and thus provide less uncertain flood predictions. Existing methods for estimating catchment rainfall, for example, the Thiessen polygon approach (Shaw *et al.*, 2011, p167) only make use of the rainfall signal. Thiessen weights for each rain gauge are computed by their relative area of influence and the area of each polygon used to weight the rainfall amount of the station in the center of the polygon. If any station is missing, the polygons must be recalculated. Thiessen polygons do not take elevation effects into account and are not related to streamflow generating processes (Schumann, 1998). Reverse hydrology takes the information present in the streamflow, that incorporates catchment information, and uses it to infer the rainfall that generates the discharge and thus could result in a better estimate of the flow hydrograph.

#### **1.4. Hydrological modelling – a brief introduction**

Hydrological processes are extremely complex. This complexity is obvious but requires simplifications, which must be stated, in order to describe them mathematically. It is also the reason why there is no common approach to hydrological modelling (Beven, 2012a). There are a wide range of hydrological models available with the choice often being down to the purpose of the modelling exercise (Todini, 2007). Often modelling is carried out to extrapolate existing data in both space and time, for example, into

ungauged catchments or into the future to assess the effects of change, as compensation for weaknesses in measurement techniques. It is often very difficult or impossible to measure all the processes and states required to describe and understand the system, for example, storage. Modelling for research purposes aims to improve understanding of the processes involved in the hydrological system with most being learnt when the data does not support existing theories which then have to be modified (Beven, 2012a). The ultimate aim of most modelling is to improve decision making in, for example, water resource management, flood control, pollution mitigation or to supply boundary conditions to atmospheric circulation models (Wagener *et al*, 2004).

Models range from physics-based distributed models, with many parameters that try to reproduce the heterogeneity of the catchment characteristics and hydrological processes, to black-box models with very few parameters based only on the observations of inputs and outputs without any reference to physical reality of the processes involved. In between these extremes are lumped physics-based models that assume that the processes and characteristics can be averaged over the catchment, and grey-box models based on the relationship between the system inputs and outputs but with some physical interpretation. Data-based mechanistic (DBM) modelling used in this study falls into the latter category (see section 2.4).

Physics based models assume that mass and momentum are conserved. Model parameters may be derived, at least in part, from catchment characteristics. Theoretically, distributed models route runoff through the stream network enabling predictions to be made at any point in the network, however many parameters are required to calibrate the model. Fully distributed models can have many parameters which must be estimated and even measurable parameters may lose their realism once adjusted so that the model produces acceptable results (Vieux *et al*, 2014). Geospatial data, now widely available, may provide future improvements in parameterisation, however overlays based on soil and vegetation do not directly describe the rainfall transformation processes in the catchment (Beven, 2012a). Geographical Information Systems (GIS) can also be used to incorporate remote sensing data (Brocca, 2014). SHE (Système Hydrologique Européen) is an example of a fully distributed model. It can incorporate information on topography, vegetation and soils and may be used to



investigate the effects of land-use change on flooding or water quality (Abbott *et al.*, 1986).

Semi-distributed models lump the characteristics of similar areas of catchments together (may be described as Hydrological Response Units (HRUs) - Flügel, 1995). This has the effect of reducing the number of parameters that need to be estimated. HRUs may be defined using GIS data. A grid-based approach can also be used where calculations are made based on every grid element, for example, LISFLOOD (De Roo *et al.*, 2000). Parameters are averaged for each HRU or grid so they can be thought of as a collection of small scale lumped models (Beven, 1989). HRUs can be mapped back into space using GIS but scale dependence of the parameters and calibration can be a problem (Vinogradov *et al.*, 2010).

Lumped physics based models regard the catchment as a single unit using average parameter values that are assumed to be representative of the whole catchment. They have only a few parameters however spatial variation cannot be represented by a single value (Sharma and Luxmoore, 1979). Calibration can be automated but there is a danger of over-parametrisation and problems may be caused by parameter inter-action (Ibbitt and O'Donnell, 1971). It has been suggested that 5 parameters explain most of the information contained in hydrological data (Hornberger *et al.*, 1985).

All models are simplifications of the 'real world' and, as such, are 'wrong', however they are often useful (Box, 1976) as long as they are used for the purpose for which they were developed and all limitations and simplifications are stated. Currently, there is no evidence that highly parameterised, process based models deliver better results than simpler stochastic models based on mathematical and statistical concepts (Shaw *et al.*, 2011), however this may change if reliable measurements of processes currently unmeasurable should become feasible. Many models can be defined by the calibration data that will perform well in practice – the problem of equifinality (Beven, 2006) – however it is questionable whether a model having no physical explanation should be accepted even if the results are satisfactory. A model may produce acceptable results for the conditions used to define it but, unless it has hydrological validity, it is difficult to have confidence in the results outside these limits (Kirchner, 2006).

Not only the time-step but also the choice of model should be defined by the purpose of the modelling exercise. If the aim is to predict discharge from rainfall without any consideration of the processes involved, then a simple black box model may be good enough. Black box models are usually lumped at catchment scale and, in contrast to distributed physics based models only have a very few parameters. These models attempt to extract as much information as possible from the available data by relating the inputs to the outputs, that is, the problem becomes one of systems analysis (Young, 1998). It can be argued that the data may not be good enough to identify a complex highly parameterised model (Jakeman and Hornberger, 1993) so successfully transforming the inputs into outputs without any knowledge of the processes by which this occurs is good enough. This is data-based modelling. It is dependent on suitable data being available so this approach could not be used in ungauged catchments. The concept has been extended by suggesting that the models identified should have some physical explanation (Young and Beven, 1994). The objective approaches used in black box modelling are used to identify a range of parsimonious models from the data. Only models that have a physical interpretation are retained (Young and Lees, 1993). This is Data-Based Mechanistic modelling. It combines elements of white box, physics based models with black box techniques and is often termed grey box modelling (Lees, 2000).

As models are approximations of the real world (Oreskes and Belitz, 2001) they have built-in uncertainties which may include the modeller's perception of the system, the simplifications involved in building the mathematical model, model structure, parameter estimates, the scale of the processes involved (do micro-level physical laws apply at catchment scale?), the time interval (does a model that has been calibrated for one time interval apply to another?), spatial scale (does a model calibrated for one catchment apply to another one?), the non-linearity of hydrological processes and the quality of the data. In order for the results from the modelling process to be useful, some measure of the uncertainties involved is needed to supply some indication of the limitations to its applicability. These uncertainties must be communicated in a way that is easily understandable to the non-expert.

Beven (2012a) describes the modelling process from perceptual through conceptual, procedural, calibration and evaluation stages. An adaption of his flow diagram showing the steps of the modelling process in order of increasing approximation is shown in

Figure 1-1. The perceptual model is the ‘Big Picture’ in the mind of the modeller. It will be unique to the individual, being the way they perceive the complexity of the hydrological system. The conceptual model is the mathematical simplification of this concept and the procedural model is the code needed to run it. Calibration uses observed data to determine model parameters whilst evaluation may use a different set of data to evaluate whether the model produces acceptable results. Measures used to assess model performance may be objective, for example, the Young Information Criterion (*YIC*) (Young, 1984, 2011) or Nash-Sutcliffe Efficiency ( $R_t^2$  or *NSE*) or subjective based on the experience of the modeller with reference to the model’s purpose. Acceptance requires not just that a model is a good fit but also has a physical explanation. If the criteria for acceptance are not met at any stage, then modifications may be made and the model reassessed. It can be argued that it is not possible to prove that a model is valid, only that it is wrong - the concept of falsification (Wagener *et al.*, 2004).

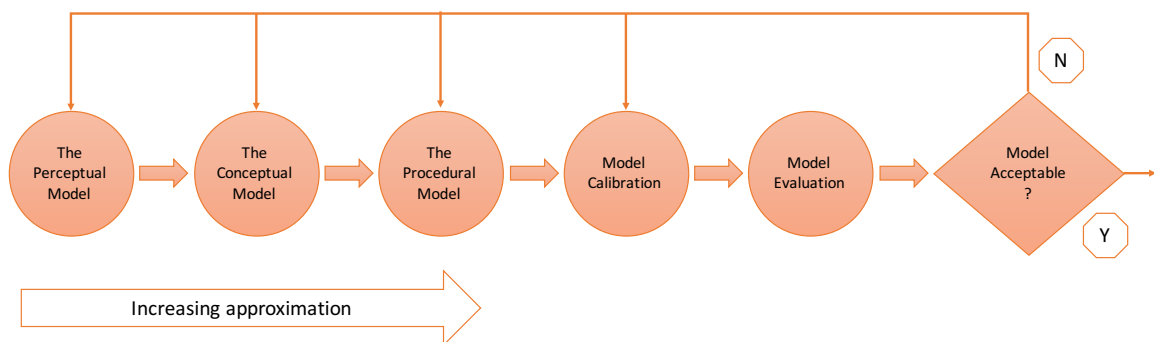


Figure 1-1: Schematic showing the steps in model development/ selection in order of increasing approximation (adapted from Beven, 2012a)

DBM modelling takes a top-down approach to model identification and parameter estimation. Models are identified from the data (in this study, rainfall and streamflow) that have as few parameters as are necessary to adequately define the dominant processes of the (hydrologic) system. Model structure is identified using objective systems analysis methods that minimise the bias introduced by prior assumptions (Taylor *et al.*, 2007) and enable the dominant modes of a system to be identified (Ockenden, 2010). Models are only accepted if they have a physical explanation (Young and Beven, 1994). DBM modelling often makes use of linear transfer functions however no real-world process is truly linear although it may be treated as such over a limited range of conditions (Leedal, 2006). If this is not the case, some means of

accounting for the non-linearity must be applied before identifying the parameters of the linearised system.

### 1.5. Why reverse hydrology?

Managing and reducing flood risk is becoming more important due to man's increased vulnerability. Deriving a relationship between rainfall and flow is key but extremely complex and, because many of the processes involved are unmeasurable, often inferred from point or laboratory measurements. It is necessary to think laterally about the way models are identified and novel approaches such as the one presented in this thesis are necessary to provide new insights into the processes and their identification. Although rainfall is the key driver and often the major input to hydrological models, it is only part of the story. Streamflow contains information about both the rainfall and the catchment processes that generated it. Inversion utilises the information in both rainfall and streamflow so could be a tool to aid improved understanding of flow generation and its links to rainfall, leading to more reliable flood predictions.

The terms 'inverse' and 'reverse' are often used interchangeably but this is not strictly correct. Inversion of a system has a different meaning to reversing the system, which is known in Information Science as unknown input estimation, and in Control Engineering as the Input Observer technique (Bhattacharyya, 1978). In order to invert a model, the transformation between the system inputs and outputs, usually the structure and parameters of the model, must first be identified from the observations. These parameters may have physical significance but are often difficult to measure accurately or at all. Estimation of the Unit Hydrograph, a widely used technique, is an example of this (Laurenson and O'Donnell, 1969; Boorman, 1989). Other examples may be found in areas such as astronomy, medicine, meteorology, geophysics, sub-surface hydrology and inverse streamflow routing (*c.f.*, Günther *et al.*, 2006; Pasquier and Marquette, 2006; De Campos Velho *et al.*, 2007; Devaney, 2012; Pan and Wood, 2013). Once identified, the system model is inverted enabling it to be run backwards – this is 'reverse hydrology'. For example, instead of using rainfall and the identified model to produce an estimate of streamflow, streamflow is used to infer the rainfall that has generated it by use of an inverted model. The integrative dynamics of the process mean that it is not feasible to simply fit a model 'in reverse' (that is, identify a model that

takes streamflow as its input and generates rainfall as its output) because it is numerically poorly defined, particularly for non-linear systems, and, very importantly, because the catchment processes involve differentiation in both space and time. A forward model, linking the conversion of rainfall to streamflow, must first be identified and inverted to obtain a reverse model. Reverse hydrology does ‘hydrology backwards’ using an inverted model allowing rainfall to be inferred from streamflow (Kirchner, 2009).

Reverse hydrology takes the information present in the streamflow that incorporates catchment information, and uses it to infer Discharge Generating Rainfall for the catchment. Accurate streamflow hydrograph simulation depends on the availability of highly sampled rainfall data and also its spatial distribution (Littlewood and Croke, 2013). Estimating the short-term rainfall characteristics which are important in producing the hydrograph (Obled *et al.*, 1994) may be useful for filling gaps in existing rainfall records, for example, due to equipment malfunction or periods when snow is the dominant precipitation (Hudson *et al.*, 1997), where corresponding flow records exist and extending rainfall series for catchments which have long streamflow but only short rainfall records.

The proposed method utilises the DBM methodology (for example, Young, 1998, 1999; Young and Garnier, 2006) to identify a simple, parsimonious model of the catchment dynamics based on the data (rainfall and streamflow) sampled at sub-hourly intervals. Non-linearity (*c.f.* section 2.3) is applied as a separate step using the bi-linear power law (Beven, 2012a). Other methods for accounting for non-linearity exist, for example, the non-linear loss model used by the IHACRES model (Jakeman *et al.*, 1990), which included a power law relationship between soil moisture index and effective rainfall (Ye *et al.*, 1997) and was updated by Evans and Jakeman (1998) to a catchment moisture deficit version and modified by Croke and Jakeman (2004), or the approach taken in the Bedford-Ouse model (Whitehead *et al.*, 1979) which modulates rainfall by a temperature dependent factor that is then filtered to give a measure of soil moisture content and used to modulate the modified rainfall. These approaches require extra data to be available so it was decided to use the simpler bi-linear power law in this study. A linear continuous time transfer function (CT-TF) model describes the relationship between the linearised rainfall and streamflow. The term ‘linearised’ is used in

preference to ‘effective’ rainfall here because the bi-linear transform has been applied to the rainfall data so that a linear TF can be identified. Effective rainfall is defined by Beven (2012a) as the part of the rainfall that is equal to the volume of streamflow generated. This is not the same as the linearised rainfall calculated here.

Continuous time models are used because their parameters have a direct physical interpretation and allow a wide range of system dynamics typical of hydrological systems to be modelled – so called ‘stiff’ systems where there is a wide range in the time constants (Young, 2010). Given that sampling is frequent enough to capture the system dynamics, parameters are not sampling interval dependent. The rational transfer function model is trivially inverted (*c.f.* section 2.5 and Chapter 4). Where the resultant model would be ‘improper’, that is, the order of the numerator of the CT-TF is greater than that of the denominator, the inversion requires derivatives of the streamflow. Regularised Derivatives are used, hence the algorithm has been called *RegDer*. Application of the regularisation procedure (described in sections 4.2 and 4.3) makes inversion possible without amplification of the noise in the inferred rainfall series. The general approach used could be applied within any DBM or top-down modelling framework.

The rainfall sequence inferred by the *RegDer* method from a single gauge (Kretzschmar *et al.*, 2016) may indicate that any one gauge may not be providing full information (Andrews *et al.*, 2011). The *RegDer* method of inversion could be used to assess the positioning and efficacy of rain-gauges in a network. Examination and comparison of the flow sequences generated from observed rainfall, catchment average rainfall and inferred rainfall may be able to highlight periods when flow is influenced by rainfall not captured by the rain-gauge or times when rainfall is registered but the flow does not respond (for example, when the catchment is wetting-up after a dry period). Periods of inconsistent data could influence the initial model identification but also help promote understanding of the rainfall distribution and integration processes especially if combined with a network of rain-gauges. The temporal resolution of the inferred rainfall appears to be affected by the slow time constant, the rainfall regime and the goodness-of-fit of the forward model. A well-fitting forward model that inverts well should be robust in terms of replicating the catchment system.

Possible applications and benefits of reverse hydrology include:

- 1) Filling gaps in rainfall records
- 2) Assessing rain-gauge networks (no. and position of gauges)
- 3) Identifying inconsistent or uninformative rainfall or flow data
- 4) Improved understanding of catchment processes
- 5) Improved understanding of rainfall distribution
- 6) Extraction of the essential rainfall dynamics required to generate flow from the broad-spectrum input signal.
- 7) For identifying convective storm cells or snowmelt events that effect the streamflow exiting the catchment but are not represented by the rain-gauge record (Kirchner, 2009).

## 1.6. Aims and objectives

This study aimed to:

- 1) **Improve understanding** of the information content of space-time distributed rainfall data for flood modelling
- 2) **Develop tools and techniques** for improving rainfall datasets for catchment modelling

These aims will be met by the following objectives:

- 1.i **Develop a new method** for inferring rainfall from sub-hourly streamflow data based on a **novel regularisation technique**
- 1.ii **Evaluate the regularisation technique** by comparison with existing inversion methods utilising data from two catchments with contrasting rainfall characteristics and flow-paths using a range of metrics
- 1.iii Assess the ability of the regularisation technique to capture the **dominant modes** of the rainfall-runoff behaviour using methods of **temporal aggregation and spectral analysis**
- 1.iv Assess the ability of the regularisation technique to capture the **spatio-temporal structure** of catchment rainfall
  
- 2.i **Quantify local rainfall records** that are **misinformative** for flood modelling
- 2.ii **Quantify the spectral components** of the rainfall signal responsible for flood generation
- 2.iii **Develop a new technique** for in-filling and extending rainfall records based on a combination of **regularisation and spectral decomposition**

## 1.7. The story so far .....

This thesis is based on a number of articles, either already published or prepared for publication (Chapters 4-8):

Chapter 2 provides background to the methodology used in the following papers. The data and catchments used for testing are described in chapter 3. Five papers which tell the story of this project are presented in chapters 4-8 followed by an overall summary and conclusions with recommendations for follow-up work in Chapter 9. A consolidated reference list covering all chapters follows.



Chapter 4 (Kretzschmar *et al.*, 2014) presents the **novel inversion method** utilising regularised derivatives (**RegDer**) and compares it with an existing method using the direct inversion of a discrete transfer function (**InvTF**). Tests are carried out using data from two contrasting catchments – the tropical Baru catchment in Borneo and the temperate Blind Beck, a tributary of the River Eden, in North-west England. Using both methods, the hydrograph generated from the inferred rainfall is much closer to the observed hydrograph than one generated using the forward model. However, the direct inverse method shows evidence of high frequency artefacts which would cause it to fail the criteria for DBM modelling. The output from the **RegDer** method shows evidence of loss of resolution however tests show that the essential catchment dynamics are being captured.

This theme is continued into Chapter 5 (Kretzschmar *et al.*, 2015) where **spectral analysis** was used to confirm that despite the loss of time resolution in the rainfall output from the *RegDer* method, the catchment dynamics necessary for streamflow generation are being captured. Estimates of time resolution from spectral analysis are compared with estimation of the time resolution from aggregation of the observed rainfall time-series. Both confirm that the essential dynamics are being captured and that the loss of resolution is the price paid for numerical stability of the inversion process.

Chapter 6 (Kretzschmar *et al.*, 2016) continues this topic but this time applied to the heavily instrumented Brue experimental catchment in south-west England. The spatial element of catchment rainfall is picked up and it is demonstrated that the loss of time-resolution and **representation of the essential rainfall characteristics applies everywhere in the catchment.**

Chapter 7 resumes the spatial theme presented in chapter 6 and introduces the concept of **Discharge Generating Rainfall (DGR)**, the part of the rainfall required to generate discharge. DBM modelling and the DGR concept are applied to the identification of which rain-gauge or gauges are representative of the catchment as a whole. This approach has been the subject of two conference presentations (Hydro-informatics 2016; EGU 2017). How well a model fits a rainfall-runoff combination is taken to

indicate its representativeness. A hydrograph generated using DGR shows an improved fit to the observed hydrograph over using a forward model and observed rainfall.

Chapter 8 takes the concept of Discharge Generating Rainfall and applies a **Spectral Decomposition** approach to the problem of generation of a new rainfall sequence that may be used to fill in gaps in the rainfall record or extend existing records (if flow records exist where rainfall does not).

## Chapter 2 Background to methods used

### 2.1. Introduction

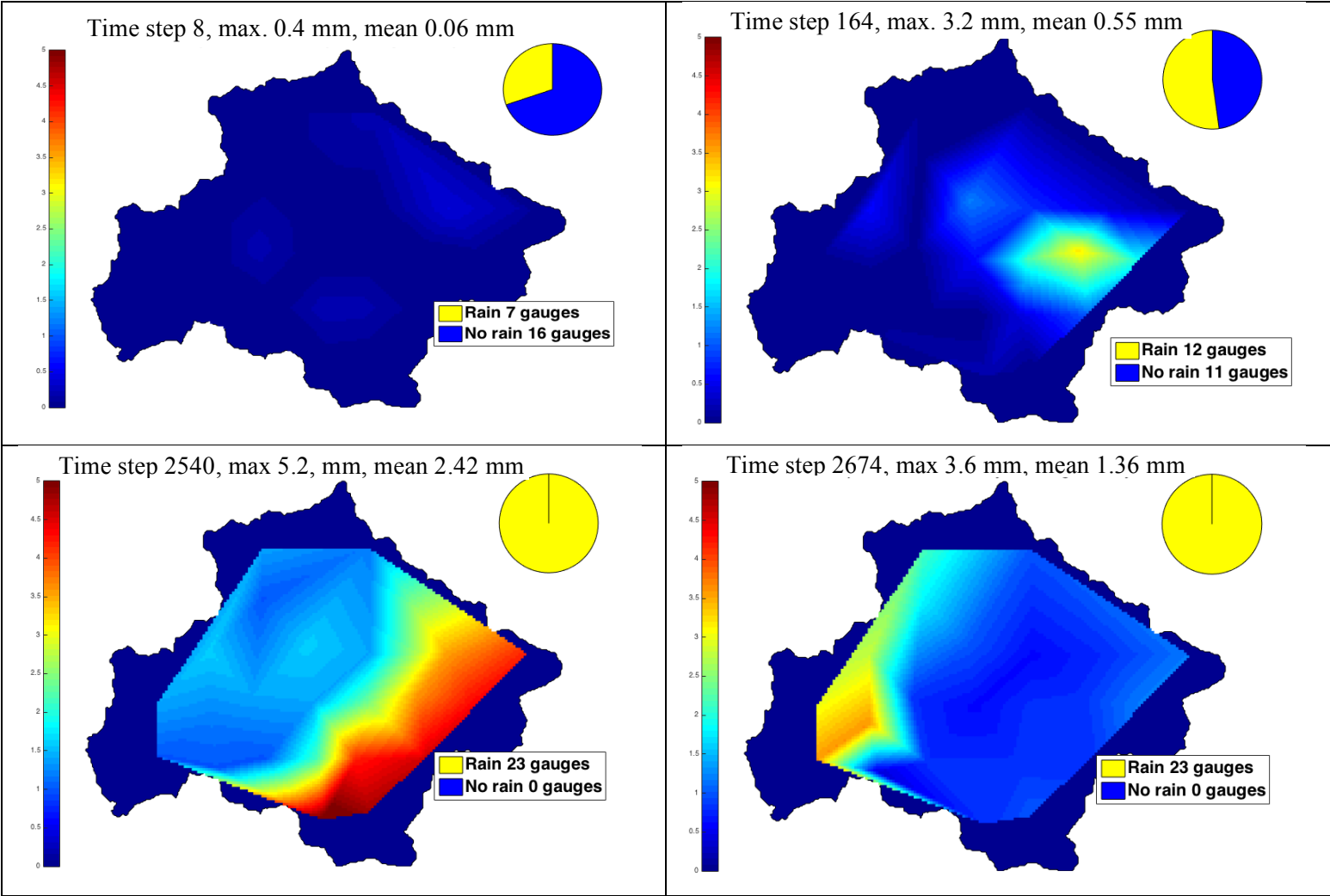
This chapter aims to introduce the ideas and methods used throughout the papers included in this thesis. The pertinent methods are included in each paper but are of necessity often lacking in detail. The relevant sections will be referred to where appropriate.

### 2.2. Spatial and temporal variability

Rainfall is the key driver of flow generation processes, however it is highly variable in both space and time. The effect of spatial variability on streamflow hydrograph generation has been widely investigated over many years resulting in varying conclusions which have yet to be resolved (Emmanuel *et al.*, 2015). Every catchment and every rainfall event is different which, when coupled with errors, that may be large enough to obscure any patterns, lead to a complexity which make it difficult to draw any general conclusions (Emmanuel *et al.*, 2015; Segond *et al.*, 2007). Timescale and sampling interval may also have an impact.

Rainfall variability in both space and time over the 135 km<sup>2</sup> Brue catchment in South-west England is illustrated in Figure 2-1 below. The Brue catchment is unusual due to density of the rain-gauge network. It has 49 rain-gauges in a catchment of 135 km<sup>2</sup>. Many of the gauges are very close together and therefore highly correlated (see Figure 7-3 in chapter 7). The 23 gauges used in this study, a density of 1 gauge per 5.9 km<sup>2</sup>, maintain geographical coverage. In practice, it is likely that a catchment of this size would only have a network of 2 or maybe 3 gauges (in 2010, the UK average was one gauge per 76 km<sup>2</sup>, Met. Office, 2010). The density of the gauge network makes it ideal for investigating the effect of spatial rainfall distribution on flow generation. It was set up as part of the Hydrological Radar Experiment (HYREX) by the UK Natural Environment Research Council (NERC) that ran from May 1993 to April 1997. The broad aim of HYREX was to gain a better understanding of rainfall variability, as sensed by weather radar, and how this variability impacts on river flow at the catchment scale (Moore *et al.*, 2000). For further discussion, see chapter 3, section 3.3.

Figure 2-1: Maps of rainfall over the Brue catchment showing the variability in time and space. The brighter the color, the higher the rainfall. The pie chart at top right shows the proportion of gauges measuring rain in the illustrated time step (more yellow - more gauges with rain).



Beven and Hornberger (1982) suggested, on the basis of a simulation study, that spatial variability is important, leading to significant differences in peak timing, distributions of peak flow and affecting volume - getting the volume right seems to be most important. The effects of spatial variation are tied to the question of how many gauges are needed to achieve an accurate estimate of catchment rainfall (Adhikary *et al.*, 2015). Dense gauge networks which might be expected to give a better estimate are expensive to install and maintain but sparse networks may miss the detail of rainfall variation especially under convective conditions. There is an example of two gauges only 300m apart in Walnut Gulch, Arizona showing a difference of 10mm from one convective storm (Faurès *et al.*, 1995). A large body of research exists aimed at answering the question of rain gauge location and network density. A very brief overview is given here. For further details, refer to the referenced literature.

The variability of rainfall is damped by the catchment processes so streamflow shows less variability. If rainfall variability is not organised enough to overcome the damping effect, then spatial variation need not be taken into account however reliable information on spatial patterns is important in order to make accurate estimates of total volume. This may be more important than spatial variation in itself (Obled *et al.*, 1994; Segond *et al.*, 2007). The importance of spatial variation may be catchment specific and dependent on the characteristics of the catchment and the rainfall regime. Younger *et al.*, (2009) studied the effect of rainfall input on model output on an event-by-event basis in the Brue catchment. They concluded that errors in the rainfall can lead to changes in the estimated model parameters to compensate for these observation errors. This may lead to a set of parameters for a single average model that is uniquely adjusted to simulate the erroneously observed event or events.

A well-designed network is required to evaluate an accurate estimate of the rainfall (Adhikary *et al.*, 2015), one that is dense enough to give a good estimate with gauges in the right locations but without redundancy. One of the earliest studies of the effect of network density was carried out by Eagleson (1967) using a combination of harmonic analysis and distributed linear systems (having some similarity to the techniques used in this study). He claimed that incorporating catchment dynamics into network design reduces the number of gauges required. Bras and Rodriguez-Iturbe (1976) used a multivariate state-space rainfall model together with a runoff model to investigate how

detailed the description of the rainfall field needed to be. Both Eagleson and Bras and Rodriguez-Iturbe concluded that gauge location appeared to be important and that catchments are more sensitive to storms dominated by over-land flow near their outlets. The HYREX experiment (Moore *et al.*, 2000) was set up to investigate rainfall variability and its impact on catchment scale flow regimes by combining radar and remote sensing data with information derived from a dense rain gauge network over the Brue catchment. Zhang and Han (2017) investigated spatial variability using the same catchment as a case study. They presented a framework for assessing spatial variation based on a combination of Coefficient of Variation and Moran's I (Moran, 1950) and concluded that a simple lumped model was adequate for simulating simple events but models with higher spatial resolution were required for more complex spatially variable events.

Lebel *et al.*, (1987) used scaled estimation error variance to compare Thiessen polygon, spline and Kriging interpolation methods for a range of network densities. Lebel *et al.*, (1987), Obled *et al.*, (1994) and Shah *et al.* (1996) all stated that a dense network has advantages over sparse networks whilst Sugawara (1992) said that rain gauge weighting should be by meteorological conditions rather than location. Several other studies looked at the impact of the density of gauge networks on rainfall estimation and hydrograph generation (*c.f.* for example, Anctil *et al.*, 2006; Bardossy and Das, 2008). The introduction of weather radar and other remote sensing techniques has led to several studies aimed at reducing uncertainties in rainfall forecasts by combining radar and remote sensing data with information derived from rain gauges (*c.f.* for example, Moore *et al.*, 2000; Bradley *et al.*, 2002; Brocca *et al.*, 2013). Chandler and Wheeler (2002) applied Generalised Linear Models (GLM) to a cluster of flood events in western Ireland and suggested that GLMs could be a powerful tool for analyzing historical records for rainfall variability patterns potentially associated with climate change. With advances in Geographical Information Systems (GIS), greater use is being made of geostatistical techniques both to investigate the effects of rainfall variability and to improve rainfall estimates (*c.f.* for example, Naoum and Tsanis, 2004; Yeh *et al.*, 2011; Shaghagian and Abedini, 2013; Adhikary *et al.*, 2015) however these techniques require that a large number of gauges are available for analysis.

It is often the case that a single gauge or sparse gauge network is assumed to represent the catchment as a whole. In this study, a method for assessing which gauges are representative using DBM modelling is proposed (see Chapter 7). It can be shown that representativeness varies with time due to the movement of rainfall over the catchment. The method highlights that spatial rainfall distribution does indeed have an impact on runoff (surface and sub-surface) generation. It is proposed, in Chapter 7, that reverse hydrology can be used to overcome this problem.

### **2.3. Non-linearity**

Hydrological processes are highly non-linear. The same amount of rainfall does not always generate the same amount of streamflow. If the rainfall follows a dry period, soil moisture will be low and initially rainfall will be used in ‘wetting-up’ the catchment before its effects can be seen in the runoff. If soil moisture is high, runoff will occur much more quickly and more of the rainfall will be operative in producing runoff. The reason why storm Desmond (5/6<sup>th</sup> December 2015) caused so much damage in the U.K. was because record amounts of rain fell on already saturated soils. Had that much rain fallen 2 months earlier, following a dry spell, it is possible that the effects would not have been so devastating.

A transfer function is a linear dynamic relationship, in this case between rainfall and streamflow. As stated above, the relationship between rainfall and streamflow is, in reality, highly non-linear so it must be ‘linearised,’ that is, the non-linearity accounted for in a separate step before the TF model is identified. (see Figure 6-2 for workflow diagram). This approach to compartmentalising a non-linear system into a static non-linearity and linear dynamics is known as a Hammerstein structure. This study uses a bi-linear power law relationship (Equation 2-1) between rainfall and flow (Young and Beven, 1994; Beven, 2012a; Young, 2003) with flow being used as an index of antecedent wetness, that is, the wetness of the catchment at the start of a rainfall event or period. This process introduces an extra parameter that determines the variable fraction of rainfall converted into flow which must also be estimated from the data. The power law coefficient ( $\alpha$ ) estimation is carried out ‘off-line’ and the non-linearity, as a power function, can easily be inverted when applied in the reverse modelling process.

The power law is given by:

$$P_e = P_{obs} * Q_{obs}^{\alpha} \quad (\text{Equation 2-1})$$

where  $P_{obs}$  is the measured rainfall,  $Q_{obs}$  is the measured catchment outflow in the previous time period and  $\alpha$  the parameter of the power law determining the fraction of the rainfall that generates discharge.  $P_e$  is the resultant linearised rainfall (often termed ‘effective rainfall’ but as this term has other connotations, the term ‘linearised rainfall’ is mainly used in this study). The higher the value of alpha, the greater the non-linearity and the less linearised rain there is available for discharge generation. If  $\alpha=0$ , linearised rainfall and measured rainfall are the same and the system can be said to be linear. At first sight, using flow as a surrogate for soil moisture might seem unusual, however it makes physical sense, that is, when flow is low, catchment storage is low and will be filled before runoff occurs – less of the rainfall is effective in influencing the flow – conversely, when flow is high, soil moisture (catchment storage) is high and runoff will occur more quickly – more of the rainfall is effective (Ratto *et al.*, 2007) in generating discharge. To avoid confusion and to correspond with chapter 7, the term Discharge Generating Rainfall (DGR) is introduced here. It is not the same as linearised rainfall but is the part of the rainfall effective in generating flow.

#### 2.4. Data-Based Mechanistic (DBM) modelling

Data Based Mechanistic modelling (Young and Lees, 1993) was first applied to water quality modelling and river flow by Young and Beck (1974) and Young (1974). It was developed over a number of years and now has been applied in areas as diverse as ecology and economics (Young, 2011). In contrast to physically based models, which are often complex and have many parameters that need to be defined, data based models have a simple structure and as few parameters as can be justified by the data (they are parsimonious). DBM modelling is often based on transfer functions which exemplify this philosophy however, any model class where model structure can be identified from the data could be used (Young, 1993, page 137).

The first stage of DBM modelling is effectively ‘black-box’ modelling, that is, models are fitted using statistical or systems analysis techniques with no consideration given to whether they have any physical explanation (Young *et al.*, 2004), and only once this



stage is complete are models accepted or rejected according to whether they have a meaningful physical explanation with respect to the system in question and the modelling objectives. DBM modelling requires that sufficient data be available at the scale under consideration and that prior assumptions (perceptions) about model structure and complexity are minimized. The model structure and necessary complexity is identified from the data and is often based on linear transfer function models, hence the necessity for linearising the input (depending on the existing catchment nonlinearity). It is the physically meaningful interpretation of the models which differentiates DBM modelling from black-box modelling. Many models may be identified that fit the input data equally well (the equifinality concept of Beven, 2006). However, if models do not have a physically meaningful explanation (that is, they are not behavioural) they are rejected.

Transfer function models may be defined in both discrete and continuous time (CT). Hydrological time-series are usually sampled at discrete time-intervals so it would seem that discrete-time (DT) models are ideal for modelling. They are widely used and can be applied easily to numerical methods of data assimilation and forecasting, for example, using the Kalman filter and fixed interval smoothing. CT formulations have several advantages over DT models, however historically they were difficult to estimate, so they tend to have been avoided. CT models can provide an insight into the properties of the system and the model's parameters have direct physical interpretation that is not related to the sampling interval as is the case for DT models. CT modelling allows a wide range of time constants, characterising dynamic modes typical of hydrological systems (termed stiff systems), to be modelled and can be better estimated from data with a high sampling frequency such as the data used in this study. A CT model, as it is sampling rate independent, can be converted into a DT model with the same dynamic properties at any sampling interval.

A transfer function (TF), a ratio of polynomials, can be described by their orders, the absolute time delay and the parameter alpha which is used to measure non-linearity. Most TF models, as identified and applied in hydrology, have orders of 3 or less – higher orders are difficult to describe mechanistically and are therefore rejected by the DBM philosophy. The general structure of a TF can be defined by:

$$TF = [n, m, \delta]^\alpha \quad (\text{Equation 2-2})$$

where  $n$  is the order of the denominator polynomial and  $m$  the order of the numerator polynomial.  $\delta$  is the pure time-delay in time-units and  $\alpha$  the coefficient of the power-law function that indicates the strength of the non-linearity in the system – higher values of  $\alpha$  indicate a more non-linear system. Both DT and CT formulations are included for completeness and because the novel *RegDer* inversion method (Kretzschmar *et al.*, 2014) is compared to the direct inversion of a discrete model (Andrews *et al.*, 2010).

A general DT-TF can be written as:

$$y(k) = \frac{B(z^{-1})}{A(z^{-1})} u(k - \delta) \quad (\text{Equation 2-3})$$

where  $u(k)$  is the input at the  $k^{\text{th}}$  time interval and  $y(k)$  is the output at the same interval.  $\delta$  is the pure time delay in the system. The polynomials A and B are defined as:

$$A(z^{-1}) = 1 + a_1 z^{-1} + a_2 z^{-2} + \dots + a_n z^{-n} \quad (\text{Equation 2-4})$$

and

$$B(z^{-1}) = b_0 + b_1 z^{-1} + b_2 z^{-2} + \dots + b_m z^{-m} \quad (\text{Equation 2-5})$$

where  $z^{-i}$  is the backward shift operator, that is,  $z^{-i} y(k) = y(k - i)$ . The orders of the polynomials are  $n$  and  $m$  respectively.

CT-TF models are similarly formulated but in terms of  $s$  where  $s \sim d/dt$ , the Laplace operator of derivative:

$$Y(s) = \frac{B(s)}{A(s)} U(s) e^{-s\tau} \quad (\text{Equation 2-6})$$

Polynomials A and B are defined as:

$$A(s) = s^n + a_1 s^{n-1} + a_2 s^{n-2} + \dots + a_n s^0 \quad (\text{Equation 2-7})$$

and

$$B(s) = b_0s^{m-1} + b_1s^{m-2} + b_2s^{m-3} + \dots + b_ms^0 \quad (\text{Equation 2-8})$$

while  $Y(s)$  and  $U(s)$  (denoted often simply as  $Y$  and  $U$ ) are Laplace transforms of  $u(k)$  and  $y(k)$  respectively, and  $e^{-s\tau}$  is the Laplace transform of time delay  $\tau$ . The process of model structure identification is described in chapter 4.

### 2.4.1. Physical interpretation

The important aspect of DBM modelling that sets it apart from black-box modelling is the requirement that the model has a physically meaningful interpretation. The time and frequency domain properties, model decomposition and how these might be interpreted in hydrological terms are explored in this section (Young, 2011). Only first and second order models are considered as models of a higher order have not been used as they failed the final criteria for the objectives of this study – they could not be successfully inverted.

As previously stated, one of the advantages of using a CT model formulation is that the parameters have direct physical interpretation independent of the model's sampling rate (Young, 2010). The continuous time model formulation for a 1<sup>st</sup>-order model is given by:

$$Y = \frac{b_0}{s + a_1} U e^{-s\tau} = \frac{SSG}{sTC + 1} U e^{-s\tau} \quad (\text{Equation 2-9})$$

where the steady state gain (SSG) for this first order system is given by:

$$SSG = \frac{b_0}{a_1} \quad (\text{Equation 2-10})$$

and the time constant (TC) by:

$$TC = \frac{1}{a_1} \quad (\text{Equation 2-11})$$

A 2<sup>nd</sup> order model is given by:

$$Y = \frac{b_0s + b_1}{s^2 + a_1s + a_2} U e^{-s\tau} \quad (\text{Equation 2-12})$$

which must have negative real roots for the system to be stable and non-oscillatory – if these conditions are not met, the model has failed DBM criteria for catchment systems

and must be rejected. Assuming these criteria have been met, a 2<sup>nd</sup> order system can be decomposed by partial fraction expansion into two first order systems whose *SSG* and *TC* can be determined using Equation 2-10 and Equation 2-11 (Young, 2011). Stable higher order systems may also be decomposed in the same way.

Equation 2-12 can be rewritten as:

$$Y = \frac{SSG_1\left(s+\frac{1}{TC_2}\right)+SSG_2\left(s+\frac{1}{TC_1}\right)}{\left(s+\frac{1}{TC_1}\right)\left(s+\frac{1}{TC_2}\right)} U e^{-s\tau} \quad (\text{Equation 2-13})$$

where  $TC_1$  and  $TC_2$  are the system time constants and are often significantly different – a ‘stiff’ system.  $TC_1$  and  $TC_2$  are often referred to as the fast (or quick) and slow pathways and designated  $TC_q$  and  $TC_s$ . The model can be decomposed into a parallel form:

$$Y = \left( \frac{SSG_q}{1+TC_q s} + \frac{SSG_s}{1+TC_s s} \right) U e^{-s\tau} \quad (\text{Equation 2-14})$$

where  $SSG_q$  and  $TC_q$  are the steady state gain and time constant of the fast response component and  $SSG_s$  and  $TC_s$  are the steady state gain and time constant of the slow response component. The total *SSG* of the system is given by:

$$SSG_t = SSG_q + SSG_s \quad (\text{Equation 2-15})$$

where  $SSG_t$  is the total gain of system. The fraction of the flow along each pathway can be calculated from:

$$P_q = \frac{SSG_q}{SSG_t} \quad P_s = \frac{SSG_s}{SSG_t} \quad (\text{Equation 2-16})$$

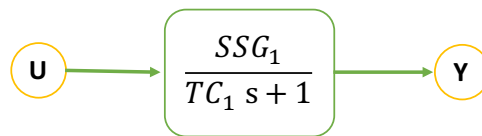


Figure 2-2 - Block diagram of a basic first order system

A simple first order model can be represented by the block diagram in Figure 2-2. A second order system can be decomposed into two first order systems. These may be

connected in a number of ways as shown in Figure 2-3. Higher order TF can be broken down in the same way but the number and the nature of connections become more complex.

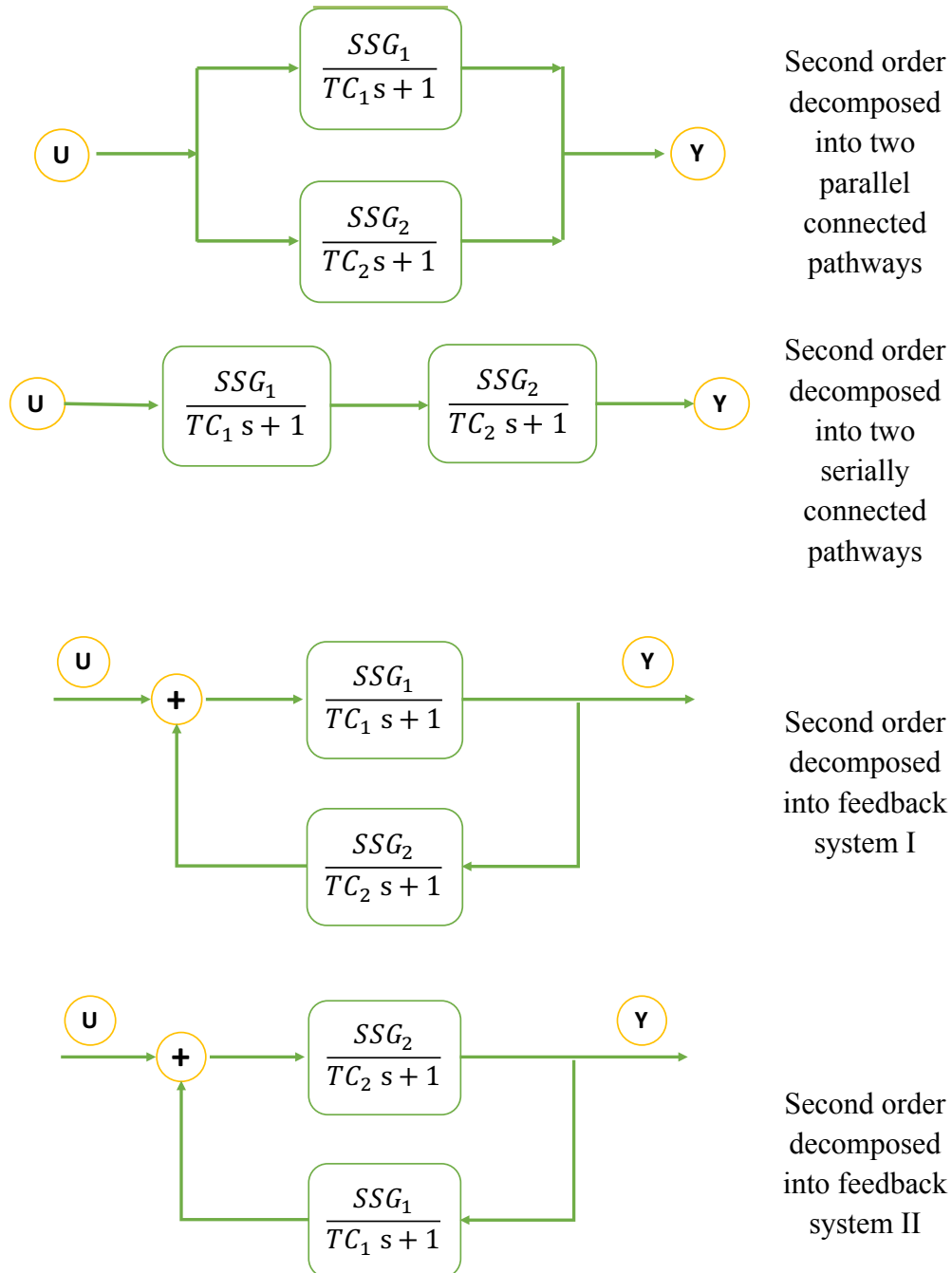


Figure 2-3 - Decomposition of a second order TF into first order systems connected by different pathways.

Similar analysis can be carried out on discrete time systems *c.f.* Beven (2012a, p108). Although the system pathways are referred to as ‘fast’ (or ‘quick’) and ‘slow’ these do

not generally correspond directly to surface runoff and baseflow. The fast pathway may include some near surface flow and the slow pathway may include any sub-surface flow not just baseflow. For further discussion, see section 5.8.

## 2.5. Transfer function inversion methodology

In order to obtain a well-defined inverse transformation, the transformation itself must be well-defined and it must characterise the system without excessive complexity. Inversion is based on differentiation and is, therefore, numerically poorly defined by definition. In this study, a novel solution to estimating Discharge Generating Rainfall has been proposed utilising the inverse of a continuous-time transfer function and regularisation, termed the *RegDer* method (Kretzschmar *et al.*, 2014). It is compared to the direct inverse of a transfer function (Andrews *et al.*, 2010) termed *InvTF* in chapter 4.

The general inversion of a linear system, as described in Section 1.3, is shown in Figure 2-4. If  $G$  ( $G: U \rightarrow Y$ ) is a true representation of the system and  $G^{-1}$  ( $G^{-1}: Y^* \rightarrow U^*$ ) is the true dynamic inverse then the overall system input,  $U$ , is the same as the output,  $Y^*$  (Buchholz and Grünhagen, 2004)

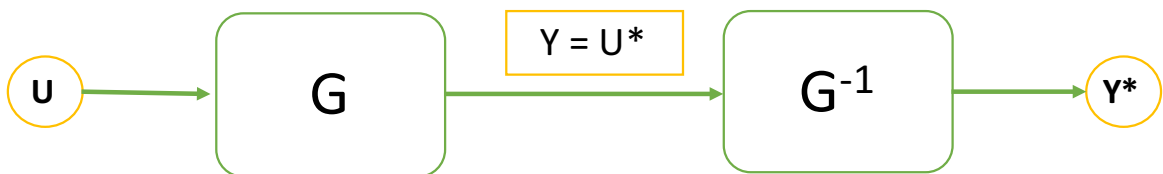


Figure 2-4 - A schematic representation of a general identity system assuming a perfect model and a perfect inverse. In the ideal case, the system input  $U$  is identical to the system output  $Y^*$  (adapted from Buchholz and Grünhagen, 2004)

The general system,  $G$ , can be represented a transfer function of the form:

$$G = \frac{B(s)}{A(s)} \quad (\text{Equation 2-17})$$

with  $A$  and  $B$  polynomials of orders  $n$  and  $m$  respectively. Transfer functions are linear operators so once the time delay and parameters have been identified, the model can be rewritten as:

$$G^{-1} = \frac{A(s)}{B(s)} \quad (\text{Equation 2-18})$$

from which a series of linearised rainfalls may be inferred. As shown in Figure 2-4, in an ideal situation, the series of inferred rainfalls would exactly equal the rainfall inputs to the system. In the real world, this is unlikely and how well  $Y^*$  matches  $U$  is dependent on the rainfall regime, the catchment dynamics, the quality of the data and how well the model represents the physical processes as well as the efficiency of the inversion.

A ‘proper’ transfer function depends on the relative orders of the numerator (order  $m$ ) and denominator (order  $n$ ). To be proper,  $n \geq m$  is required. If this is not the case, the TF model will not be realisable due to the fact that perfect derivatives do not exist (as involving knowledge of the future), and thus will be rejected by DBM methodology. An improper TF can be seen to be responding to future events now, which is clearly impossible (Dokuchaev, 2016). This problem arises with the inverse TF models – a common situation with many systems being ‘strictly proper’ where  $n > m$  resulting in an inverse where the opposite is true, which therefore is unrealisable.

Two approaches to resolving this issue are taken in this study.

### 2.5.1. Regularised derivative estimate approach

The Regularised Derivative method was developed from an idea first mooted by Jakeman and Young (1984) in combination with developments in the identification of CT-TF models (for example, Young and Garnier, 2006). The transfer function is inverted as in Equation 2-18 but is then split into a ‘proper’ realisable part and the unrealisable part which will require the use of derivatives. The realisable part takes  $Y$ , the original system output, as its input whilst the part requiring derivatives, uses regularised estimates of the derivatives as input.

Regularisation is a mathematical technique that introduces extra information allowing an ill-posed problem to be solved numerically. The additional information in this case takes the form of imposing a loss of temporal resolution (increasing the smoothness of the solution), thus effectively limiting the number of estimated values or parameters, and so simplifying the model. This process is sometimes interpreted as imposition of

Occam's Razor on the solution (the law of parsimony which states that the simplest answer is often correct). Regularisation is necessary here because minimising the objective function (residual sum of squares) leads to exaggeration of high frequency components of the estimated signal, particularly for catchments with large storage and slow and multiple time constants. The tuning parameter introduced is the NVR (equation 4-9) which is reciprocally related to the smoothness of the estimate. It is applied only to the higher derivative estimates (*c.f.* equation 4-4) allowing the amount of smoothing and therefore loss of resolution to be tuned to give the best fit to the observed rainfall.

The derivative estimates are obtained using a regularisation technique using higher order Integrated Random Walk models in a stochastic state-space framework, a technique available in the Captain Toolbox for Matlab (Taylor *et al.*, 2007). For detailed explanation, section 4.3. The following example shows a CT-TF model linking linearised rainfall and streamflow:

$$Q = \frac{A(s)}{B(s)} Pe = \frac{b_0s + b_1}{s^2 + a_1s + a_2} Pe \quad (\text{Equation 2-19})$$

where the order of the numerator  $m=1$  and the order of denominator  $n=2$ .

This is a proper TF where  $n>m$  so when the inverse is written as:

$$Pe = \frac{B(s)}{A(s)} Q = \frac{s^2 + a_1s + a_2}{b_0s + b_1} Q \quad (\text{Equation 2-20})$$

where the order of the numerator  $m=2$  and the order of denominator  $n=1$ . This is an improper TF because  $n<m$  and it involves a pure derivative of  $Q$ . It can be transformed to:

$$Pe^* = \frac{s^2 + a_1s + a_2}{b_0s + b_1} Q = \frac{s}{b_0s + b_1} (sQ) + \frac{a_1s + a_2}{b_0s + b_1} Q \quad (\text{Equation 2-21})$$

where the TFs are proper but involves the derivative of  $Q$ ,  $sQ$ , which is estimated using the regularised estimate of the derivative of  $Q$  obtained from an Integrated Random Walk model of  $Q$  (IRWSM in the Captain toolbox) (Jakeman and Young, 1984; Young *et al.*, 1999). The inverse transform can be rewritten using the regularised derivative estimate approximation  $(sQ)^*$ :



$$Pe^* = \frac{s}{b_0s + b_1} (sQ)^* + \frac{a_1s + a_2}{b_0s + b_1} Q \quad (\text{Equation 2-22})$$

which is realisable and straightforward to implement.

### 2.5.2. The alternative fast compensating mode approach

Equation 2-18 can be rewritten in a realisable (or ‘proper’, that is not involving direct derivatives) form (Zadeh and Desoer, 1963) given by:

$$G^{-1} = \frac{A(s) b(s)}{B(s) a(s)} \quad (\text{Equation 2-23})$$

where  $\frac{b(s)}{a(s)}$  is a compensating transfer function which makes the overall inverse realisable with no pure differentiation. The order of the denominator  $a(s)$  is chosen to be of an order such that the overall denominator is of higher order than the numerator. The compensating TF has a SSG of 1 and the roots of the numerator (poles) are chosen to be fast, that is, well above the upper range of the original model spectrum so that the inverse dynamics are not affected. The Direct Inverse approach taken by Andrews *et al.*, (2010) was used as comparison with the novel regularised derivative method in chapter 4.

## 2.6. Goodness of fit metrics

There is a difference between model selection and evaluating model performance (Bennett *et al.*, 2013). Selection may include criteria other than how well the model fits the data, and may be dependent on the purpose of the model. It may include subjective factors such as cost, applicability, simplicity and whether it has a physical explanation. Testing of model performance requires that some observational data, which is assumed to be error free (Moriassi *et al.*, 2007), is available for comparison. Ideally, this should not have been used for model identification or calibration. Metrics commonly result in a single value that is assumed representative of the whole series. This may, however, hide or misrepresent localised behaviour in both space and time.

### 2.6.1. Model selection criteria

The routines used for model selection in this study, contained in the Captain Toolbox for Matlab (Taylor *et al.*, 2007) do so on the basis of  $R_t^2$  – the Nash-Sutcliffe Efficiency

(NSE) – and the Young Information Criterion (*YIC*) proposed by Young (1984). The NSE is based on the coefficient of determination Equation 2-24 and is given by:

$$R_t^2 = 1 - \frac{\sum_{i=1}^N (Q_o^i - Q_m^i)^2}{\sum_{i=1}^N (Q_o^i - \bar{Q}_o)^2} \quad (\text{Equation 2-24})$$

where  $Q_m$  is the modelled value and  $Q_o$  the observed value at  $i$ .  $\bar{Q}_o$  is the mean of the observed series. It can range between  $1 > R_t^2 > -\infty$  where 1 indicates a perfect fit. A value of 0 indicates that the model performs no better than using the average of the observed data. Negative values mean performance is worse than using the average (Blöschl *et al.*, 2013). It measures the magnitude of the residual variance (noise) relative to the information contained (variance of observed data) and indicates how well the observed versus simulated data fit the 1:1 line (Moriasi *et al.*, 2007). The NSE is sensitive to differences in means and variances but, due to the residual squaring, it is over-sensitive to extreme values. The NSE uses the observed mean as a baseline which can result in over-estimation of the model skill especially when highly seasonal variables are involved (Gupta *et al.*, 2009).

The Young Information Criterion (*YIC*) is an objective measure combining model fit with a measure of over-parameterisation. It is given by:

$$YIC = \ln \frac{\sigma_r^2}{\sigma_o^2} + \ln\{NEVN\} \quad (\text{Equation 2-25})$$

where  $\sigma_r^2$  and  $\sigma_o^2$  are the variances of the residual series and observed series respectively and NEVN (the normalised error variance norm) is given by:

$$NEVN = \frac{1}{np} \sum_{i=1}^{np} \frac{\sigma_r^2 P_{ii}}{a_i^2} \quad (\text{Equation 2-26})$$

where  $np$  = the number of parameters,  $P_{ii}$  is the  $i^{th}$  diagonal element of the parameter covariance matrix and  $a_i^2$  is the square of the  $i^{th}$  parameter. The first term is a measure of how well the model fits the data and the second is a measure of parameterisation. A large negative value indicates a good fit with lowest number of parameters necessary to capture the system dynamics. In general, a higher order model will show a better fit but the parameters will have a greater uncertainty and the model may only fit the calibration data. *YIC* is a compromise between model fit and model complexity (Young *et al.*, 1996; Ockenden, 2010).

A further consideration in this study is how well a model inverts. In general, a model which fits the data and inverts well is likely to be a robust representation of the system. Final model choice was based on  $R_t^2$  (as high as possible),  $YIC$  (large negative value preferred) and the ability of the inverted model to recover the rainfall as measured by the NSE and termed  $IR_t^2$ .  $IR_t^2$  should be as high as possible and is the deciding factor between similar models.

### 2.6.2. Model Evaluation

To be useful, models need to pass some criteria of acceptability. Deciding what those criteria should be often depends on the purpose of the model. Quantitative measures allow for objective comparison of models highlighting the similarities and, possibly more importantly, the differences between observed and modelled series. A single value may not be enough to characterise differences in space and time. Different metrics can be used to characterise different states of the system, for example, dry periods, wetting up, wet periods or drying (Choi and Beven, 2007). Different metrics highlight different behaviours and target different parts of the hydrograph, for example, peak magnitude, peak timing, rising limb, recession or low flows, so a range of metrics may be necessary to assess performance over the whole range (Krause *et al.*, 2005). Seibert (2001) and Schaefli *et al.*, (2007) advocate comparing performance of a model against a benchmark model that is easily understood by end-users and stake-holders and suggest a variation to the basic  $R_t^2$  formulation (Equation 2-34). Many reviews of performance measures have been published discussing the pros and cons (*c.f.*, for example, Legates and McCabe, 1999; Krause *et al.*, 2005; Moriasi *et al.*, 2007; Ritter and Muñoz-Carpena, 2013; Bennett *et al.*, 2013). A brief overview is given here with focus on those used in this study. Alternatives to be found in the literature are also mentioned.

Performance measures can be categorised as regression metrics that measure the strength of a modelled relationship, dimensionless metrics that give a relative assessment, error indices that generate metrics in the same units as the measurements and graphical comparisons that provide useful visual assessments. Some metrics fit into more than one category.

The importance of graphical comparison should not be underestimated despite its subjectivity. Comparing hydrographs can show differences in peak magnitudes and timing and how well the shape of the recession is defined (Moriassi *et al.*, 2007). Scatter plots between observed and simulated series indicate whether model performance is the same over the whole range or is dependent on magnitude or whether there are any relationships that are not 1:1 (indicating bias in the simulated series). Scatter plots and box-plots may also highlight the presence of outliers (Ritter and Muñoz-Carpena, 2013).

Bias may be quantified using the error index, PBIAS (Moriassi *et al.*, 2007). It is given by:

$$PBIAS = \left[ \frac{\sum_{t=1}^T (Q_o^t - Q_m^t)}{\sum_{t=1}^T Q_o^t} \right] \times 100 \quad (\text{Equation 2-27})$$

where  $Q_o$  and  $Q_m$  are the observed and modelled values at time,  $t$ . The optimal value is 0 (no bias) with positive values indicating under-estimation and negative over-estimation. Andr ssian *et al.*, (2001) suggest an alternative which they use to quantify the over- or under-estimation of a sample of rainfall (for example, rainfall measured at a single gauge) compared to the reference or ‘true’ rainfall (for example, catchment average rainfall). It is given by:

$$BALANCE = \frac{\sum_{t=1}^T ER_t}{\sum_{t=1}^T TR_t} \quad (\text{Equation 2-28})$$

where ER is the estimated rain at time  $t$  and TR is the true or reference rain at the same time. A value of 1 indicates no bias. Values greater than 1 indicate that the sample over-estimates and values less than 1 indicate the sample under-estimates.

There are many other error indices, discussed in the referenced literature, that quantify error in the units of the measured values. Root mean square error (RMSE) and Mean absolute error (MAE) are two of the most commonly used. They are given by:

$$RMSE = \sqrt{\frac{\sum_{t=1}^N (Q_o^t - Q_m^t)^2}{N}} \quad (\text{Equation 2-29})$$

and

$$MAE = \frac{\sum_{t=1}^N |Q_o^t - Q_m^t|}{N} \quad (\text{Equation 2-30})$$

where  $N$  is the number of observations and  $Q_o$  and  $Q_m$  are the corresponding observed and modelled values. If  $RMSE > MAE$  the presence of outliers is indicated (Legates and McCabe, 1999).

Correlation based metrics such as the coefficient of determination ( $r^2$  or  $R^2$ ), NSE and Index of Agreement ( $d$ ) (c.f. Krause *et al.*, 2005) are commonly used in hydrology. They are over-sensitive to extremes and are insensitive to additive and proportional differences so may indicate that a model is a good predictor when it obviously is not (Legates and McCabe, 1999). Use of graphical methods and summary statistics should be used in addition.

Blöschl *et al.*, (2013, p27) give two different definitions of the coefficient of determination –  $r^2$  and  $R^2$  – where  $r^2$  is the square of the correlation coefficient and is given by:

$$r^2 = \frac{[\sum_{t=1}^T (Q_m^t - \bar{Q}_m)(Q_o^t - \bar{Q}_o)]^2}{\sum_{t=1}^T (Q_m^t - \bar{Q}_m)^2 \sum_{t=1}^T (Q_o^t - \bar{Q}_o)^2} \quad (\text{Equation 2-31})$$

where  $Q_o$  and  $Q_m$  are the observed and modelled values at time  $t$  and  $\bar{Q}_m$  and  $\bar{Q}_o$  are the means of the modelled and observed series.  $r^2$  measures the degree of linear association and ranges from 0 for no correlation to 1 for a perfect fit. One of the major drawbacks to  $r^2$  is that it is dependent only on the amount of dispersion that is explained by the predictions so a systematically biased model will give an  $r^2$  value close to 1 even though all the predictions are wrong. Krause *et al.*, (2005) suggest taking the gradient ( $b$ ) and intercept ( $a$ ) of the regression line into account (for a good fit,  $a$  should be close to 0 and  $b$  close to 1). They suggest a weighted version of  $r^2$  that includes the slope,  $b$ :

$$wr^2 = \begin{cases} \{b\}.r^2 & \text{for } b \leq 1 \\ \{b\}^{-1}.r^2 & \text{for } b > 1 \end{cases} \quad (\text{Equation 2-32})$$

$wr^2$  quantifies over or under-predictions at the same time as the dynamics.

The alternative formulation is:

$$R^2 = 1 - \frac{\sum_{t=1}^T (Q_m^t - Q_o^t)^2}{\sum_{t=1}^T (Q_o^t - \bar{Q}_o)^2} \quad (\text{Equation 2-33})$$

It is a composite measure of bias and random error where 1 is a perfect fit and 0 indicates the model is no better than the average of the observations, A negative value indicates that the model is worse than the average. The NSE (Equation 2-24) is based on this formulation. A further variation on the NSE that allows model performance to be compared to a benchmark model was suggested by Seibert (2001) and Schaepli *et al.*, (2007). It is given by:

$$BE = 1 - \frac{\sum_{t=1}^T (Q_m^t - Q_b^t)^2}{\sum_{t=1}^T (Q_o^t - Q_b^t)^2} \quad (\text{Equation 2-34})$$

where  $Q_b$  is the value at time  $t$  generated by the benchmark model.

The reliance on squared errors in these metrics means that they tend to emphasize larger errors and do not account for residual correlations. These tend to be associated with higher streamflows so they show a better fit to peaks than lower flows. Data transformations such as taking logs can increase sensitivity to low flows because the peaks are flattened whilst low flows change very little. The sensitivity to over- or under-prediction is increased (Krause *et al.*, 2005).

A variation of the *NSE* was suggested by Andr ssian *et al.* (2001) and is used alongside BALANCE (Equation 2-28) to estimate how well a rainfall subset matches the reference or ‘true’ rainfall. It is termed the Goodness of Rainfall Estimation (GORE) index and uses a square root transformation of the variables to reduce the impact of extreme events. It is given by:

$$GORE = 1 - \frac{\sum_{i=1}^n (\sqrt{ER_i} - \sqrt{TR_i})^2}{\sum_{i=1}^n (\sqrt{TR_i} - \sqrt{\overline{TR}})^2} \quad (\text{Equation 2-35})$$

where  $n$  is the number of observations,  $ER$  is the estimated (or sampled subset) rain and  $TR$  is the ‘true’ or reference rain (often catchment average rainfall). For application see section 6.4.

The metrics discussed so far apply to the whole dataset. On an event basis, metrics such as Peak Difference (PDIFF) and Percentage Error in Peak (PEP) (Bennett *et al.*, 2013)

are useful for quantifying differences in hydrograph peaks which may be evident from visual inspection. They are given by:

$$PDIFF = Max(Q_o) - Max(Q_m) \quad (Equation 2-36)$$

and

$$PEP = \left( \frac{Max(Q_o) - Max(Q_m)}{Max(Q_o)} \right) \times 100 \quad (Equation 2-37)$$

where  $Q_o$  and  $Q_m$  are the observed and modelled datasets for the event. PDIFF is the measured difference between the magnitude of the peaks and PEP the percentage difference (see Figure 4-6).

### 2.6.3. Summary

There are a wide range of evaluation metrics available however choosing a suitable one depends on the purpose of the model and the data. Many metrics assume a normal distribution and independence and are generally not suitable for use with hydrological data which usually is not normally distributed, and are therefore not discussed here. The independence assumption is often ignored and may result in information remaining in the residual series which is not explained by the model leading to biased estimates of the statistical properties. The metric most widely employed, NSE, should be used alongside additional methods including graphical and error measures such as PBIAS. NSE (as an  $\mathcal{L}^2$  - a quadratic norm based criterion) tends to favour good fit at higher flows and will tend to indicate a model is a good fit even if low flows are not well reproduced. Combining regular  $R_r^2$  with the log-transformed version,  $R_r^2 L$ , provides a better overall picture of model performance across the whole range (see section 7.8).

## 2.7. Spectral analysis

Transformation of time-series into the frequency domain enables features that are hard to see in the time domain to be detected. Although spectral analysis has been applied for several decades in hydrology (*c.f.* review in Kendall and Hyndman, 2007) it has seen little practical use (Fleming *et al.*, 2002), however Kendall and Hyndman (2007) used it to extract quantitative information and demonstrate linkages between hydrological processes. This is, paradoxically, in spite of the fact that transfer function models, intrinsically constructed in the frequency domain, are commonly used in

hydrology. Transfer functions are easily interpreted as spectral expressions, as the Laplace operator,  $s = i\omega$ , and the backward shift operator  $z^{-1} = e^{-i\omega\Delta t}$  in this dual interpretation (with:  $\omega = 2\pi f$ ,  $f$  - the signal frequency, and  $i$  - the imaginary unit). These identities are used in Chapter 5 – as they provide direct spectral relationships between the signals and illustrate the spectral decomposition occurring in the regularisation process.

Model evaluation usually entails comparing model output with observed values of the same quantity to ensure a good fit (see section 2.7.2). A good fit in the time-domain implies a good fit in the frequency domain but this may not be the case. Fleming *et al.*, (2002) suggested that comparing periodicities in the frequency domain could be a valuable approach for assessing model performance. Montanari and Toth (2007) attempted model calibration based on the spectral density function suggesting that the technique could be applied to sparse data or ungauged catchments. Cuchi *et al.*, (2014) used frequency analysis to investigate the non-linearities in a karst system in Spain. Spectral analysis has also been applied to fractal system behavior (*c.f.* for example Kirchner *et al.*, 2000). Wavelet analysis can extract both time and frequency information from a signal capturing information at a range of resolutions. It was used by Schaepli *et al.* (2007) to detect potential flood generating meteorological conditions due to its ability to explore co-variation of different processes at differing time-scales and is becoming a popular tool for analysis (Dadu and Deka, 2016). In Chapter 5, spectral analysis is used to confirm that the inferred rainfall time-series retains the characteristics of the input rainfall series.

A catchment acts as a low-pass filter. A broad-spectrum rainfall signal input is low-pass filtered by the catchment's spatio-temporal integration processes into a lower frequency range streamflow signal – as illustrated in Figure 2-5. The loss of time resolution (*c.f.* Chapter 4 and Chapter 5 for detail and discussion) in the inferred rainfall signal is to be expected given that the regularisation procedure also acts as a low-pass filter. The streamflow spectrum is the result of mapping the rainfall spectrum by the catchment dynamics. Regularisation is a necessary step here in order to obtain a well-defined inverse of the catchment dynamics.



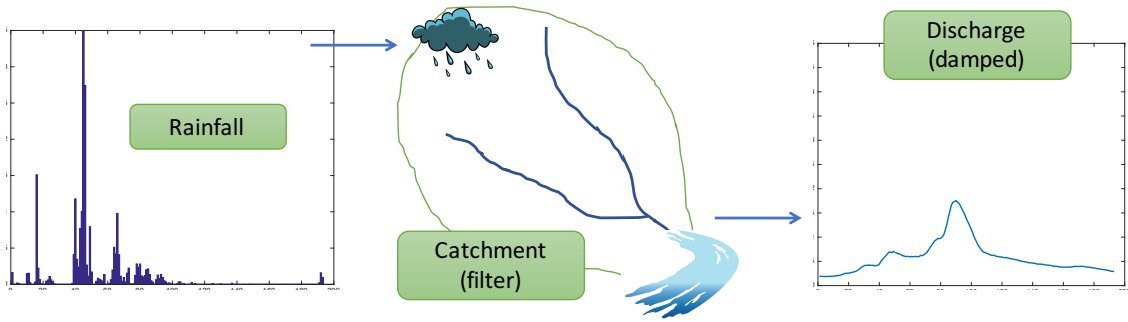


Figure 2-5 - The low-pass filtering (damping) effect of the catchment (storage) as the high frequency rainfall signal is converted into lower frequency discharge (adapted from Smith *et al.*, 2004)

The Fourier transform (FT) maps the time domain signal into the frequency domain:

$$G(f) = \int_{-\infty}^{\infty} g(t)e^{-2\pi ift} dt \quad (\text{Equation 2-38})$$

where  $t$  is time,  $f$  is frequency and the imaginary unit  $i = \sqrt{-1}$ .  $G(f)$  and  $g(t)$  can be said to be two different ways of expressing the same signal or operator (kernel function such as the unit hydrograph). The frequency signal can be converted back to the time domain using the inverse FT:

$$g(t) = \int_{-\infty}^{\infty} G(f)e^{2\pi ift} df \quad (\text{Equation 2-39})$$

An alternative formulation using angular units, by substituting  $\omega = 2\pi f$ , is often found in the literature however the formulations given here are easier to implement. (Fleming *et al.*, 2002). The FT can be thought of as decomposing the time-series into sine waves of different amplitudes, phases and periodicities.

Figure 2-6 illustrates basic waveform definitions  $y(t) = D + A \cdot \sin(2\pi ft - \varphi)$  with  $f = \frac{1}{T}$ . Period is defined as the distance from one peak to the next and amplitude as the half-wave height (the distance from the centre line to a peak or trough).

Frequency is how often something happens in one time unit and is defined as:

$$f = 1/T \quad (\text{Equation 2-40})$$

where  $T$  is the Period and  $f$  is given in cycles per time unit. Frequency is often expressed in Hertz or cycles per second. Frequency may refer to spatial dimensions (for example, cycles per metre) as well as time.

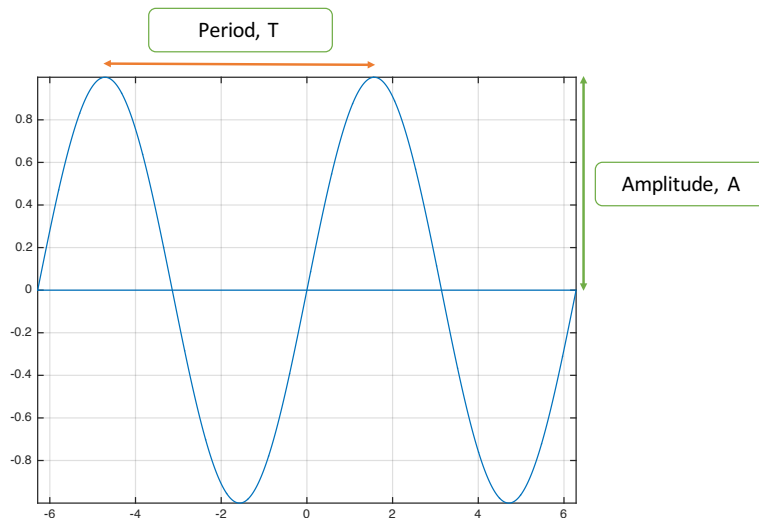


Figure 2-6 - Definition of period and amplitude of a sinusoidal waveform

Phase shift  $\phi$  is a measure of how far in time (or along the x-axis) a wave function is from its base position and vertical shift,  $D$ , the constant, or DC component in electronics jargon indicates the vertical distance of the centre line from 0 – illustrated in Figure 2-7.

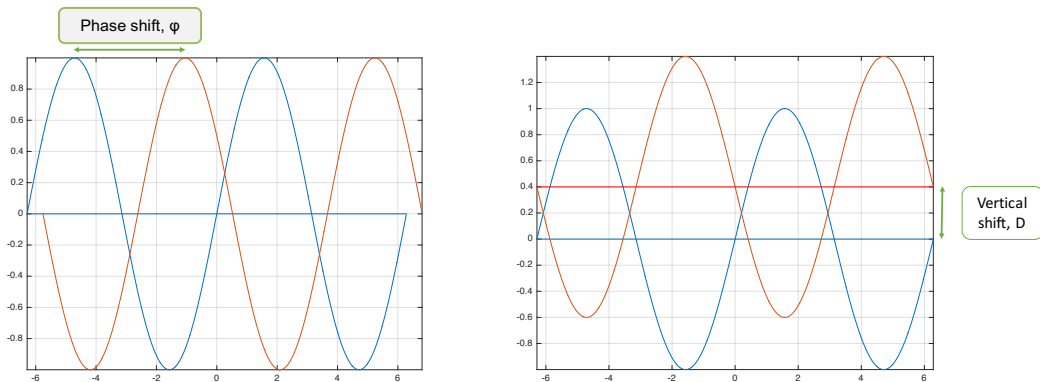


Figure 2-7 - Phase shift and vertical shift of a sinusoidal function

A periodogram is the frequency domain expression of a signal, strictly speaking, its amplitude spectrum estimate, showing the amplitudes of all the spectral components – at all the frequencies - adding up to produce the observed signal. In this study, periodograms are obtained using the Fast Fourier Transform implemented in Matlab using the FFT or periodogram functions. Figure 2-8 shows the time-series and periodogram plots for the same set of rainfall and flow data. Peaks in the amplitude spectrum indicate frequencies that make a significant contribution to the signal. At low frequencies the two signals run close together (the signals in Figure 2-8 have been

shifted vertically for clarity. The frequency spectrum is not affected by this shift). At the position of the catchment time constant, the flow spectrum drops off sharply. When it has dropped 6dB in amplitude, the cut-off point is reached. Below that point the frequency spectrum has little power and has very little effect.

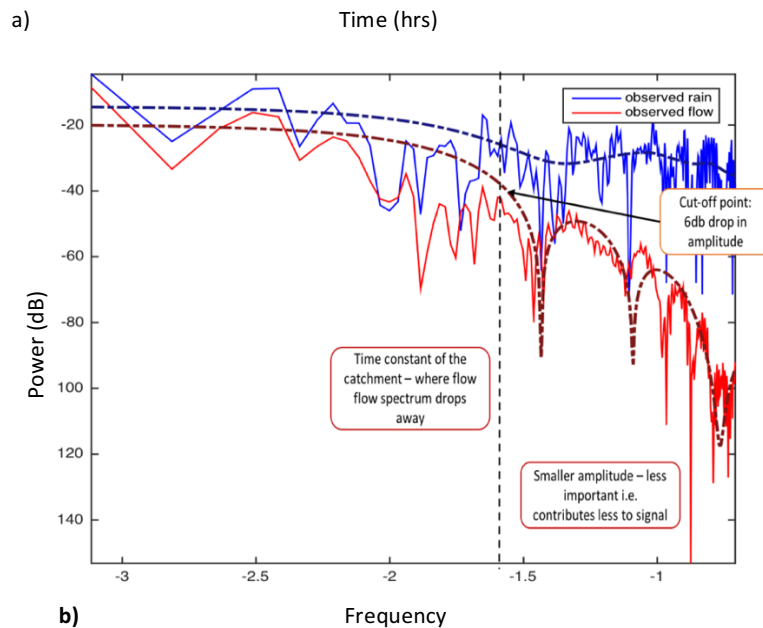
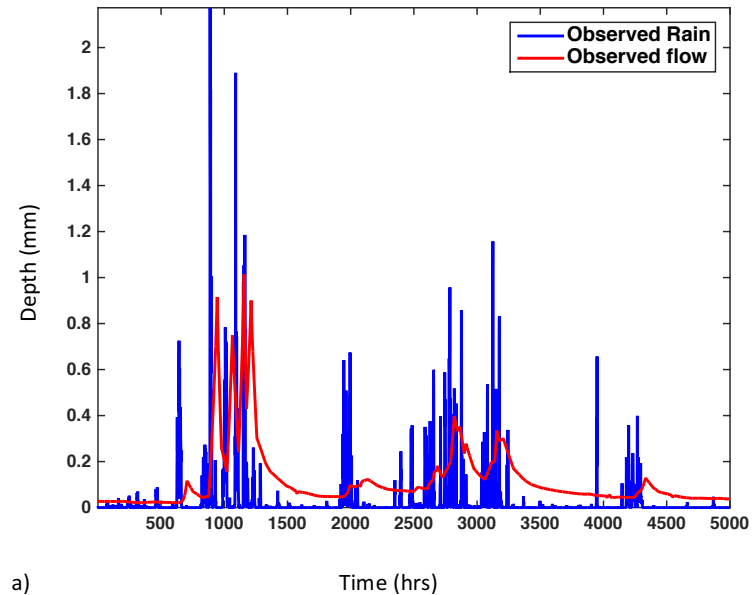


Figure 2-8: a) Time-series and b) frequency plots (periodogram) for the same set of rainfall and flow data. The periodogram pair shows the low-pass filtering effect of the catchment on the rainfall signal. The high frequency attenuation strength is illustrated in this double-logarithmic scaled graph.

There are many sequences of rainfall that give the same output however the signal beyond the band-pass of the catchment is filtered out and therefore cannot be recovered hence the loss of resolution in the inferred rainfall. Regularisation gives a unique signal

which can be adjusted by choosing an appropriate regularisation parameter, noise variance ratio (NVR).

The sampling rate of a system must be high enough to fully define it without over-sampling. The Nyquist-Shannon frequency gives the upper limit on the size of the sampling interval,  $\Delta t$ , that will enable the system dynamics to be represented without distortion (aliasing - Bloomfield, 1976, p21). The Nyquist frequency – the limit frequency represented in the spectrum - is defined as half the sampling frequency:

$$f_c = \frac{1}{2\Delta t} \quad (\text{Equation 2-41})$$

where  $f_c$  is the Nyquist frequency and  $\Delta t$  is the sampling interval. If the sampling interval is small enough to uniquely define the system, that is, less than  $1/2f_c$ , a CT model should be independent of the rate of sampling. This means that if the maximum observed signal frequency is below the Nyquist limit then the model is capturing the full system dynamics.

## 2.8. Uncertainty

Models are simplified approximations of the real world (*c.f.* section 1.2) so predictions made using these models are approximations also. It follows then that there is uncertainty in the predictions, which should be quantified and reported, along with the assumptions made when building the model. In some cases, the uncertainty may be large enough to affect decisions taken based on these predictions, for example, the design of flood defences.

Uncertainty comes from a range of sources and may be divided into epistemic and aleatory uncertainties. Epistemic uncertainties result from gaps in knowledge and understanding. They tend to be non-stationary, arbitrary in occurrence and are difficult to deal with by probabilistic methods. It is possible that epistemic errors may be so large that the data may not be informative when identifying and calibrating model and parameters (Beven and Westerberg, 2011). Aleatory uncertainties are random and can be characterised by a formal error model. They are assumed to be stationary and can provide probabilistic estimates of uncertainty (Beven and Lamb, 2014).

Epistemic uncertainties include:

- Measurement or estimation errors in the inputs and boundary conditions, for example, rain gauge measurements, radar estimates or inappropriate conversions from remote sensing data
- Lack of knowledge about the extent and effect of spatial rainfall
- Choice of interpolation method used to estimate catchment rainfall
- Biases in meteorological variables, for example, rain-gauge under-catch
- Model structural errors including the assumptions made
- Parameter estimates
- Scale of the processes involved (do micro-level physical laws apply at catchment scale?),
- Time interval (does a model that has been calibrated for one time interval apply to another?)
- Unknowns that affect the system and are known about but cannot be represented
- Unknowns that may affect the system but have not yet been recognised (Beven and Young, 2013; Beven and Lamb, 2014).

There are several methods widely used for uncertainty estimation (*c.f.* Beven, 2004) including:

1. Optimisation based on regression
2. Bayesian statistical methods
3. Multi-objective Pareto approach
4. Generalised Likelihood Uncertainty Estimation (GLUE)
5. Fuzzy set methods.

Traditionally, model calibration has focussed on minimising some cost function, looking for the ‘optimal’ model, the right answer. Uncertainty is only evaluated around the optimal model. The optimisation problem in the presence of uncertainty is often ill-posed and, with limited data, it may be difficult to know if the minimum of the objective function has been found or merely a local minimum depending on the shape of the response surface so several runs with different starting points maybe required. Changes in the calibration data, search algorithm or criteria may result in a different optimum. Models are complex and many parameter sets or model structures may give acceptable

model outputs. This is the concept of equifinality (Beven, 2006). Equifinality recognises that there may be structural or input errors and that the procedural model may not be a good representation of the perceptual model or even that the perceptual model may not be a true understanding of the system (*c.f.* Figure 1-1).

DBM modelling recognises the equifinality concept in that many models with a similar fit may be identified from the data. The modeller must choose between them based on the performance measures such as  $R_t^2$  and  $YIC$ . Usually the models with the highest  $R_t^2$  are chosen then selection between them is made using the lowest (highest negative)  $YIC$ . In this study, a third criteria was introduced: how well does a model invert? A set of the models with the highest  $R_t^2$  was chosen for inversion then the model that inverts the best, that is, has the highest inverse  $R_t^2$  ( $IR_t^2$ ) was chosen from these. If  $IR_t^2$  for more than one model were similar, then  $R_t^2$  and  $YIC$  were also taken into account.

Ideally predictions of the future should be 100% certain however this is not likely to happen due to the many uncertainties in any real system. Aleatory uncertainty can be reduced by using longer records (assuming stationarity of the processes) but reductions in epistemic uncertainty require improvements in knowledge, for example, better measurement techniques or enhanced understanding of the rainfall distribution.

## Chapter 3 Test catchments and data

The methods presented in papers 1 and 2 were tested on two catchments at opposite ends of the rainfall spectrum, the humid temperate Blind Beck catchment in the North-west UK and the humid tropical Baru catchment in Borneo. The choice of these two experimental catchments allowed the initial evaluation of the novel method for estimation of catchment rainfall from streamflow to be made using the extremes of a basin with tropical convective rainfall and shallow flow pathways to a basin with temperate low-intensity frontal rainfall and deep flow pathways leading to greater damping or temporal integration. Spatial applications were tested on the heavily instrumented Brue catchment in South-west England, an area known for historic and recent flooding (*c.f.* chapter 6 and chapter 7). The density of the gauge network makes it ideal for investigating the influence of rainfall spatial distribution on catchment outflow. Details of the catchments and the test data are summarised in this chapter.

### 3.1. Blind Beck - temperate catchment

The Blind Beck catchment has an area of 8.8 km<sup>2</sup> and lies in the headwaters of the Eden basin in North West England, UK (54.51°N 2.38°W). The location is shown in Figure 3-1. Superficial cover is glacial till (61%) and riverine and fluvial clays with floodplain sands and gravels underlain by Penrith Sandstone, a major aquifer, and limestone/mudstone. Land cover is mostly grassland (both improved and rough) with some arable land (BGS, 2017). Soils are 53% brown earth, 21% stagnogley, 17% brown alluvial and 9% lithomorphic (Ockenden, 2010). Stagnogley soils have slowly permeable subsoil which is prone to water-logging (see Figure 3-4).

The basin's response shows evidence of deep hydrological pathways due to the presence of deep limestone and sandstone aquifers, and this has resulted in a damped hydrograph response (Mayes *et al.*, 2006; Ockenden and Chappell, 2011; Ockenden *et al.*, 2014). Winter rainfall in this basin is derived from frontal systems with typically lower intensities than the convective systems in the tropics (Reynard and Stewart, 1993). Data from a single tipping-bucket rain-gauge (that is, 0.1 gauges per km<sup>2</sup>) located in the middle of the catchment was used in this study. The data used in the analysis covers the period from 26<sup>th</sup> Dec 2007 at 16:45 to 31<sup>st</sup> December 2007 at 21:45

sampled at 15 minute intervals (Figure 3-2) and was previously modelled by (Ockenden and Chappell, 2011). A summary of the statistics of the observed rainfall and flow for the event modelled are shown in Table 3-1.

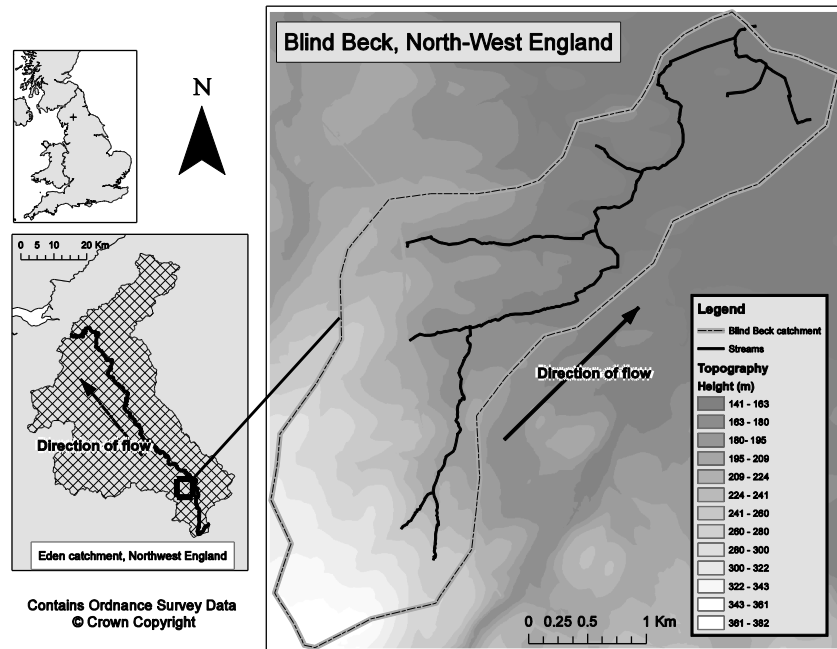


Figure 3-1 - Location and topography of the 8.8 km<sup>2</sup> Blind Beck catchment, NW England

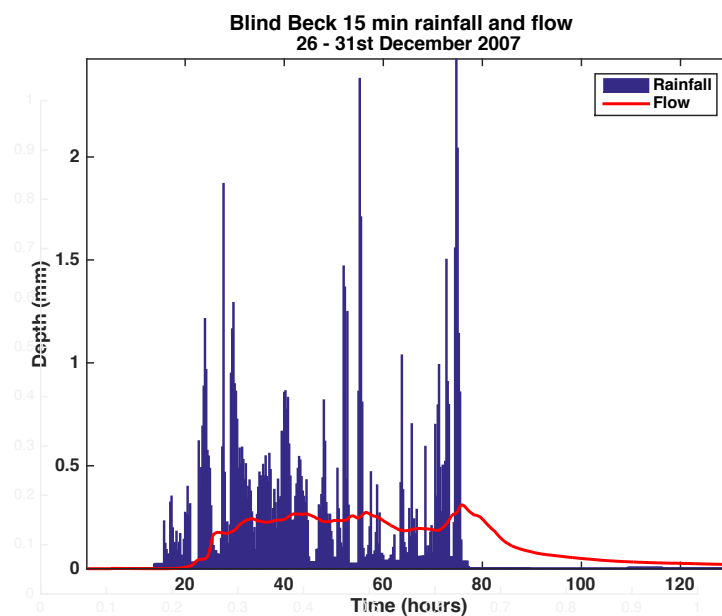


Figure 3-2 - Rainfall and flow in the Blind Beck catchment on 26-31st December 2007 sampled at 15 minute intervals



Table 3-1 – 15-minute rainfall and flow statistics for 26th - 31st December 2007 in the Blind Beck catchment

	Mean	Median	Standard deviation	Skewness	Kurtosis	Maximum	Total
Rainfall (mm)	0.141	0.025	0.335	3.15	15.93	2.48	90.7
Flow (mm)	0.003	0.112	0.010	0.15	1.35	0.33	70.6



Figure 3-3 - a) The WISER water quality monitoring system at the main weir, Blind Beck Experimental Catchment, Cumbria, UK, b) The water-level recorder (left) and WISER water quality monitoring system (centre) at the main weir, Blind Beck Experimental Catchment, Cumbria, UK (Photos courtesy of: NA Chappell)

Blind Beck is part of the Eden catchment and was monitored as part of the CHASM project (Catchment Hydrology and Sustainable Management), a long-term research program investigating the issue of scale and how catchments might respond to future changes in climate (CHASM, 2016). Mayes *et al.*, (2006) monitored a multi-day flood event at a range of scales and noted a large spatial rainfall variation related to elevation. Ockenden (2010) investigated hydrological pathways, important for addressing problems such as flooding, chemical loads and pollutant pathways, by chemical characterisation of stream-water, rainwater and borehole water (Monitoring equipment shown in Figure 3-3). Saturated areas were identified (see Figure 3-4) and contributing landscape features assessed using paired sites analysed using geospatial techniques. Low order transfer function models were used to identify the dominant modes of stream

response (Ockenden and Chappell, 2011). Modelling results were confirmed by Ockenden *et al.*, (2014) using a hydro-chemical mixing model.



Figure 3-4 - Saturated area close to the Low Hall stream gauging station within the Blind Beck Experimental Catchment, Cumbria, UK (Photo courtesy of NA Chappell)

### 3.2. Baru - tropical catchment

The 0.44 km<sup>2</sup> Baru catchment is situated in the headwaters of the Segama river located in Sabah on the northern tip of Borneo, East Malaysia (4° 58' N 117° 49' E). (Location shown in Figure 3-5). The climate is equatorial with a twenty-six year (1985-2010) mean rainfall of 2,849 mm (Walsh *et al.*, 2011) showing no marked seasonality but tending to fall in short convective events (see Figure 3-7c) showing high spatial variability and intensities much higher than those of temperate UK (Bidin and Chappell, 2003; 2006). Due to the high spatial variability, a network of 6 automatic rain-gauges (13.6 gauges per km<sup>2</sup>) was used to derive the catchment-average rainfall using the Thiessen Polygon method. Haplic alisols, typically 1.5 m in depth and with a high infiltration capacity (Chappell *et al.*, 1998) are underlain by relatively impermeable mudstone bedrock resulting in the dominance of comparatively shallow sub-surface pathways in this basin (Chappell *et al.*, 2006). As a result of the high rainfall intensity and shallow water pathways the stream response is very flashy (that is, rapid recession in the impulse response function).

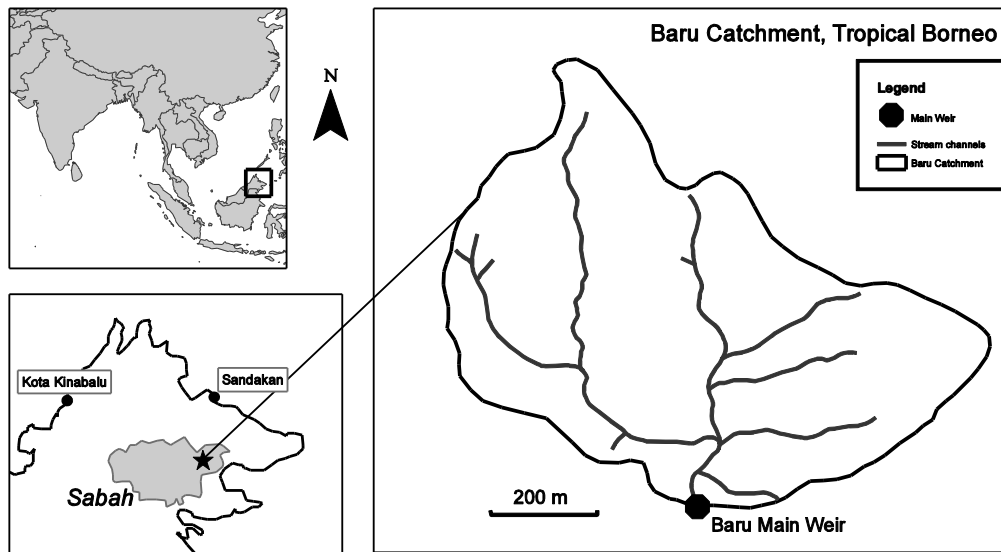


Figure 3-5 - Location of the 0.44 km<sup>2</sup> tropical Baru catchment

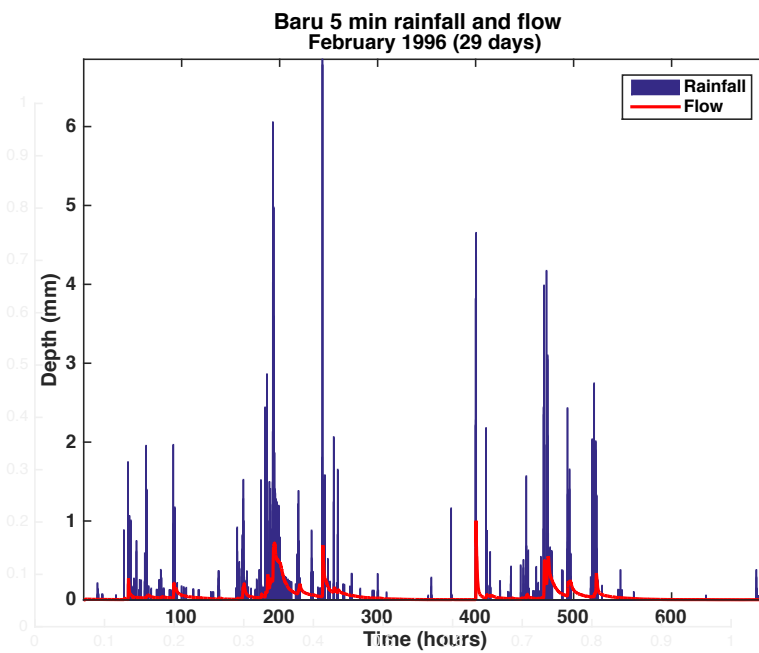


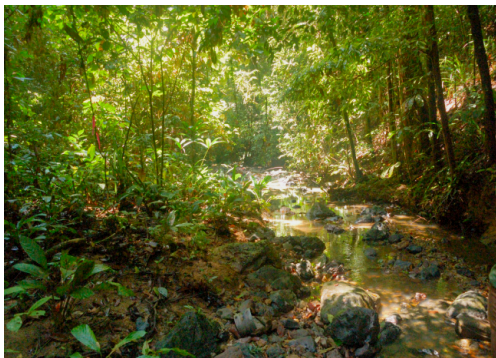
Figure 3-6 – 5 minute rainfall and flow data from the 0.44 km<sup>2</sup> Baru catchment (February 1996)

The data used in the analysis are from February 1996 sampled at 5 minute intervals (Figure 3-6) and have been modelled previously by Chappell *et al.*, (1999) and Walsh *et al.*, (2011). The rainfall and flow statistics for the period modelled are shown in Table 3-2 - Statistics of 5-minute rainfall and flow for February 1996. The character of the

Baru catchment is shown in Figure 3-7 and may be compared with Blind Beck (Figure 3-3 and Figure 3-4).



a) Preparing to collect a water sample (for suspended sediment determination) at the main station of the Baru Experimental Catchment, Sabah, Malaysian Borneo



b) The main channel of the Baru catchment 100m upstream of the main station (Sabah, Malaysian Borneo)



c) The DVFC meteorological station during heavy rain, Sabah, Malaysian Borneo

Figure 3-7: Images showing the character of the Baru catchment (Photos courtesy of N.A. Chappell and W. Tych)

Table 3-2 - Statistics of 5-minute rainfall and flow for February 1996

	Mean	Median	Standard deviation	Skewness	Kurtosis	Maximum	Total
Rainfall (mm)	0.050	0.000	0.284	11.24	180.1	6.85	418.6
Flow (mm)	0.051	0.021	0.092	4.03	23.1	1.00	424.0

Previous research includes DBM modelling relating suspended sediment load to rainfall in areas affected by selective logging (Chappell *et al.*, 1999). This was followed up (Chappell *et al.*, 2004) when a 10-year rainfall event triggered a landslide and culvert collapses highlighting that although sources of sediment were recovering from road construction and harvesting, localized events must be taken into account when considering sustainable forestry. 21 years on, Walsh *et al.* (2011) showed that although storm sediment response had reduced, there was still a need for forestry to stabilise steep slopes and reduce landslide risk. DBM modelling has also been used (Chappell *et al.*, 2006) to examine rainfall- streamflow data and component pathways such as overland flow, subsurface flow and transpiration though these pathways may not correspond directly to the fast and slow partitions of the decomposed TF model (*c.f.* section 2.4.1). The catchment streamflow showed a flashy response to rainfall but the relationship between infiltration and over-land flow showed a much less flashy response.

### **3.3. Brue, Somerset, UK**

This paper utilises the heavily instrumented Brue catchment in South-west England. It has 49 rain gauges in an area of 135.2 km<sup>2</sup>, from which 23 were chosen for analysis, enabling spatial variability to be investigated. Because of the rationale behind the original experimental network design (Moore *et al.*, 2000), many gauges are in very close geographical proximity and very highly correlated so a sub-set of 23 gauges from the original 49 was selected for analysis (*c.f.* section 6.4). The catchment is fed by springs in the Mendip Hills and Salisbury Plain (NRFA, 2012). There is an elevation change of approximately 300m from south-west to north-east across the catchment. The underlying geology is a combination of mudstone and limestone with a limestone ridge running in an arc across from north to south across the eastern upland area (see Figure 3-8). The catchment can largely be split into impermeable lowland to the west, higher land to the east where the limestone ridge is permeable, and the far east of the catchment which is largely impermeable (only 0.5% is moderate to high permeability, (NRFA, 2012)). Land use is mostly pasture on clay soils with some woodland on the elevated eastern side (Wood *et al.*, 2000) with very little urbanisation (NRFA, 2012). A flood storage reservoir was built in 1983 to protect Bruton after widespread flooding. It drains 21% of the upland, fast responding part of the catchment.

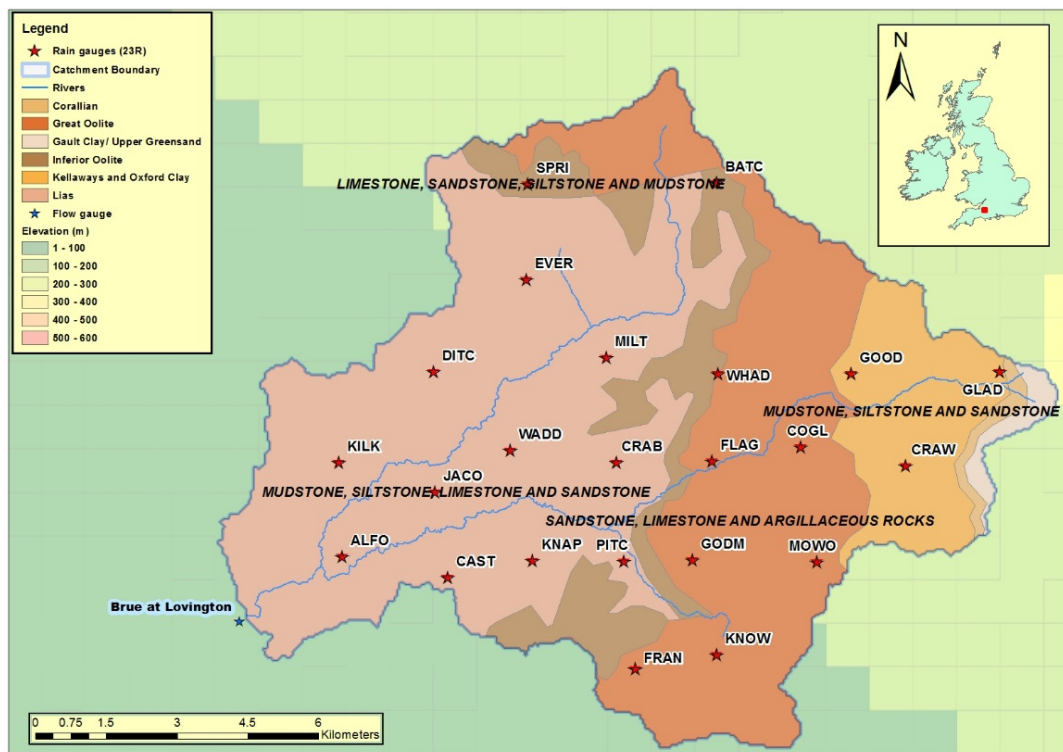


Figure 3-8 - Brue catchment geology, location and gauge network. (Crown Copyright/database right 2016. A British Geological Survey/EDINA supplied service; National River Flow Archive, 2012)

The Brue research catchment was set up in 1993 as part of a Natural Environment Research Council (NERC) special topic research programme – the Hydrological Radar Experiment (HYREX) (Wood *et al.*, 2000). It ran for six years and the data has been extensively used in many subsequent research projects (for example, Wood *et al.*, 2000; Moore *et al.*, 2000; Bell and Moore, 2000; Villarini *et al.*, 2008 a,b, Dai *et al.*, 2015; Zhang and Han, 2017). The Brue Valley Living Landscape, managed by the Somerset Wildlife Trust, is an ecological conservation project aiming to restore habitats that will support wildlife in the face of climate change whilst enabling farmers to continue profitable use of their land (Somerset Wildlife Trust, 2017). Figure 3-9 shows some typical views of the catchment.



*Figure 3-9 - The Brue catchment: The weir at Lovington (NRFA, 2012) and a typical river channel near Glastonbury. Upstream rain causes levels to rise and flooding when the embankments overtop. Flooded fields near Glastonbury (Edwin Graham, geograph.org.uk).*

Figure 3-11 shows cumulative rainfall plots for each of the gauges grouped into geographical blocks. In block A, FLAG has slightly lower rainfall than the other two gauges. ALFO and KILK in block B have lower rainfall than the other 3 gauges. The gauges in C are split into two pairs, SPRI and BATC have higher rain than EVER and MILT. GLAD has significantly higher rainfall than GOOD and CRAW in block D. The gauges in block E all have very similar rainfall whereas those in block F are paired with PITC and CRAB having slightly higher rainfall than WADD and KNAP. Rainfall tends to be lowest near the catchment outflow where the ground is the lowest and highest in the east where elevations are greater.

Table 3-3 - Statistics for the Brue catchment October 1994 - September 1997. Rainfall statistics for each rain-gauge. Gauges are grouped geographically (see Figure 3-10)

	Mean	Median	Standard deviation	Skewness	Kurtosis	Maximum	Total
Flow (mm)	0.011	0.004	0.019	11.24	40.7	0.26	1124
Rainfall (mm)							
ALFO	0.020	0.000	0.131	18.02	610.8	8.6	2054
KILK	0.020	0.000	0.141	21.15	942.9	11.6	2130
DITC	0.022	0.000	0.146	18.26	636.2	9.0	2341
JACO	0.022	0.000	0.151	19.55	700.3	10.2	2288
CAST	0.021	0.000	0.142	17.20	538.8	9.2	2228
WHAD	0.024	0.000	0.156	23.37	1122.5	11.8	2268
FLAG	0.022	0.000	0.146	19.34	724.5	9.6	2320
COGL	0.023	0.000	0.142	14.86	408.3	8.1	2434
SPRI	0.024	0.000	0.147	14.78	379.9	6.4	2528
BATC	0.024	0.000	0.147	18.73	727.2	10.2	2475
EVER	0.022	0.00	0.142	19.29	744.4	10.6	2283
MILT	0.022	0.000	0.136	14.11	336.4	7.2	2318
GOOD	0.023	0.000	0.140	14.79	407.1	7.8	2414
CRAW	0.022	0.000	0.138	15.59	452.4	8.4	2345
GLAD	0.025	0.000	0.158	20.49	878.3	11.6	2626
PITC	0.023	0.000	0.158	23.94	1336.9	14.4	2470
KNAP	0.022	0.000	0.146	20.93	966.6	13.0	2288
CRAB	0.023	0.000	0.157	18.41	571.8	8.2	2442
WADD	0.021	0.000	0.141	16.97	503.8	7.8	2268
FRAN	0.023	0.000	0.151	17.20	569.7	10.2	2458
KNOW	0.023	0.000	0.147	16.94	564.2	10.1	2420
MOWO	0.023	0.000	0.140	13.44	304.7	6.2	2418
GODM	0.023	0.000	0.151	19.30	796.3	11.8	2450



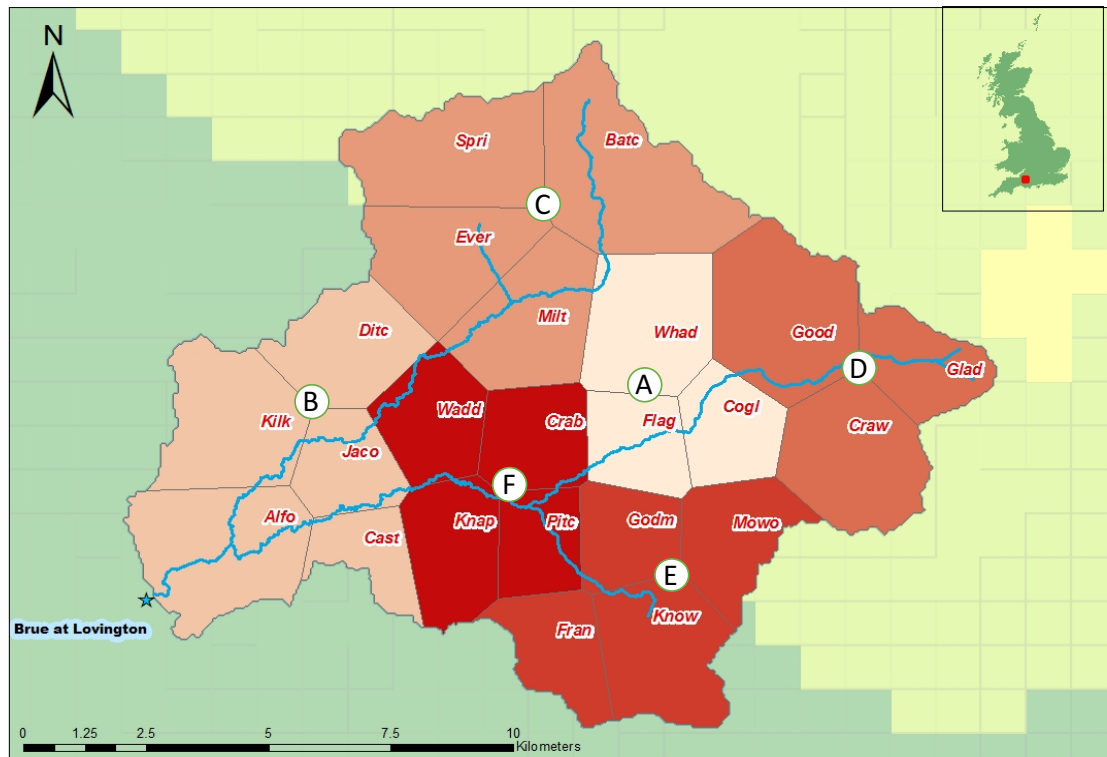


Figure 3-10- Brue catchment showing how rain-gauges are grouped geographically for convenience. Colouring units are the Thiessen polygons

Gauge ALFO has 2054 mm over the 3-year period (685mm per year) compared with GLAD which has a total of 2626 mm (875 mm per year). These two gauges are at the extreme ends of the catchment. Rainfall distributions vary from year to year, season to season and event to event. Figure 3.12 shows the rainfall distribution in space and time for each of the 3 water years studied. The statistics for catchment average rainfall (TP method) by year and season are shown in Table 3-4.

In WY1 and WY2 the majority of the rain falls in the winter whereas in WY3 it is more evenly distributed. Examination of the 3D plots shown in Figure 3-12 highlights the rainfall distribution both temporally and spatially. Winter rain tends to be lower intensity and distributed across the whole catchment though WY3 shows some localised high intensity events even in the winter. Spring tends to be drier and summer into autumn dominated by more high intensity localised events. The variation in time suggests that one average rainfall-flow response model may not be adequate for simulation of all events, and the variation in space that not all rainfall gauges will be representative of the whole catchment and the representativeness may vary with time and from event to event.

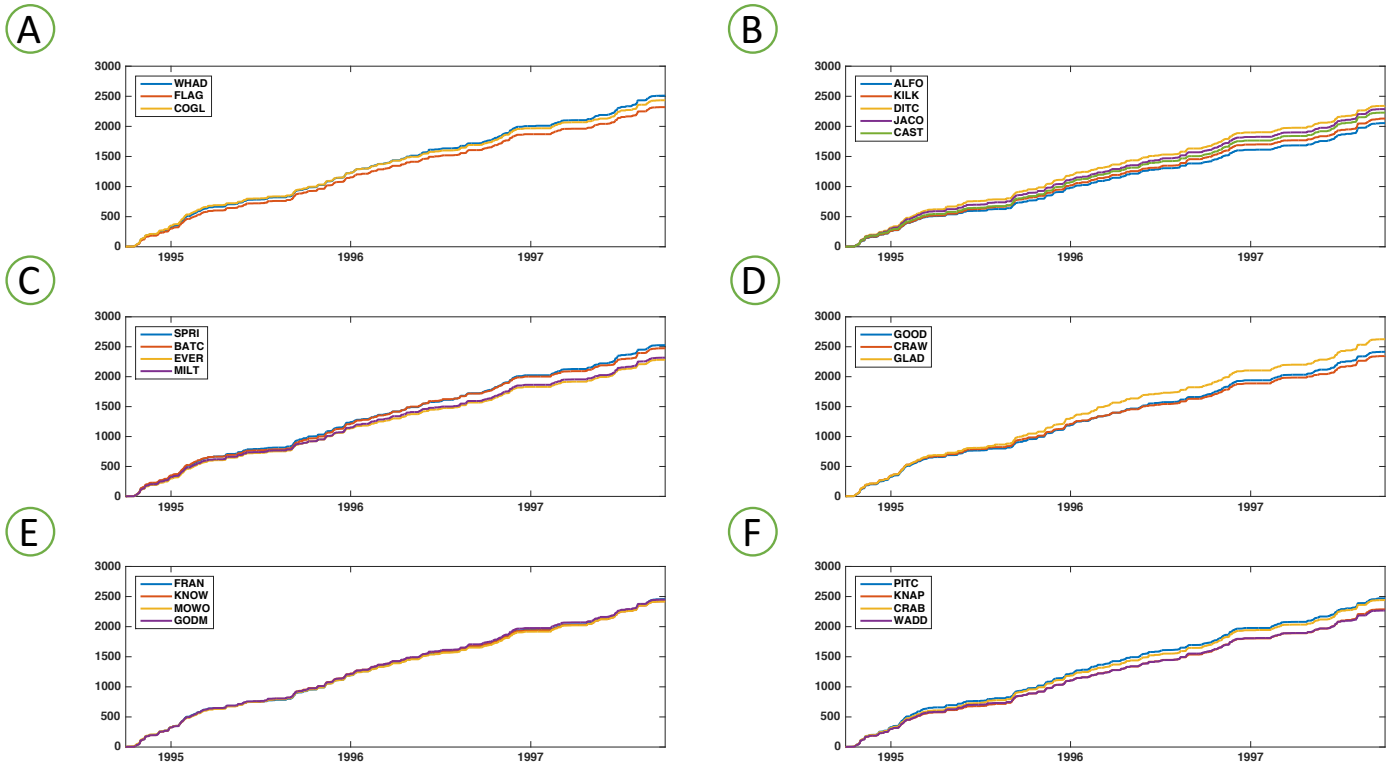


Figure 3-11 - Cumulative rainfall for groups of rain-gauges (geographical grouping – see Figure 3-10) across the Brue catchment. Variation between gauges even over a 3 year period is obvious as is the similarity between FRAN, KNOW, MOWO and GODM, all situated at the southern edge of the catchment



Table 3-4 - Statistics of rainfall measured in mm at 15 minute intervals over the Brue catchment showing the differences between winter and summer for the 3 years studied (catchment average rainfall estimated using Thiessen polygon method).

	October 1994 – September 1995 (WY1)			October 1995 – September 1996 (WY2)			October 1996 – September 1997 (WY3)		
	Year	Winter	Summer	Year	Winter	Summer	Year	Winter	Summer
Total (mm)	929	635	294	755	461	294	728	344	384
Mean (mm)	0.027	0.036	0.017	0.022	0.026	0.017	0.020	0.019	0.022
Standard Deviation (mm)	0.128	0.138	0.116	0.114	0.113	0.114	0.111	0.103	0.118
Maximum (mm)	3.5	3.1	3.5	4.8	4.3	4.8	3.0	3.0	3.0

The Brue experimental catchment was set up to gain a better understanding of rainfall spatial and temporal resolution by combining information from a dense rain-gauge network with weather radar and its impact on flow generation. A network of 49 gauges was set up and combined with information from 3 overlapping radar installations – a Doppler C-band at Cobbacombe Cross, a C-Band at Wardon Hill and an experimental dual polarisation S-Band radar at Chilbolton. Details of the network design are given by Moore *et al.* (2000). The ideal design had to be modified on the ground due to issues with siting and permissions from land-owners. Unsurprisingly, given the gauge network density, much of the follow-up research using the data from the Brue has been related to combining rain-gauge and radar measurements (Wood *et al.*, 2000), sensitivity of model outputs to spatial and temporal variability of rainfall (Bell and Moore., 2000) and spatial sampling error related to network density (Villarini *et al.*, 2008b) and sampling scales in both space and time (Villarini *et al.*, 2008a). More recently, it was used as part of a study by Mazzoleni *et al.*, (2017) investigating the use of crowd-sourcing to improve flood forecasting by data assimilation and by Zhang and Han (2017) who investigated spatial variability using very different methods to this study concluding that a simple lumped model gave an adequate representation of simple events but more complex spatially variable events required models with a higher spatial resolution.

## Chapter 4 Reversing hydrology: estimation of sub-hourly rainfall time-series from streamflow

Kretzschmar, A., Tych, W and Chappell, N. A. (2014) *Reversing hydrology: Estimation of sub-hourly rainfall time-series from streamflow*. Environmental Modelling & Software 60: 290-301.

### Abstract

A novel solution to the estimation of catchment rainfall at a sub-hourly resolution from measured streamflow is introduced and evaluated for two basins with markedly different flow pathways and rainfall regimes. It combines a continuous-time transfer function model with regularised derivative estimates obtained using a recursive method with capacity for handling missing data. The method has general implications for off-line estimation of unknown inputs as well as robust estimation of derivatives. It is compared with an existing approach using a range of model metrics, including residuals analysis and visuals; and is shown to recover the salient features of the observed, sub-hourly rainfall, sufficient to produce a precise estimate of streamflow, indistinguishable from the output of the catchment model in response to the observed rainfall data. Results indicate potential for use of this method in environment-related applications for periods lacking sub-hourly rainfall observations.

### 4.1. Introduction

Accurate simulation of stream hydrographs is strongly dependent on the availability of rainfall data at a sufficiently high, sub-daily sampling intensity (Hjelmfelt, 1981; Littlewood and Croke, 2013). Additionally, hydrograph simulation may be sensitive to the spatial intensity of rainfall sampling (Ogden and Julien, 1994; Bardossy and Das, 2008) or to the uncertainties arising from local calibrations of rainfall radar (Cunha *et al.*, 2012) or individual rain-gauges (Yu *et al.*, 1997). Despite this importance, most gauged basins lack the necessary long-term, sub-hourly rainfall records (and adequate spatial rainfall sampling) to combine with the streamflow records that are, by contrast, typically monitored at sub-hourly intervals for several decades. If those short-term rainfall characteristics responsible for producing stream hydrographs (see Eagleson, 1967; Obled *et al.*, 1994) can be estimated from streamflow, the resultant synthetic rainfall series may be useful in many applications. For example, synthetic rainfall

records could be derived for basins with long-term streamflow, but only short-term rainfall, to: (1) evaluate long-term, rainfall estimates from Global Circulation Models for specific catchments (see Fujihara *et al.*, 2008), (2) provide long-term rainfall records for long-term aquatic ecology studies (for example, Ormerod and Durance, 2009), and (3) identify localised rainfall cells or snowfall events that affect the streamflow but are poorly represented in rain-gauge records (Kirchner, 2009).

This study uses a Data-Based Mechanistic (DBM) modelling approach to identify linear Continuous-Time Transfer Function (CT-TF) models (Young and Garnier, 2006) between sub-hourly rainfall and streamflow. These forward CT-TF models are then inverted to derive rainfall time-series using a novel method that utilises regularisation techniques. Algorithms within the CAPTAIN Toolbox (Taylor *et al.*, 2007) are used for this modelling and the methodology evaluated by application to two micro- or headwater-catchments with contrasting rainfall and response characteristics, namely the humid tropical Baru catchment and the humid temperate Blind Beck catchment. Classical rainfall-runoff non-linearity utilises a power law relationship between measured and effective rainfall (Beven, 2012a) implemented as a Hammerstein type non-linearity (Wang and Henriksen, 1994) separated from the linear dynamics of the transfer function. As the power function is monotonic, it is easily inverted, making it trivial to apply in combination with the effective rainfall estimate generated by the proposed method as illustrated in Figure 4-1.

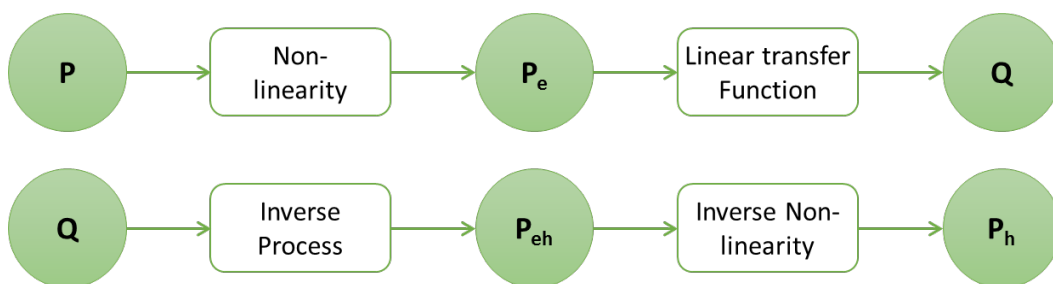


Figure 4-1: The use of Hammerstein-type non-linearity in the model identification (a) and inversion (b) processes where  $P$  is the observed rainfall,  $P_e$  is the effective rainfall,  $Q$  is the observed streamflow,  $P_{eh}$  is the inferred effective rainfall and  $P_h$  is the inferred rainfall with the non-linearity reapplied.

The graphical expression of the forward CT-TF model of a rainfall-streamflow response in discrete time is the impulse response function and this is directly equivalent to the unit hydrograph or UH developed by Sherman (1932). Inversion of the UH or its CT-TF equivalent to derive rainfall from streamflow has been attempted by Hino (1986), Croke (2006), Kirchner (2009), Andrews *et al.* (2010) and Young and Sumińska (2012). These studies have used a range of different approaches. For example, Hino (1986) applied a standard regularised Least Squares (LS) solution to the inversion of a catchment model of ARX form (that is, autoregressive with exogenous variables: see Box *et al.*, 2008). This approach differs from the CT-TF based approach proposed here, in that potentially huge matrix inversions are needed. Kirchner (2009) used a very different method that involved the construction of a first-order, non-linear differential equation linking rainfall, evaporation and streamflow through the sensitivity function, resulting in a compound measure of precipitation and evaporation, which is then reduced to rainfall through making assumptions about the relationship between the rainfall and residual rainfall (that is, rainfall minus evaporation). Kirchner's method has been applied to the Rietholzbach catchment in Switzerland (Teuling *et al.*, 2010) and to 24 diverse catchments in Luxembourg (Krier *et al.*, 2012) where it reproduces the streamflow and storage dynamics for catchments characterised by a single storage – discharge relationship but cannot explain more complex travel times. Andrews *et al.* (2010) used inverse filtering, applying similar CAPTAIN modelling methods to the ones proposed here, but using a direct inverse transfer function in discrete time. As this is methodologically the nearest approach to the proposed one and, at the same time, highlights the practical problems with direct inversion of transfer function models, it was chosen as a comparison in this study. Young and Sumińska (2012) applied non-minimal state-space feedback control methods to inversion of discrete time transfer function models, based on the work of Antsaklis (1978).

Jakeman and Young (1984) were the first to indicate that recursive regularisation might be a useful approach to derive rainfall time-series from the UH, but without offering an implementation of the algorithm or examples. The novel method proposed here has been developed by combining these ideas with developments in the identification of CT-TF models (for example, Young and Garnier (2006)) and improvements in the CAPTAIN routines (Taylor *et al.*, 2007). The inverse process is based on differentiation (Young, 2006), and so may be expected to be ill-posed and sensitive to noise in the

streamflow data (O'Sullivan, 1986; Neumaier, 1998; Tarantola, 2005). The direct inverse of the discrete transfer function method involves differencing, the key issue addressed in the proposed method by using regularised derivatives, potentially its major advantage.

The generality of our approach indicates that it could be used within any modelling framework involving DBM or top-down catchment modelling. Integrating it within other frameworks, for instance to assess the information content of hydrological data (Beven and Smith, 2015) is already a part of an existing project which partly funded this study (NERC CREDIBLE project –see Acknowledgements for details). Another good example of the use for this approach would be within the **hydromad** framework (Andrews *et al.*, 2011) where it could be a part of either model or data evaluation process. Such application could be based on the reasoning that a model and data combo (the principle of DBM approach), which invert well should be more reliable (this assertion will be the subject of future work). Within the same **hydromad** framework a similar reasoning could be used to verify the placement of rain gauges within a catchment. If the inversion generates poorly fitting inferred rainfall with many negative periods it could indicate that the present rain gauges do not provide full information about the catchment rainfall due to their placement. Andrews *et al.* (2011) also indicate the use of such inversion routines in calibration of full hydrological models.

Reaching further out, beyond the discipline of hydrology, there are many other situations where either input estimation of a dynamic system (for example, Maquin *et al.*, 1994, Yang and Wilde, 1988 and many others), or more generally, robust derivative estimation problems (De Brabanter *et al.* 2011) could benefit from the solution provided here. The off-line character of the method, characteristic for regularisation-based methods, excludes on-line applications, such as input observers in control engineering, but provides more flexibility, for instance by easy compensation of pure time delays in the transfer functions.

#### **4.2. Novel parsimonious method for input estimation using reduced order output derivatives**

To obtain a well-defined and effective inverse of any transformation (for example, UH or equivalently a TF), the transformation itself must be well defined. It must capture



the character of the system without any unnecessary complexity that would result in the transformation itself being ill-defined. This is the essence of the philosophy of the Data-Based Mechanistic (DBM) approach of Young (1998; 1999) that aims to produce models that fit the data well with as few parameters as are necessary to capture the dominant dynamic modes of the system. CAPTAIN tools are used to identify models using this underlying philosophy.

The relationship between rainfall and streamflow expressed as a purely linear CT-TF may be given by:

$$Q = \frac{\beta_0 s^m + \beta_1 s^{m-1} + \dots + \beta_m}{s^n + \alpha_1 s^{n-1} + \dots + \alpha_n} e^{-s\tau} R \quad (\text{Equation 4-1})$$

where  $Q$  and  $R$  are Laplace transforms of  $Q(t)$  (streamflow) and  $R(t)$  (discharge),  $s^r$  is the Laplace operator for  $r^{\text{th}}$  time derivative, ( $s^r = \frac{d^r}{dt^r}$ ),  $e^{-s\tau}$  is the Laplace transform for pure time delay between rainfall and the initial streamflow response  $\tau$ , with the model parameter vector:  $\theta = [\alpha_1 \alpha_2 \dots \alpha_n \beta_0 \beta_1 \dots \beta_m]^T$  of dimension  $n+m+1$ . These parameters are estimated from the data along with their covariance matrix,  $C_\theta$ , using the Refined Instrumental Variable (RIV) method (Young and Jakeman, 1980) within the CAPTAIN toolbox. With CT-TFs, fast responding modes of catchment response can be estimated at the same time as very slow modes; one of their key advantages over discrete time approaches. Systems with widely-spaced time constants ('stiff systems') are known to be difficult to handle numerically including estimation of their parameters.

By its very nature (that is, point measurements of rainfall), a transfer function model encapsulates both temporal and spatial modes of integration of the rainfall by the catchment.

The inverse relationship expressing the streamflow-derived rainfall using the transfer function (Equation 4-2) will have the general form of:

$$\hat{R} = \frac{b_0 s^n + b_1 s^{n-1} + \dots + b_n}{s^m + a_1 s^{m-1} + \dots + a_m} e^{s\tau} Q \quad (\text{Equation 4-2})$$

where  $a_i = \beta_i / \beta_0, i = 1, \dots, m$  and  $b_i = \alpha_i / \beta_0, i = 1, \dots, n$  to ensure the denominator polynomial is monic, with  $n \geq m$  as in (Equation 4-2). The negative time delay is accounted for by off-line data-offset adjustment. The ill-posed nature of this inverse relationship is aggravated by the fact that often  $n$  is greater than  $m$  by more than one, reflecting the strong integrative character of catchment systems. This results in pure derivatives of the output that are often of an order higher than one (Equation 4-2). Indeed, most software environments such as Matlab do not even allow simulation of such systems, labelling them as improper. It should be noted here that the danger of obtaining unstable inverse models when the original model is non-minimum-phase (that is, has zeroes in the right half-plane) is avoided altogether, as the DBM modelling methodology means that such models will be rejected at an early stage as non-physical.

The proposed solution (Equation 4-3) consists of using regularised derivative estimates that is consistent with, but extending the approach proposed by Jakeman and Young (1984), namely:

$$\hat{R} e^{-s\tau} = \frac{b_0 \{s^n Q\}^* + b_1 \{s^{n-1} Q\}^* + \dots + b_n Q}{s^m + a_1 s^{m-1} + \dots + a_m} \quad (\text{Equation 4-3})$$

where  $\{s^n Q\}^* = \mathcal{L} \left\{ \frac{d^n}{dt^n} Q \right\}$  is the Laplace transform of the optimised regularised estimate of the  $n^{\text{th}}$  time derivative of  $Q$ :  $\frac{d^n}{dt^n} Q$ .

Note that for  $n > m$  this equation is equivalent to

$$\hat{R} e^{-s\tau} = \frac{b_0}{A(s)} \{s^n Q\}^* + \frac{b_1}{A(s)} \{s^{n-1} Q\}^* + \dots + \frac{b_{m+1}}{A(s)} \{s^{m+1} Q\}^* + \frac{b_m s^m + \dots + b_n}{A(s)} Q \quad (\text{Equation 4-4})$$

where:

$$A(s) = s^m + a_1 s^{m-1} + \dots + a_m \quad (\text{Equation 4-5})$$

In the latter, the final component is a proper transfer function, the preceding components are weighted (by  $b_0 \cdots b_{m-n}$  respectively) regularised derivatives of order  $n \dots m + 1$ , all of them filtered with  $A(s)$ . It is worth noting that because of the filtering, the  $n^{\text{th}}$  regularised derivative estimate is not indeed required, instead the  $((n-m)^{\text{th}}, \dots, 1^{\text{st}})$  order regularised derivative filtered with proper transfer functions is used, as shown below:

$$\frac{b_0}{A(s)} \{s^n Q\}^* \approx \frac{b_0 s^m}{A(s)} \{s^{n-m} Q\}^* \quad (\text{Equation 4-6})$$

Equation 4-4 (with substitution based on Equation 4-6) can be interpreted as a bank of filtered regularised derivatives added together, weighted by the inverse TF numerator coefficients  $b_0, b_1, \dots, b_n$ . In practical implementation therefore, the number of regularised derivatives estimated is limited to the difference between the orders of the numerator and the denominator of the original transfer function (Equation 4-3), that is,  $(n-m)$ , as the remaining derivatives are used implicitly in their filtered form making the algorithm more robust than its alternatives using a discrete transfer function inverse. Use of regularisation results in a trade-off between moderating the noise-amplifying ill-effects of the inversion process, and of the temporal resolution of the resulting rainfall time-series estimated. In order to obtain regularised estimates of derivatives of streamflow time-series up to order  $n-m$ , the output rainfall time-series is modelled as an  $(n-m)^{\text{th}}$  order Integrated Random Walk (IRW) process described in the following section.

### 4.3. Estimation and implementation of regularised derivatives (RegDer method)

The use of regularised derivatives in model estimation is not a new development - Jakeman and Young (1984) show how recursive Kalman Filter (KF) algorithms (Kalman, 1960) and Fixed Interval Smoothing (FIS, for example, Norton, 2009) produce reliable estimates of derivatives of time-series. Finite difference numerical schemes normally involve forms of direct differencing of signals, and so, while many will be stable, they will amplify the high frequency components of the discharge signal, thus producing noise artefacts. When they form filters with a degree of smoothing, they introduce filter artefacts, that is, side lobes; (FIR or polynomial filters effectively using combined central differences). Representative examples of this approach can be found

*i.a.* in Luo *et al.* (2005), where the complicated spectra of Savitzky-Golay differentiators are shown. Other approaches to non-parametric derivative estimation (parametric estimation is seen as constraining) often involve forms of approximation in suitable functional bases including splines and other kernel smoothing forms. Derivative estimation or approximation is the subject of many studies, for example, De Brabanter *et al.* (2011), who use the kernel approach within a more complicated framework. Regularisation based derivative estimation has been introduced several decades ago (Anderssen and Bloomfield, 1974) using a matrix-based method, that involves operations on large matrices of the size of the data series, which is not practical for the long, frequently-sampled series used in hydrology and other environmental applications, unlike the recursive approach implemented here. Moussaoui *et al.* (2005) evaluated the possibilities of estimating derivatives and inputs of dynamic systems using regularisation techniques by applying a Tikhonov regularisation and then using Poisson filtering to jointly estimate parameters and signals. Their use of filtering techniques resulted in issues arising from phase lags in the estimated signals. They referred to Jakeman and Young (1984) with respect to possible solutions involving smoothing, but without proposing a method. In any case, smoothing is only applicable when rainfall is present at all times, which is not the case that this method is being developed to address.

As the rainfall and streamflow data are normally of time series nature with a fixed sampling rate, a discrete-time State-Space approach is employed to estimate the derivatives. This can be done because values between the sampling time instances are not used, and there is a direct equivalence between continuous-time and discrete-time models in regularly sampled data.

A basic discrete time Stochastic State-Space formulation is used (see for example, Young *et al.*, 1999) with the state transition equation as in Jakeman and Young (1984):

$$x_{k+1} = \begin{bmatrix} 1 & 1 \\ 0 & 1 \end{bmatrix} x_k + \begin{bmatrix} 0 \\ 1 \end{bmatrix} v_k \quad (\text{Equation 4-7})$$

where the state  $x_k = [Q_k \quad dQ_k]^T$  is composed of level state  $Q_k$  and slope state  $dQ_k$  of the Integrated Random Walk process which is used to describe  $Q(t)$  with  $t = k\Delta t$  where  $\Delta t$  is the sampling interval. It is this second component of the state  $dQ_k$  that

provides the estimated time derivative of the observed process (given  $\Delta t$ ). It is assumed that the discrete time is sampled uniformly with samples every time unit. The assumption is based on the fact that stage (and hence streamflow) is normally sampled uniformly by data-loggers. Rainfall is sampled normally using tipping-bucket rain-gauges and converted onto the same time basis as the streamflow data. The process is not observed directly, but through the observation equation:

$$Q_k^{obs} = [1 \quad 0]x_k + e_k \quad (\text{Equation 4-8})$$

where  $e_k$  and  $v_k$  are zero-mean, serially uncorrelated white noise sequences.

Equation 4-7 shows the manner of obtaining the 1<sup>st</sup> order derivative estimate, but it is easy to build up the State-Space to generate estimates of higher order derivatives.

The ratio of variances of the state- and observation-disturbance is termed the Noise Variance Ratio (NVR):

$$NVR = \frac{\sigma_v^2}{\sigma_e^2} \quad (\text{Equation 4-9})$$

which is related, reciprocally, to the smoothness of the estimate, or the regularisation parameter (Jakeman and Young, 1984). This form of Stochastic State-Space formulation lends itself to the state estimation procedures of the KF and FIS (Bryson and Ho, 1969), noting that the combined KF/FIS algorithms produce not only optimal smooth estimates of both states but also estimates of their uncertainty bounds. The variance parameters  $\sigma_v^2$  and  $\sigma_e^2$ , or in this simplified case the *NVR* parameter of the KF/FIS algorithm, are normally estimated using optimisation, usually involving Maximum Likelihood (ML) objective functions. Variants of the objective function are discussed by Tych *et al.* (2002) and Taylor *et al.* (2007). In the proposed approach, the objective function is modified from the usual ML approach to a measure of how well the estimated rainfall fits the actual rainfall time series. As the method is based primarily upon the use of Regularised Derivatives it is further called the *RegDer* method.

#### 4.4. Comparison with the discrete-time inversion procedure (*InvTF* method)

For comparison with the *RegDer* method, the method of Andrews *et al.* (2010) based on the use of the direct inverse of a discrete transfer function, was also applied to the two catchment datasets. Since a discrete TF is used, the inverse is easy to simulate directly by differencing or near-differencing (that is, no explicit differentiation). In discrete time form, this gives:

$$Q_k = \frac{\beta_0 + \beta_1 z^{-1} + \dots + \beta_m z^{-m}}{1 + \alpha_1 z^{-1} + \dots + \alpha_n z^{-n}} R_{k-\delta} \quad (\text{Equation 4-10})$$

Where the backward shift operator  $z^{-1}y(k) = y(k-1)$  and  $t = k\Delta t$  is the sample time of the  $k^{\text{th}}$  sample. The operator  $z$  is used here instead of  $q$  (often used in system identification literature) to avoid confusion with standard hydrological practice that uses letter  $q$  to denote streamflow. The same notation and model orders were used for the parameters vector as for the CT-TF model (Equation 1). Estimation of the discrete model was undertaken using the discrete version of the RIV method, implemented in the CAPTAIN Toolbox. The estimated rainfall time-series was then obtained simply by rearranging the above equation, as in Andrews *et al.* (2010):

$$R_{k-1} = \frac{1}{\beta_0} \{(Q_k + \alpha_1 Q_{k-1} + \alpha_2 Q_{k-2}) - (\beta_1 R_{k-2} + \beta_2 R_{k-3})\} \quad (\text{Equation 4-11})$$

This is shown here for  $n = m = 2$  and  $\delta = 1$  for clarity. As with the continuous-time form, the time delay, estimated from the data, can be removed during the off-line processing. This approach, based on a direct inverse of a discrete transfer function (Andrews *et al.*, 2010), is here called *InvTF*.

#### 4.5. First evaluation of the new *RegDer* methodology (including *InvTF* comparisons)

In order to evaluate the *RegDer* algorithm's performance, data from two headwater experimental catchments exhibiting both contrasting rainfall regimes and hydrological pathways were compared. Previous studies have identified linear models for both catchments (Chappell *et al.*, 2006 - Baru; Ockenden and Chappell, 2011 - Blind Beck). Subsequent analysis using the classic bilinear power law (Beven, 2012a) has confirmed this assumption. On this basis, linear modelling was applied in both cases. Streamflow

was sampled uniformly by data-loggers, while rainfall was sampled using tipping-bucket rain-gauges then converted onto the same time basis as the streamflow data.

#### 4.6. Choice of evaluation metrics

Alexandrov *et al.* (2011) suggest a general framework for model assessment and a wide variety of possible metrics are available. Bennett *et al.* (2013) present a range of possible tests including numerical, graphical and qualitative techniques and a selection of these was employed in this study. Some were found to be inappropriate as they involve a normal distribution of data and/or residuals or other critical assumptions. Q-Q plots of the residuals (not shown here) clearly indicated that the assumption of normality cannot be made. In future work, decision theory may provide a framework for choosing between both modelling methods and competing model structures.

Commonly, the simplified Nash-Sutcliffe Efficiency (NSE or  $R_t^2$ ) is used to compare the performance of hydrological models. Several models may be identified which fit the data well (that is, equifinality: Beven, 2006) so the Young Information Criterion (*YIC*: Young, 2001) can be used to differentiate between these models. The *YIC* is an objective measure combining the goodness of fit with a measure of over-parameterisation.

Once acceptable forward models (that is, rainfall-runoff) have been selected (using  $R_t^2$  and *YIC*) they are inverted and the performance of the inverse models compared using a range of metrics including  $R_t^2$ , basic statistics of the residuals and visual ability to match peak values. The inferred (or synthetic) rainfall sequences were also compared visually with each other and with the observed rainfall. Inferred and observed rainfall series were then used as inputs to the original forward models and the generated modelled flow sequences compared using the  $R_t^2$  values and visual comparisons. Statistical analysis of the residuals of both models gives an additional insight into the differences between the catchments and rainfall regimes, as well as the differences between the inversion approaches.

Model uncertainty is evaluated using Monte Carlo Simulations (MCS) for both the forward and the inverse models utilising the covariance matrix generated as part of the

output from the estimation routines contained in the CAPTAIN Toolbox for Matlab (Taylor *et al.*, 2007). In this analysis, the guidelines for validation of DBM models published by Young (2001) are followed. The models thus generated can be used to investigate the sensitivity of the inversion process to the parameterisation of the forward model.

## 4.7. Data

### 4.7.1. Baru - tropical catchment responses

The 0.44 km<sup>2</sup> Baru catchment is situated in the headwaters of the Segama river located in Sabah on the northern tip of Borneo, East Malaysia (4° 58' N 117° 49' E). The climate is equatorial with a twenty-six year (1985-2010) mean rainfall of 2,849 mm (Walsh *et al.*, 2011) showing no marked seasonality but tending to fall in short (< 15 min) convective events showing high spatial variability and intensities much higher than those of temperate UK (Bidin and Chappell, 2003; 2006). Due to the high spatial variability, a network of 6 automatic rain-gauges (13.6 gauges per km<sup>2</sup>) was used to derive the catchment-average rainfall using the Thiessen Polygon method. Haplic alisols, typically 1.5 m in depth and with a high infiltration capacity (Chappell *et al.*, 1998) are underlain by relatively impermeable mudstone bedrock resulting in the dominance of comparatively shallow sub-surface pathways in this basin (Chappell *et al.*, 2006). As a result of the high rainfall intensity and shallow water pathways the stream response is very flashy (that is, rapid recession in the impulse response function). The data used in the analysis are from February 1996 sampled at 5 minute intervals (Figure 4-2a) and have been modelled previously by (Chappell *et al.*, 1999) and (Walsh *et al.*, 2011).

### 4.7.2. Blind Beck - temperate catchment response

The Blind Beck catchment has an area of 8.8 km<sup>2</sup> and lies in the headwaters of the Eden basin in North West England, UK (54.51°N 2.38°W). The basin's response shows evidence of deep hydrological pathways due to the presence of deep limestone and sandstone aquifers, and this has resulted in a damped hydrograph response (Mayes *et al.*, 2006; Ockenden and Chappell, 2011; Ockenden *et al.*, 2014). Winter rainfall in this basin is derived from frontal systems with typically lower intensities than the convective systems in the tropics (Reynard and Stewart, 1993). Data from a single



tipping-bucket rain-gauge (that is, 0.1 gauges per km<sup>2</sup>) located in the middle of the catchment was used in this study. The data used in the analysis covers the period from 26<sup>th</sup> Dec 2007 at 16:45 to 31<sup>st</sup> December 2007 at 21:45 sampled at 15 minute intervals (Figure 4-2b) and was previously modelled by (Ockenden and Chappell, 2011).

The choice of these two experimental catchments, therefore, allowed the initial evaluation of the estimation of catchment rainfall from streamflow for the end-member extremes of a basin with tropical convective rainfall and shallow flow pathways to a basin with temperate frontal rainfall (that is, much lower intensity) and deep flow pathways (that is, much greater basin damping or temporal integration).

#### 4.8. First results and discussion

Forward CT-TF models identified for Blind Beck data explained over 98% of the variance in the streamflow, whilst those for the Baru fit slightly less well, explaining 88% - see Table 4-1 for the  $R_t^2$ ,  $YIC$  (Young, 2001), and time-constants of the best forward models for each catchment, based on a high  $R_t^2$  with a large negative  $YIC$  value according to DBM methodology. The simulated streamflows from a 2<sup>nd</sup>-order model for the two basins are shown in Figure 4-2. The impulse response function (that is, unit hydrograph) for the Baru catchment (Figure 4-2b) showed a considerably faster recession in comparison to that of the Blind Beck catchment (Figure 4-2a) by a factor of 6, confirming the flashier nature of the shallow, tropical catchment, as noted by previous transfer function studies (Chappell *et al.*, 1999, 2006; Walsh *et al.*, 2011; Chappell *et al.*, 2012).

*Table 4-1: The best CT-TF models fitted to subsets of data for Blind Beck (sampled at 15 minute intervals) and Baru (sampled at 5 minute intervals). There is little difference in efficiency ( $R_t^2$ ) between the different models so selection was based on the lowest order model with the lowest  $YIC$  (Young, 2001). The  $YIC$  is an objective measure combining the goodness of fit with a measure of over-parameterisation. A model with a large negative  $YIC$  fits the data well with a small number of parameters.*

Catchment	Model Structure [n,m,d]	$R_t^2$	$YIC$	Time Constants (hours)	
				1st	2nd
Blind Beck	[2,2,3]	0.983	-6.711	6.35	22.10
Baru	[2,2,3]	0.878	-8.054	1.14	20.56

The identified well-fitting, forward models selected according to the DBM methodology were then inverted using the *RegDer* method and, for comparison, the *InvTF* method to estimate catchment rainfall from streamflow for the two catchments. The results of the inversions using the two techniques are shown in Figure 4-3 and the reverse models' fit in Table 4-2.

Table 4-2: Efficiency ( $R_t^2$ ) values for the rainfall sequences estimated by inverting the models selected for Blind Beck and Baru using the *InvTF* and ***RegDer*** methods of inversion.

$R_t^2$	Blind Beck [2,2,3]	Baru [2,2,3]
<i>InvTF</i>	0.512	-0.349
<i>RegDer</i>	0.515	0.433

Both approaches applied to the streamflow data for the Blind Beck catchment produced very similar inferred rainfall time-series (Figure 4-3b). Both approaches produce slightly smoothed rainfall time-series compared to the observed 15-minute sampled rainfall. The smoothing effect is small when compared with the time constant of 6.4 hours for the main component of the forward CT-TF model for the Blind Beck catchment (Table 4-1). Both produce some briefly negative rainfall values during periods of hydrograph recession. Estimated periods of negative rainfall are likely to be due to the point (that is, highly localised) rainfall measurements not fully characterising the entire catchment rainfall, so, at times, there is discharge with no locally measured rainfall that could be attributed to it, and *vice-versa*; an effect also described by Young and Sumisławska (2012).

In general, the forward models fit very well so the uncertainty bounds demonstrated by Monte Carlo runs are very narrow as illustrated in Figure 4-3.

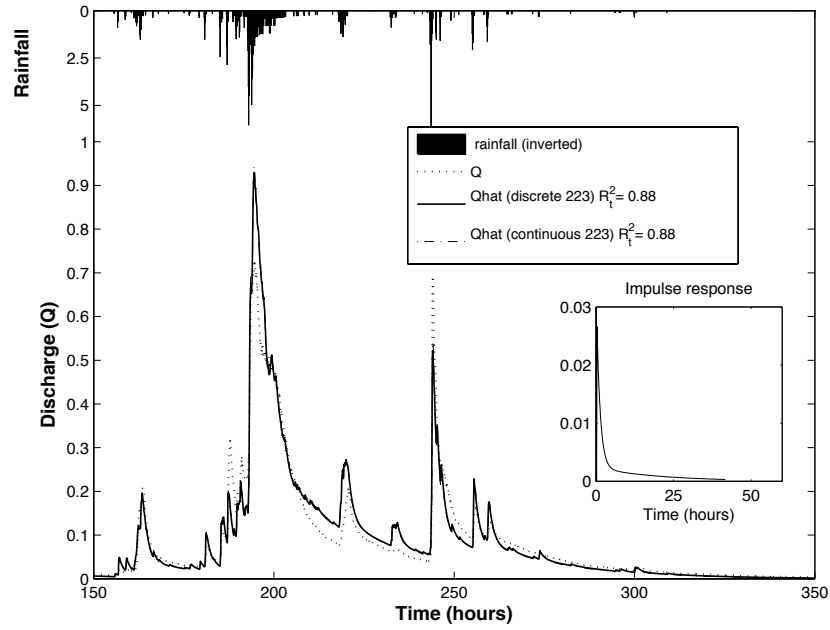
When applied to the Baru data, the *RegDer* and *InvTF* approaches do, however, give simulated or synthetic rainfall time-series with some different characteristics (Figure 4-3a). The *InvTF* method, while capturing some of the peaks better (illustrated in Figure 4-4 and Table 4-3) gives a time-series with very high frequency noise component, of such a high intensity that it produces momentary negative rainfall values. These very high frequency components are the result of direct differencing involved in this method of inversion, which severely amplify high frequency noise in the signal. In contrast, the

*RegDer* method again produced smoothed inferred rainfall time-series with dynamics faster than the time constant of 1.14 hours for the faster component of the forward CT-TF model for the Baru catchment (Table 4-1). An interesting insight is gained by examining the inset in Figure 4-3b, where the two inferred rainfall series clearly follow the same trajectory, but the *InvTF* results include the high frequency noise, very clearly not related to the observed rainfall. The observed rainfall is indeed smoother than its *InvTF* estimate. These artefacts manifest themselves to a much higher degree in the fast responding Baru catchment with a different rainfall regime.

This last observation is confirmed by the residuals analysis. Residuals plots are shown in Figure 4-4a and Figure 4-4b for Baru and Blind Beck respectively. It is apparent from the plots how much more high frequency noise is involved in the *InvTF* estimates, even for the Blind Beck data, where both methods perform in a similar manner (see the residuals variance values in the plots). Figure 4-5 shows comparative plots of the residuals autocorrelation function (RACF) for both models and both catchments. As expected the RACFs for Blind Beck are similar, quickly disappearing within their confidence bounds and it is just the variance level that differentiates the results for both methods. For Baru the RACFs are quite different, with RACF for *RegDer* quickly attenuated and not showing the negative ACF values characterising the fast switching, noisy *InvTF* residuals.

Table 4-3 shows that while the residuals statistics for Blind Beck show good similarity between the methods, the residuals for Baru show large discrepancies, with *InvTF* showing some extreme values and a completely different distribution shape, as characterised by the calculated moments: means are similar, variance doubles for *InvTF*, and higher moments are radically different and not realistic. The Mean Absolute Error statistics (MAE) show similar relationships to the variance.

a)



b)

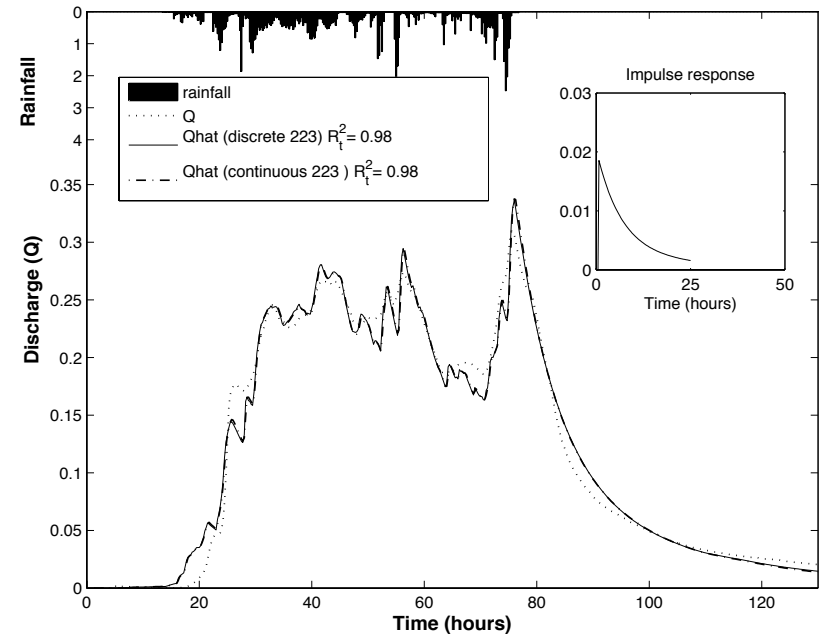


Figure 4-2: Measured and estimated streamflow for: a) Baru (at 5 minute intervals) and b) Blind Beck (at 15 minute intervals), together with the associated hyetograms and impulse responses

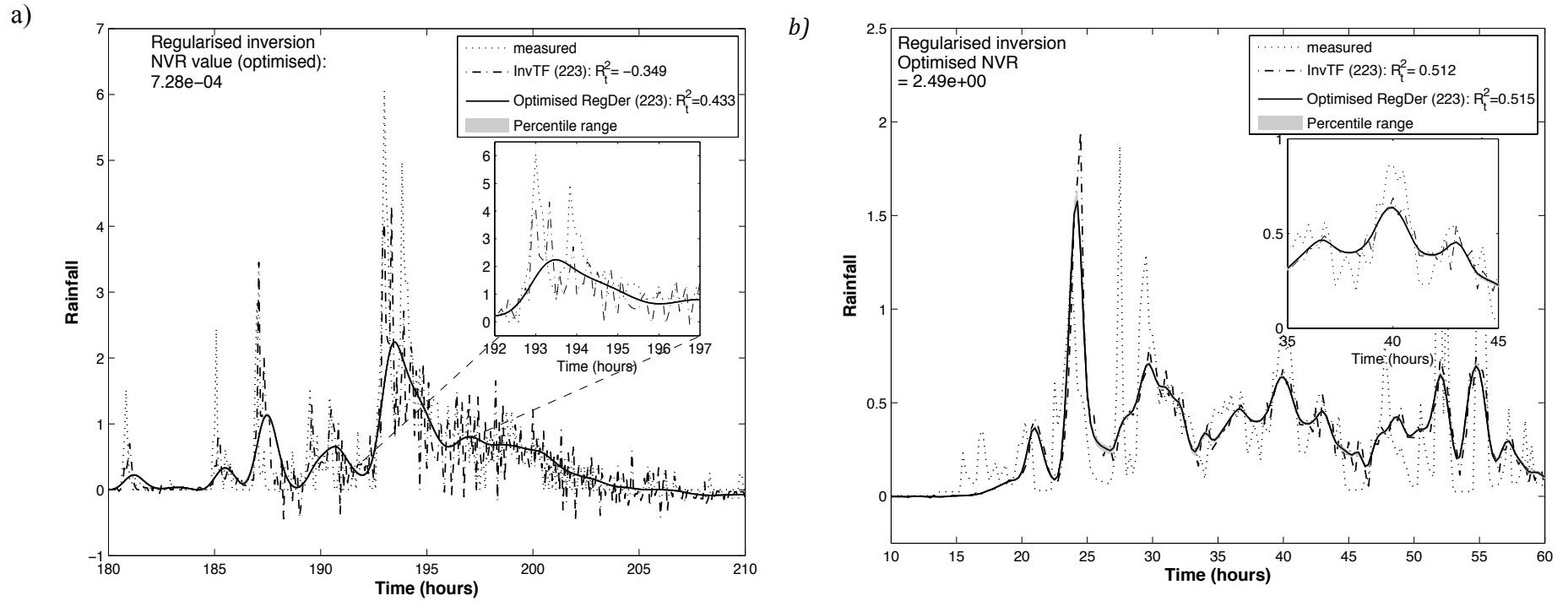


Figure 4-3: Comparison of rainfall simulated using the InvTF and RegDer (NVR optimised) methods for a) Baru and b) Blind Beck. Examination of the inset confirms that the RegDer method estimates the Baru catchment rainfall better (see Table 4-2) whilst there is little difference between the methods for Blind Beck rainfall. 99% uncertainty bands generated by Monte Carlo analysis are shown and can be seen to be very narrow

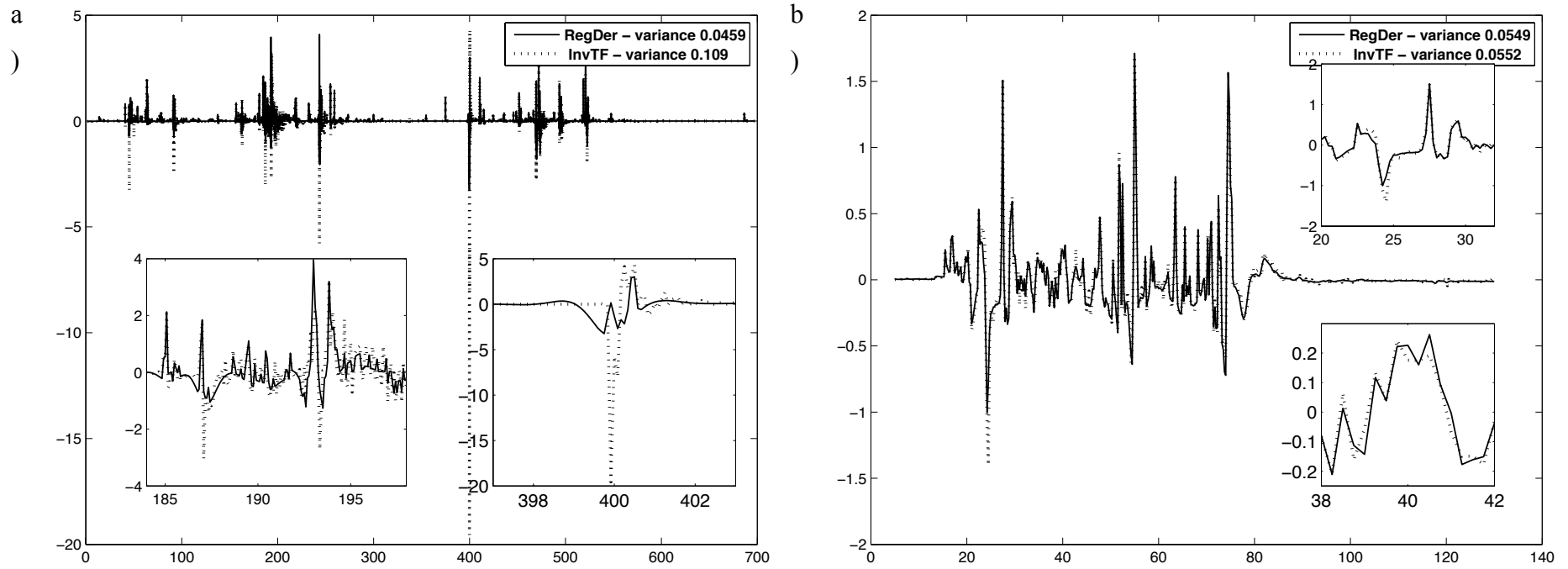


Figure 4-4: Comparison of residuals for a) Baru and b) Blind Beck for the two inversion methods showing the similarities in performance between the methods when used for Blind Beck (with a minor increase in noise for InvTF) and the differences when used for Baru (with large artefacts in InvTF)

Table 4-3: Residuals analysis for Blind Beck and Baru for both inversion methods showing the similarity between the methods for Blind Beck and the differences for Baru.

	Mean	Mode	Var	Skew	Kurt	Max	Min	Rng	MAE
<i>Blind Beck</i>									
RegDer	-0.0004	-0.0119	0.0549	2.54	20.1	1.71	-1.00	2.71	0.117
InvTF	0.0001	-1.4012	0.0552	1.77	19.4	1.69	-1.40	3.09	0.118
<i>Baru</i>									
RegDer	-0.004	0.0001	0.0459	3.51	112.3	4.09	-3.25	7.34	0.057
InvTF	-0.0036	0	0.1092	-27.17	1549.2	4.31	-19.56	23.9	0.066

Similar effects are shown by the peaks statistics (Bennett *et al.*, 2013) in Figure 4-6. In the figure  $P_e$  denotes effective rainfall, while  $P_{eh}$  – inferred effective rainfall. The errors in peak estimates are of similar magnitude. Inferred in this figure refers to the values of peaks of inferred rainfall. Baru results show considerable improvement of these peak error statistics achieved using *RegDer* approach.

Despite the presence of smoothing effects and/or high frequency noise components, models simulating observed streamflow from synthetic rainfall using either method were able to simulate the observed streamflow equally well, and with a very high efficiency (Table 4-4), resulting in virtually indistinguishable model outputs given the observed rainfall or *RegDer* or *InvTF* rainfall as inputs. This is demonstrated in Figure 4-7a and b.

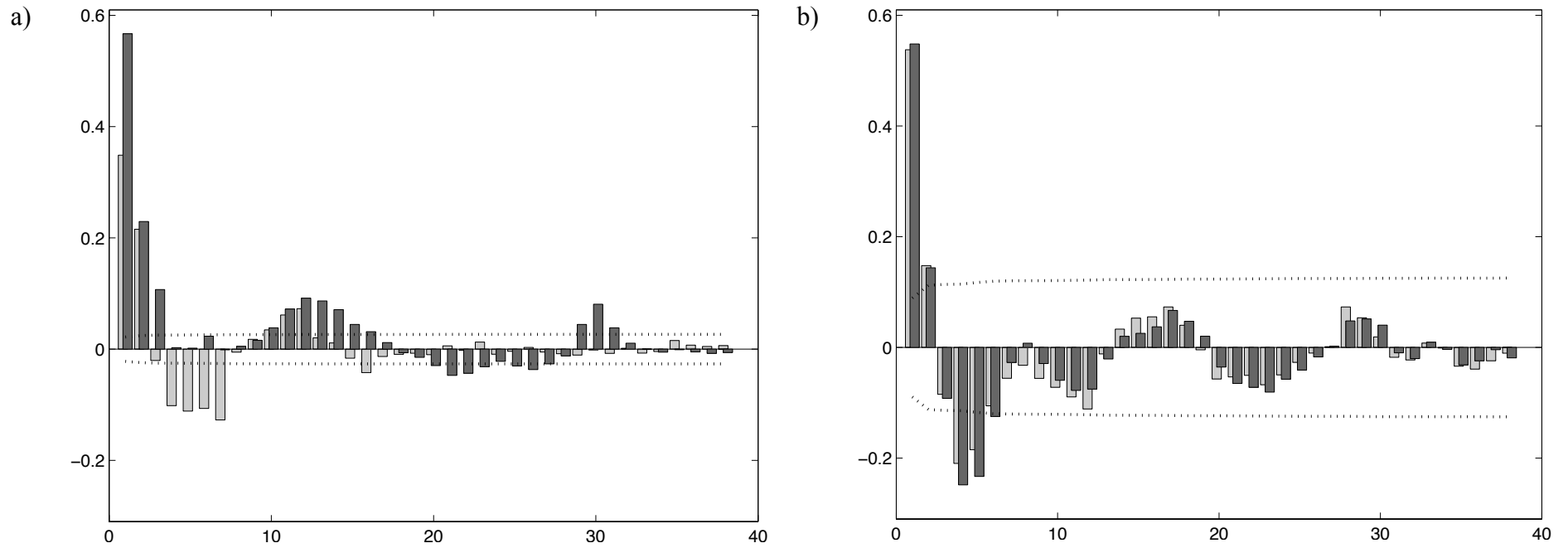


Figure 4-5: comparative plots of the residuals autocorrelation function (RACF) for InvTF (light grey bars) and RegDer (dark grey bars) and both catchments (Baru in (a) and Blind Beck in (b)) showing the differences between methods of inversion. In both cases, RegDer quickly attenuates whereas InvTF shows negative ACF values characterising the fast switching, noisy residuals/artefacts.



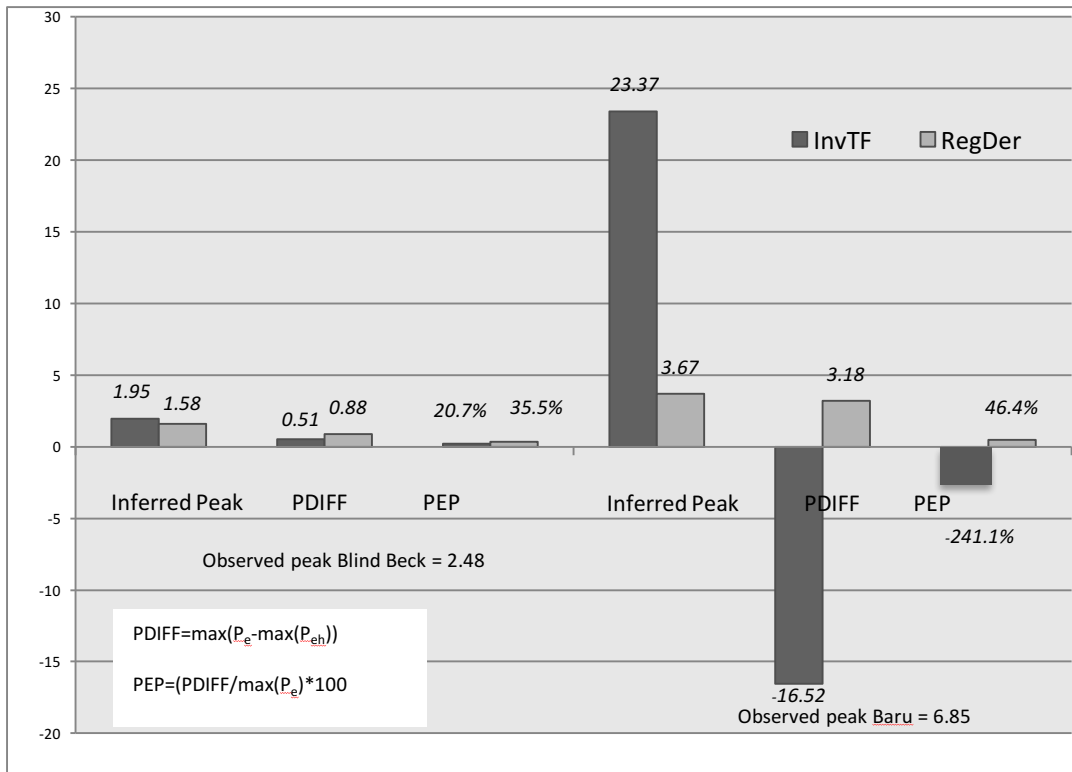


Figure 4-6: Comparison of the estimation of peaks for the two methods showing that for Blind Beck, both methods estimate the observed peak quite well with little difference between them whilst for Baru, the InvTF method hugely underestimates the peak whilst RegDer slightly over-estimates. The metrics PDIFF and PEP were taken from Bennett et al (2013).

It should be noted that while *RegDer* results appear to be ‘too smooth’ and the *InvTF* results – too ‘noisy’, the balance between the two is easily achieved using *RegDer* by balancing the NVR coefficients of the inverse model, and will ultimately be up to the researcher and the aims of modelling exercise. *RegDer* results can be interpreted as sub-sampling, or sacrificing the unobtainable (due to observation disturbance) temporal resolution. Critically, there are no such controls with *InvTF*. Quantifying this balance is a part of on-going research and is to be addressed in a forthcoming publication. Applying a smoothing algorithm to *InvTF* results would produce a different outcome, as *RegDer* only applies regularisation to the minimal number of terms within the bank of filters of Equation 4-4 as opposed to a cruder tool of smoothing the entire signal.

Table 4-4: Efficiency ( $R^2$ ) of forward CT-TF models of streamflow based on the observed rainfall or *RegDer* or *InvTF* rainfall as inputs.

Model input	Blind Beck $Rt2$	Baru $Rt2$
Observed rain	0.984	0.878
Modelled rain ( <i>InvTF</i> )	1.000	0.937
Modelled rain ( <i>RegDer</i> )	1.000	0.957

The integrating effect of the Blind Beck catchment seen in the damped hydrograph (Figure 4-7b) was expected given the presence of deeper hydrological pathways (Ockenden and Chappell, 2011; Ockenden *et al.*, 2014) however, the degree of temporal basin integration of the rainfall signal (and hence response damping) by the shallow pathways within the tropical catchment (Chappell *et al.*, 2006) was not expected, but does indicate the role of even shallow water paths in damping intense rainfall. The degree of catchment integration indicates that the slight smoothing of the simulated rainfall time-series (by the *RegDer* method) has no impact on its ability to be used in forward CT-TF models to simulate streamflow. On the basis of their utility for creating synthetic rainfall time-series for use in periods lacking observed rainfall, the new *RegDer* method and *InvTF* method of Andrews *et al.* (2010) seem of equal value. Perhaps the new *RegDer* method is marginally better than the *InvTF* method because of the high frequency behaviour that can be produced by the *InvTF* method with some data sets where high frequency noise is amplified by the derivative action, for example, the proposed approach is more robust for stiff systems (those with a wide range of time constants). Further, this high frequency behaviour has no physical interpretation so might be considered to fail the final evaluation criterion of the DBM modelling philosophy (Chappell *et al.*, 2012). These findings from the first evaluation of the new *RegDer* method are very positive and highlight the potential value of this method for generating synthetic rainfall time-series for a range of rainfall regimes and catchment settings. These preliminary findings have stimulated a much more extensive programme of evaluation of the *RegDer* method against a range of other methods (including the *InvTF* method of Andrews *et al.*, 2010) for a much larger set of catchments with differing rainfall and catchment settings.

A number of basic statistics of the observed and inferred (*RegDer* and *InvTF*) rainfall series are shown in Table 4-5. It is clear that for the Blind Beck catchment most statistics for both observed and inferred series are similar in magnitude (they were not expected to be too close due to the smoothing effect of both methods), which is consistent with other results reported above. For Baru however, there are significant differences between the methods. There is an indication of mean-smoothing effects of both methods showing in variance and range. *InvTF* inferred rainfall shows large changes and unusual values in range, minima and maxima, as well as higher order moments being of different order of magnitude from those of the actual rainfall and *RegDer* results. This is an indication of the artefacts of explicit differencing of the streamflow data when using *InvTF*. In addition, the high skewness of the observed rainfall measurements adds to the argument regarding non-Gaussian distribution, and hence many of the standard model metrics not being applicable.

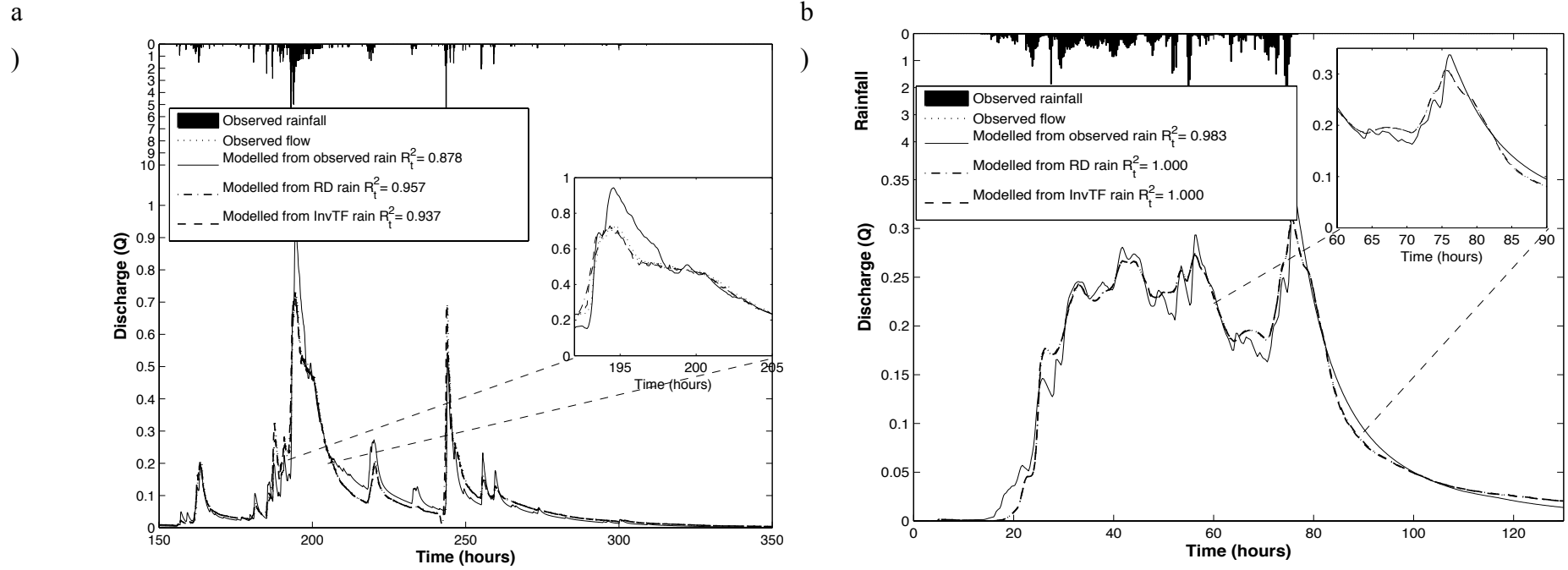


Figure 4-7: Outputs modelled from observed and modelled rainfall sequences for a) Baru and b) Blind Beck showing that the outputs (discharges) are indistinguishable over much of the figure despite the differing characteristics of the rainfall inputs

Table 4-5: Data and model output statistics (rainfall (mm)). The following abbreviations were used: Var – variance, Kurt – kurtosis, Skew- skewness, IQR – inter-quartile range, prct – percentiles. Obs refers to observed rainfall. The Wet prefix in the table rows refers to statistics calculated only for samples with non-zero rainfall (>0 for inferred).

Blind Beck	Mean	Var	Skew	Kurt	Max	Min	Range	25% prct	75% prct	IQR
Obs. All	0.181	0.112	3.154	15.934	2.476	0.003	2.474	0.004	0.233	0.230
Obs. Wet	0.181	0.112	3.152	15.925	2.476	0.000	2.476	0.004	0.233	0.230
RegDer	0.182	0.061	1.744	7.451	1.576	-0.156	1.733	0.010	0.319	0.309
InvTF	0.181	0.067	2.120	10.591	1.948	-0.198	2.146	0.008	0.311	0.303
Wet RegDer	0.202	0.062	1.658	7.289	1.576	-0.129	1.705	0.012	0.342	0.330
Wet InvTF	0.198	0.069	2.065	10.581	1.948	-0.198	2.146	0.010	0.345	0.335
<hr/>										
Baru										
Obs. All	0.050	0.081	11.230	179.694	6.853	0.000	6.853	0.000	0.000	0.000
Obs. Wet	0.253	0.403	4.383	27.969	6.056	0.000	6.056	0.000	0.213	0.213
RegDer	0.054	0.054	7.549	76.584	3.674	-0.392	4.066	0.001	0.018	0.017
InvTF	0.054	0.169	29.739	1411.93	23.374	-3.630	27.004	0.001	0.018	0.018
Wet RegDer	0.055	0.042	6.751	60.481	2.763	-0.336	3.099	0.001	0.020	0.019
Wet InvTF	0.051	0.095	18.517	567.320	12.644	-1.461	27.004	0.001	0.017	0.017

## 4.9. Conclusions

Robust identification techniques were used to identify continuous-time transfer function models for two catchments with contrasting rainfall and flow path regimes. Following the DBM methodology, the models fitted the data well with a minimal number of parameters as indicated by a large negative value of the *YIC*. The identified (DBM) models for both catchments were of 2<sup>nd</sup>-order. This is a typical model order for many catchments. The models were inverted using the new *RegDer* method and, for comparison, the *InvTF* method used by Andrews *et al.* (2010). Both methods were able to produce synthetic rainfall time-series that were then able to simulate almost all of the dynamics in the streamflow time-series for both catchments (Figure 4-4ab). In comparison to the *InvTF* method of Andrews *et al.* (2010), the *RegDer* method did, however, produce synthetic rainfall containing much less high frequency noise. This was particularly visible in the synthetic rainfall of *InvTF* for the tropical basin with convective rainfall (Figure 4-3a). The smoothing introduced by the *RegDer* method is

on a much smaller temporal scale than the dominant dynamics of the catchment indicating that the detailed temporal distribution of the rainfall series may not be important for the modelling the observed streamflow (depending on the reasons for modelling) so long as the series recreates the short-term (that is, sub-hourly) characteristics responsible for producing stream hydrographs sufficiently well, which is consistent with the findings of Eagleson (1967) and Obled *et al.* (1994). These findings are confirmed by comparative evaluation of several model metrics, including peak modelling errors and a detailed residuals analysis. It is worth noting that applying a smoothing algorithm to *InvTF* results would produce a different outcome, as *RegDer* only applies regularisation to the minimal number of terms within the bank of filters of Equation 4-4, as opposed to a cruder tool of smoothing the entire signal.

Further evaluations of the new *RegDer* method against *InvTF* and other methods need to be undertaken using a more diverse range of global rainfall and flow-path regimes. This work will include catchments where the derivation of long-term rainfall time-series by *RegDer* would support hydrological, climatological or ecological studies requiring such long time-series of synthesised rainfall (Ormerod and Durance, 2009).

## Chapter 5 Reversing Hydrology: quantifying the temporal aggregation effect of catchment rainfall estimation using sub-hourly data

Kretzschmar, A., Tych, W., Chappell, N. A., Beven, K. J., (2015) *Reversing hydrology: quantifying the temporal aggregation effect of catchment rainfall estimation using sub-hourly data*, Hydrology Research, Jun 2016, 47 (3) 630-645; DOI: 10.2166/nh.2015.076

### Abstract

Inferred rainfall sequences generated by a novel method of inverting a continuous time transfer function show a smoothed profile when compared to the observed rainfall however streamflow generated using the inferred catchment rainfall is almost identical to observed streamflow ( $R_t^2 > 97\%$ ). This paper compares the effective rainfall inferred by the regularised inversion process (termed inferred effective rainfall) proposed by the authors with effective rainfall derived from the observed catchment rainfall (termed observed effective rainfall) in both time and frequency domains in order to confirm that, by using the dominant catchment dynamics in the inversion process, the main characteristics of catchment rainfall are being captured by the inferred effective rainfall estimates. Estimates of the resolution of the inferred effective rainfall are found in the time domain by comparison with aggregated sequences of observed effective rainfall, and in the frequency domain by comparing the amplitude spectra of observed and inferred effective rainfall. The temporal resolution of the rainfall estimates is affected by the slow time constant of the catchment, reflecting the presence of slow hydrological pathways, for example, aquifers, and by the rainfall regime, for example, dominance of convective or frontal rainfall. It is also affected by the goodness-of-fit of the original forward rainfall-streamflow model.

### 5.1. Introduction

Rainfall is the key driver of catchment processes and is usually the main input to rainfall-streamflow models. If the rainfall and/or streamflow data used to identify or calibrate a model are wrong or disinformative, the model will be wrong and cannot be

used to predict the future with any certainty. Blöschl *et al.* (2013) state that if the dominant pathways, storage and time-scales of a catchment are well defined then a model should potentially reproduce the catchment dynamics under a range of conditions. It is often the case that hydrological variables, such as rainfall and streamflow, are measured at hourly or sub-hourly intervals then aggregated up to a coarser resolution before being used as input to rainfall-streamflow models resulting in the loss of information about the finer detail of the catchment processes (Littlewood and Croke, 2008; Littlewood *et al.*, 2010; Littlewood and Croke, 2013). Kretzschmar *et al.* (2014) have proposed a method for inferring catchment rainfall using sub-hourly streamflow data. The resulting rainfall record is smoothed to a coarser resolution than the original data but should still retain the most pertinent information.

This paper investigates the implications of the reduced resolution and the potential loss of information introduced by the regularisation process in both the time and frequency domains. Both temporal and spatial aggregation are incorporated in the transfer function model however only the temporal aspect is considered here. The effect of spatial rainfall distribution using sub-catchments will be the subject of a future publication.

The method developed and tested by Kretzschmar *et al.* (2014) – termed the **RegDer** method - inverts a continuous-time transfer function (CT-TF) model using a regularised derivative technique to infer catchment effective rainfall from streamflow with the aim of improving estimates of catchment rainfall arguing that a model that is well-fitting and invertible is likely to be robust in terms of replicating the catchment system. In the context of this study, observed catchment rainfall (may be derived from one or more rain-gauges by any suitable method, for example, Thiessen polygons) is converted to observed effective rainfall (*OER*) by a non-linear transform designed to render the relationship between the rainfall input and streamflow output (via a continuous time transfer function) linear. The inversion process takes the catchment streamflow and, using a regularisation process, infers effective rainfall (*IER*), which is then converted to inferred catchment rainfall (*ICR*) by the reverse of the non-linear transform (illustrated in Figure 5-3). The effective rainfall (both *OER* and *IER*) may be termed scaled rainfall (related to Andrews *et al.*, 2010) as it is derived from the overall catchment rainfall.



The classical approach to inverse (as opposed to reverse) modelling involves the estimation of non-linearity (rainfall or baseflow separation) and the unit hydrograph (UH), which is an approximation to the impulse response of the catchment. Boorman (1989) and Chapman (1996) use sets of event hydrographs to estimate the catchment UH. Boorman (1989) superimposed event data before applying a separation technique and concluded that the data required may be more coarsely sampled than might be expected because one rain-gauge is unlikely to be representative of the whole catchment. Chapman (1996) used an iterative procedure to infer rainfall patterns for individual events before applying baseflow separation. The resultant UHs had higher peaks and shorter rise times and durations than those obtained by conventional methods. He viewed the effective rainfall as the output from a non-linear store. Duband *et al.* (1993) and Olivera and Maidment (1999) used deconvolution to identify mean catchment effective rainfall, which was redistributed using relative runoff coefficients whilst Young and Beven (1994) based a method for inferring effective rainfall patterns on the identification of a linear transfer function. In that study a gain parameter, varying with time accounted for the non-linearity in the relationship between rainfall and streamflow.

In recent years, a range of different approaches has been used to explore reverse modelling in hydrology, that is, estimating effective rainfall from streamflow. Notable publications include Croke (2006), Kirchner (2009), Croke (2010), Andrews *et al.*, (2010), Young and Sumislawska (2012), Brocca *et al.* (2013, 2014) and Kretzschmar *et al.* (2014). Kirchner's method links rainfall, evapo-transpiration and streamflow through a sensitivity function making assumptions which allow rainfall to be inferred from the catchment streamflow. The method has been applied by Teuling *et al.* (2010) and Krier *et al.* (2012) to catchments in Switzerland and Luxembourg and has been found to work for catchments with simple storage-streamflow relationships and limited hysteresis. Brocca *et al.* (2013) employed a similar method based on the water balance equation but inferred the rainfall series from soil moisture. In a further study, Brocca *et al.* (2014) used satellite derived soil moisture to infer global rainfall estimates. Rusjan and Mikos (2015) applied Kirchner's simple dynamic system concept to a catchment in south-west Slovenia characterised most of the time by subsurface storage but showing a response that by-passed this storage after intense rainfall. They combined two separate sensitivity functions to enable the simulation of a range of contrasting

hydrological conditions. Croke (2006) derived an event-based unit hydrograph from streamflow alone but his approach was limited to ephemeral quick-flow-dominant catchments whilst Andrews *et al.* (2010) and Young and Sumislawska (2012) use a discrete model formulation inverted directly or via a feedback model (which could be adapted to CT formulation). Croke (2010) explores a similar approach to the one presented in Andrews *et al.* (2010) for several catchments. This is done in the context of slow flow, recharge and quickflow separation, relating the derived general model to existing ones (such as IHACRES). He also includes measures to constrain the rainfall estimate uncertainty. The flow components are estimated as individual discrete-time transfer functions separated using a relaxation procedure. The equivalent effective rainfall estimate is then obtained as a form of inverse discrete-time transfer function with the separated flow components as inputs. The approach proposed by Kretzschmar *et al.* (2014) combined a continuous time transfer function (CT-TF) model with regularised derivative estimates to infer the catchment rainfall from sub-hourly streamflow data, including comparisons to the direct inverse of a discrete transfer function model, similar to those used by Croke (2010) and Andrews *et al.* (2010).

Littlewood (2007) applied the IHACRES model (for example, Jakeman *et al.*, 1990) to the River Wye gauged at Cefn Brwyn showing that the values for the model parameters for that catchment changed substantially as the data time step used for model calibration decreased. Littlewood and Croke (2008) extended this work to include a second catchment and found that as the time-step decreased the parameter values approached an asymptotic level (on a semi-log plot) concluding that, at small enough time-steps, parameters become independent of the sampling interval. They suggested further investigation using data-based mechanistic modelling (DBM) methods as described by Young and Romanowicz (2004) and Young and Garnier (2006) for estimating CT models from discrete input data. Such models generate parameter values independent of the input sampling rate – as long as the sampling rate is sufficiently high in comparison to the dominant dynamics of the system. Advantages of using the CT formulation include allowing a much larger range of system dynamics to be modelled, for example, ‘stiff’ systems that have a wide range of time-constants (TC), typical of many hydrological systems. The outputs from such a model can be sampled at any time-step, including non-integer, and the parameters have a direct physical interpretation (Young, 2010).

Krajewski *et al.* (1991) compared the results from a semi-distributed model and a lumped model and concluded that catchment response is more sensitive to rainfall resolution in time than space, whilst a study by Holman-Dodds *et al.* (1999) demonstrated that models calibrated using a smoothed rainfall signal (due to coarse sampling) may result in under-estimation of streamflow. Further calibration, required to compensate, leads to the loss of physical meaning of parameters. They also concluded that parameters estimated at one sampling interval were not transferable to other intervals; a conclusion echoed by Littlewood (2007) and Littlewood and Croke (2008).

Studies by Clark and Kavetski (2010) showed that in some cases, numerical errors due to the time-step are larger than model structural errors and can even balance them out to produce good results. The follow-up study by Kavetski and Clark (2010) looked at its impact on sensitivity analysis, parameter optimisation and Monte Carlo uncertainty analysis. They concluded that use of an inappropriate time step can lead to erroneous and inconsistent estimates of model parameters and obscure the identification of hydrological processes and catchment behaviour. Littlewood and Croke (2013) found that a discrete model using daily data over-estimated time-constants for the River Wye gauged at Cefn Brwyn when compared to those estimated from hourly data confirming that parameter values were dependent on the time-step. They discussed the loss of information due to the effect of time-step on time constants and suggested that plots of parameter values against time step could be used as a model assessment tool. In a previous study, Littlewood and Croke (2008), compared the sensitivity of parameters for two catchments with respect of time-step and discussed the role of time-step dependency on the reduction of uncertainty. They also suggested continuous time transfer function modelling using sub-hourly data to derive sampling rate independent parameter values. Littlewood *et al.* (2010) introduced the concept of the Nyquist-Shannon (N-S) sampling theorem, which defines the upper bound on the size of sampling interval required to identify the CT signal without aliasing, and consequentially its effect on the frequency of sampling required to specify a rainfall-streamflow model. Given a frequent enough sampling rate, the CT model is time independent and can be interpreted at any interval.

Further understanding may be gained by transforming rainfall and streamflow series from the time domain to the frequency domain and using spectral analysis. Several potential uses of spectral analysis in hydrology have been explored including modelling ungauged catchments, modelling karst systems and seasonal adjustment of hydrological data series. A maximum likelihood method for model calibration based on the spectral density function (SDF) has been suggested by Montanari and Toth (2007). The SDF can be inferred from sparse historic records in the absence of other suitable data making it a potentially useful tool for modelling ungauged catchments. They also suggest that spectral analysis may provide a means of choosing between different apparently behavioural models. Cuchi *et al.* (2014) used ‘black box’ modelling and frequency analysis to study the behaviour of a karst system (located at Fuenmajor, Huesca, Spain). They concluded that the method works well for a linear system and that Fuenmajor has a linear hydrological response to rainfall at all except high frequencies. They suggest that the non-linearity issues might be addressed using appropriate techniques such as wavelets or neural networks. Szolgayova *et al.* (2014) utilised wavelets to deseasonalise a hydrological time-series and suggested that the technique had potential for modelling series showing long-term dependency (interpreted as containing low frequency components).

The method introduced by Kretzschmar *et al.* (2014) showed that given that the rainfall-streamflow model captures the dynamics of the catchment system, the high frequency detail of the rainfall distribution is not necessary for the prediction of streamflow due to the damping (or low-pass filter) effect of the catchment response. The numerical properties of the regularisation as applied to the inversion process place a mathematical constraint of smoothness balanced against a loss of some temporal resolution in the inferred rainfall time series. The regularisation and therefore smoothing level is controlled through the Noise Variance Ratio (NVR), optimised as part of the process and is only applied when necessary, that is, when the analytically inverted catchment transfer function model is improper (has a numerator order higher than the denominator order).

## 5.2. Application catchments

*RegDer* has been tested on two headwater catchments with widely differing rainfall and response characteristics – Baru in humid tropical Borneo and Blind Beck, in humid temperate UK.

### 5.2.1. Baru – tropical catchment

The 0.44 km<sup>2</sup> Baru catchment (Figure 5-1a) is situated in the headwaters of the Segama river located in Sabah on the northern tip of Borneo, East Malaysia (4° 58' N 117° 49' E). The climate is equatorial with a twenty-six year (1985-2010) mean rainfall of 2849 mm (Walsh *et al.*, 2011) showing no marked seasonality but tending to fall in short (<15 min) convective events showing high spatial variability and intensities much higher than those of temperate UK (Bidin and Chappell, 2003, 2006). Due to the high spatial variability, a network of 6 automatic rain-gauges (13.6 gauges per km<sup>2</sup>) was used to derive the catchment-average rainfall using the Thiessen Polygon method. Haplic alisols, typically 1.5 m in depth and with a high infiltration capacity (Chappell *et al.*, 1998) are underlain by relatively impermeable mudstone bedrock resulting in the dominance of comparatively shallow sub-surface pathways in this basin (Chappell *et al.*, 2006, 2007). As a result of the high rainfall intensity and shallow water pathways the stream response is very flashy (that is, rapid recession in the impulse response function). Vegetation cover is lowland, evergreen dipterocarp forest, which was subject to selective logging during 1988-89 (Greer *et al.*, 1995). The data used in the analysis are from February 1996 sampled at 5 min intervals (Figure 5-1b) and have been modelled previously by Chappell *et al.* (1999) and Walsh *et al.* (2011).

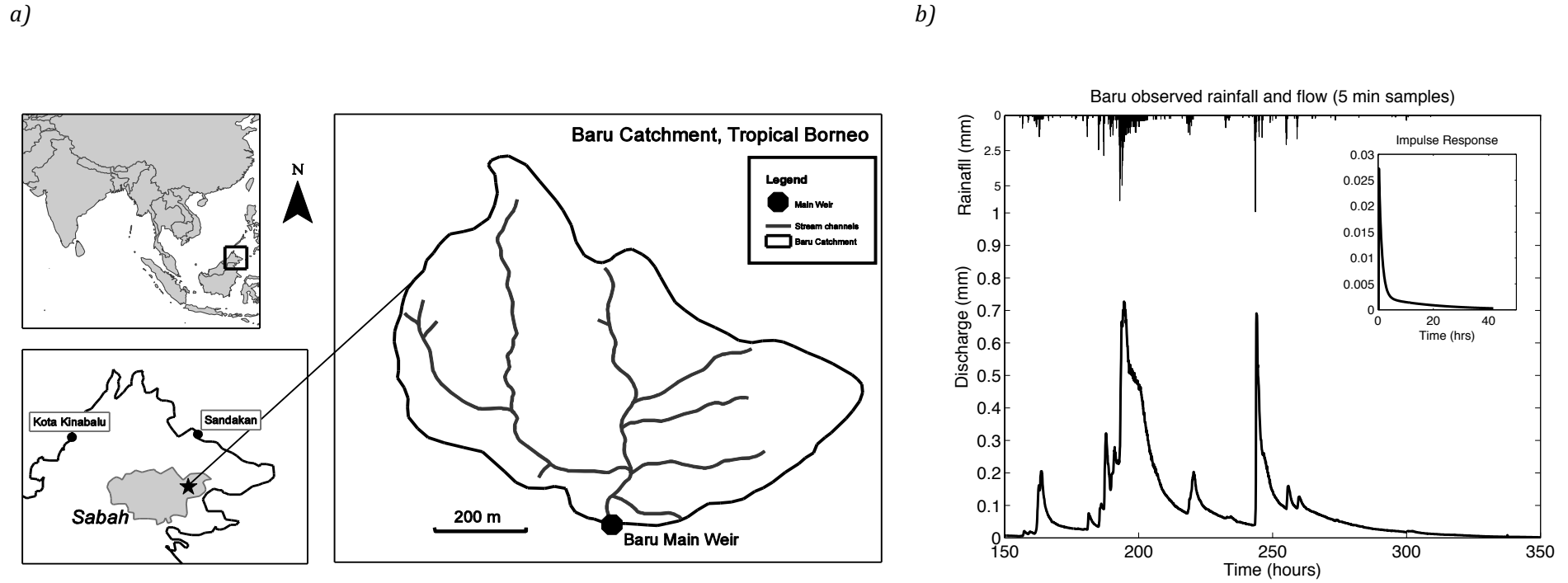


Figure 5-1: a) The location of the 0.44km<sup>2</sup> tropical Baru catchment in Sabah (dark grey area in bottom left map – Sabah Foundation Forest management concession), Borneo and b) the hydro- and hyetographs for the February 1996 sampled at 5 min intervals showing the flashy response of the catchment to the high intensity, spatially variable rainfall

### 5.2.2. Blind Beck – temperate catchment

The Blind Beck catchment (Figure 5-2a) has an area of 8.8 km<sup>2</sup> and lies in the headwaters of the Eden basin in North West England, UK (54.51°N 2.38°W). The basin's response shows evidence of deep hydrological pathways due to the presence of deep limestone (62%) and sandstone (38%) aquifers resulting in a damped hydrograph response (Mayes *et al.*, 2006; Ockenden and Chappell, 2011; Ockenden *et al.*, 2014). Winter rainfall in this basin is derived from frontal systems with typically lower intensities than the convective systems in the tropics (Reynard and Stewart, 1993). Data from a single tipping bucket rain-gauge (that is, 0.1 gauges per km<sup>2</sup>) located in the middle of the catchment was used in this study. The data used in the analysis covers the period from 26th Dec 2007 at 16:45 to 31st December 2007 at 21:45 sampled at 15 min intervals (Figure 5-2b) and was previously modelled by Ockenden and Chappell (2011) using an aggregated hourly time-step.

The choice of these two experimental catchments, therefore, allowed the initial evaluation of the estimation of catchment rainfall from streamflow for the end-member extremes of a basin with tropical convective rainfall and shallow flow pathways to a basin with temperate frontal rainfall (that is, much lower intensity) and deep flow pathways (that is, much greater basin damping or temporal integration).

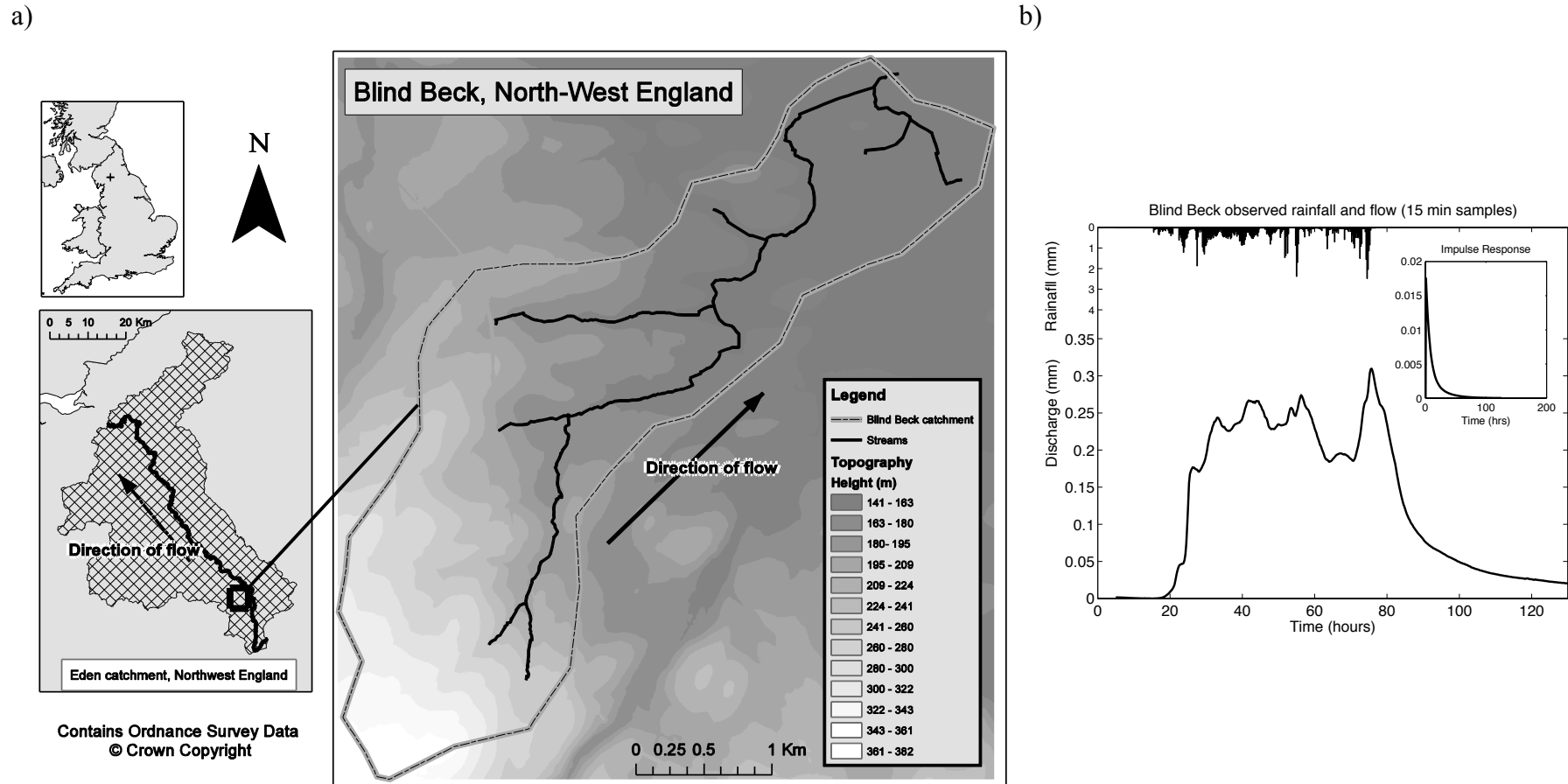


Figure 5-2: a) The location of the 8.8km<sup>2</sup> temperate Blind Beck catchment in Northwest England and b) the hydro- and hyetographs for Blind Beck for the period from 26th Dec 2007 at 16:45 to 31st December 2007 at 21:45 sampled at 15 min intervals showing its response to less intense frontal rainfall and deeper hydrological pathways



### 5.3. Model formulation and physical interpretation

This study investigated the limits of inferred catchment effective rainfall estimation from streamflow. Continuous time transfer function models identified from the observed data using Data Based Mechanistic (DBM) modelling approaches (Young and Beven, 1994; Young and Garnier, 2006), are inverted using the *RegDer* method (Kretzschmar *et al.*, 2014) and used to transform catchment streamflow into estimates of catchment inferred rainfall.

DBM modelling makes no prior assumptions about the model structure (though it often uses structures based on transfer functions), which is suggested by the observed data, and must be capable of physical interpretation. As transfer functions are linear operators, a transform structured as a bilinear power-law (Equation 5-1), also identified from the observed data, was applied to linearise the data before model fitting (Young and Beven, 1994; Beven, 2012a, p91):

$$P_e = P Q^\alpha \quad (\text{Equation 5-1})$$

where  $P$  is the observed rainfall,  $Q$  the observed streamflow in the previous time period and  $\alpha$  is a parameter, estimated from the data.  $P_e$  is the effective observed rainfall (ER) and  $Q$  is used as a surrogate for catchment wetness. Both catchments used in this study proved to be predominantly linear in their behaviour so Equation 5-1 was not used. In the initial study, a wide range of possible models was identified using algorithms from the Captain Toolbox for Matlab (Taylor *et al.*, 2007). The models selected were a good fit to the data and were suitable for inversion. The Nash-Sutcliffe Efficiency (NSE or  $R_t^2$ ) is commonly used to compare the performance of hydrological models. Often several models can be identified that fit the data well (the equifinality concept of Beven, 2006). From these, models with few parameters to be estimated that inverted well were selected. In this study, a second order linear model was found to fit both catchments. The output from the *RegDer* process is an inferred effective rainfall series to which the inverse of the power law is then applied, if necessary, to construct an inferred catchment rainfall sequence. The process is illustrated in Figure 5-3.

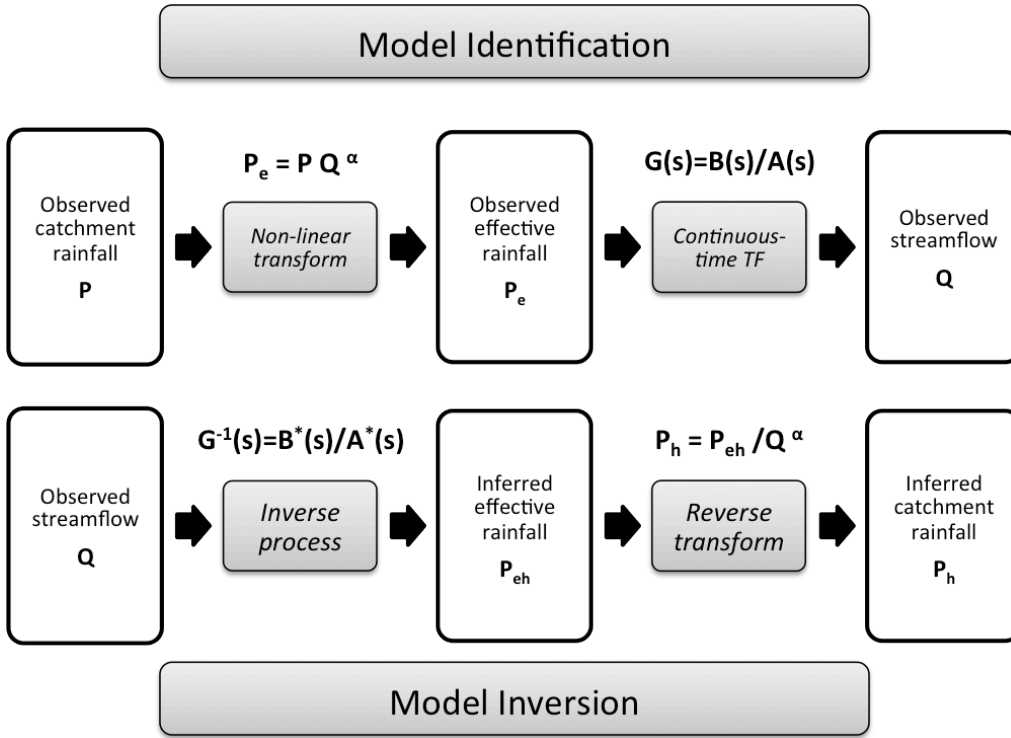


Figure 5-3: model identification and inversion workflow where  $P$  is the observed catchment rainfall,  $P_e$  is the effective rainfall,  $Q$  is the observed streamflow,  $P_{eh}$  is the inferred effective rainfall and  $P_h$  the inferred catchment rainfall. Non-linearity is represented by the bilinear power law (Beven, 2012a, p91). The continuous time transfer function is given by  $G(s)$  where  $A(s)$  and  $B(s)$  are the denominator and numerator polynomials and the inversion process is represented by  $G^{-1}(s)$  where  $A^*(s)$  and  $B^*(s)$  refer to the symbolic denominator and numerator polynomials of the regularised inverse transfer function as in (Equation 5-4).

The transfer function model inversion process has been described in Kretschmar *et al.* (2014). It involves transition from the transfer function catchment model:

$$Q = G(s)R = \frac{\beta_0 s^m + \beta_1 s^{m-1} + \dots + \beta_m}{s^n + \alpha_1 s^{n-1} + \dots + \alpha_n} e^{-s\tau} P_e \quad (\text{Equation 5-2})$$

to the direct inverse (in general non-realisable):

$$\hat{R} = \frac{b_0 s^n + b_1 s^{n-1} + \dots + b_n}{s^m + a_1 s^{m-1} + \dots + a_m} e^{s\tau} Q \quad (\text{Equation 5-3})$$

which is then implemented using regularised streamflow derivatives in the form of:

$$\hat{R} e^{-s\tau} = \frac{b_0 \{s^n Q\}^* + b_1 \{s^{n-1} Q\}^* + \dots + b_n Q}{s^m + a_1 s^{m-1} + \dots + a_m} \quad (\text{Equation 5-4})$$

where  $\{\widehat{s^n Q}\}^* = \mathcal{L}\left\{\widehat{\frac{d^n}{dt^n} Q}\right\}$  is the Laplace transform of the optimised regularised estimate of the  $n^{\text{th}}$  time derivative of  $Q$ :  $\frac{d^n}{dt^n} Q$ . The regularised derivative estimates replace the higher order derivatives in Equation 5-3, which otherwise make Equation 5-3 unrealisable (improper) – this is the core of the method in Kretzschmar *et al.* (2014). In the implementation,  $n^{\text{th}}$  derivatives (Equation 5-4) are not estimated, but advantage is taken of the filtering with the denominator polynomial, whereby only  $(n-m)^{\text{th}}$  order regularised derivative estimates of  $Q$  are required in combination with a proper transfer function.

The inferred effective rainfall (*IER*) sequences generated by *RegDer* generally have a much smoother profile (illustrated in Figure 5-4) than the observed effective rainfall inputs, however streamflow sequences generated with the inferred catchment rainfall (*ICR*) used as the model input are almost indistinguishable from the observed streamflow ( $R_t^2 > 97\%$ ) – illustrated in Figure 5-9. This indicates that the catchment dynamics, as captured by the transfer function model, renders the differences between observed and inferred rainfall immaterial. The reason for this becomes clear when looking at the frequency domain analysis of the inversion process shown in this paper.

In order to investigate this, the *IER* is compared to aggregated effective observed rainfall sequences with increasing levels of aggregation until a good match is found (high value of  $R_t^2$  or  $R$ ). Two methods of aggregation have been used: 1) averaging over a range of time-series, 2) moving average over varying time scales. Two measures are used to assess the correspondence between the IR and the aggregated effective rain: 1)  $R_t^2$ , the coefficient of determination, and 2)  $R$ , the instantaneous Pearson correlation coefficient. They are given by:

$$R_t^2 = 1 - \frac{\sum(ER - IER)^2}{\sum(ER - \overline{ER})^2} \quad (\text{Equation 5-5})$$

$$R = \frac{\sum(ER - \overline{ER})(IER - \overline{IER})}{\sqrt{\sum(ER - \overline{ER})^2} \sqrt{\sum(IER - \overline{IER})^2}} \quad (\text{Equation 5-6})$$

where  $ER$  indicates a value from the aggregated effective rainfall sequence with mean  $\overline{ER}$  and  $IER$  is the corresponding value from the inferred effective rainfall sequence

with mean  $\overline{IER}$ . Both  $R_t^2$  and  $R$  values tend towards a maximum value as aggregation increases. The aggregation level at which the maximum is reached is identified and taken as an estimate of the resolution of the inferred effective series. This value is then compared to the system fast time constant ( $TC_q$ ) and the Nyquist-Shannon (N-S) sampling limit.

#### 5.4. Continuous model formulation

One of the advantages of using a CT model formulation is that the parameters have a direct physical interpretation independent of the model's sampling rate (Young, 2010). The continuous time model formulation for a 2<sup>nd</sup>-order model is given by:

$$y(t) = \frac{\beta_0 s + \beta_1}{s^2 + \alpha_1 s + \alpha_2} u(t - \delta) \quad (\text{Equation 5-7})$$

where  $y$  is the measured streamflow at time  $t$ ,  $\delta$  is the transport delay and  $u$  is the effective rainfall at time  $t - \delta$ . If the denominator can be factorized and has real roots, (Equation 5-7) can be rewritten as:

$$y(t) = \frac{\beta_0 s + \beta_1}{(s + \frac{1}{TC_q})(s + \frac{1}{TC_s})} u(t - \delta) \quad (\text{Equation 5-8})$$

where  $TC_q$  and  $TC_s$  are the system time constants and are often significantly different – a ‘stiff’ system. Decomposing the model into a parallel form gives:

$$y(t) = \left( \frac{g_q}{1 + TC_q s} + \frac{g_s}{1 + TC_s s} \right) u(t - \delta) \quad (\text{Equation 5-9})$$

where  $g_q$  and  $TC_q$  are the steady state gain and time constant of the fast response component and  $g_s$  and  $TC_s$  are the steady state gain and time constant of the slow response component. The steady state gain of the system as a whole is given by:

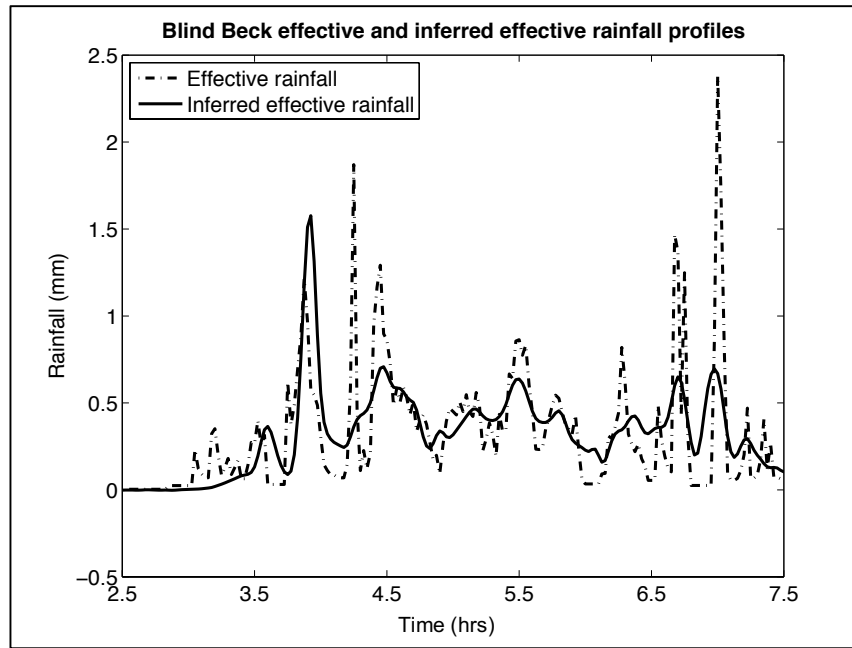
$$g = g_q + g_s \quad (\text{Equation 5-10})$$

so the fraction of the total streamflow along each pathway can be calculated from:

$$P_q = \frac{g_q}{g_q + g_s}; P_s = \frac{g_s}{g_q + g_s} \quad (\text{Equation 5-11})$$

The fraction of streamflow attributed to the slow response component is sometimes termed the Slow Flow Index (SFI) (Littlewood *et al.*, 2010). This example shows a second order model but the general principle can be extended to higher order models.

a )



b )

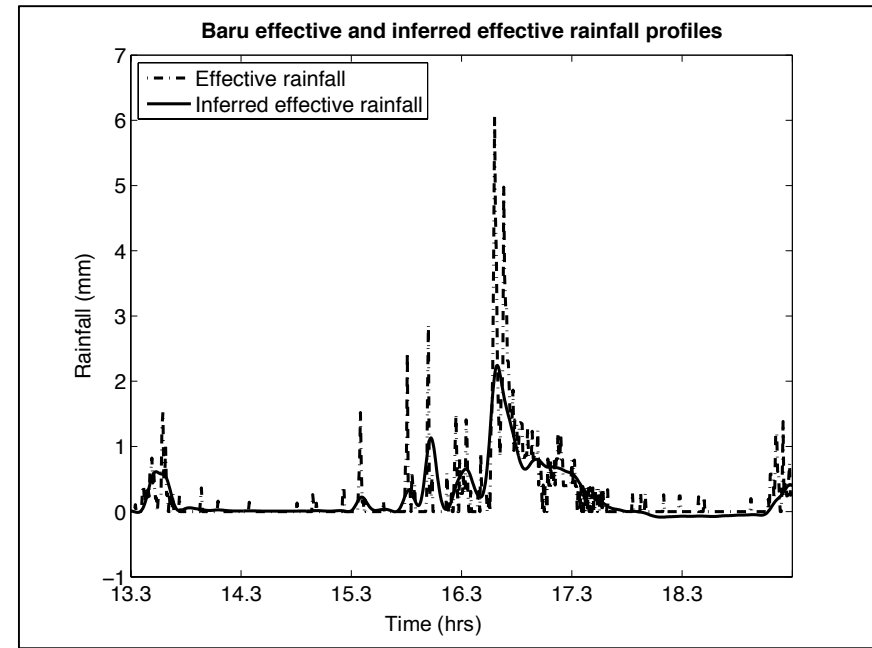


Figure 5-4: observed effective and inferred effective rainfall profiles generated using the RegDer inversion method for a) Blind Beck and b) Baru

Details of the inversion and regularisation processes can be found in Kretzschmar *et al.* (2014).

### 5.5. Sampling frequency

When using CT modelling, the Nyquist-Shannon frequency gives the upper limit on the size of the sampling interval,  $\Delta t$ , that will enable the system dynamics to be represented without distortion (aliasing - Bloomfield, 1976, p21). Aliasing occurs when a system is measured at an insufficient sampling rate to adequately define the signal from the data. The Nyquist-Shannon theorem states that the longest sampling step for a signal with bandwidth  $\Omega$  (maximum frequency, where  $\Omega = 2\pi f$  in cycles per time unit) to be represented is:

$$\Delta t \leq \frac{1}{2\Omega} \quad (\text{Equation 5-12})$$

in order to completely define the system in absence of observation disturbance (Young, 2010). If the sampling interval is small enough to uniquely define the system, the estimated CT model should be independent of the rate of sampling. Conversely, if the frequency of the inferred output is less than the N-S limit, then the system dynamics should be adequately captured. Other estimates of the sufficient sampling interval, designed to avoid proximity to the Nyquist limit, have been made by Ljung (1999) and Young (2010). In terms of system TCs, these limits are given by:

$$\text{Nyquist} = \pi TC_q \text{ time units} \quad (\text{Equation 5-13})$$

$$\text{Ljung} = \frac{\pi TC_q}{5} \text{ time units} \quad (\text{Equation 5-14})$$

$$\text{Young} = \frac{TC_q}{6} \text{ time units} \quad (\text{Equation 5-15})$$

### 5.6. Temporal aggregation of effective rainfall

Two methods for aggregating *ER* were used to estimate the time resolution of the *IER*. Rainfall is the total volume accumulated over the sampling interval so the *ER* was aggregated over progressively longer sampling periods of 2 to 24 times the base sampling period and averaged to form a new smoothed sequence that could be compared with the *IER*. For comparison, aggregation was also performed via a moving average process utilising the convolution method available in Matlab. Both methods

may be affected by the aggregation starting point and edge effects. The aggregated *ER* sequences were compared to the *IER* using the coefficient of determination ( $R_t^2$ ) and the correlation ( $R$ ).  $R_t^2$  and  $R$  tend towards a maximum value as aggregation increases. The aggregation time-step at which this value is established is used to estimate the resolution of the *IER*.

## 5.7. Spectral Analysis

Periodograms of the amplitude spectra of the observed and modelled series were plotted to test whether the *ER* and *IER* have the same dynamics in the critical frequency range, despite the loss of time resolution (related to low pass filtering due to regularisation). A periodogram is the frequency domain representation of a signal; transforming the signal into the frequency domain may reveal information that is not visible in the time domain. A transfer function shown in its equivalent frequency domain form describes the mapping between the input and the output signals' spectra for the linear dynamic systems used here. Signals may be easily transformed between the time and frequency domains (Wickert, 2013).

Periodograms are obtained using the Matlab implementation of the Fast Fourier Transform and smoothed using the Integrated Random Walk (for example, Young *et al.*, 1999); the same regularisation approach as used in the calculation of the *IER*, implemented in the Captain Toolbox (Taylor *et al.*, 2007). Periodograms of *ER*, *IER* and catchment streamflow are compared on a single plot showing how the spectral properties of the inversion process are used to obtain the *IER* estimates (see Figure 5-6). The streamflow spectrum is the result of mapping the rainfall spectrum by the catchment dynamics. To make a full inversion of that mapping would involve very strong amplification of high frequencies with all the negative consequences discussed by Kretzschmar *et al.* (2014). The most significant implications of full inversion include the introduction of high amplitude, high frequency noise artefacts into the rainfall estimates. The regularisation of estimated derivatives introduces the effect of low-pass filtering into the inversion process, avoiding the excessive high frequency noise. Regularisation does not introduce any lag into the process, unlike traditional low pass filtering.

## 5.8. Results and discussion

Figure 5-4 illustrates the smoothed rainfall distribution of the IER sequence obtained using the *RegDer* method. Similar streamflow sequences are generated using either the observed rainfall or *ICR* sequences as model input (see Kretzschmar *et al.*, 2014). The implication is that the catchment system dynamics are being captured despite the apparent difference in the rainfall distribution and that the detail of the rainfall series in time may not be important when modelling the dominant mode of streamflow dynamics.

In order to assess the degree of resolution lost by estimating rainfall using the *RegDer* method, the ER was aggregated using two methods (that is, simple aggregation by resampling and a moving average) and the resulting sequences compared to the *IER* sequence in the time domain. Plots of progressively more aggregated sequences are shown in Figure 5-5. It can be seen that as aggregation increases, peaks become lower and more spread out and the sequence is effectively smoothed. The coefficient of determination ( $R_t^2$ ) and the correlation ( $R$ ) between the aggregated sequence and the *IER* tends to a maximum then decreases as aggregation time increases – ultimately the variation in the sequence would be completely smoothed out. The point at which the maximum value is reached is taken as an estimate of the resolution of the *IER*. Plots of  $R_t^2$  or  $R$  values are shown in Figure 5-6 (aggregation by resampling) and Figure 5-7 (moving average estimate). Time resolution estimates are shown in Table 5-1 and compared with the fast time constant ( $TC_q$ ) and the Nyquist-Shannon sampling limit.

Table 5-1 shows that the estimated resolution of the *IER* sequence for Blind Beck is around 9-10 time periods (that is, 2.25-2.5 hours) and for Baru it is 11-12 time periods (that is, 55 mins – 1hr). Both estimates are within the Nyquist-Shannon safe sampling limit and below the fast time constant for both catchments indicating that even though resolution has been lost – the regularisation trade-off for numerical stability – the dominant mode of the rainfall-streamflow dynamics has been captured. Table 5-2 shows that the estimated resolution of the inferred effective rainfall for both catchments is well within the Nyquist limit and, whilst the Blind Beck resolution is within the safe limits suggested by Ljung (1999) and Young (2010), the estimated resolution for Baru is close to the fast TC and outside the suggested limits. The estimates of resolution of



the inferred sequence made from the aggregation plots are not always well defined and may be dependent on the length of record which will affect the number of aggregation periods that may be meaningfully calculated given the finite length of the data series. A better means of estimation of resolution may be achieved by examining the frequency spectra of the rainfall and streamflow sequences.

*Table 5-1: The sampling frequency (hrs) and time constants (TC<sub>q</sub> – fast and TC<sub>s</sub> – slow) are listed for each of the study catchments together with the slow flow index (SFI – the percentage of the flow taking the slow pathway), the Nyquist-Shannon safe sampling limit (hrs) and the time resolution of the inferred effective rainfall (IER) estimated by both resampling and moving average methods. Also shown is the frequency domain estimate of the resolution – the cut-off point beyond which the signal carries very little information (illustrated in Figure 5-8) and can be considered unimportant. Time resolution of the inferred effective rainfall sequences estimated by both resampling and moving average methods are less than the dominant (fast) mode of the catchments and considerably less than the ‘safe’ Nyquist-Shannon limit.*

Catchment	Sampling frequency (hours)	TC <sub>q</sub> (hrs)	TC <sub>s</sub> (hrs)	SFI	Nyquist-Shannon Limit (hours)	Time resolution estimates		
						Aggregation by resampling	Aggregation by Moving Average	Cut-off point (hrs)
Blind Beck	.25	6.3	22.1	47%	19.9	2.5 hours (10 time periods)	2.25 hours (9 time periods)	3.8
Baru	.083	1.1	18.7	62%	3.4	0.9 - 1 hours (11-12 time periods)	1 hour (12 time periods)	1.7

*Table 5-2: The estimated resolution of the inferred effective rainfall for Blind Beck is well within both the Nyquist limit and the safe sampling limits suggested by the Ljung (1999) and Young (2010) whereas the resolution for Baru, whilst well within the Nyquist limit, is close to the fast TC<sub>q</sub> and outside the suggested safe sampling limits of Ljung and Young.*

Catchment	TC <sub>q</sub> (hours)	Nyquist limit (hours)	Ljung interval (hours)	Young interval (hours)	Estimated resolution (hours)
Blind Beck	6.3	19.9	3.98	3.32	2.25-2.5
Baru	1.1	3.4	0.68	0.57	0.91-1.0

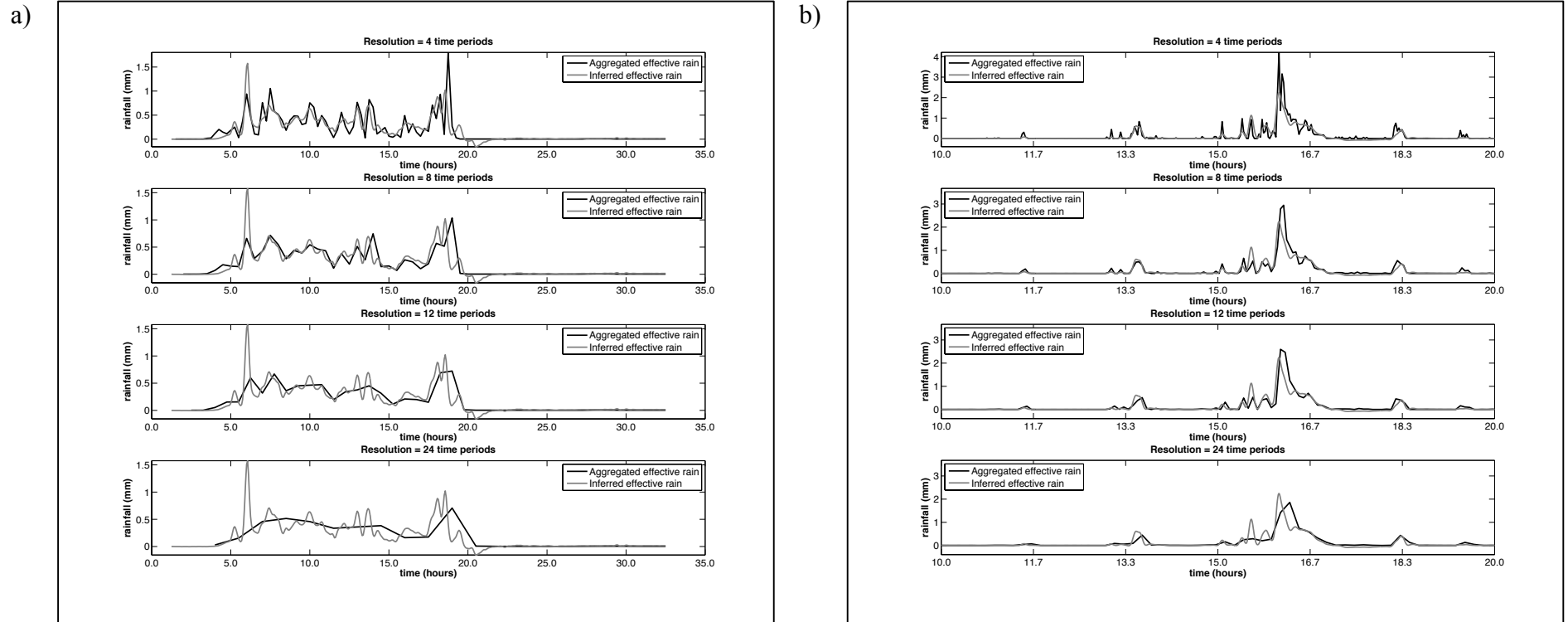


Figure 5-5: Comparison of aggregated sequence to the Inferred effective rainfall sequence for a) Blind Beck (sampling interval 15 mins) b) Baru (sampling interval 5 mins) at aggregations of 4, 8 12 and 24 time periods (samples) illustrating how aggregation lowers the peak and spreads the volume of rainfall over a longer time period. The inferred effective rainfall sequence is plotted for comparison

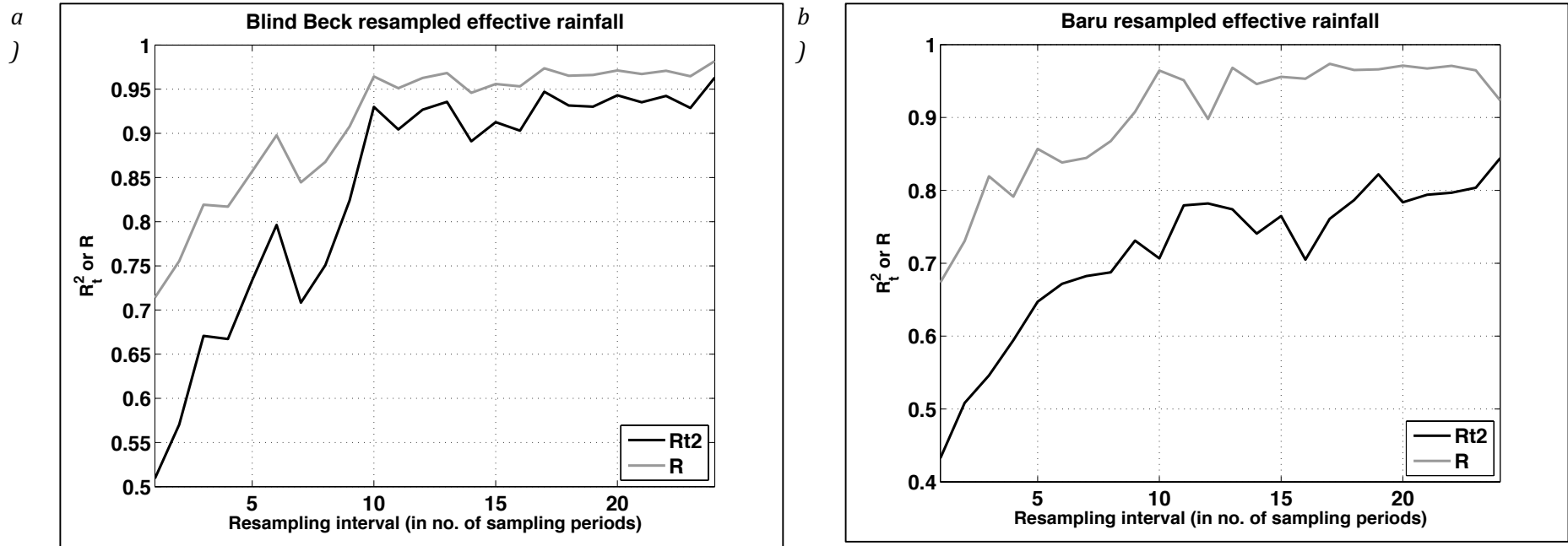


Figure 5-6: The  $R_t^2$  and  $R$  tend to a maximum value as aggregation increases for a) Blind Beck and b) Baru. The resolution of the inferred effective rainfall is taken to be point at which the maximum is reached or very little change is apparent. For Blind Beck, this value is reached at 10 periods for both  $R_t^2$  and  $R$ . The result for Baru is not quite as clear but can be estimated to be 10 periods from  $R$  and 11 or 12 from  $R_t^2$  though  $R_t^2$  continues to increase up to 24 time periods perhaps due to higher variability of the rainfall

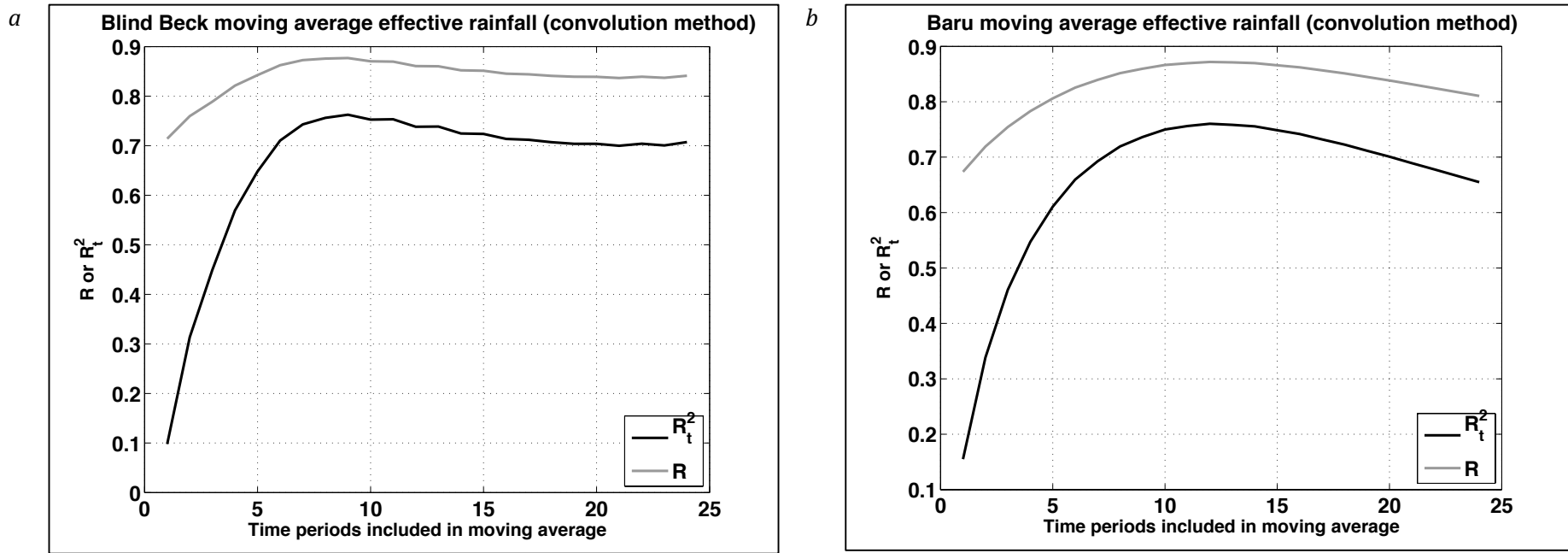


Figure 5-7: A similar plot to Figure 5-6 with aggregation by Moving Average for a) Blind Beck and b) Baru. Rather than reaching an asymptotic level, the  $R_t^2$  and  $R$  values maximize at 9 time periods for Blind Beck and 12 time periods for Baru (determined graphically in Matlab). These values have been used as the estimates of the resolution of the inferred effective rainfall and agree well with the estimates made by resampling. Convolution term in the caption is with reference to the method of calculating the moving average

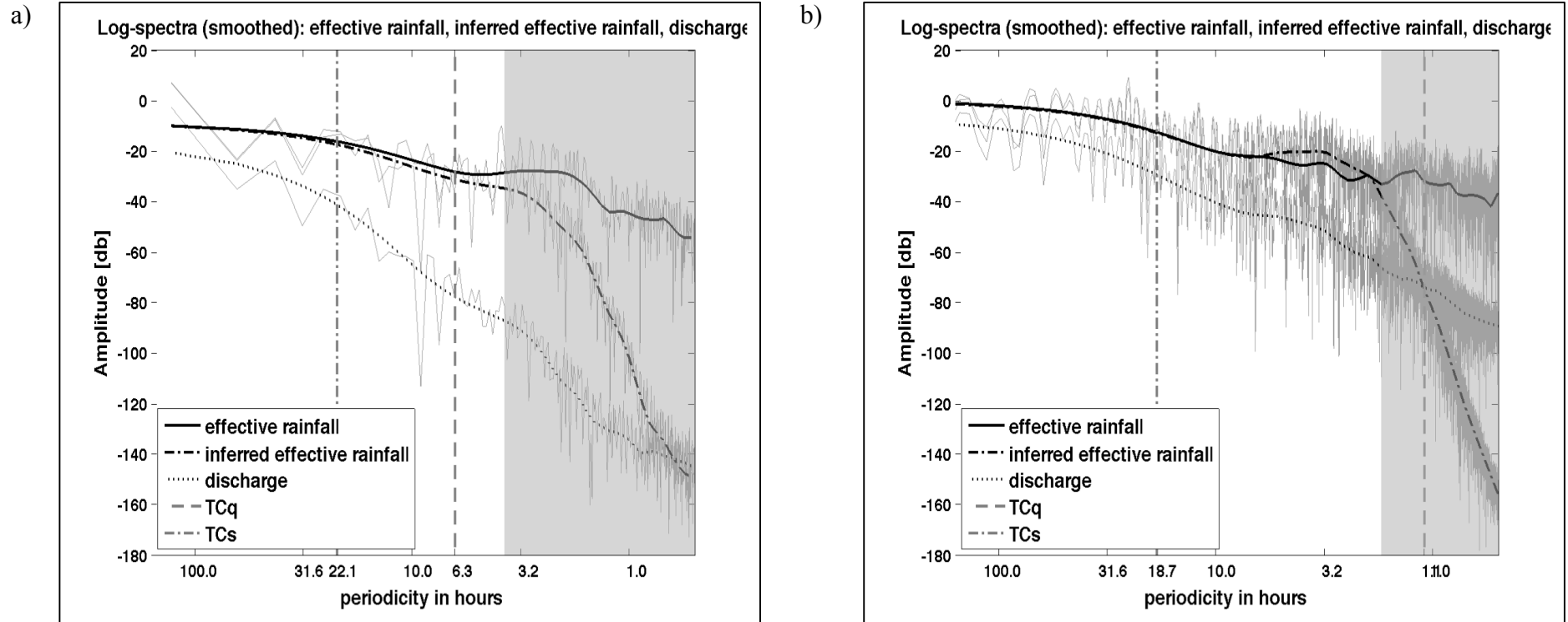


Figure 5-8: Periodograms for a) Blind Beck and b) Baru showing the frequency structure of the effective rain, inferred effective rain and streamflow sequences. The grey area shows frequencies beyond the 6dB difference between smoothed ER and IER spectral point. Both catchments show a similarity in the frequency spectra of effective and inferred effective rainfall within the catchment system. The inferred effective rainfall spectrum is very close to that of the actual effective rainfall within a wide range of frequencies mostly covering those corresponding to the catchments' time constants. There is also a strong low pass filtering effect cutting off high frequencies with low amplitudes instead of boosting this high frequency noise.

In Figure 5-8, the amplitude spectra of inferred effective and observed effective rainfall are very close (overlapping when smoothed) within a broad range of frequencies. The cut-off frequency, where the difference between the smoothed ER and *IER* spectra is approximately -6dB, provides a frequency domain estimate of the resolution. The cut-off period for Blind Beck is 3.8 hours and for Baru is 1.7 hours. For frequencies above this value, a very strong low pass filtering effect shown is by the rapid decrease in the IR spectrum. The frequency range beyond the cut-off point, shaded in Figure 5-8, carries a very small proportion of the power of the signal and can be considered non-significant.

Table 5-1 lists the time constants, SFIs and cut-off points for both catchments. The cut-off point for Blind Beck (3.8 hrs) is outside the range of the catchment time constants (6.3 ...22.1 hrs) probably reflecting the frontal rainfall regime, which is relatively uniform in time and space. Flow along both pathways is almost evenly split indicating that they are both important in terms of flow generation. On the other hand, Baru's *TCq* (1.1 hrs) is beyond the cut-off point (1.7 hrs) in the area where the spectra contain little power or information indicating why the catchment's variable, high intensity, high frequency, highly localised convective rainfall may not be easy to estimate. It is worth noting that the forward rainfall-discharge model does not fit the Baru catchment (88%) characterised by its highly variable, both spatially and temporally rainfall, as well the Blind Beck catchment (98%) with its relatively uniform predominantly frontal rainfall (Kretzschmar *et al*, 2014).

The processes and characteristics limiting the inferred effective rainfall accuracy include the slow components of the catchment dynamics and the rainfall regime. These can be seen as the 'usual suspects' affecting the inversion process. The general goodness of fit of the initial catchment model (rainfall-streamflow) appears to be a factor as well (see Figure 5-9), indicating that the inferred effective rainfall estimation method presented here can be used to assess the quality of available data and the degree to which the data characterise the catchment. Further work is required using a range of catchment and rainfall regimes to confirm these results and explain them in terms of rainfall and catchment characteristics, as well as investigating spatial relationships. The latter will be evaluated using catchment data with multiple rain-gauges, and are the subject of the forthcoming work. Rainfall is the key driver of streamflow with the

pattern varying from event to event however the underlying catchment characteristics, for example, soil, geology, topography, may modify this. A combination of inversion and spectral analysis may provide a method for untangling the effects of catchment characteristics and rainfall regime on streamflow generation and has the potential for characterising the effects of future changes in catchment and/or rainfall characteristics due to, for example, climate change.

## 5.9. Conclusions

A combination of time and frequency domain techniques have been used to show that the inferred effective rainfall time-series generated by the RegDer inversion method does indeed approximate the direct inverse of a transfer function to a high degree of accuracy within the frequency range which includes the dominant modes of the rainfall-streamflow dynamics. The direct inverse exaggerates low-amplitude high frequency noise, which is filtered out by the regularisation process involved in the *RegDer* method. The smoothing of the signal resulting from regularisation is quantified in the time-domain by comparison with aggregated observed input data using standard model fit measures - coefficient of determination,  $R_t^2$ , and correlation coefficient,  $R^2$ - and analysed as a low-pass filtering process in the frequency domain. The smoothing effect is minimised within the constraints of the available data and catchment dynamics, through optimisation of the regularisation constants (NVRs) to obtain the best fit of the inversion process where both rainfall and discharge data are available.

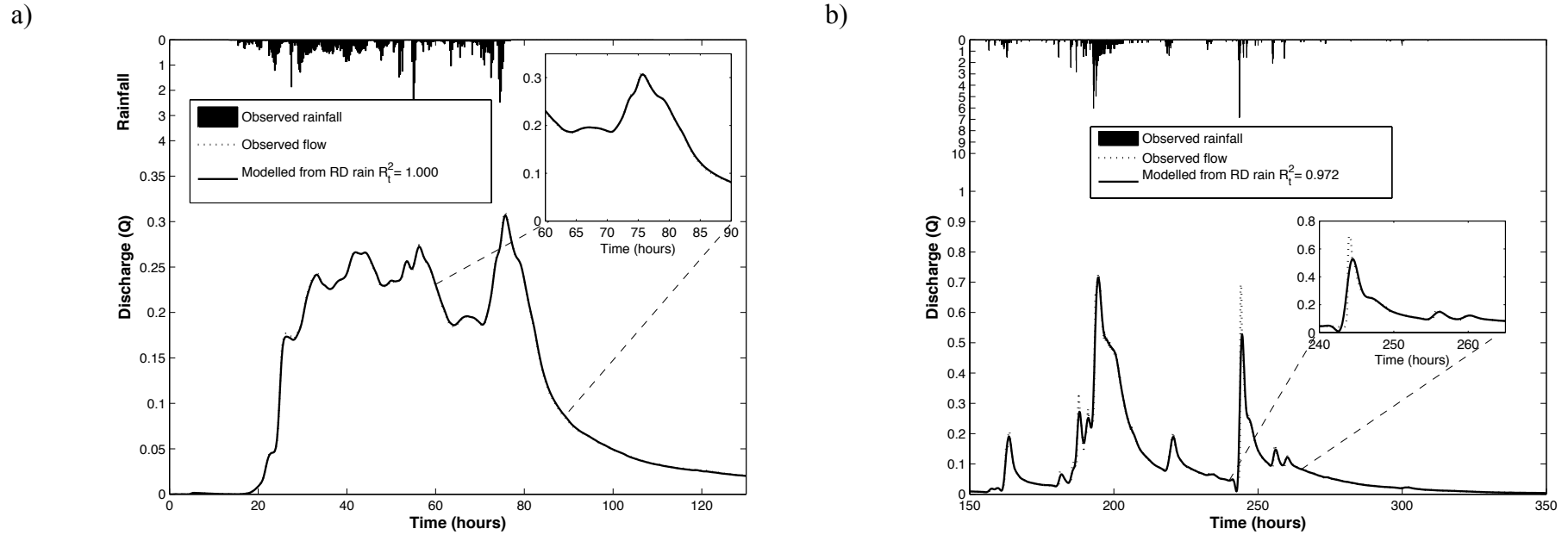


Figure 5-9: Comparison of observed discharge and discharge generated from the Inferred Effective Rainfall for a) Blind Beck and b) Baru. The flow sequences match almost perfectly in the case of Blind Beck and very closely in the case of Baru where the peak flows are under-estimated. Note that the forward (rainfall-discharge) model fit for Blind Beck (98%) is better than for Baru (88%) (Kretzschmar et al, 2014).



## **Chapter 6 What really happens at the end of the rainbow? – paying the price for reducing uncertainty (using reverse hydrology models)**

Kretzschmar, A, Tych, W, Chappell, NA & Beven, KJ (2016), What really happens at the end of the rainbow?: paying the price for reducing uncertainty (using reverse hydrology models) *Procedia Engineering*, vol 154, pp. 1333-1340.  
DOI: 10.1016/j.proeng.2016.07.485

### **Abstract**

Modelling of environmental processes is subject to a high degree of uncertainty due to the incorporation of random errors and a lack of knowledge about how processes operate at the scale of interest. Use of uncertain data when identifying and calibrating a model can lead to disinformative data being included in the procedure, resulting in uncertain parameter estimation and ambiguity in the outcomes. Rainfall-runoff modelling where a single rain-gauge is often assumed to be representative of the potentially highly variable (in both space and time) rainfall field is a good example. The noisy pattern of rainfall inputs is transformed by the catchment into streamflow. The streamflow pattern is dependent on the spatio-temporal pattern of rainfall and of the dominant processes operating within the catchment. Inverse modelling of the catchment dynamics, that is, inferring catchment rainfall from streamflow, provides a possible means of improving the estimated rainfall input because all rain falling on the catchment becomes streamflow, and thus, providing improved forecasts of the streamflow output. A combination of inverse modelling, time series analysis, spatial analysis and spectral analysis may also help to provide an insight into the complex processes operating within the catchment system. This paper applies a novel method for inferring true catchment rainfall from streamflow highlighting that the streamflow is better estimated using inferred rainfall than observed rainfall (from a single gauge) because a single gauge only gives a partial description of the rainfall field. However, reducing uncertainty in this way comes at a price, in this case, the reduction in time-resolution of the inferred rainfall series.

## 6.1. Introduction

Rainfall is the most important input to most hydrological models. The rainfall field is variable in both time and space and thus has inherent uncertainty. This is amplified by the fact that rainfall measured at a point by a single rain gauge is often assumed to be representative of a catchment many kilometres squared in area. Figure 6-1 shows the variability in the rainfall field across the Brue catchment (in the south-west of the UK) measured at 15-minute intervals by a 23-gauge network. The pie charts at the top right of each image indicate how many gauges are measuring rainfall at each time interval – the more yellow, the more gauges have rainfall.

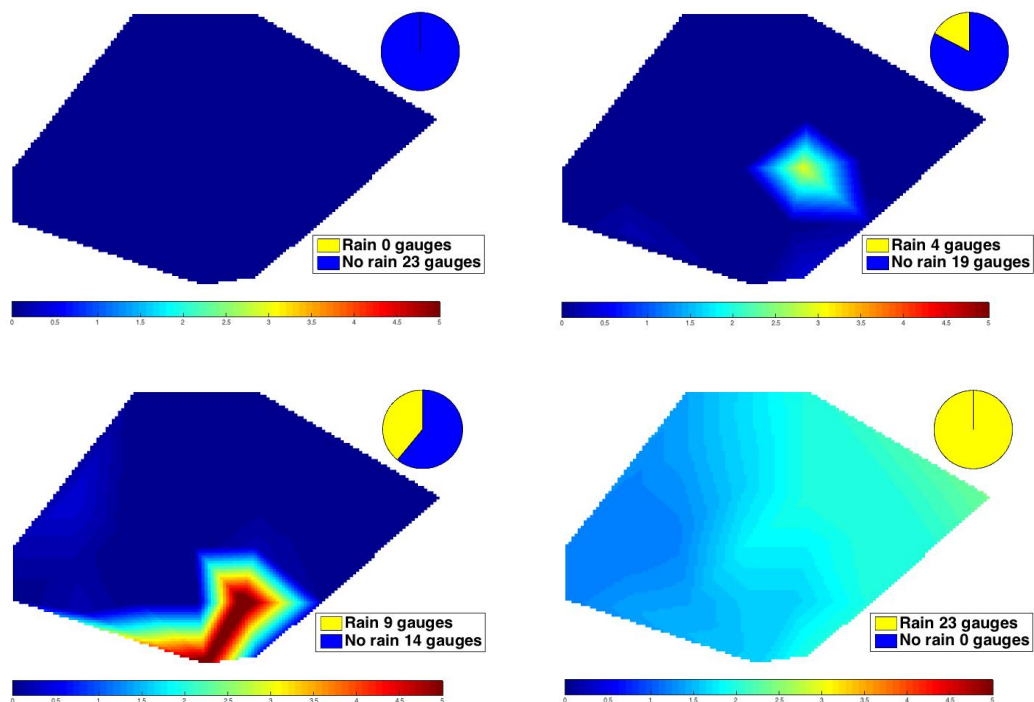


Figure 6-1 – The variability in the rainfall field in space and time over the Brue catchment – brighter colours mean more rain (mm). Rainfall sampled at 15 minute intervals. The pie charts show how many gauges measure rain - the more yellow, the more gauges are measuring rainfall.

Estimates used to design flood defences are based on historic records of rainfall and streamflow which are subject to uncertainty from many sources including measurement techniques, instrumentation, changes to the system, model structure, lack of understanding of the processes at the scale of interest and those all-important unknowns some of which are ‘unknown unknowns’. The ideal would be to provide a 100% certain

forecast of the future. However, uncertainty dictates that this is unlikely to happen. The best that can be done is to strive for improved understanding of the processes and better measurement techniques that will help to reduce uncertainty.

So how can rainfall estimates be improved? As can be seen, rainfall is variable in time and space (Figure 6-1) and a single gauge may not be representative of the rain that falls over the whole catchment, however, all the rain that falls on the catchment is integrated, by the active processes, into streamflow that can be measured at the catchment outlet. Working backwards from the measured streamflow, it should be possible to use the information in the streamflow to estimate the rainfall.

Considerable interest has been shown in ‘reverse hydrology’ in recent years. Although streamflow is itself subject to uncertainty, it is assumed that errors in measurement are much smaller than the errors in estimates of catchment rainfall (Henn *et al.*, 2015) especially in mountainous catchments where altitude also plays a role in rainfall distribution. Studies in this area include those by Croke (2006, 2010), Kirchner (2009), Andrews *et al.* (2010), Young and Sumisławska (2012), Brocca *et al.*, (2013, 2014) and Kretzschmar *et al.* (2014, 2015). Reverse hydrology could be an important tool in promoting understanding of catchment rainfall distribution and the processes by which it is converted to streamflow and the identification of periods of inconsistent input-output data.

## 6.2. Methodology

Distributed models that attempt to take account of the variations in rainfall and catchment characteristics have a large number of parameters that must be estimated in order to fit the model. Many of these parameters have no physical meaning or lose their meaning in the calibration process when adjusted to make the model outputs a better fit to the observed measurements. Given the uncertainty involved at all stages of the process, it is hard to justify these highly parameterised models though they have a place in attempting to explain the processes involved. This study uses the Data Based Mechanistic (DBM) modelling approach (Young and Beven, 1994), which allows the data to suggest the form of the model. Several models that fit the data well may be

identified (the equifinality concept described in Beven (2006)) but only those that have few parameters (are parsimonious) and have a physical interpretation are accepted.

The method presented here uses systems analysis techniques, implemented using the Captain toolbox in Matlab (Taylor *et al.*, 2007) to identify a continuous time (CT) transfer function model utilising the high-resolution data (in this case, rainfall and streamflow) needed to capture the dynamics of the catchment. The model (or models) thus identified can be inverted using a novel regularisation process detailed in Kretzschmar *et al.*, (2014). The output from the regularisation process is an inferred rainfall series. The transfer function model is a linear relationship so non-linearity is modelled as a separate process as shown in Figure 6-2.

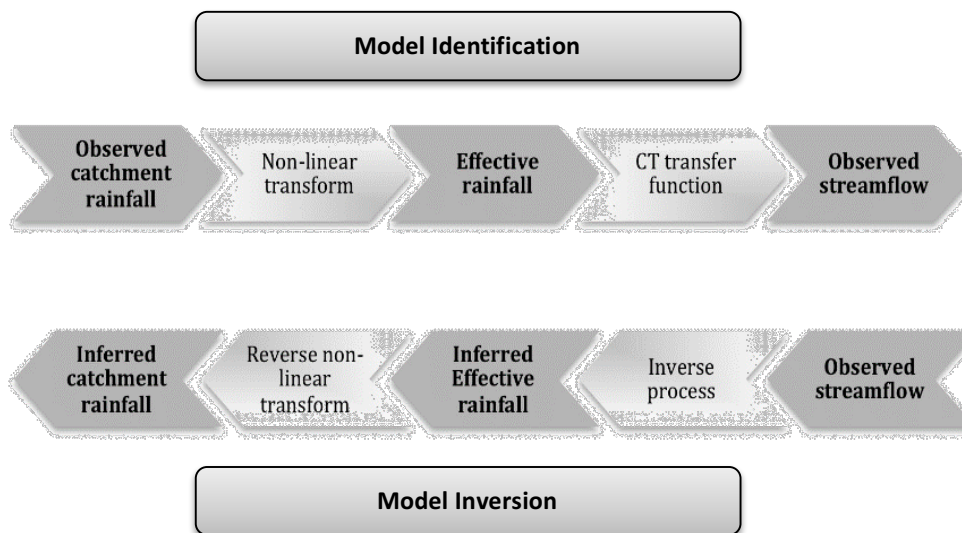


Figure 6-2 - the model identification and inversion workflow showing the off-line non-linear transformation

Advantages of using a CT formulation are that a wide range of catchment dynamics can be modelled and the parameters have a direct physical interpretation that is independent of the sampling rate (Young, 2010). The inversion itself is necessarily badly posed due to the need to invert processes which have been integrated in both time and space. However, applying the regularisation technique to CT models makes inversion possible without the amplification of the noise present in the data as is the case with direct inversion of the transfer function (Andrews *et al.*, 2010; Kretzschmar *et al.*, 2014). Kirchner's method (Kirchner, 2009) links rainfall and streamflow through a storage sensitivity function but it is limited to simple catchments that behave as single-reservoir (first-order) systems (Henn *et al.*, 2015). Discussion of other approaches is made in the

referenced literature (for example, Croke, 2006, 2010; Kirchner, 2009; Andrews *et al.*, 2010; Young and Sumislawska, 2012; Brocca *et al.*, 2013, 2014; Kretzschmar *et al.*, 2014, 2015). Working with sub-hourly data from two contrasting catchments, Kretzschmar *et al.*, (2014) showed that while the direct inverse of a transfer function produced an inferred effective rainfall series characterised by high frequency noise components, the regularisation process produced a much smoother rainfall profile sacrificing time resolution in favour of numerical stability. They also showed that both rainfall sequences resulted in similar modelled flow sequences, which fitted the observed streamflow data more closely than flow modelled using the observed rainfall implying that the dynamics of the catchment were being effectively captured in both cases. The high frequency behaviour of the direct inverse method has no physical interpretation so can be deemed to fail the criteria of the DBM methodology. Further investigation (Kretzschmar *et al.*, 2015) made use of sub-sampling and spectral analysis to quantify the loss of resolution and showed that the inferred rainfall sequences were still able to capture the catchment dynamics. Catchments integrate the rainfall falling on them in space as well as time when converting the rainfall into flow. This paper presents an initial investigation of spatial uncertainty utilising the inverse regularisation method outlined above.

### **6.3. Test catchment**

This paper utilises the heavily instrumented Brue catchment in South-west England. It has 49 rain gauges in an area of 135.2 km<sup>2</sup> enabling spatial variability to be investigated. There is an elevation change of approximately 300m from south-west to north-east across the catchment. The underlying geology is a combination of mudstone and limestone with a limestone ridge running in an arc across from north to south across the eastern upland area (see Figure 6-3). The catchment can largely be split into impermeable low-land to the west, higher land to the east where the limestone ridge is permeable, and the far east of the catchment which is largely impermeable. Land use is mostly pasture on clay soils with some woodland on the elevated eastern side (Wood *et al.*, 2000). The Brue research catchment was set up in 1993 as part of a Natural Environment Research Council (NERC) special topic research programme – the Hydrological Radar Experiment (HYREX) (Wood *et al.*, 2000). It ran for three years but the data has been extensively used in many subsequent research projects [for

example, (Wood *et al.*, 2000; Moore *et al.*, 2000; Bell and Moore, 2000; Villarini *et al.*, 2008 a,b).

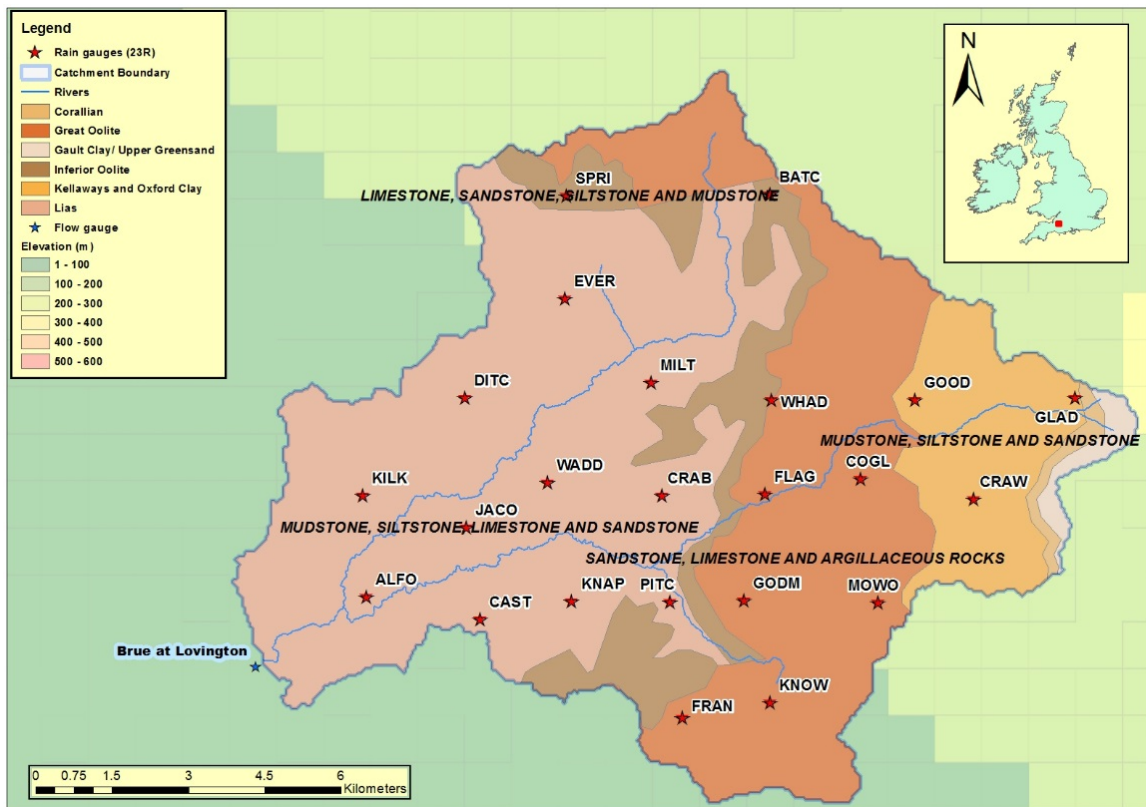


Figure 6-3 - Brue catchment geology, location and gauge network. (Crown Copyright/database right 2016. A British Geological Survey/EDINA supplied service; National River Flow Archive, 2012)

#### 6.4. Initial spatial analysis

Due to the geographical proximity of many of the gauges in the Brue catchment, the most highly correlated gauges were rejected and a network of 23, retaining the geographical spread, was chosen for analysis – the reduced network is shown in Figure 6-3 against the underlying geology of the catchment. A detailed analysis of the effect of the number of gauges and the ability of the inversion process to highlight disinformative sections of data is planned. Early results comparing the results from the full gauge set (49F) with the reduced gauge set (23R) and individual gauges is presented here. Two basic methods of averaging are investigated – simple arithmetic averaging (AV) and Thiessen polygons (TP) where the gauges are weighted by their area of influence. Both methods are well documented (for example, Shaw *et al.*, 2011, p166). Given the number of gauges, the effect of elevation is not included *per se* as it is expected to vary from event to event.

Firstly, the set 23R was compared to the 49F using the GORE (Goodness of Rainfall Estimate - that is, how well the sub-sample represents the true rainfall) and BALANCE (a measure of over/under estimation of the sub-sample with respect to the true rainfall) metrics presented by Andréassian *et al.* (2001) and shown Equation 6-1 and Equation 6-2

$$GORE = 1 - \frac{\Sigma(\sqrt{ER} - \sqrt{TR})^2}{\Sigma(\sqrt{TR} - \sqrt{TR})^2} \quad (\text{Equation 6-1})$$

where ER is the sample rainfall in a single time-step and TR is the corresponding observation from the true (or reference) rainfall. GORE can vary between  $-\infty$  and 1 where 1 indicates that the sub-sample (ER) perfectly represents the true rainfall (TR).

$$BALANCE = \frac{\Sigma ER}{\Sigma TR} \quad (\text{Equation 6-2})$$

If  $BALANCE > 1$ , the sub-set over-estimates, if  $BALANCE < 1$ , the sub-set under-estimates and a value close to 1 indicates a good fit.

Table 6-1 shows the comparison between the TR (49F) and ER (23R) for the two averaging methods and indicates that the reduced network (23R) is a good estimator of the TR as estimated using the full gauge set (49F). For this catchment and gauge set, there is little to choose between the methods. Gauges drawn from set 23R (Thiessen polygon method) are thus used to estimate the average CT transfer function for the catchment.

*Table 6-1 - Validation of the 23 gauge network with respect to the full 49 gauges using the BALANCE and GORE criteria.*

	BALANCE	Percentage over/under estimation	GORE
Arithmetic average	1.005	+0.5%	0.985
Thiessen Polygon	1.004	+0.4%	0.987

## 6.5. Initial Results and Discussion

Models were identified using the observed rainfall series for each individual gauge drawn from set 23R and the catchment outflow then inverted using the regularisation method. In order to compare the inferred and observed rainfall sequences and determine

the time resolution of the inferred sequence, aggregation by sub-sampling at increasing sampling intervals was performed. Nash-Sutcliffe Efficiency ( $R_t^2$ ) was calculated at each interval and the time interval with the closest fit to the observed (aggregated) rainfall (highest  $R_t^2$ ) was taken to be the time resolution of the inferred rainfall (Kretzschmar *et al.*, 2015). The  $R_t^2$  of the aggregated sequence was compared with the  $R_t^2$  of the fitted model and the results plotted in Figure 6-4 indicating that, despite the loss of time-resolution, the results are closely comparable.

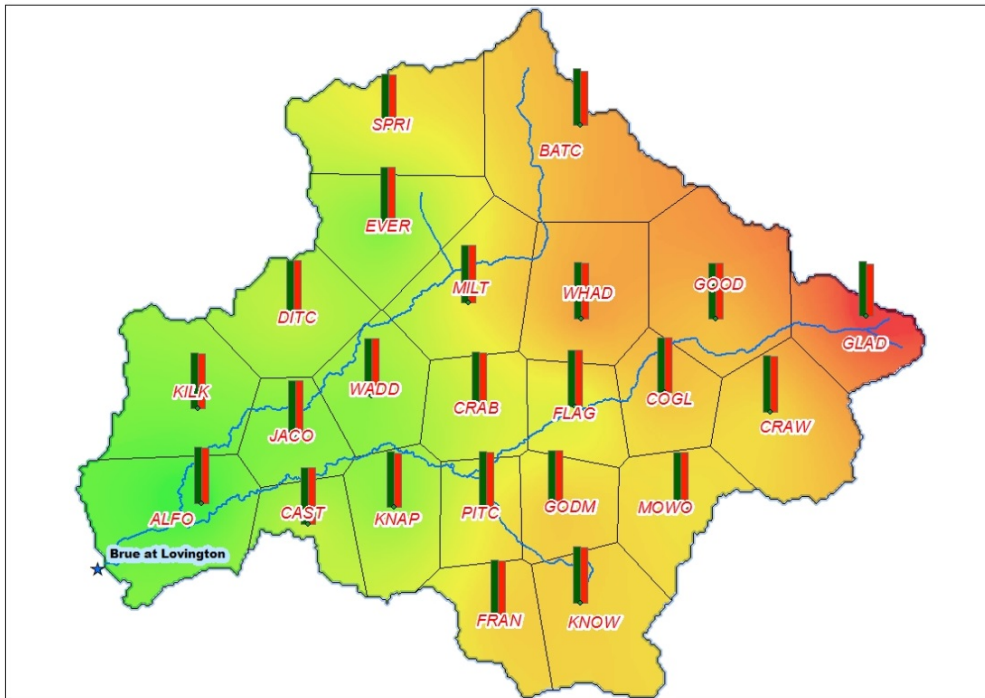


Figure 6-4 - Comparison of modelled  $R_t^2$  (green bars) with inferred, aggregated  $R_t^2$  (red bars) for each individual gauge. (Crown Copyright/database right 2016. A British Geological Survey/EDINA supplied service; National River Flow Archive, 2012)

For all gauges, the aggregation period (estimate of time resolution) of the inferred rainfall sequence is less than the fast time constant ( $TCq$ ) implying that the catchment dynamics are being captured. Flow was generated using the inferred rainfall sequence from each individual gauge. The resulting flow sequences were found to more closely match the observed flow (typically  $R_t^2 = 0.996$ ) than flows generated from models fitted to individual gauges ( $R_t^2 = 0.804$  to  $0.831$ ) or flow generated from a model fitted using the catchment average rainfall calculated from the 23R (TP average) gauge set ( $R_t^2 = 0.852$ ). This is consistent with the results presented in Kretzschmar *et al.* (2015).



Examination of the observed rainfall (top plots in Figure 6-5) shows the variability of the rainfall field across the catchment and emphasises that it can be raining hard in one place whilst it is dry in another (see also Figure 6-1) resulting in artificial spikes in the generated flow - particularly evident in the plot for KILK, one reason why some events can be disinformative when used for model calibration (Beven and Smith, 2015). Further work is planned to investigate the effects of different densities and numbers of rain gauges, identification of disinformative periods of data, and how it might be possible to measure how representative individual gauges or gauge sets are of the catchment as a whole.

## **6.6. Conclusions**

As has been demonstrated, reverse hydrology utilises the information in the streamflow exiting the catchment to infer the rain that has fallen over the whole catchment rather than the amount measured at an individual rain gauge where the latter may not be representative of the total rainfall field and may even lead to spurious spikes in the modelled flow where rain has been measured at the gauge but not elsewhere in the catchment. This technique could deliver an improved estimate of the total rainfall. However, the reduction in uncertainty in the rainfall estimates comes at a price – a reduction in the time resolution of the rainfall series. As has been demonstrated, this is not a problem as long as the resolution is still fine enough to capture the dynamics of the catchment.

Reverse hydrology could be an important tool in developing understanding of catchment rainfall distribution and the processes by which it is converted into streamflow leading to a reduction in uncertainty and an improvement of future flow predictions that might result in saved lives, reduced damage to property and infrastructure and ultimately to decreased costs.

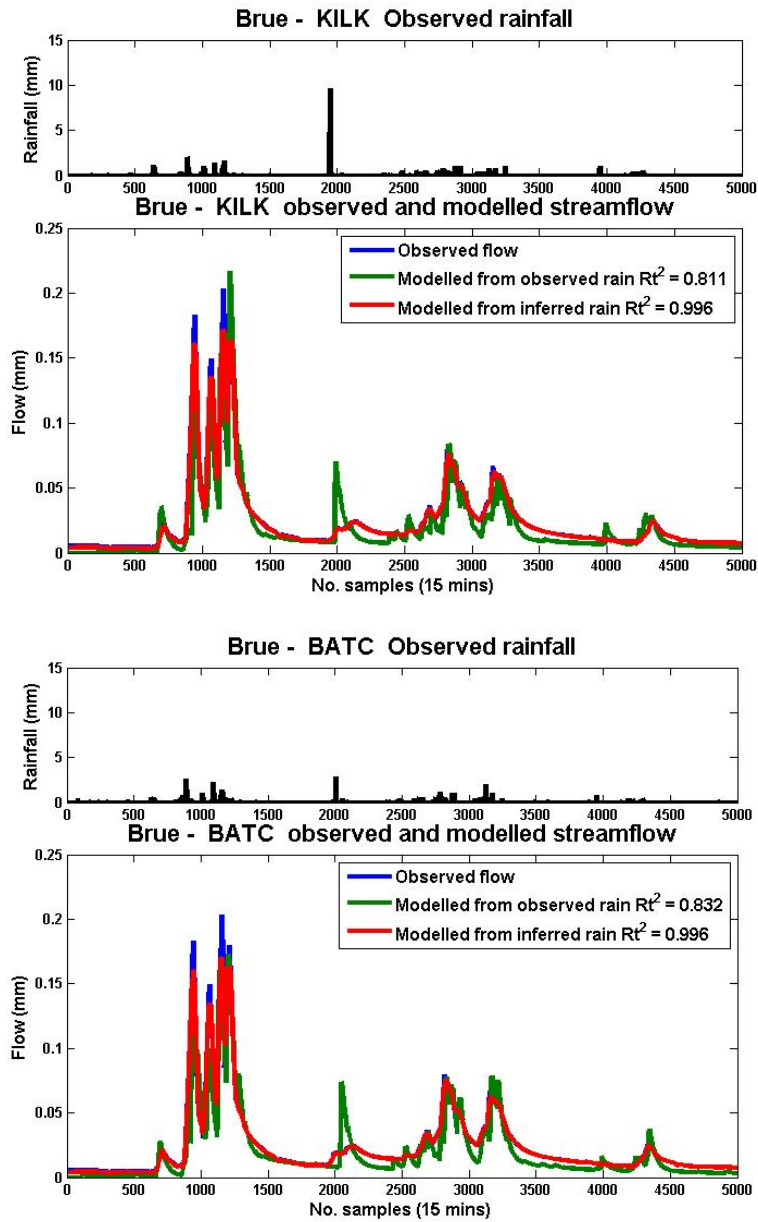


Figure 6-5 - Observed rainfall from example gauges comparing flow generated using the observed and inferred rainfall with the observed flow

## **Chapter 7 Implications of spatio-temporal sampling of a rainfall field when generating a streamflow hydrograph: An investigation of Discharge Generating Rainfall using Reverse Hydrology**

Kretzschmar, A., Tych, W., Beven, K.J. and Chappell N.A.  
Lancaster Environment Centre

### **Abstract**

Prediction of floods requires an accurate estimate of rainfall and despite recent advances in measurement techniques, reliance is still largely on, often sparse, rain gauge networks to supply information on catchment rainfall. The densely instrumented Brue catchment provided the opportunity to develop and evaluate a method for assessing the ability of rain gauge observations to represent the spatio-temporal variability of a rainfall field. A parsimonious model is identified between rainfall observations from individual gauges in a 23-gauge network and the degree of model fit ( $R_i^2$ ) used as a measure of the ‘representativeness’ of the rain gauge. It was recognised that all rain gauges are required to estimate catchment average rainfall, the performance of gauges in terms of discharge generation capability varies with time and space. The part of the rainfall spectrum that generates discharge – Discharge Generating Rainfall (DGR) – can be extracted using the *RegDer* inversion technique proposed by Kretzschmar *et al.* (2014). If DGR is used to generate a flow hydrograph, further knowledge of the spatio-temporal structure of the rainfall may not be required. DGR is the low frequency part of the rainfall spectrum analogous to the low-pass filtering effect of the catchment storage. The high frequency part of the rainfall signal, which has been filtered out, appears to have little or no impact on flow generation.

## 7.1. Introduction

Flood prediction is an uncertain science. Flooding is a worldwide problem affecting the lives and property of thousands each year. There is evidence to suggest that the hydrological cycle is intensifying (Huntington, 2006) however there is ongoing discussion about whether the increase in precipitation is reflected in an increase in peak flows (Kundzewicz *et al.*, 2014). There is no doubt that the UK is in a flood-rich period (Wilby *et al.*, 2008) whether linked to climate change or due to natural variability. Notable events in recent years include Boscastle (2004), Carlisle, Cumbria (2005), Gloucestershire, Sheffield and Hull (2008), Cockermouth, Cumbria (2009), south and south-west England (2013/2014) and most recently Cumbria, Yorkshire and some areas of southern Scotland (2015/2016). These events caused widespread damage to property and infra-structure. Several recent flood events have been linked to atmospheric rivers, elongated belts of high winds and high water vapour, conveying depressions across the Atlantic towards the UK (Lavers *et al.*, 2011). Whatever the cause of the current period of frequent floods, it is important to increase understanding of the processes by which precipitation becomes streamflow in order to aid future planning for prevention and mitigation measures against the devastating effects of flooding. Data-based mechanistic modelling and reverse hydrology are tools which may be used for this purpose.

Streamflow forecasts are based on models, simplified representations of the processes acting within a catchment, whose main input is usually rainfall. The rainfall field, variable in both space and time, is integrated (damped) by the catchment storage, which also may vary in space and time, as it becomes streamflow. Uncertainty is introduced into forecasts from many sources including model selection, model structure, measurement errors in both the inputs and outputs, lack of knowledge of the processes at work and other sources some of which are known about and some of which are not (Beven, 2012b; 2016). Despite improvements in radar coverage, which provides a greater appreciation of the temporal and spatial variations in the rainfall field, much rainfall data still comes from point gauges often at hourly or even daily intervals. It is important to have data at a sufficiently high temporal resolution, too long a time step, particularly in small catchments, may mean that storm and response dynamics are missed. In large catchments, spatial variation is more important and a coarser temporal resolution may be sufficient (Beven, 2012a, p51). Accurate estimates of rainfall input

are important, however there is no consensus on how much effect rainfall errors have on hydrologic systems (Michaud and Sorooshian, 1994a). Troutman (1982, 1983) suggested that large events tend to over-predict whilst small events under-predict. Obled *et al.*, (1994) showed that accurate estimates of total rainfall volume may be more important than spatial variation as the spatial variation may not be organised enough to overcome the damping effect of the catchment. However, knowledge of spatial variation is important when trying to accurately estimate the volume of rainfall over the catchment area.

Reverse hydrology allows an estimate of the rainfall required to get a good prediction of discharge given a forward model derived from one or more rain gauge inputs. The system model is run backwards, that is, instead of using rainfall and the identified model to produce an estimate of streamflow, streamflow is used to infer the rainfall that has generated it using an inverted model. The integrative dynamics of the process mean that it is not feasible to simply fit a model ‘in reverse’ (that is, use streamflow as the model input and rainfall as the output) but a forward model, linking the transformation of rainfall to streamflow, must first be identified and the parameters inverted to obtain a reverse model allowing rainfall to be inferred from streamflow. A poor forward model might indicate that a rain gauge (or combination of gauges) is not representative of the catchment as a whole while the inverted rainfall will implicitly compensate for rain gauge position(s), rainfall variability for specific events and runoff generation in other parts of the catchment etc.

## 7.2. Review

The effects of spatial rainfall patterns on streamflow generation have been extensively studied. Seyfried and Wilcox (1995) suggested that the interactions between processes change with time and space resulting in a picture of great complexity. Segond *et al.* (2007) and Emmanuel *et al.*, (2015) agreed that knowledge of when spatial variability of catchment characteristics and rainfall becomes important is limited by the complexity and the diversity of situations making it difficult to see a clear interpretation. However, they agree with Obled *et al.* (1994) in saying that spatial variability may not be well enough organised to overcome the damping effect of the catchment. If this is the case, then it may not be necessary to include spatial variability in a model as the response will not be greatly improved by the knowledge of the pattern

if there is sufficient knowledge of the volume of the input. Emmanuel *et al.*, (2015) said that measurement errors may have a greater effect than spatial variability while Krajewski *et al.* (1991) suggest that catchment response may be more sensitive to temporal than spatial effects. Many studies agree that sensitivity to spatial influence may be catchment specific (Obled *et al.*, 1994; Singh, 1997; Arnaud *et al.*, 2002; Segond *et al.*, 2007, Wheater *et al.*, 2006) and related to the size and shape of the catchment, catchment properties, for example, soils, geology, topography, land-use that affect flow processes, rainfall regime, storm dynamics (Surkan, 1974), channel morphology and antecedent conditions (Shah *et al.*, 1996). Segond *et al.*, (2007) and Obled *et al.*, (1994) agree that sensitivity to spatial effects may be greatest in urban catchments whilst Michaud and Sorooshian (1994a) found that spatial resolution is a significant factor in semi-arid catchments where any event may cover only part of a catchment area.

Spatial rainfall distribution may influence volume, peak flows and timing of peaks (Arnaud *et al.*, 2002) and, thus, the shape of the hydrograph (Singh, 1997) with the most important effect being on volume (Beven and Hornberger, 1982; Obled *et al.*, 1994). Widespread stratiform events with lower spatial variability can produce significant flow volumes however, particularly in small catchments, the greatest flow volumes come from convective events (Bell and Moore, 2000; Arnaud *et al.*, 2002). Spatial knowledge is more important for extreme or convective events (Michaud and Sorooshian, 1994b, Ajami *et al.*, 2004) or when soils are saturated (Anquetin *et al.*, 2010) whereas low intensity rainfall is not sensitive to spatial averaging (Pessoa *et al.*, 1993). Zoccatelli *et al.* (2010) found that there was a 30% loss of efficiency, when looking at flash flooding in Rumania, if spatial effects were ignored. Studies conducted in the semi-arid Walnut Gulch Experimental Catchment in Arizona, USA showed that even at small scale (4.4 km<sup>2</sup>) representing the rainfall pattern is crucial (Goodrich *et al.*, 1995; Faurés *et al.*, 1995) and demonstrated that assuming uniform rainfall measured at a single gauge can lead to large uncertainties in the hydrograph. They found that four gauges (1 per hectare) predicted realistic hydrographs. Michaud and Sorooshian (1994a, b) used a gauge network with a density of 1 per 20 km<sup>2</sup> to study 24 severe localized thunderstorms concluding that spatial averaging even at small scale could lead to a consistent reduction in flood peaks suggesting that 58% of the error was due to the sparsity of gauge network and half due to rainfall sampling errors.

### 7.3. Aims of the paper

The question this paper will attempt to answer is: What are the implications of sampling the spatio-temporal structure of the rainfall field when generating streamflow taking into account the uncertainties inherent in modelling?

The aims of the paper are defined below:

- A. Evaluate the effect of temporal aggregation on the estimation of the sub-daily statistics of the rainfall field by aggregating measured 15 min measurements at progressively longer time-scales up to 1 day.
- B. Evaluation of the Reverse Hydrology approach on a well instrumented, spatially diverse catchment with a view to reducing the uncertainty in simulated hydrographs. This is achieved by the introduction of the concept of Discharge Generating Rainfall (*c.f.* 7.4) inferred by using Reverse Hydrology as described in chapter 4. Discharge Generating Rainfall (DGR) – based on the rainfall estimated using the Reverse Hydrology, is the part of the broad rainfall spectrum responsible for generating the flow hydrograph.
- C. Identification of misinformative rain-gauges based on the forward and reverse hydrology models' performance. This is achieved by:
  - a. Identification of the 'best fit' model to a series of rainfall and catchment outflow derived from one or more rainfall gauges (an estimate of catchment average rainfall). The goodness-of-fit of the rainfall-outflow model may indicate whether the gauge combination is a good representation of the flow generating processes in the catchment.
  - b. Identification of the 'best fit' model to a series of rainfall and catchment outflow derived from each rainfall gauge (models are unique to the individual gauge). The magnitude of the goodness-of-fit metric ( $R_i^2$ ) provides a measure of the ability of the gauge to represent the flow generating processes of the catchment as a whole.

### 7.4. Reverse Hydrology and Discharge Generating Rainfall

Despite developments in rainfall measuring techniques, reliance is still often on a small number of rain gauges in making inferences and predictions about catchment responses.

In some cases, it has been shown that this can lead to inconsistent input-output data for specific events. Rain gauges measure how much rain has fallen at a point in the catchment but what happens between the gauges can only be estimated by some methods of interpolation. However, hydrologists have long used a method of analysis that equates a cumulative “effective” rainfall with the discharge measured at a catchment outlet, (*c.f.* for example, Boorman, 1989; Chapman, 1996; Croke, 2006). Kretzschmar *et al.*, (2014, 2015) have developed a technique that takes the measured outflow from a catchment and infers the amount of rain that has generated it. Estimating the characteristics of the Discharge Generating Rainfall (DGR) - the rainfall responsible for producing the hydrograph - in this way allows simulation of synthetic rainfall series that may be used in many applications including input to flood forecasting models, in-filling gaps in rainfall records (see chapter 8) and investigation of the importance of the spatial and temporal structure of a rainfall field with respect to streamflow generation.

The dynamic part of the discharge generation process is described by linear, time invariant dynamics, modelled using a continuous time transfer function model, and the rainfall-runoff nonlinearity is modelled using Hammerstein memoryless input non-linearity (*c.f.* Young and Beven (1994) and Beven (2012), for the hydrology perspective, also Wills *et al.*, (2013) for a general system perspective) as shown in Figure 7-1. Systems analysis techniques, implemented using algorithms from the Captain Toolbox for Matlab (*c.f.* Taylor *et al.*, 2007; Kretzschmar *et al.*, 2014), were used to identify a continuous time (CT) transfer function model using high-resolution rainfall and streamflow data to capture the dynamics of the catchment (specifically: functions RIVCBJ and RIVCBJID). The model (or models) thus identified can be inverted using a regularisation approach (*RegDer*) presented in Kretzschmar *et al.* (2014). The output from the *RegDer* process is an inferred rainfall series that is an estimate of the flow generating rainfall, which is termed here: Discharge Generating Rainfall (DGR). The inferred rainfall sequence is the part of the broad rainfall spectrum required to generate discharge and is not generally the same as catchment average rainfall.



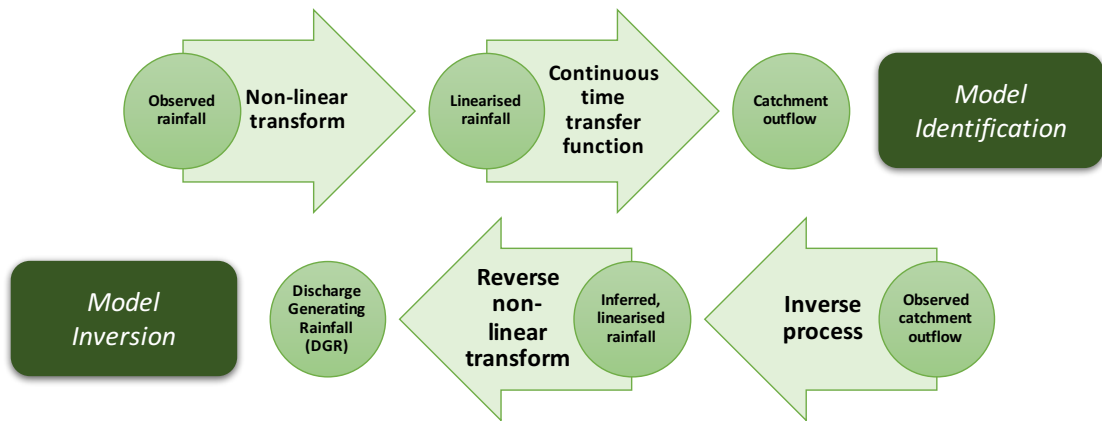


Figure 7-1 - Model identification and inversion workflow showing the off-line linear transformation.

The advantages of using a CT formulation are that a wide range of catchment dynamics can be modelled and the parameters have a direct physical interpretation that is independent of the sampling rate (Young, 2010). The inversion itself is badly posed due to the need to invert processes which have been integrated in both time and space. However, applying the regularisation technique to CT models makes inversion possible without the amplification of the noise present in the data as is the case with direct inversion (Andrews *et al.*, 2010; Kretzschmar *et al.*, 2014). Other approaches are discussed in the referenced literature (Croke, 2006, 2010; Kirchner, 2009; Andrews *et al.*, 2010; Young and Sumislawska, 2012; Brocca *et al.*, 2013, 2014; Kretzschmar *et al.*, 2014, 2015, 2016).

Working with sub-hourly data from two contrasting catchments, Kretzschmar *et al.* (2014) showed that the regularisation process produced a rainfall profile that sacrificed time resolution in favour of numerical stability, resulting from the damping effect of the catchment in both space and time. They showed that this rainfall sequence resulted in modelled flow sequences that fitted the observed streamflow data more closely than flow modelled using the observed rainfall, implying that the dynamics of the catchment were being effectively captured. Further investigation by Kretzschmar *et al.* (2015) made use of sub-sampling and spectral analysis to quantify the loss of resolution and showed that the inferred rainfall sequences were still able to capture the full discharge dynamics to the same degree as the best rainfall-discharge model given the measured rainfall data.

### 7.4.1. Model selection criteria

The routines used for model identification and selection in this study, contained in the Captain Toolbox for Matlab (Taylor *et al.*, 2007) do so on the basis of  $R_t^2$  – the Nash-Sutcliffe Efficiency (*NSE*) – and the Young Information Criterion (*YIC*) proposed by Young (1984). (*c.f.* section 2.6.2). The *NSE* is based on the coefficient of determination Equation 7-1 and is given by:

$$R_t^2 = 1 - \frac{\sum_{i=1}^N (Q_o^i - Q_m^i)^2}{\sum_{i=1}^N (Q_o^i - \overline{Q_o})^2} \quad (\text{Equation 7-1})$$

where  $Q_m$  is the modelled value and  $Q_o$  the observed value at  $i$ .  $\overline{Q_o}$  is the mean of the observed series. It can range between  $1 > R_t^2 > -\infty$  where 1 indicates a perfect fit. A value of 0 indicates that the model performs no better than using the average of the observed data. Negative values mean performance is worse than using the average (Blöschl *et al.*, 2013).

The Young Information Criterion (*YIC*) is an objective measure combining model fit with a measure of over-parameterisation. It is given by:

$$YIC = \ln \frac{\sigma_r^2}{\sigma_o^2} + \ln\{NEVN\} \quad (\text{Equation 7-2})$$

where  $\sigma_r^2$  and  $\sigma_o^2$  are the variances of the residual series and observed series respectively and NEVN (the normalised error variance norm) is given by:

$$NEVN = \frac{1}{np} \sum_{i=1}^{np} \frac{\sigma_r^2 P_{ii}}{a_i^2} \quad (\text{Equation 7-3})$$

where  $np$  = the number of parameters,  $P_{ii}$  is the  $i^{th}$  diagonal element of the parameter covariance matrix and  $a_i^2$  is the square of the  $i^{th}$  parameter. The first term is a measure of how well the model fits the data and the second is a measure of parameterisation. A large negative value indicates a good fit with lowest number of parameters necessary to capture the system dynamics. *YIC* is a compromise between model fit and model complexity (Young *et al.*, 1996).

A third criteria, introduced because it is important to not just have a good fitting forward model but one that inverts well, is  $R_t^2$  measuring the fit of the inferred rainfall series,  $IR_t^2$ . Final model choice was based on  $R_t^2$  (as high possible), *YIC* (large negative value

preferred) and the ability of the inverted model to recover the rainfall ( $IR_i^2$  as large as possible).

### **7.5. Case study – Brue Experimental Catchment, South-west England**

This study utilises the heavily instrumented Brue catchment in South-west England. It has 49 rain gauges in an area of 135.2 km<sup>2</sup> enabling spatial as well as temporal variability in the rainfall field to be investigated. Outflow from the catchment is measured at a single flow gauging structure, a crump weir, at Lovington. Weed growth down-stream in the summer has an effect on the stage-discharge relationship however all except the highest flows are contained within the section (NRFA, 2012). There is an elevation change of approximately 300m from south-west to north-east across the catchment and the underlying geology is a combination of mudstone and limestone with a limestone ridge running in an arc from north to south across the eastern upland area (see Figure 7-2). The catchment can largely be split into impermeable low-land to the west, higher land to the east where the limestone ridge is permeable, and the far east of the catchment which is largely impermeable. Land use is mostly pasture on clay soils with some woodland on the elevated eastern side. The Brue research catchment was set up in 1993 as part of a Natural Environment Research Council (NERC) special topic research programme – the Hydrological Radar Experiment (HYREX) (Wood *et al.*, 2000). It ran for three years but the data has been extensively used in many subsequent research projects (for example, Wood *et al.*, 2000; Moore *et al.*, 2000; Bell and Moore, 2000; Villarini and Krajewski, 2008; Villarini *et al.*, 2008).

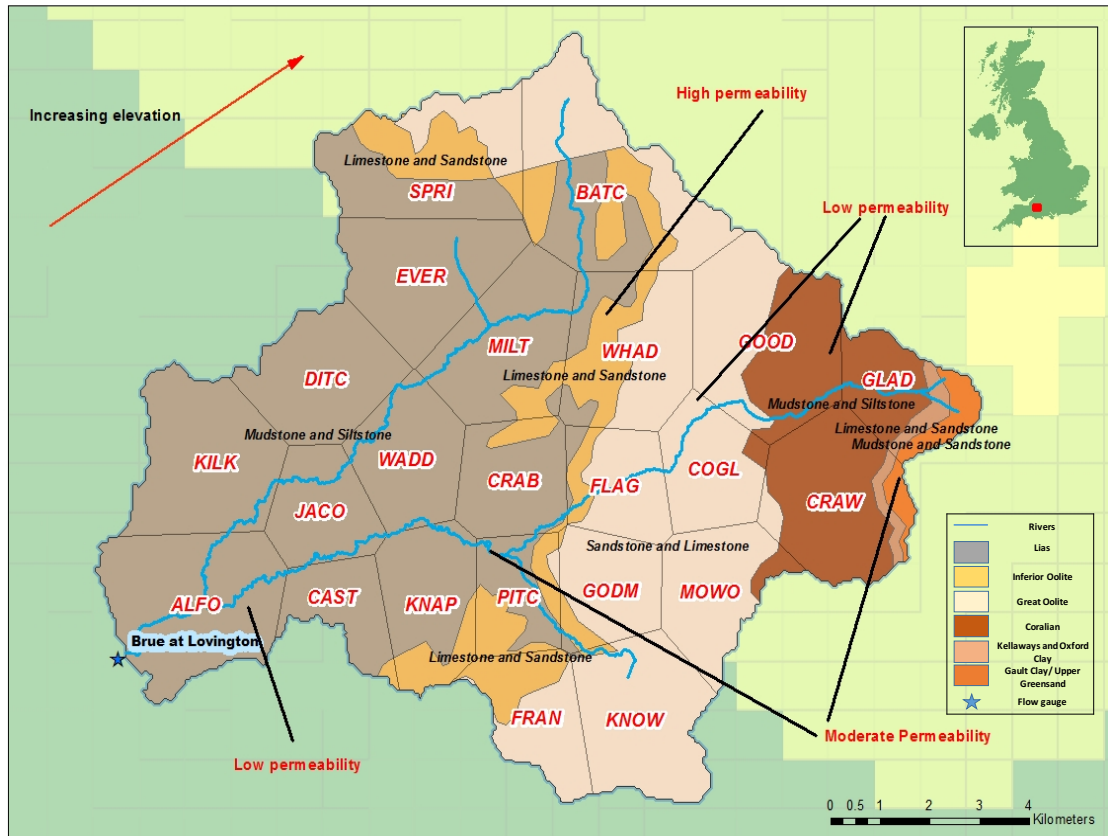


Figure 7-2 - Brue catchment showing location of 23 gauges used in the study and the underlying geology. (Note that this map is also used elsewhere in a different context, so is provided here for clarity.)

Rainfall and flow data sampled at 15 minute intervals for 23 rain gauges selected from the 49 available from the Brue catchment and a single flow gauge at the catchment outlet (station 52010, NRFA, 2012) for the period October 1994 to September 1997 (3 years) were used in this analysis. The 23 gauges selected maintain geographical coverage whilst reducing the inter-gauge correlation (see Figure 7-3). Kretzschmar *et al.* (2016) justified the reduction of the study gauge network from 49 to 23 gauges and showed that an estimate of catchment average rainfall obtained from 23 gauges is within 0.4% of that obtained from 49 gauges using the Thiessen polygon method. Figure 7-3 shows a plot of correlation against distance between each pair of gauges indicating that correlation increases as inter-gauge distance decreases and justifying the removal of gauges in close geographical proximity. The rainfall measured at each gauge was used to calculate the catchment average rainfall. It is reasonable to assume that the density of the gauge network (1 gauge per 5.9 km<sup>2</sup>) is enough to give good estimate of the true catchment rainfall (termed here CAR).

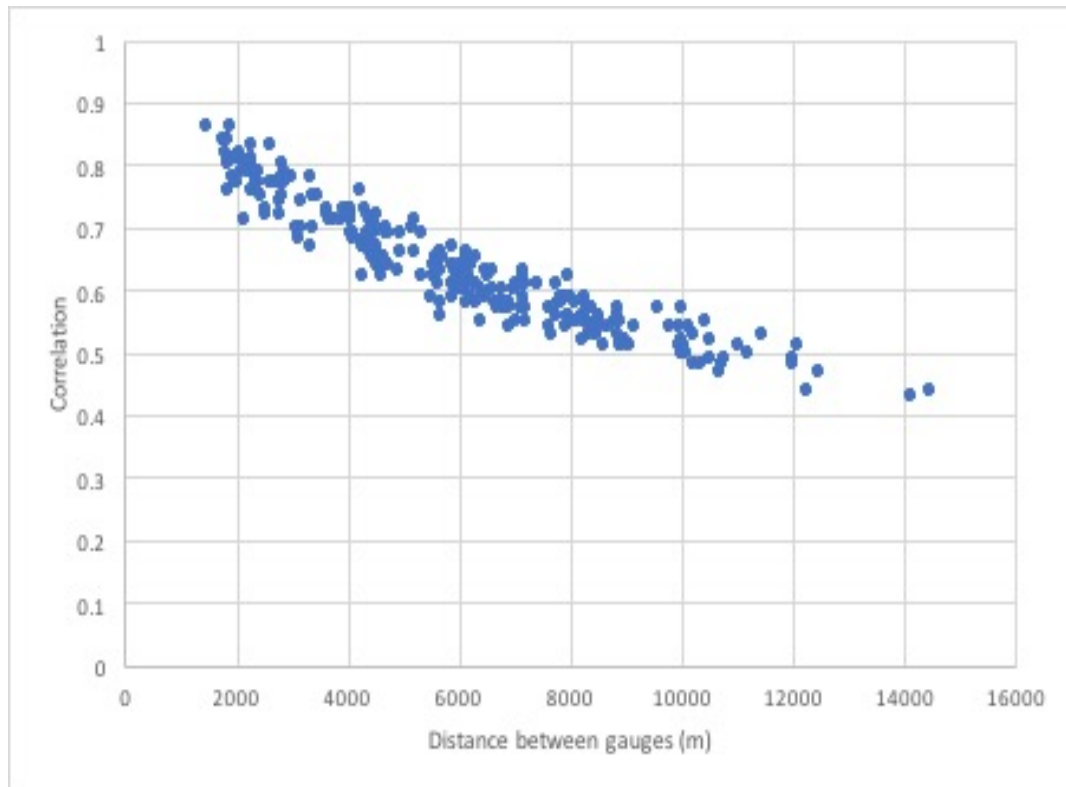


Figure 7-3 - Correlation against distance between gauge pairs for the Brue catchment. As expected, correlation decreases as distance between gauges increases providing justification for removing highly correlated gauges in close geographical proximity

## 7.6. Annual data

Figure 7-4 shows plots of the catchment average rainfall and Figure 7-5 catchment outflow for the 3 years under consideration (October 1994 to September 1997) and illustrates the year on year temporal variability. Both WY1 (October 1994 - September 1995) and WY2 (October 1995 – September 1996) have wetter winters and drier summers whereas WY3 (October 1996 – September 1997) has a wetter summer than winter. Rainfall is more variable in WY1 than WY2 and WY3. Discharge patterns show even greater differences. Both WY1 and WY2 have wet winters whilst flow in WY3, although greater in the winter, occurs in distinct events that can be related to the rainfall patterns though this is less obvious in the summer months despite the average rainfall differing little between winter and summer. In WY1 and WY2, summer rainfall only has significant effect on the streamflow when an event is both large and of some duration, for example, September 1995. Short-lived convective events, for example, November 1995 and June 1996 generate only relatively small increases in flow.

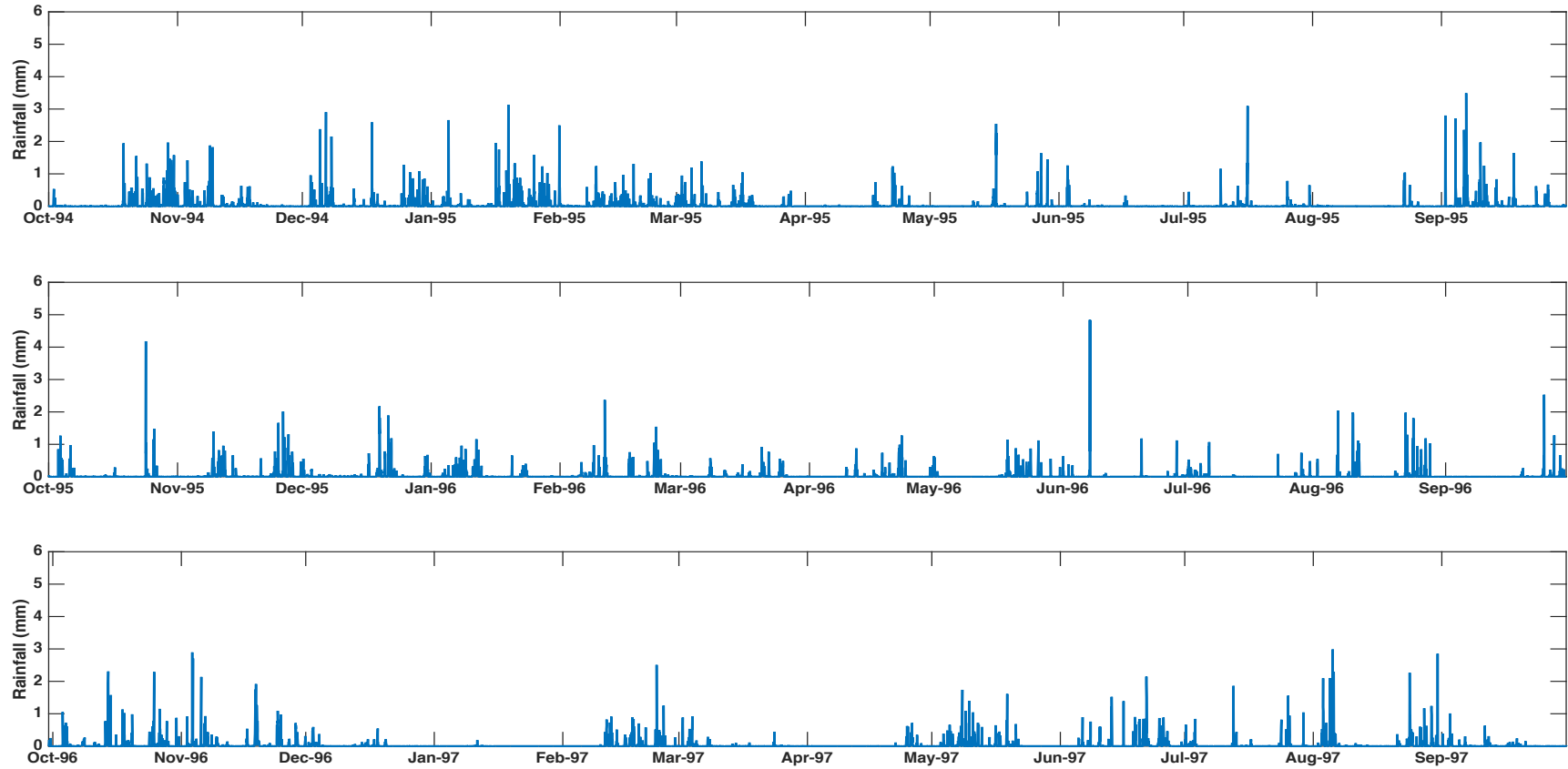


Figure 7-4 - 3 years of catchment average rainfall data sampled at 15 minute intervals for the Brue catchment plotted as water years - October 1994 to September 1997. Differences between years and between seasons are evident from these plots and from the statistics shown in Table 7-1

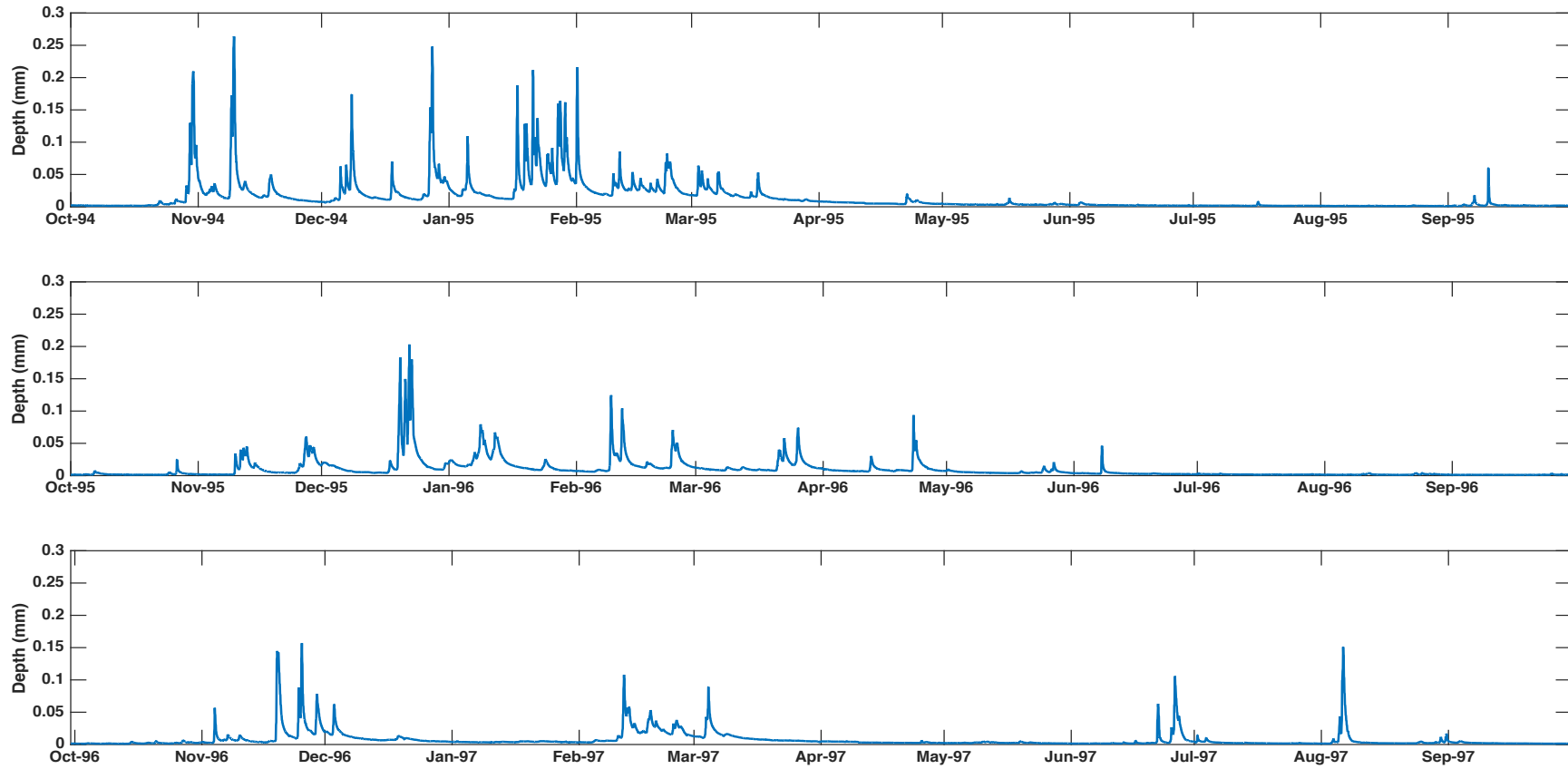


Figure 7-5 - 3 years of flow data sampled at 15 minute intervals for the Brue catchment plotted as water years - October 1994 to September 1997. Differences between years and between seasons are evident from these plots and from the statistics shown in Table 7-1.

Table 7-1 lists the statistics of the catchment average rainfall for each water year and the summer and winter seasons studied. The runoff coefficient (RC) indicates how much rainfall is being converted to flow. The RC varies from year to year and season to season with greatest contrast between seasons being in WY1 when 75% the rainfall is converted to flow in winter but only 18% in summer. The pattern is the same but not so extreme for the other years.

Table 7-1 – Characteristics of the rain by water year and summer/ winter season for October 1994 – September 1997

Rainfall (mm)	WY1			WY2			WY3		
	Annual	Winter	Summer	Annual	Winter	Summer	Annual	Winter	Summer
Mean	0.026	0.036	0.017	0.021	0.026	0.017	0.020	0.019	0.022
Standard deviation	0.128	0.138	0.116	0.114	0.113	0.114	0.111	0.103	0.118
Skewness	10.3	7.9	14.1	14.6	10.9	18.2	11.2	11.6	10.8
Kurtosis	160.0	97.3	277.4	387.9	223.2	548.8	181.1	200.8	164.5
<b>Flow (mm)</b>									
Mean	0.015	0.027	0.003	0.010	0.015	0.004	0.007	0.011	0.004
Standard deviation	0.025	0.031	0.003	0.015	0.019	0.005	0.013	0.015	0.009
Skewness	4.3	3.4	7.8	4.9	3.9	6.9	5.5	4.4	8.9
Kurtosis	18.1	18.1	131.7	37.6	23.8	76.7	42.9	30.4	96.6
<b>Runoff Coefficient</b>	0.57	0.75	0.18	0.46	0.60	0.25	0.37	0.58	0.19

### 7.7. The effect of aggregation on rainfall structure

Rainfall variability decreases as sampling interval increases (Shaghagian and Abedini, 2013) and the correlation between topography and rainfall increases (Bárdossy and Pegram, 2013). Table 7-2 shows the effect of increasing the sampling interval (by aggregation) on the characteristics of the rainfall over the 3 years studied for the Brue catchment. Aggregation is a basic form of low-pass filtering so links with the loss of time resolution due to regularisation and the filtering effect of the catchment. The most



striking features are the decrease in variability as illustrated by the change of distribution, demonstrated by a decrease in standard deviation with increasing sampling period (see Figure 7-6a), the consistency in the lag-1 autocorrelation (see Figure 7-6b), the increase in the proportion of wet time periods and the decrease in maximum rainfall intensity. Lag-1 autocorrelation is consistent at a sub-daily level but at longer aggregation periods the familiar decrease may be observed until it disappears completely (Chandler *et al*, 2006; Wilderer, 2011).

Table 7-2 - The effect of increasing sampling period from 15 mins to 24 hrs on the statistics of rainfall structure for the 3 water years studied (October 1994- September 1997).

	Sample period	Mean (mm)	Standard deviation (mm/hr)	Skew	Kurtosis	Lag1 ACF	Median (mm)	Proportion wet time periods	Max intensity (mm/hr)
WY1	15 min	0.026	0.51	10.3	160.0	0.759	0.000	0.19	14.8
	1hr	0.104	0.26	5.35	47.4	0.760	0.009	0.58	4.6
	6hr	0.625	0.10	2.21	11.1	0.724	0.475	0.99	0.9
	12hr	1.250	0.07	2.03	10.3	0.740	1.057	1.00	0.66
	24hr	2.501	0.05	1.39	6.19	0.726	2.280	1.00	0.39
WY2	15 min	0.021	0.46	14.6	387.9	0.760	0.000	0.17	20
	1hr	0.085	0.24	7.61	108.1	0.774	0.003	0.50	5.5
	6hr	0.508	0.10	3.26	22.0	0.765	0.347	0.99	1.00
	12hr	1.016	0.06	2.41	13.1	0.714	0.862	1.00	0.51
	24hr	2.032	0.04	1.67	7.34	0.705	1.844	1.00	0.29
WY3	15 min	0.020	0.44	11.2	181.1	0.765	0.000	0.17	11.6
	1hr	0.081	0.22	5.59	47.1	0.760	0.009	0.52	3.00
	6hr	0.489	0.09	1.95	7.82	0.777	0.291	0.99	0.67
	12hr	0.977	0.06	1.25	4.52	0.773	0.810	1.00	0.34
	24hr	1.954	0.041	0.74	3.36	0.745	1.831	1.00	0.22

The change of distribution shape is also characterised by skewness and kurtosis reduction with increasing sampling period (see Figure 7-6c and d). The lag-1 autocorrelation shows a slight increase in variability with increasing sampling interval but the pattern is not consistent year-on-year (Figure 7-6b). The proportion of wet time periods increases with increased sampling interval because rain in any 15-minute period within the sampling interval will cause it to be classified as a wet-period. This would imply that if sampling period is 6hrs or more, it appears to be wet all the time. Perhaps a change in definition needs to be applied, for example, a threshold value greater than 0 for a time period to be classified as wet. The maximum rainfall intensity decreases as sampling interval increases (see Figure 7-6f) because the same amount of rainfall is

spread over a longer time-period. This is a characteristic which may be of importance when the differences between frontal and convective rainfall events are considered, as it is likely that more rain will fall in low intensity frontal events lasting for a longer period of time, than in the short lived, high intensity convective events with the consequential effect on runoff.

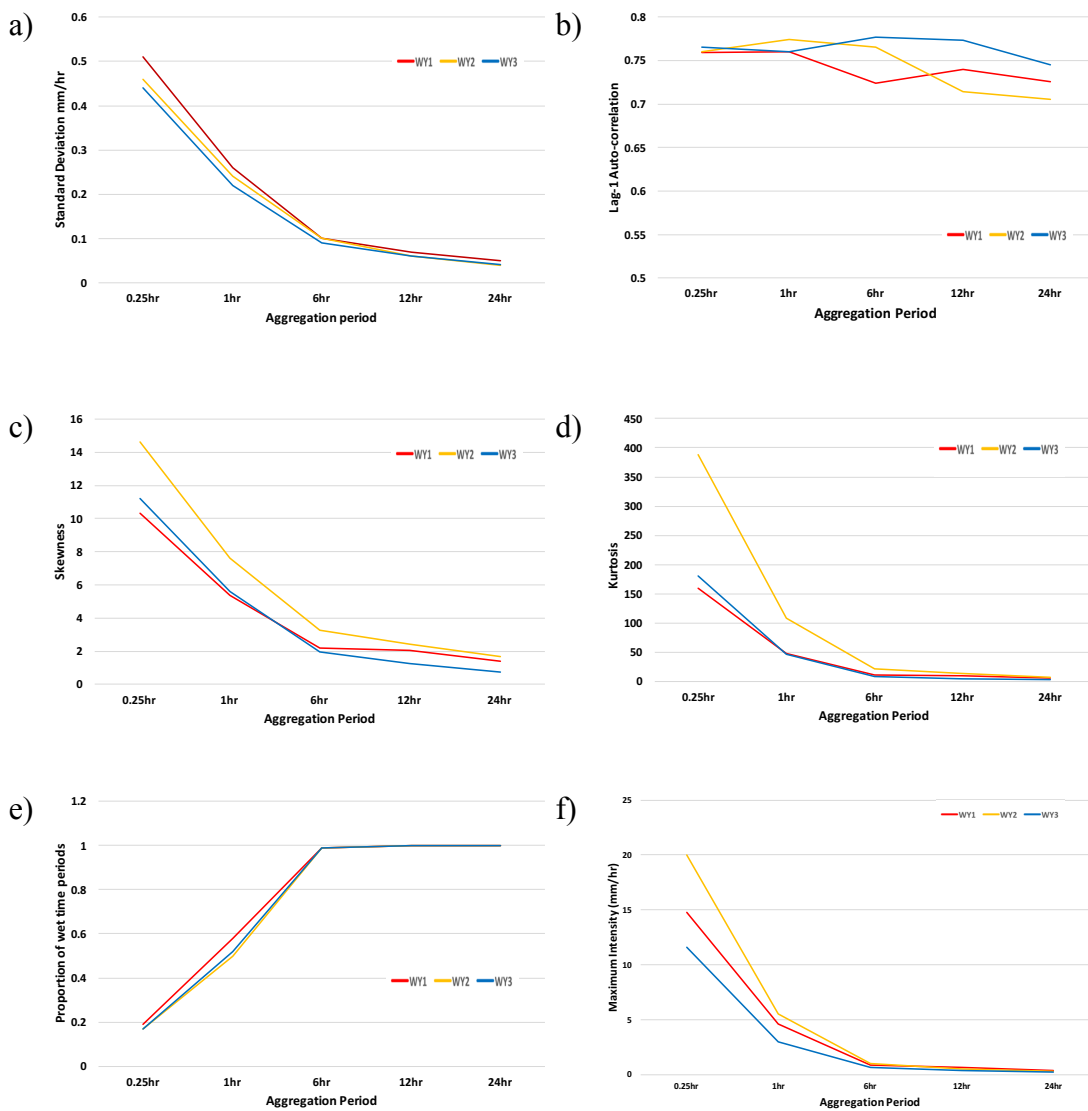


Figure 7-6 - Key characteristics of the rainfall series showing the effect of increasing sampling period a) Standard deviation (mm), b) Lag-1 auto-correlation coefficient c) Skewness d) Kurtosis e) Proportion of wet time periods f) Maximum intensity (mm/hr)

### 7.8. Comparison of catchment average rainfall with rainfall at individual gauges

Catchment average rainfall is estimated by spatial averaging of rainfall measured at rain gauges in an, often sparse, network by methods such as simple averaging, Thiessen polygons, inverse distance weighting or kriging (Shaw *et al*, 2011). The density of the rain gauge network in the Brue catchment (23 gauges in 135.2 km<sup>2</sup>) has the potential for calculating a good estimate of the catchment average rainfall. Kretzschmar *et al.* (2016) compared estimates for the Brue calculated using the Thiessen polygon (TP) and simple averaging (AV) methods. The estimates were within 0.1% but, as the TP method weights gauges by their area of influence, it was used to calculate catchment average rainfall in this study. The eastern side of the catchment is of a higher elevation than the west (see Figure 7-2) and there is evidence of some orographic effect (increased rainfall) however the density of the gauge network means it does not need to be explicitly considered.

The high density and geographical distribution of rain gauges in the Brue catchment enabled the comparison of rainfall measured at individual rain gauges with the averaged catchment rainfall. In practice, the catchment average rainfall would not be available so rainfall measured at the individual gauges must be used to estimate it. DBM modelling provides a method for assessing how much reliability can be placed on a gauge or gauge set with respect to estimates of CAR and the rainfall driving the catchment discharge.

Uncertainty may be introduced by the spatial and temporal variability of the rainfall field. Rain may be recorded at one (or more) gauges that does not affect the outflow or there may be observed changes in the flow although no rain is recorded. This may be because rain falling between the gauges is not measured but still enters the river system and affects the catchment outflow. Simulating a hydrograph from the recorded rain may show peaks where none occur in the observed hydrograph or may show evidence of missing rainfall. A hydrograph simulated using DGR very closely matches the observed hydrograph because DGR is only the part of the rainfall spectrum that drives discharge generation. High frequency rainfall that has little effect on the generation of flow has been filtered out by the *RegDer* process in the same way that the catchment acts as a

low-pass filter. Uncertainty in the generated hydrograph has been reduced (*c.f.* section 7.8). Therefore, in one context, using the model output driven by DGR can be seen as circular reasoning, while, in the present context of hydrograph uncertainty reduction, it is a ‘cleaned-up’ discharge signal. As stated in section 7.4, CAR and DGR are not generally the same. CAR is an estimate of the areal average rainfall over the whole catchment whilst DGR is an estimate of the part of the rainfall signal that generates the flow.

Rainfall at each individual gauge together with the catchment average rainfall and the number of gauges where rain was recorded are shown for an example period in Figure 7-7. The plot shows the temporal variability in the rainfall at each gauge (SGR) and the spatial variability, indicated by the number of gauges where rain is measured, and the variation in the magnitude at each time period. Comparing the CAR with the SGR shows how averaging the rainfall across the catchment lowers the peaks and increases the number of time periods with rain. For example, rain occurs at all gauges around the 24th October at similar intensities so averaging only reduces the peak by a small amount however there are occasions where all gauges experience rain but some only receive small amounts while others receive much higher amounts thus the resultant average is much lower than the peak intensity when this amount is spread evenly over the catchment. This has implications for the representativity of individual gauges at that time. CAR estimates the amount of rainfall over the catchment but does not say anything about the spatial distribution or which area of the catchment is driving discharge generation.

Gauges represent an area of the catchment which may not have any relationship to the Thiessen polygon used in the averaging method. The area of representation will be influenced not just by rainfall distribution but by the distribution of catchment characteristics, for example, topography, soils, geology and land use, although characteristics of rainfall events, for example, size, cell size, intensity and direction of movement, will also have an effect. All gauges are generally used to estimate the CAR but not all contribute equally to discharge generation at any given time. The implication of this is that although the depth of rainfall when spread over the catchment may be correct, the catchment average series may not be representative of the catchment flow generation processes. The fit of the best model identified from CAR against outflow

can only give an indication of how well CAR describes the catchment processes, on average, over that time-period.

Study of the box plots in Figure 7-8 shows the mean of the catchment average rainfall (black +) is in the middle of the means of the individual gauge sequences however, all the remaining quantities show a bias where the value for the catchment rainfall is either above or below the individual values. The distributions of the statistics vary from year to year however the bias in the characteristics of the CAR with respect to the characteristics of the rainfall from the individual gauges remains similar.

In practice, it is likely there would be between one and three rain gauges in a catchment the size of the Brue (135.2 km<sup>2</sup>) – the UK average is 1 gauge per 76 km<sup>2</sup> (Met. Office, 2010). The rainfall sequence from each single gauge or combination of gauges could be used as an estimate of the catchment average rainfall, but how representative can it be assumed to be? The box plots in Figure 7-8 indicate that the individual sequences are biased estimators of the catchment average due to spatial averaging. However, there are many sequences of rainfall that can generate almost identical hydrographs. Identification of gauges supplying non-representative information is based on the performance of the forward and reverse hydrological models measured by comparing simulated hydrographs. A poor forward model performance suggests that the gauge or gauge combination may not be representative of the catchment processes as a whole with respect to flow generation.

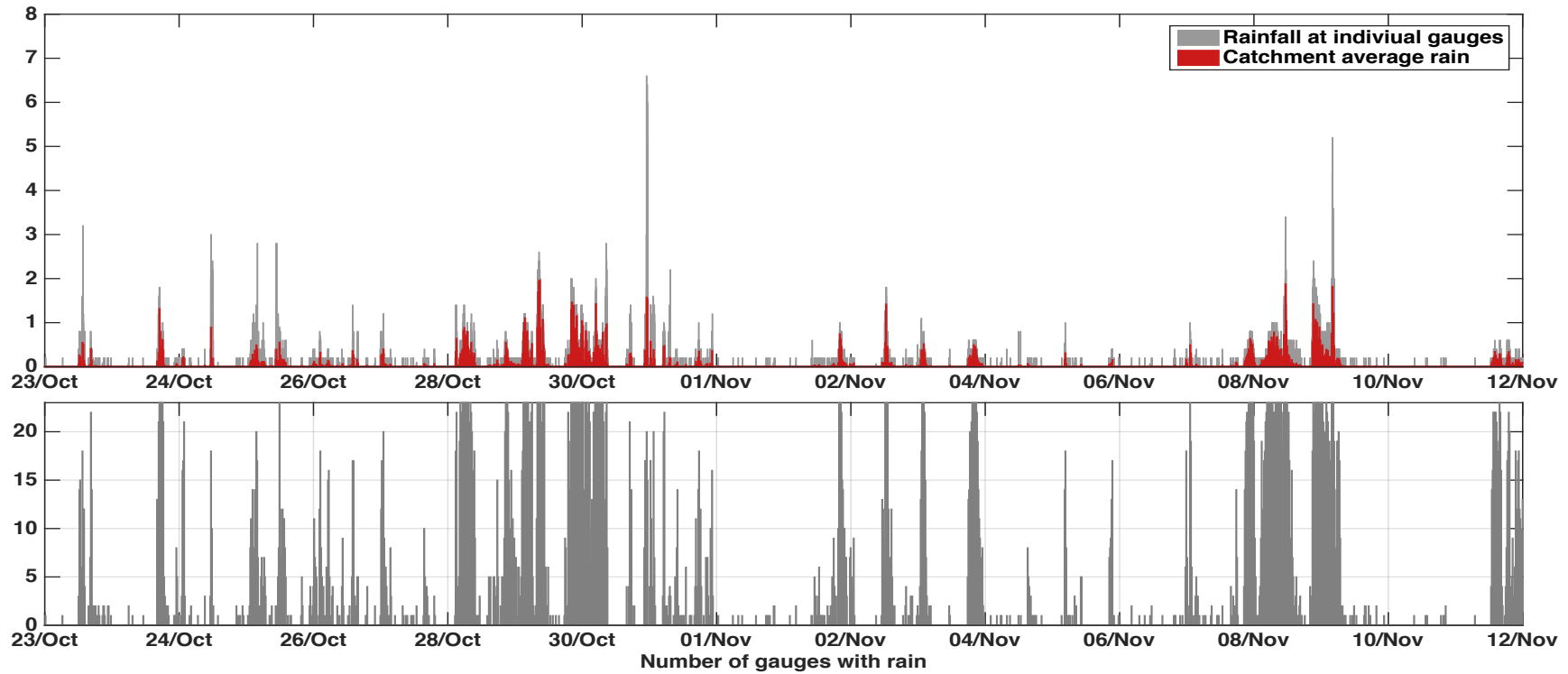


Figure 7-7 – Top plot – An example of rain at individual gauges (grey bars) over-plotted with catchment average rain (red bars); Bottom plot – the number of gauges with rain measured at each time period. The plots given an idea of the temporal and spatial variation in rainfall and illustrate how spreading rainfall evenly over the catchment lowers the rainfall peaks. This maybe the case even when all gauges have rain if some gauges have high rainfall and others low

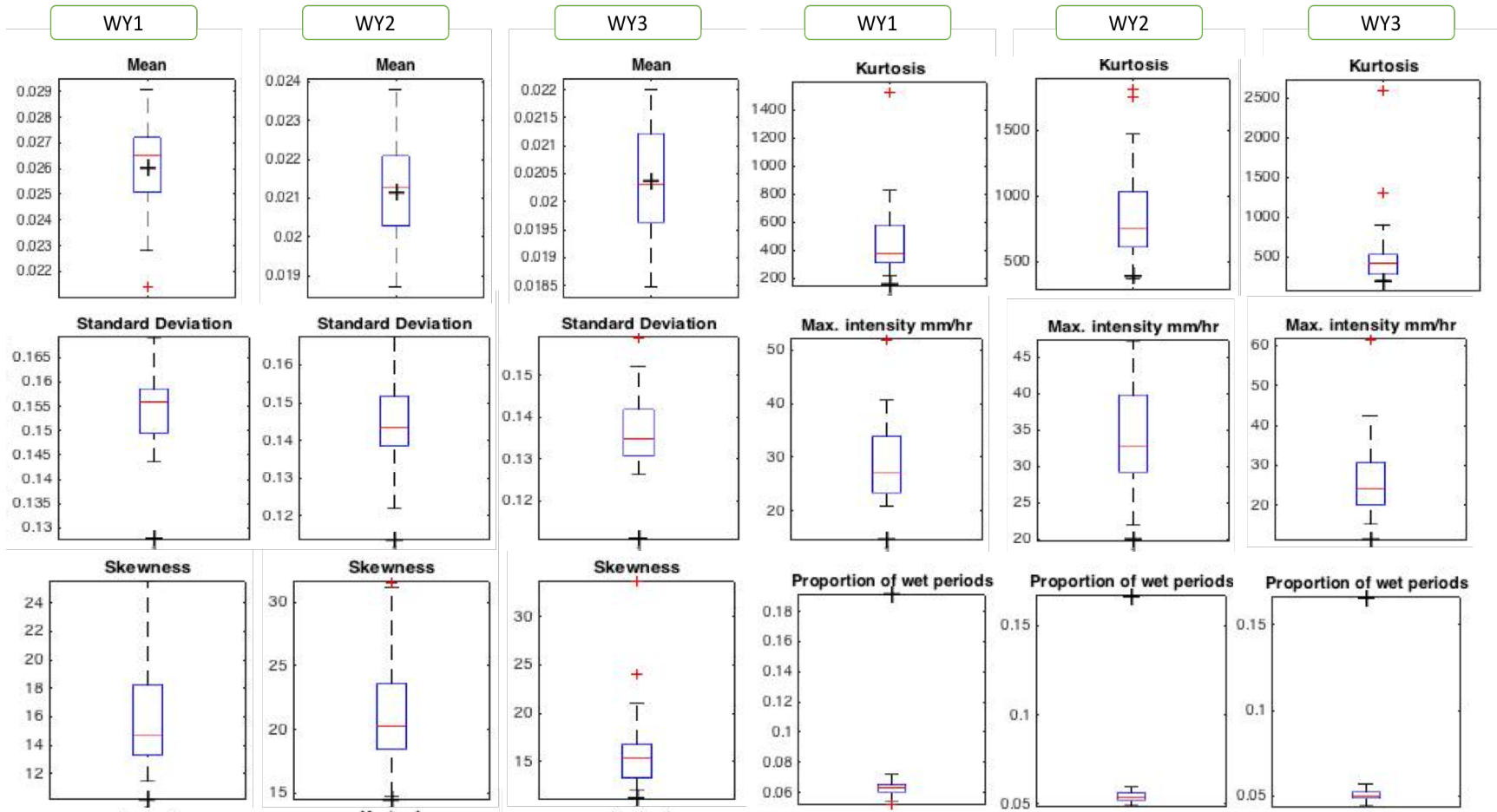


Figure 7-8 – Box plots of the 4 basic statistics, maximum rainfall intensity and proportion of wet time periods for the 23 gauges across the Brue catchment sampled at 15 minute intervals. The catchment average value is shown as a black +

All gauges contribute rainfall to the catchment average but not all gauges contribute equally to the rainfall that generates the flow, and this can change over time. Using a dense network of gauges to estimate the catchment average should give a good estimate of the depth of rainfall spread over the whole catchment but that rain may not be representative of the rainfall generating the discharge hydrograph. Identification of misinformative gauges can be made by modelling the rainfall measured at each one with the catchment outflow and comparing its performance with the observed hydrograph (which is the same whatever gauge or gauge combination is used). Any uncertainty in the discharge, for example, due to weed growth (NRFA, 2012) will apply equally to all gauges so comparisons for the same time-period should remain valid. The value of the goodness-of-fit metric ( $R_t^2$ ) gives some measure of the confidence that the rainfall measured at a gauge or averaged over a gauge-set is representative of the rainfall driving discharge generation over that time period. This method could be applied to groups of gauges, for example, pairs of gauges where each gauge individually shows a poor fit (is not representative) but the two together are representative (show a good fit).

The variance based  $R_t^2$  and Least Squares methods and their derivatives favour model performance at peaks, not in recessions and lower system output levels so a log transform may be used to gain additional information on the performance of each gauge. This may be obtained by calculating  $R_t^2L$ , which is defined as  $R_t^2$  calculated from a log transform of the data.  $R_t^2$  is calculated using the square of the differences between the observed and simulated data (see Equation 7-1) and consequently gives extra weight to the peak flows. Taking logs of simulated and measured discharge series used to calculate  $R_t^2$  flattens out the higher values whilst having little effect on the lower ones (Krause *et al.*, 2005) resulting in lower values having more weight. Thus, a combination of  $R_t^2$  and  $R_t^2L$  may be used to assess how well a model fits different parts of the hydrograph, for example, high  $R_t^2$  with a low  $R_t^2L$  suggests that the peaks are being matched well but recessions and low flows not so well; low  $R_t^2$  combined with high  $R_t^2L$  implies a model that fits low flows but may not be so good at fitting the peaks. If both  $R_t^2$  and  $R_t^2L$  are high, the model fits well over the whole range of the hydrograph. Robust measures, based on absolute, not quadratic objectives, exist, but are less frequently used.



### 7.9. Model fitting and hydrograph generation

Models were fitted, using DBM modelling techniques as outlined in section 7.4, to both CAR and SGR and the observed catchment outflow ( $Q_{obs}$ ). Hydrographs generated from these models were compared with the observed hydrograph. The observed hydrograph can be used to evaluate differences in the modelled hydrographs because it remains constant whichever rain gauge or combination of gauges supplies the rainfall input series. Hydrograph shape is dependent on both climatic and physical factors (Montesarchio *et al.*, 2015) with the recession limb generally influenced by the characteristics of the catchment and features such as time-to-peak, runoff volume and peak runoff influenced by climatic factors including the spatio-temporal distribution and the state of the catchment, for example, soil moisture. Differences between the generated and observed hydrographs may be due to differences in the rainfall structure and variations in the processes responsible for transforming rainfall into flow between the individual gauges and the catchment average (variability in both space and time) given that the catchment rainfall, filtered by the catchment processes drives the hydrograph generation process. It is assumed that the essential characteristics of the non-linear dynamics of the catchment processes do not vary whilst the rainfall input varies with time when calculating the average.

The aim of the modelling exercise is to reproduce the observed hydrograph. It might be expected that the best fit might be achieved by using all available rain gauges especially for the example catchment where the gauge density is high however as discussed in section 7.8, this may not be the case because, although the rainfall contribution is being made equally to the catchment average, this may not apply to the flow generation processes where one area of the catchment may dominate. Examination of the model fit statistics (see Table 7-3) shows that the identified models fit the calibration period well at least when the peaks are considered.  $R_t^2$  values range from 0.908 in WY1 to 0.790 in WY3. Performance of models fitted for one year perform less well when used for other years but the performance is still acceptable with  $R_t^2$  ranging from 0.877 when the WY3 model is applied to WY1 to 0.703 when the WY2 model is applied to WY3. The evidence that a model fitted to data from one year gives acceptable performance in other years indicates that the catchment response year-on-year may not be as different as it appears from the plots in Figure 7-4.

As discussed in section 7.8, the fit of the simulated hydrographs to the observed is measured by the  $R_t^2$  and  $R_t^2L$  metrics. The  $R_t^2$  values show that in WY1 and WY2 fit to the hydrograph peaks is good however WY3 does not fit quite so well. The fit to the recessions and low flows is not so good as reflected in the  $R_t^2L$  values. Particularly WY3 shows a very poor fit to the lower flows and recessions – see Figure 7-9. Examination of the hydrographs and hyetographs show that the missed peaks correspond to low values in the calculated catchment rainfall probably caused by spatial averaging.

Table 7-3 - Goodness-of-fit measures for individual models for each year between observed hydrograph and hydrograph modelled from catchment average rainfall and cross-validation results for each period. All models perform reasonably well in each period when reproducing peaks ( $Rt2$ ). Low flows are reproduced well for WY1 and WY2 but not for WY3 ( $Rt2L$ )

	Calibration period					
	WY1		WY2		WY3	
Validation period	$Rt2$	$Rt2L$	$Rt2$	$Rt2L$	$Rt2$	$Rt2L$
WY1	<b>0.908</b>	0.893	0.725	0.836	0.877	0.838
WY2	0.742	0.835	<b>0.837</b>	0.811	0.793	0.806
WY3	0.744	0.479	0.703	0.438	<b>0.790</b>	0.339

Volume is maintained but rainfall peaks are lowered because the rain is being spread to a uniform depth over the whole catchment area supporting the argument that the spatial pattern is important when generating streamflow hydrographs in contrast with, for example, Obled *et al* (1994). This conclusion may, however, be catchment dependent. In other cases, there are peaks in the generated hydrograph not present in the observed hydrograph that match peaks in the calculated rainfall probably caused by rain at one part of the catchment but not another that does not directly affect the flow – see Figure 7-10 for more detail. Cross-validation plots are shown in Appendix B.

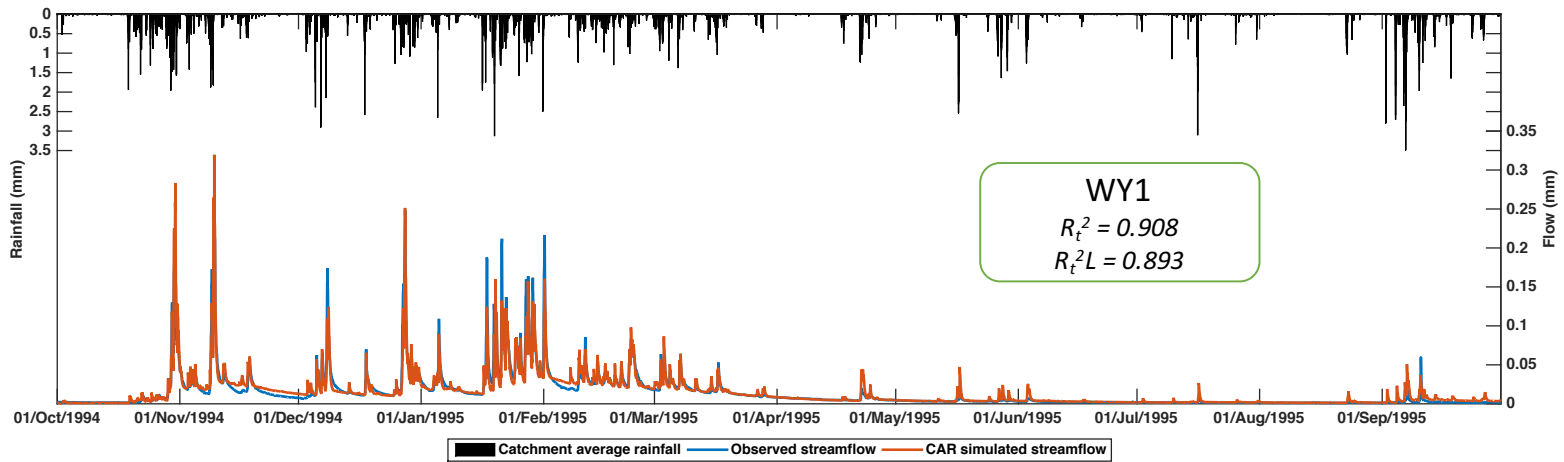


Figure 7-9a – Hyetographs (catchment average rainfall) and observed and simulated hydrographs for WY1 (using best model identified). The modelled hydrograph (red line) shows differences from the observed hydrograph (blue line). The modelled hydrograph matches both peaks and recessions well ( $R_t^2=0.908$  and  $R_t^2L=0.839$  although some differences are apparent highlighting the weaknesses in using  $R_t^2$  as a performance measure. Peaks are visible in the modelled hydrograph that do not occur in the observed hydrograph corresponding with rainfall peaks which do not influence the hydrograph.

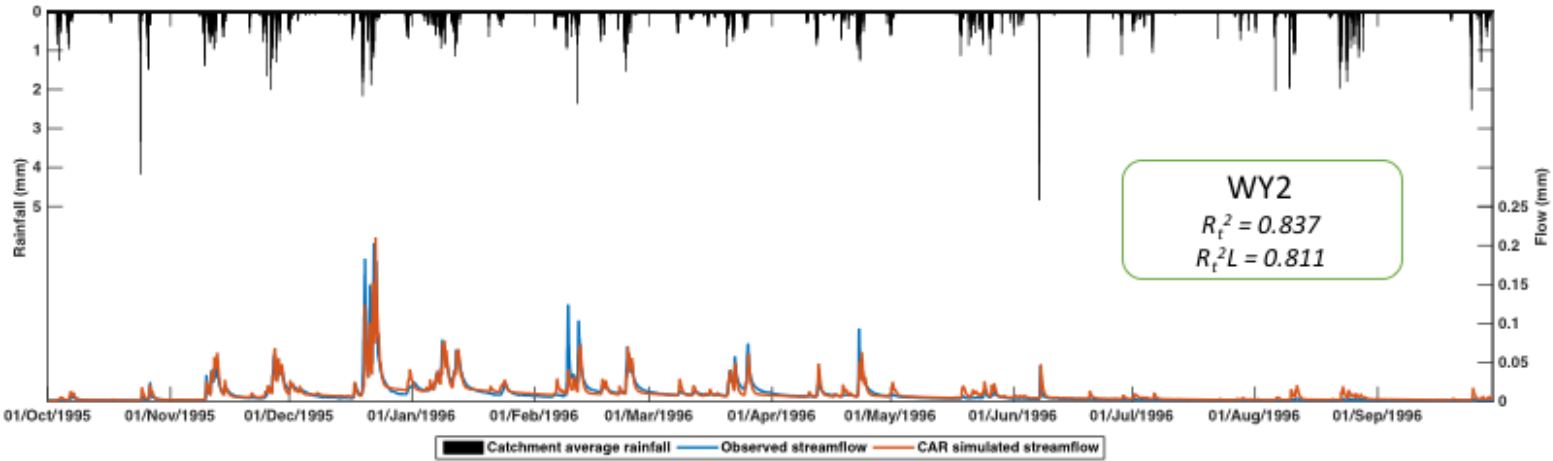


Figure 7.9b – Hyetographs (catchment average rainfall) and observed and simulated hydrographs for WY2 (using best model identified). The modelled hydrograph (red line) shows differences from the observed hydrograph (blue line). The modelled hydrograph matches both peaks and recessions well ( $R_t^2=0.837$  and  $R_t^2L =0.811$  although some differences are apparent highlighting the weaknesses in using  $R_t^2$  as a performance measure. Peaks are visible in the modelled hydrograph that do not occur in the observed hydrograph corresponding with rainfall peaks which do not influence the hydrograph.

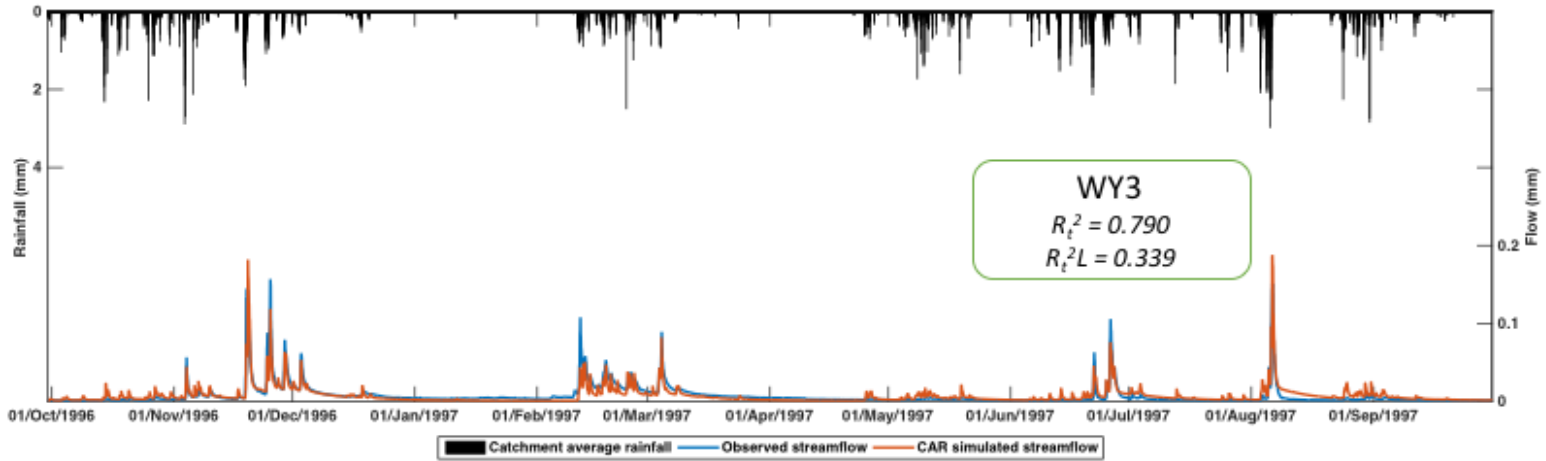


Figure 7.9c – Hyetographs (catchment average rainfall) and observed and simulated hydrographs for WY3 (using best model identified). The modelled hydrograph (red line) shows differences from the observed hydrograph (blue line). The modelled hydrograph matches peaks well ( $R_t^2=0.790$ ) however the recessions are very poorly matched as can be seen by the value of  $R_t^2L$  (0.339). Some differences in the peaks are apparent highlighting the weaknesses in using  $R_t^2$  as a performance measure. Peaks are visible in the modelled hydrograph that do not occur in the observed hydrograph corresponding with rainfall peaks which do not influence the hydrograph. An enlarged section of the hydrograph (late February) showing the both missing and extra peaks is shown in Figure 7-10

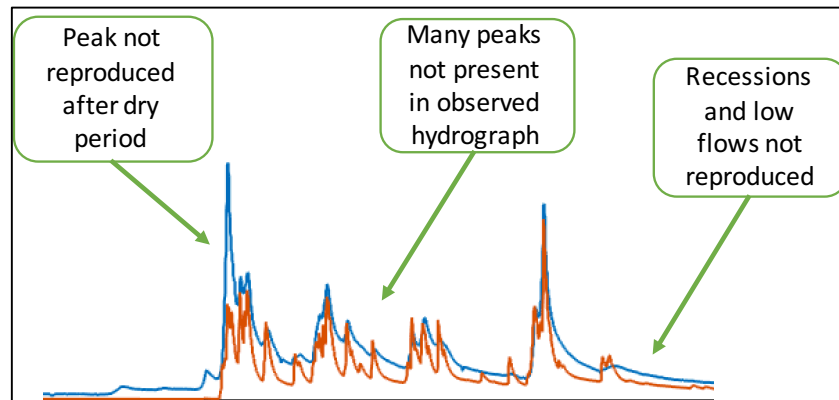


Figure 7-10 - A short section of hydrograph from WY3 showing missing peaks, extra peaks and badly reproduced recessions in more detail (blue: observed flow; red: predicted flow using CAR input)

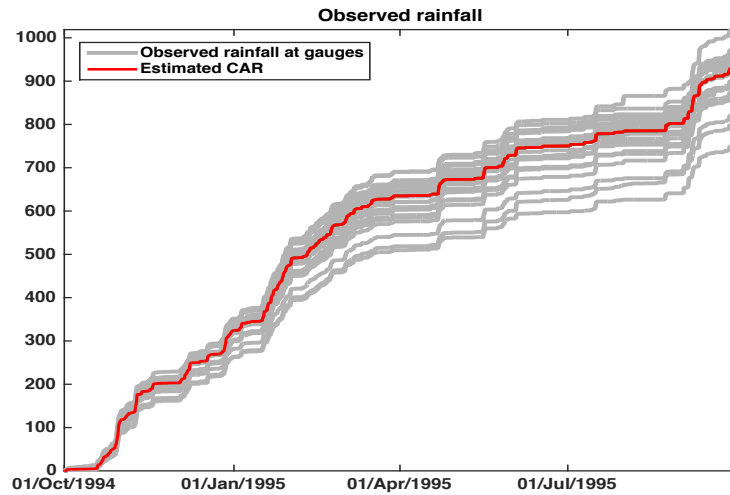
A model that fits the catchment average rainfall - outflow combination well indicates that the rainfall sequences from the gauges used to calculate that average, whether that be from one gauge, a few gauges or more, are likely to be representative of the catchment flow generation processes as a whole. If the fit is poor, then the data used to fit the model is poor in the sense that it is not representative of the rainfall-runoff transformation. Averaging is a linear process and, although various averaging methods, for example, Thiessen polygon, inverse distance weighting or kriging (Shaw *et al.*, 2011), make some attempt to take non-linearities into account, the weighting of different gauges changes with time. Thiessen Polygons attempt to weight the rainfall at a gauge by its area of influence (related to the distance between the gauges and thus the spatial resolution) however that area bears no relation to the distribution of topography, geology or soils within the catchment and is, thus, not directly related to the processes operating in the catchment that transform rainfall into streamflow. Different gauges will dominate under different conditions. Rainfall data which does not represent the flow generation processes is likely to result in a poor model. This may be due to data from some of the gauges used to estimate the average being non-representative. The modelling process attempts to compensate for errors inherent in the calibration of the forward model but if the data is too non-representative, this is unlikely to be enough to identify a model that describes the transformation of rainfall-runoff well. Investigation of the fit of models to the individual gauge rainfall and catchment outflow (which will be the same no matter which rainfall series is combined with it to identify a model) combinations may reveal which gauges have non-representative rainfall for that period.

### 7.10. Rainfall variation at single gauges

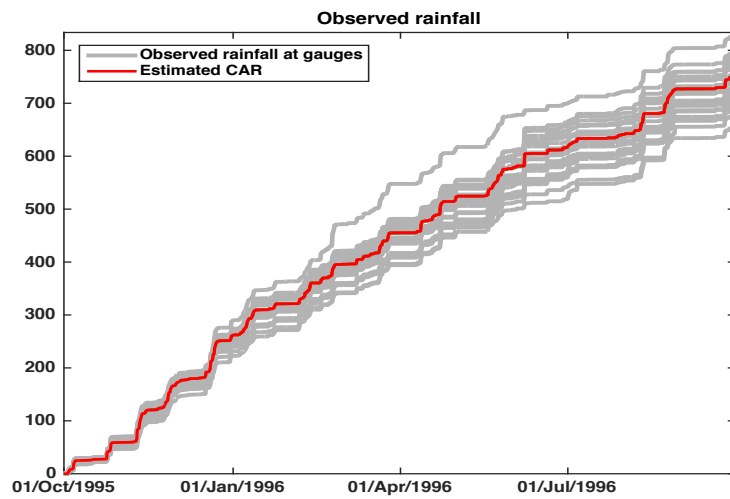
The rainfall distribution over the Brue catchment for each of the 3 water years studied is shown in the maps in Figure 7-12. Total rainfall is highest in WY1 and lowest in WY3. Some evidence of increased rainfall at higher elevations to the NE of the catchment is evident. Lowest rainfall occurs closest to the catchment outlet. The range of rainfall at each gauge compared with the catchment average is shown as cumulative plots in Figure 7-11.

The best model was identified for each gauge rainfall-flow combination, using the method described in section 7.4, and the fit examined to determine how representative the model is likely to be. How well the simulated hydrograph compares to the observed hydrograph indicates how representative the rainfall measured at that gauge is of the overall rainfall-flow transformation for that period. The time element is important as the dominant gauge(s) will change with time due to the rainfall regime (convective or frontal), the track of storms and the size and position of internal storm cells as well as conditions within the catchment, for instance, does the rain follow a dry period? Examination of Figure 7-13 shows a range of possible hydrographs could be generated dependent on the rainfall-flow combination used. Again, some peaks are overestimated, peaks occur where none were observed and recessions are sometimes not well represented. Any uncertainty in the flow estimates, for example, due to weed growth affecting the stage-discharge relationship (NRFA, 2012), will be present in all models as the same discharge is always combined with each of the different rainfall series for the time period. Examples of overestimation can be seen in Figure 7-13a around 1<sup>st</sup> January; of over-estimation of the peak and poor fit to the recession in Figure 7-13b also around 1<sup>st</sup> January where a peak not present in the observed flow also occurs. It can also be seen that that these features vary with the gauge used to measure the rainfall. Around May 1997 (WY3), a flow event shows in the individual hydrograph plots that is not present in the catchment outflow.

a: WY1



b: WY2



c: WY3

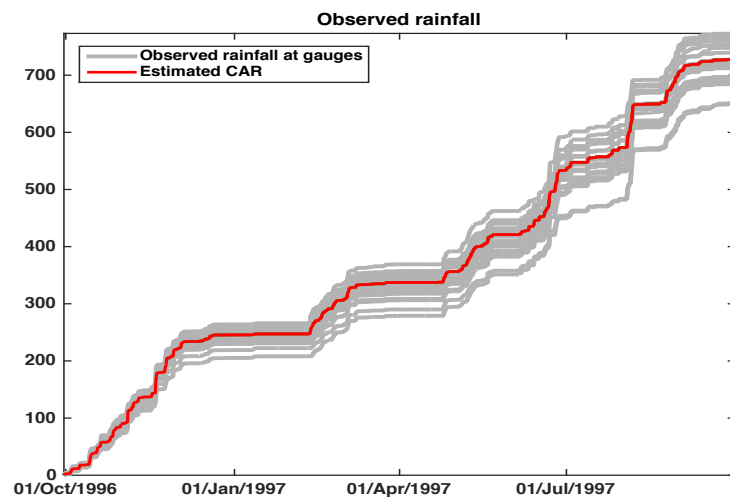


Figure 7-11: Cumulative rainfall for each water year. Variation in temporal patterns can be seen as changes in the shape of the CAR plot (red line). The grey lines show the cumulative rainfall measured at each gauge. The shape and range indicate how both spatial and temporal patterns vary from gauge to gauge and from year to year.



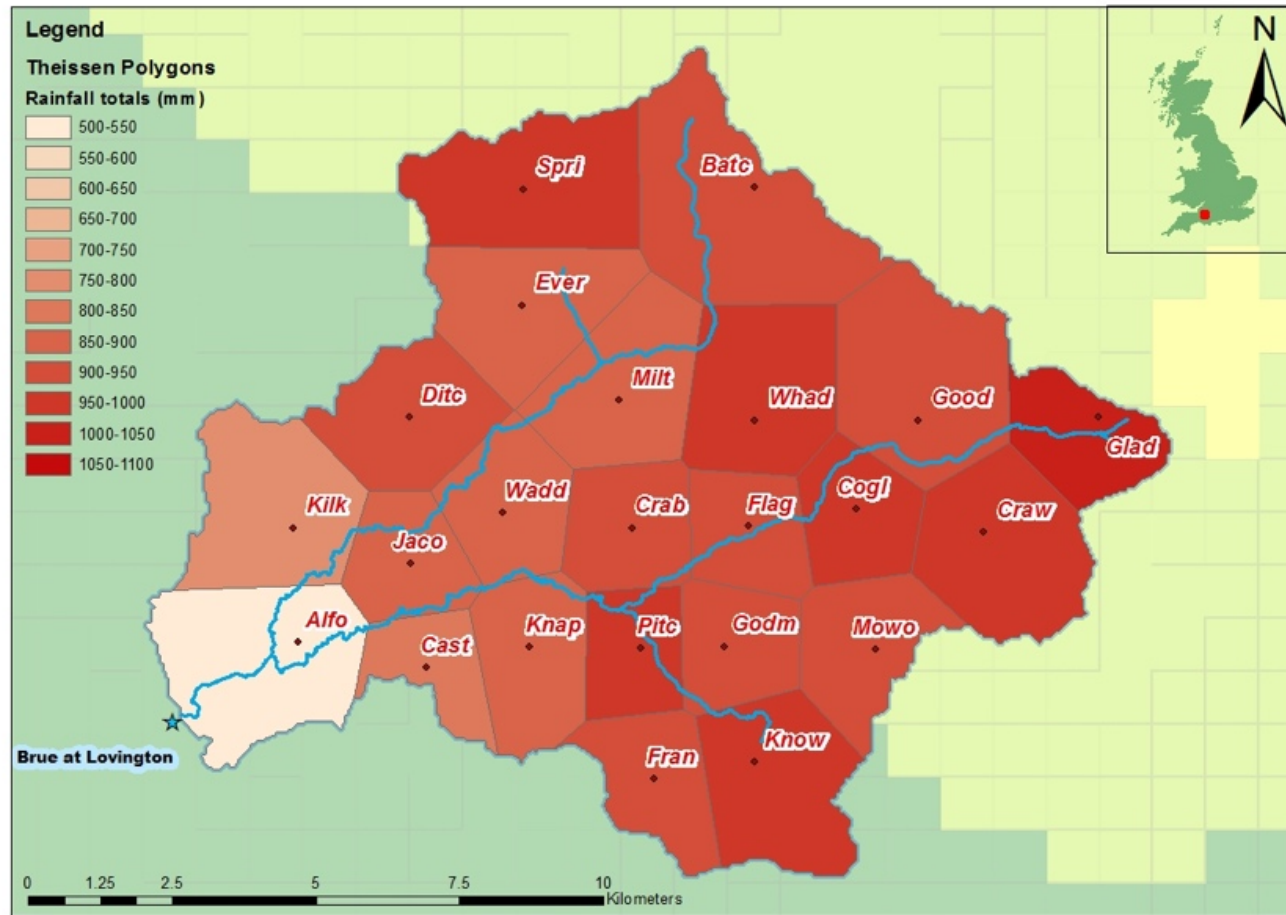


Figure 7-12a: Total rainfall over the Brue catchment in WY1 by gauge. The Thiessen polygons are coloured according to the rainfall at the gauge. Highest rainfall is on the higher ground to the north-east and lowest close to the catchment outlet.

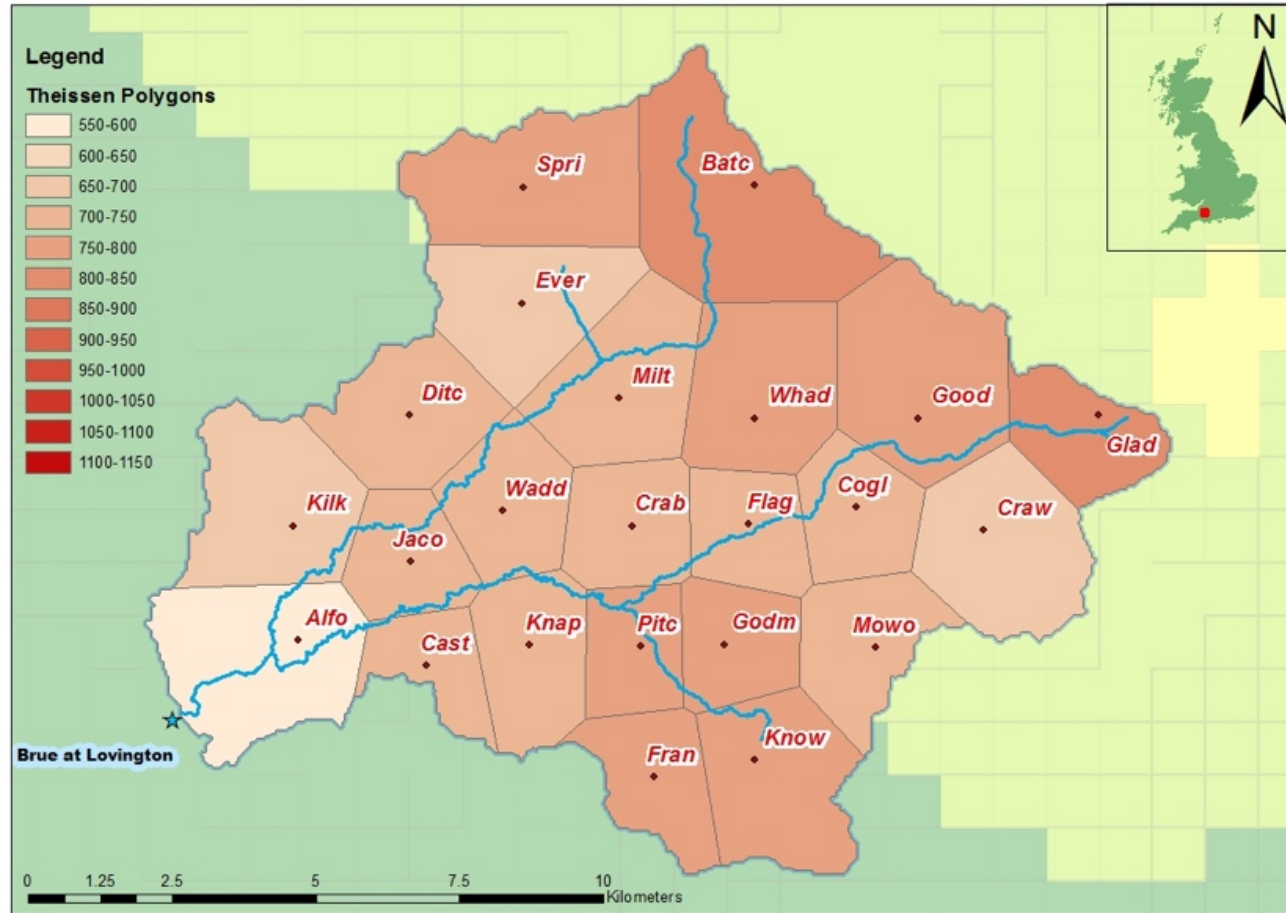


Figure 7-12b: Total rainfall over the Brue catchment in WY2 by gauge. The Thiessen polygons are coloured according to the rainfall at the gauge. Highest rainfall is on the higher ground to the north-east and lowest close to the catchment outlet.

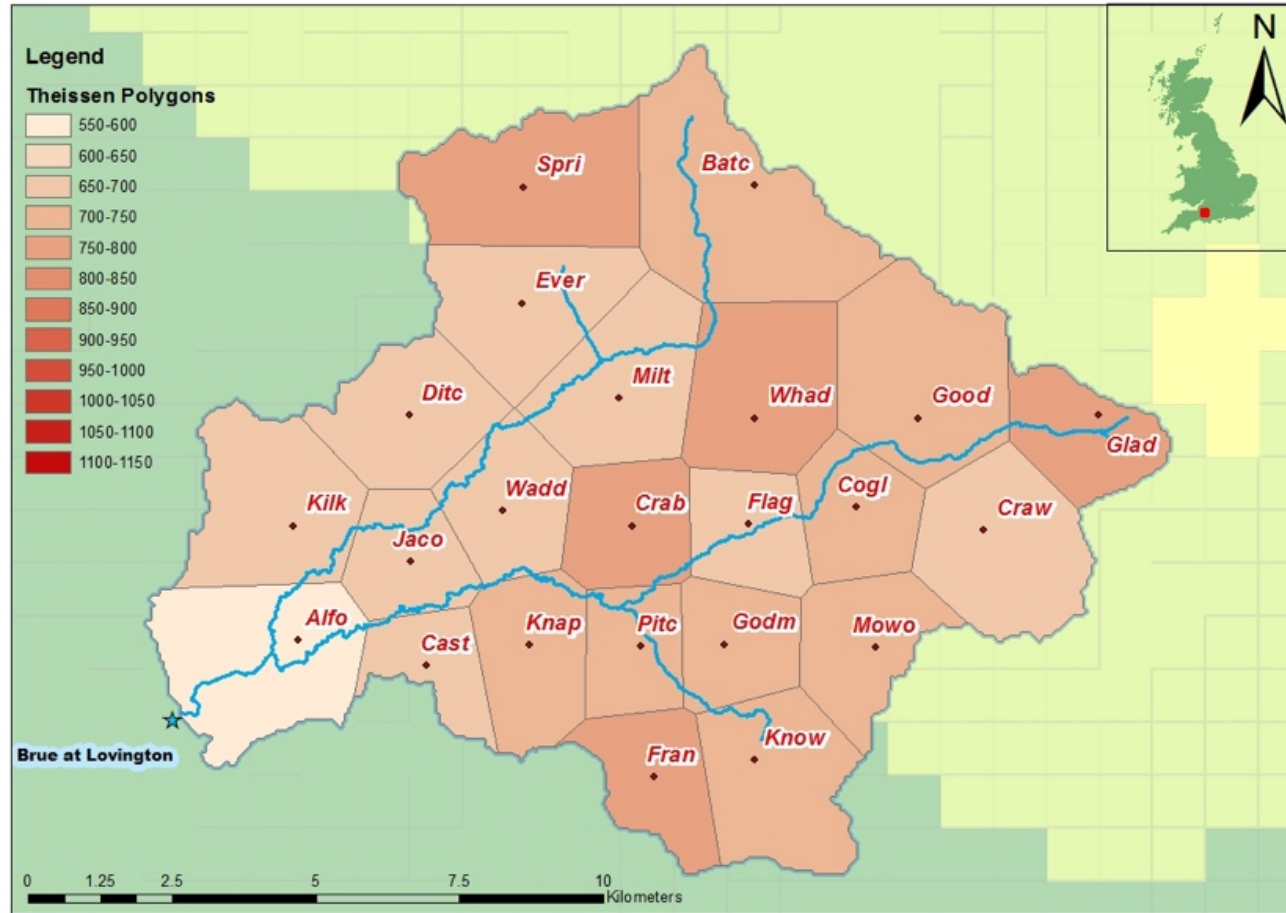


Figure 7-12c: Total rainfall over the Brue catchment in WY3 by gauge. The Thiessen polygons are coloured according to the rainfall at the gauge. Highest rainfall is on the higher ground to the north-east and lowest close to the catchment outlet

The  $R_t^2$  values mapped in Figure 7-14 give an indication of which gauges may be representative of the catchment processes, on average, during the period in question. Not only do the models that fit the data vary but how well they fit also varies. If the model fits well, the gauge rainfall series is likely to be representative of the flow generating rainfall for that period, given that the model is being fitted to the same outflow series each time. The spatial rainfall distribution over the three years is shown in Figure 7-12. Values, indicating the fit of the identified models, are shown the maps in Figure 7-14, colour coded as Table 7-4, and tabulated in Table A 1 in Appendix A.

Table 7-4 - Arbitrary thresholds for goodness-of-fit levels and associated colour coding used in Figure 7-14.






	$R_t^2$ value	Colour code
Very good fit	> 0.90	
Good fit	0.80 - 0.90	
Use with caution	0.70 - 0.80	
Poor fit	0.60 - 0.70	
Very poor fit	< 0.60	

Figure 7-14 shows the how the fit of the models identified for each rainfall-flow combination is distributed over the catchment for each of the water years. Arbitrary thresholds for goodness-of-fit and colour coding are shown in Table 7-4. In WY1 the best fit model using catchment average rainfall has an  $R_t^2$  value of 0.908 suggesting that most of the gauges are representative of the catchment during that period. Table 7-5 shows the minimum value of the  $R_t^2$  value for the individual gauges to be 0.863. Any value over 0.80 was classified as a good fit so all the gauges are a good fit in WY1. The fit to the catchment average in WY2 is 0.838. This is still a good fit but the lower value suggests that some of the gauges may not be representative in that period. The range of values for the individual gauges supports this. Most of the gauges have  $R_t^2$  values > 0.8 but two gauges (SPRI and EVER) have fits of < 0.8 suggesting that they are less representative. CAR for WY3 has an  $R_t^2$  value of 0.793 suggesting that more gauges may be unrepresentative, again supported by the range of values for the individual gauges from 0.632 to 0.843 when WY3 is considered. Study of the maps in Figure 7-14 shows that most gauges have fits between 0.70 and 0.80 with a few over 0.80 but four gauges show a fit of < 0.7. In this case, any the gauges with fits > 0.80 can be used as surrogates for CAR with some degree of confidence.

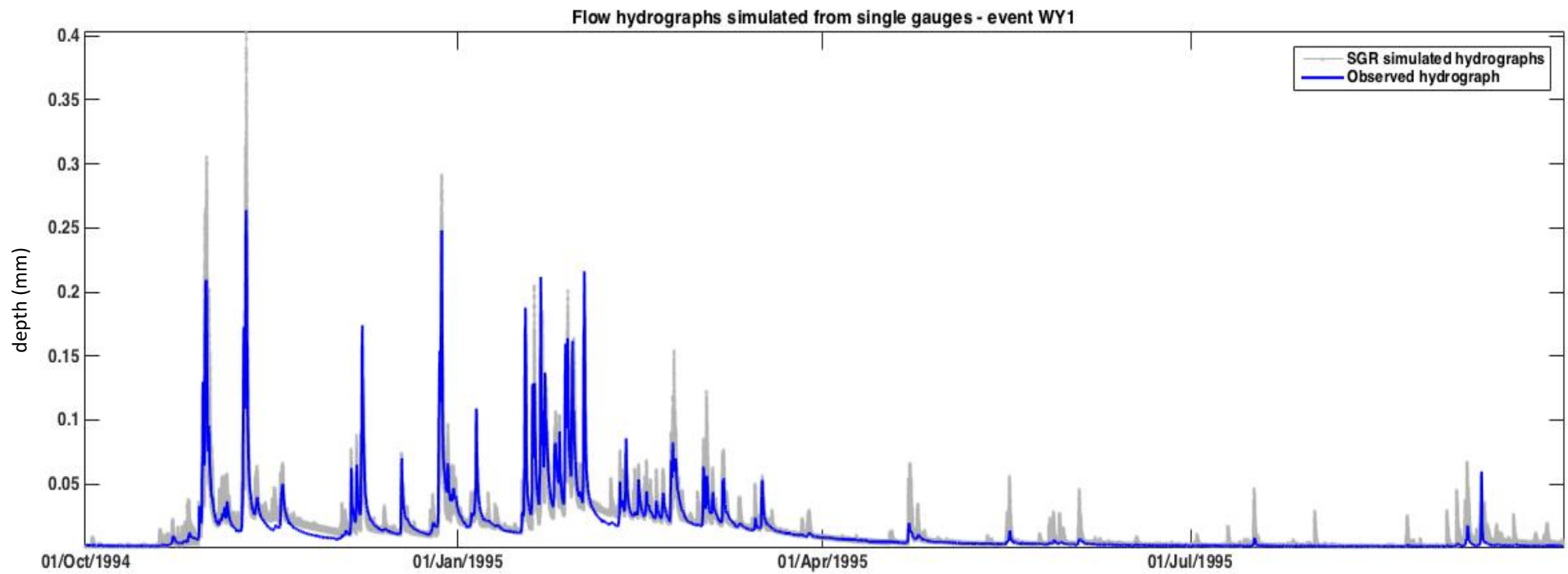


Figure 7-13a - Hydrographs simulated from rainfall measured at individual gauges (plotted in grey) over plotted by the observed hydrograph (blue line) for WY1. In many cases, the individual gauges over-estimate both the peak flow and the recessions. Also simulated peaks may be observed which do not occur in the observed hydrograph.

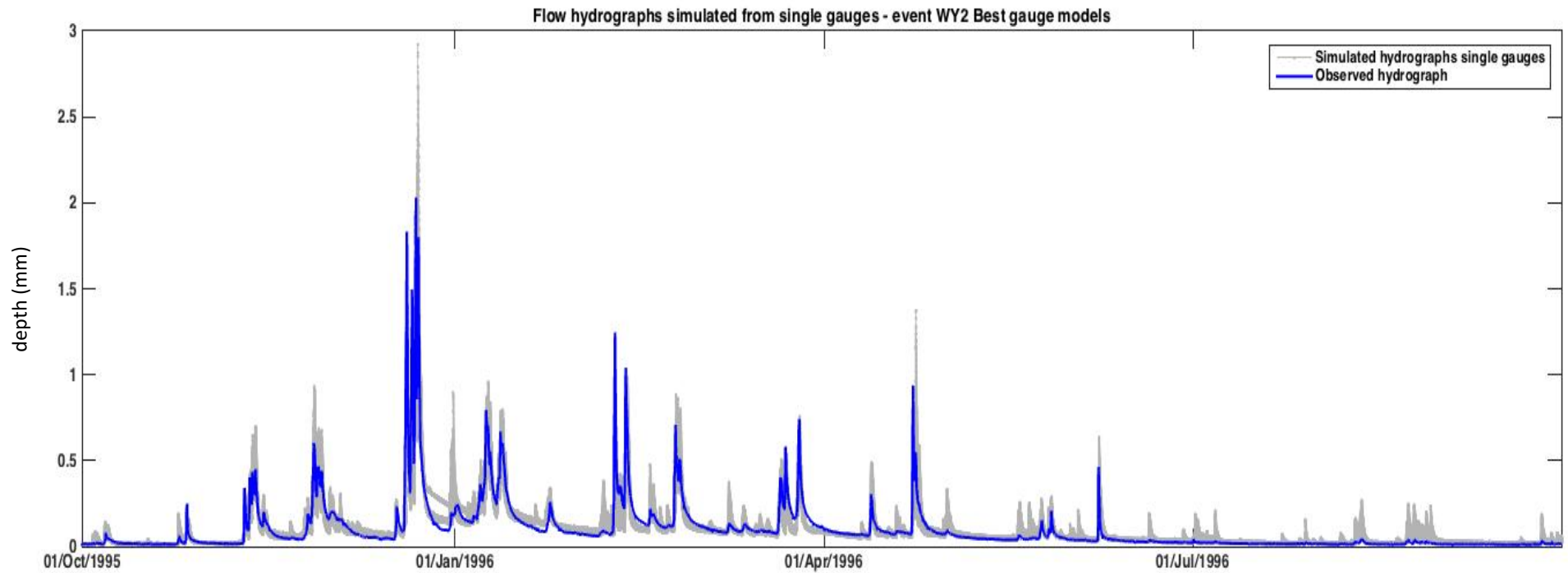


Figure 7-13b: Hydrographs simulated from rainfall measured at individual gauges (plotted in grey) over plotted by the observed hydrograph (blue line) for WY2. Individual gauges often over-estimate the peak flow and also simulate peaks which do not occur in the observed hydrograph. Around 1<sup>st</sup> January 1996, some gauges show markedly different recession profile to the rest.

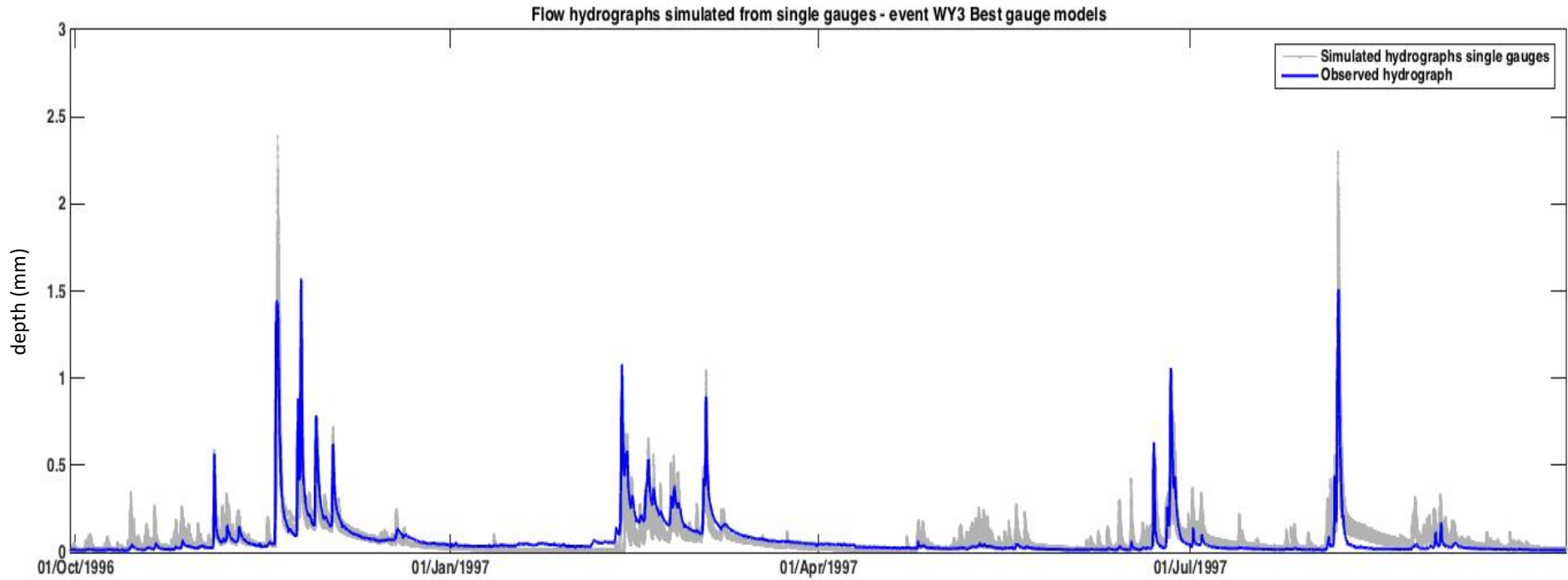


Figure 7-13c: Hydrographs simulated from rainfall measured at individual gauges (plotted in grey) over plotted by the observed hydrograph (blue line) for WY3. In many cases, the individual gauges over-estimate the peak flow but also simulate peaks which do not occur in the observed hydrograph. In several places, recessions are consistently under or over estimated and profiles differ quite markedly from the observed.

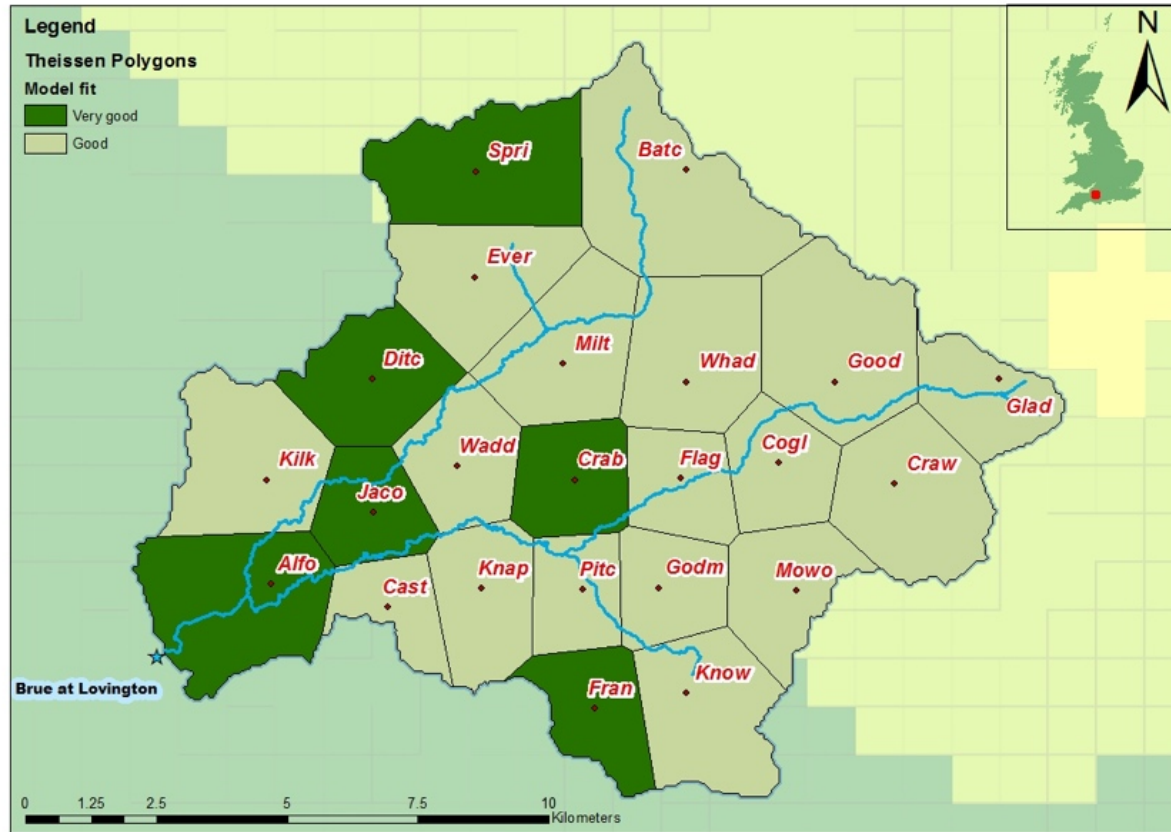


Figure 7-14a Spatio-temporal importance of the gauges is illustrated by plotting the fit of model unique to each rainfall-runoff combination on a catchment map. The theissen polygons are coloured according to the coding listed in Table 7-4. All gauges in WY1 are coded green – good fit ( $R^2 > 0.80$ ) with six over 0.9 so can be expected to be representative of the catchment as a whole. CAR model fit is 0.908.



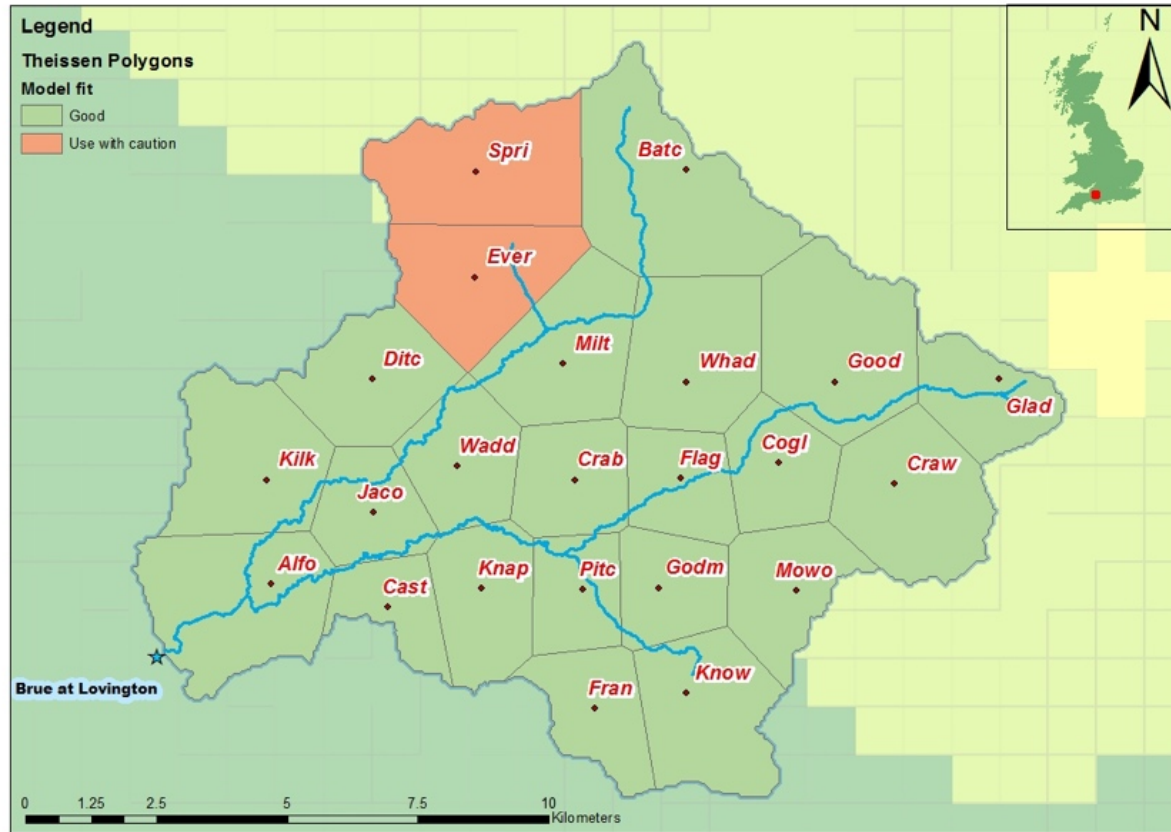


Figure 7.14b Spatio-temporal importance of the gauges is illustrated by plotting the fit of model unique to each rainfall-runoff combination on a catchment map. The theissen polygons are coloured according to the coding listed in Table 7-4. In WY2, most gauges fit well and are likely to be representative. The exceptions are the 2 gauges coloured orange at the NW edge which may not represent the catchment as well. CAR model fit is 0.838.

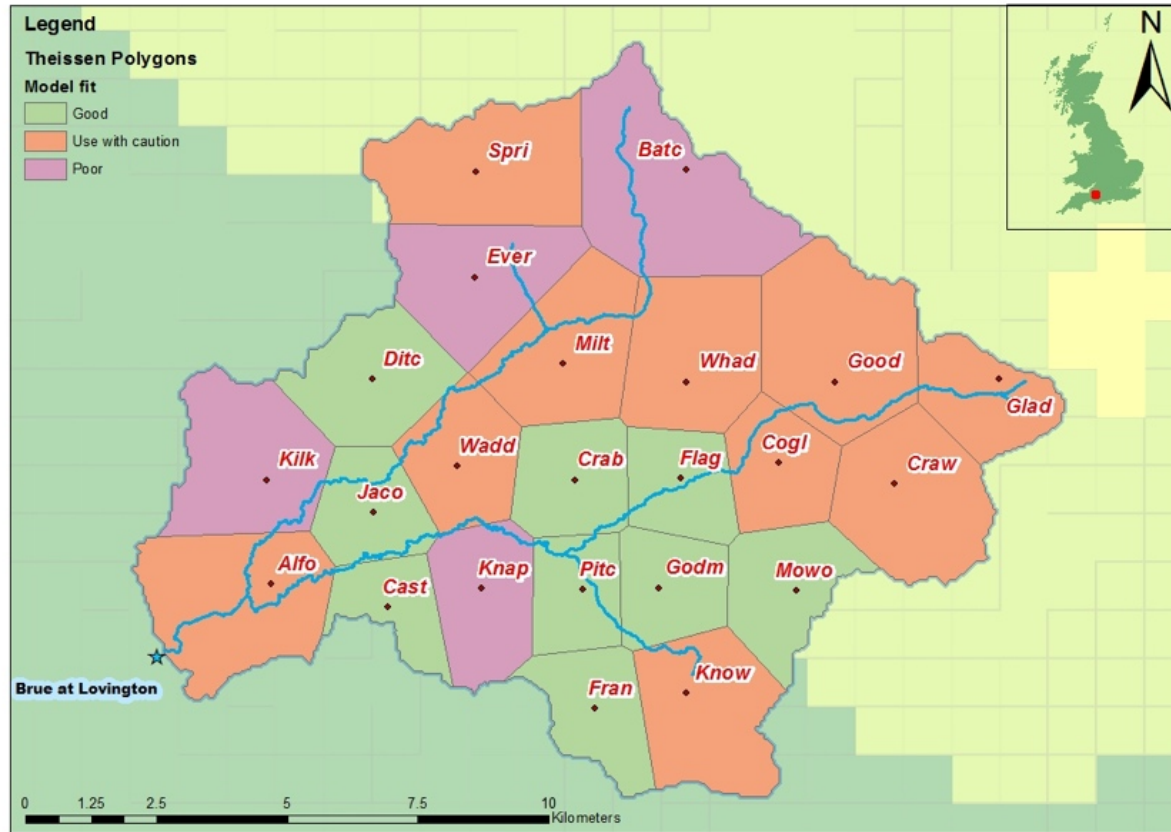


Figure 7.14c Spatio-temporal importance of the gauges is illustrated by plotting the fit of model unique to each rainfall-runoff combination on a catchment map. The theissen polygons are coloured according to the coding listed in Table 7-4. In WY3 the pattern is much less organised and there are only a few gauges that could be said to be representative (coloured green). There are four gauges have  $R^2$  values of less than 0.70 (coloured lilac) which unlikely to represent the whole catchment. CAR model fit is 0.793.

The  $R_t^2$  of the catchment average model can be used to identify whether misinformation is being supplied.  $R_t^2$  values of the models fitted using the rainfall from individual gauges may be able to identify which gauges are supplying the poor information. The magnitude of the  $R_t^2$  value for each individual gauge (assuming a unique model has been fitted to the observations at each gauge) provides a measure of the uncertainty of the information it is supplying to the average calculated for that period. Although including rainfall measured at a non-representative gauge may give a better estimate of the catchment average rainfall, it does not follow that this average is representative of the flow generation processes of the catchment as a whole and consideration should be given to whether it is more valuable to have a better average that is non-representative or a slightly worse average that is representative, the decision may depend on the purpose of the modelling exercise. Misinformative measurements do not fit the model well but may still provide substantial useful information about the flow generation processes operating in the catchment.

Table 7-5 - Comparison of the performance of the best fit catchment average model with the range of fit to individual gauges (full listing in Table A 1).

	Catchment average rainfall	Individual gauges – best fit models		
	$R_t^2$ best fit model	Min $R_t^2$	Average $R_t^2$	Max $R_t^2$
WY1	0.908	0.863	0.887	0.916
WY2	0.838	0.722	0.815	0.839
WY3	0.797	0.632	0.762	0.843

In most practical applications, the catchment average would not be available for comparison and the catchment average model would not be known. If only one gauge is available, it must be assumed that it is representative because there is no other information available. Fitting a model and studying the  $R_t^2$  value will give an indication of how much reliability can be placed on the estimate of the catchment average as estimated by that gauge.

Is it possible to do better? Traditional (forward) modelling only makes use of information present in the rainfall however reverse hydrology uses not just information in the rainfall but also information in the catchment outflow. This information may be

used to infer a rainfall series by inverting the identified model and using the catchment outflow as its input (see Kretzschmar *et al.*, (2014) for details). The output is an estimate of the rainfall which has generated the outflow. The inferred rainfall can then be used to generate a hydrograph that can be compared with the observed hydrograph.

### 7.11. Hydrographs from inferred rainfall

Figure 7-15 shows the hydrographs generated from the inferred rainfall using the best model (including structure and non-linearity – Table A1) identified for the individual rainfall-flow combinations at each gauge. All combinations show a [2,2] model structure with variations in absolute time delay and non-linearity displayed in Table A1. In WY1, the longest time-delays can be seen at gauges on the permeable section of the catchment, the exception being one gauge at the furthest point from the outlet having the shortest delay whilst the non-linearity decreases towards the outlet. In WY2 the part of the catchment furthest from the outlet shows the shortest delays with a non-linearity pattern which is the reverse of WY1. In WY3, time-delay generally increases away from the catchment outlet whilst non-linearity is lowest in the central band increasing towards the NE and SW. These patterns do not seem to correlate directly with rainfall. Models are constructed to represent the whole catchment based on limited information within the rainfall and discharge series. The catchment's dominant modes vary with time as a result of changes in rainfall patterns in the area of influence of the gauge and due also to specific catchment conditions and their complex interactions.

It can be seen that the fit of the inferred hydrographs is very close to the observed hydrograph even when the traditionally simulated (rainfall driven) hydrograph does not fit well. The  $R_r^2$  values for both forward and inferred hydrographs are tabulated in Table A1 and summarised below (Table 7-6). These examples show that using inferred rainfall from a single gauge combination may give a much closer fit to the catchment outflow than using observed rainfall from a single gauge. It could be argued that the inferred hydrographs should fit perfectly as they are being generated from rainfall derived from the flow using the same model however this is not the case because the inversion process is not perfect. Reasons for this are discussed below.

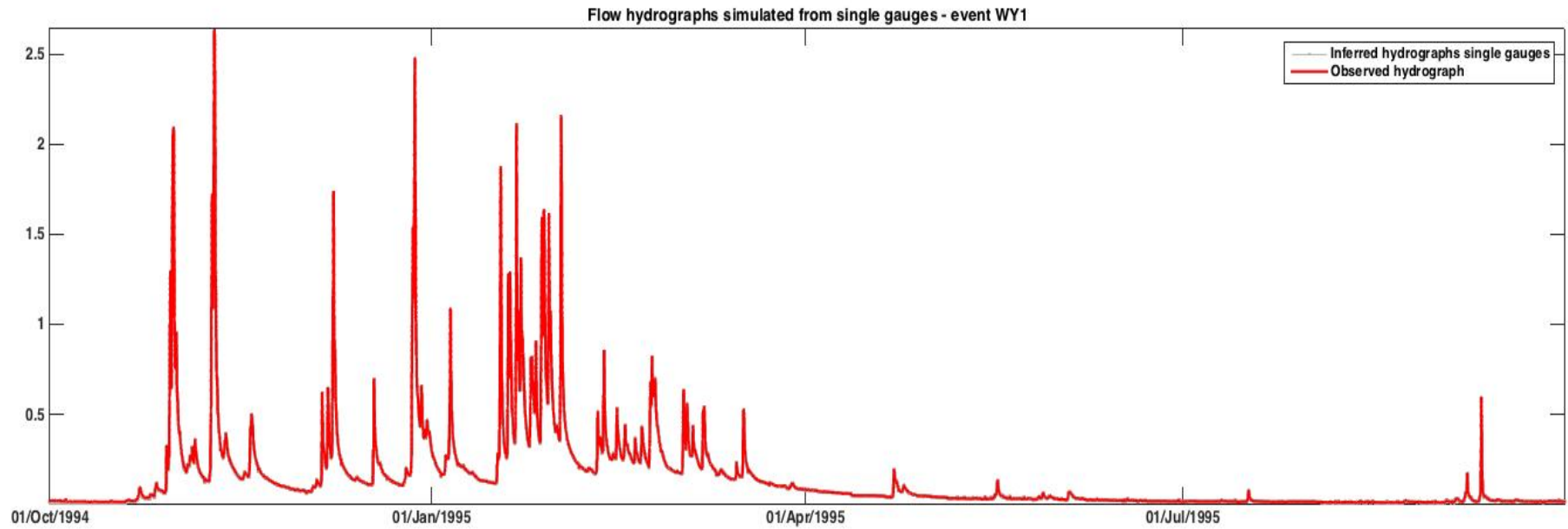


Figure 7-15a: Hydrographs generated from inferred rainfall measured at individual gauges (grey lines) compared with observed hydrograph (red line) for Water year 1 (WY1): October 1994 - September 1995. It can be seen that the simulated hydrographs are almost exact match with the observed even where the forward hydrograph does not fit well. The inferred rainfall contains only the information required to generate the hydrograph. The part of the rainfall spectrum that has no part in generating discharge is filtered out by the model.

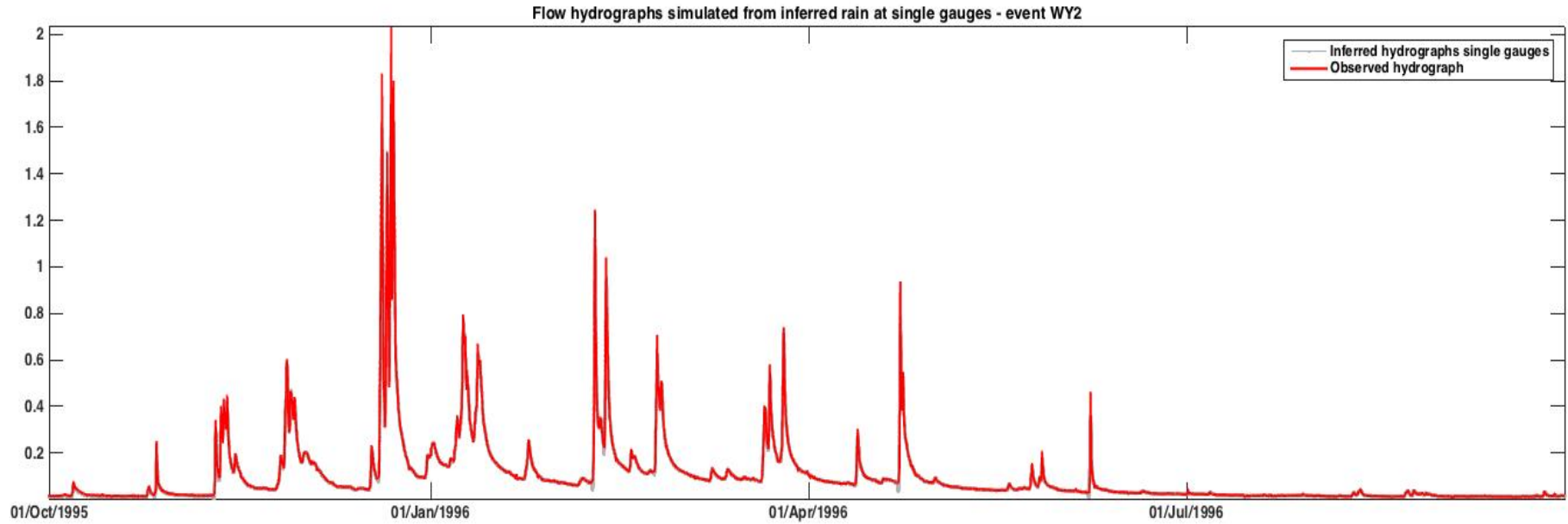


Figure 7-15b: Hydrographs generated from inferred rainfall measured at individual gauges (grey lines) compared with observed hydrograph (red line) for Water year 2 (WY2): October 1995 – September 1996. It can be seen that the simulated hydrographs are almost exact match with the observed even where the forward hydrograph does not fit well. The inferred rainfall contains only the information required to generate the hydrograph. The part of the rainfall spectrum that has no part in generating discharge is filtered out by the model.

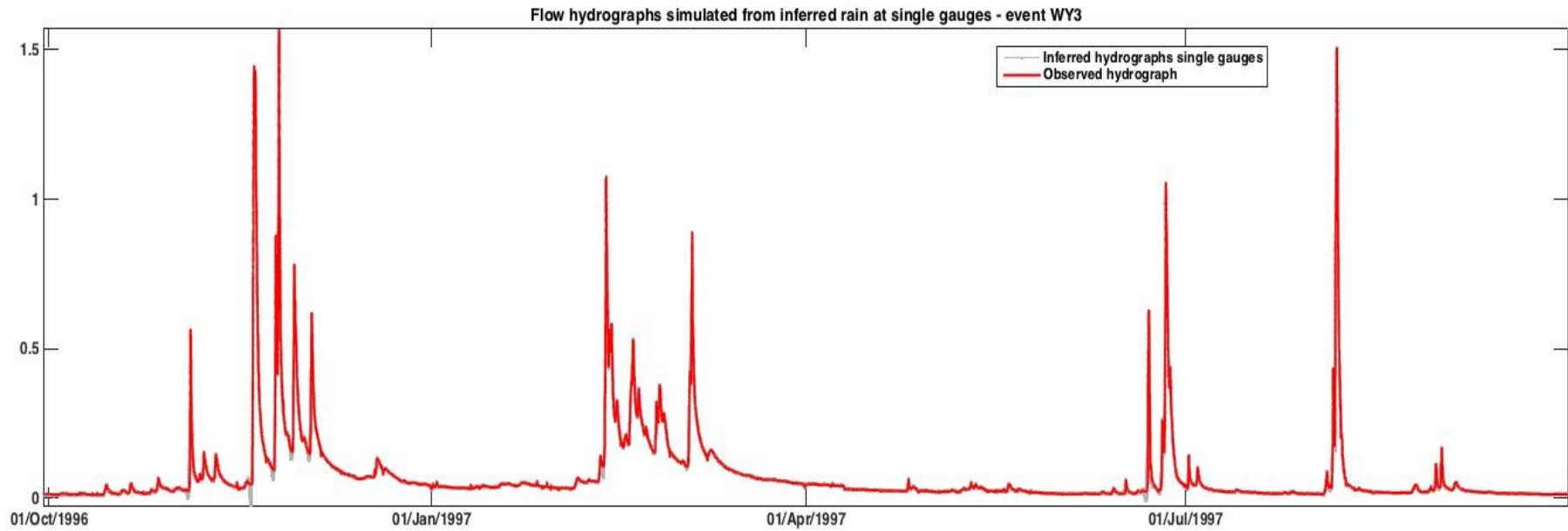


Figure 7-15c: Hydrographs generated from inferred rainfall measured at individual gauges (grey lines) compared with observed hydrograph (red line) for Water year 3 (WY3): October 1996 – September 1997. It can be seen that the simulated hydrographs are almost exact match with the observed even where the forward hydrograph does not fit well. The inferred rainfall contains only the information required to generate the hydrograph. The part of the rainfall spectrum that has no part in generating discharge is filtered out by the model.

Table 7-6 - Range of  $Rt2$  values for hydrographs generate from observed gauge rainfall and inferred gauge rainfall when compared to the observed hydrograph. In all cases use of inferred rainfall improves the hydrograph fit, usually significantly. A value of 1.000 implies perfect fit. Examination of the hydrographs shows this is not the case but the variation is in the 4<sup>th</sup> decimal place.

	$Rt2$ range – gauge rainfall	$Rt2$ range inferred rainfall
WY1	0.863 – 0.916	1.000
WY2	0.722 – 0.839	0.987 – 0.995
WY3	0.632 – 0.843	0.956 – 1.000

### 7.12. Inferred Discharge Generating Rainfall (DGR)

The inferred rainfall series generate catchment hydrographs that are very close to the observed catchment outflow, but this inferred rainfall series is quite different in character to the observed rainfall. Figure 7-16 shows the catchment average and inferred rainfall during March in each of the three years. The inferred rainfall sequence can be seen to be much smoother, usually with lower peaks than the observed sequence. It has a lower time resolution, however Kretzschmar *et al.* (2015; 2016) have shown that the inferred rainfall series captures the dynamics of the catchment despite the loss of resolution - the price paid for the numerical stability of the inversion process. The inversion process extracts the Discharge Generating Rainfall (signal) from the measured rainfall with its broad-spectrum. This is termed Discharge Generating Rainfall (DGR).

It can also be seen that the inferred rainfall sometimes goes negative. This can be explained in terms of catchment behaviour and rainfall spatial distribution by comparing the rainfall and flow plots. Negative inferred rainfall may occur during a recession because, in a recession, the flow is driven by the catchment not the rainfall (Montesarchio *et al.*, 2015). Small negative spikes occur where the inversion process is compensating because it has stopped raining at the gauge, but the flow is still increasing or rain elsewhere in the catchment is affecting the flow. These negative periods of rainfall are an artefact of the inversion and do not hinder its use as a tool for generating catchment outflow, in fact they are an important part of the mechanism.



a)  
WY1

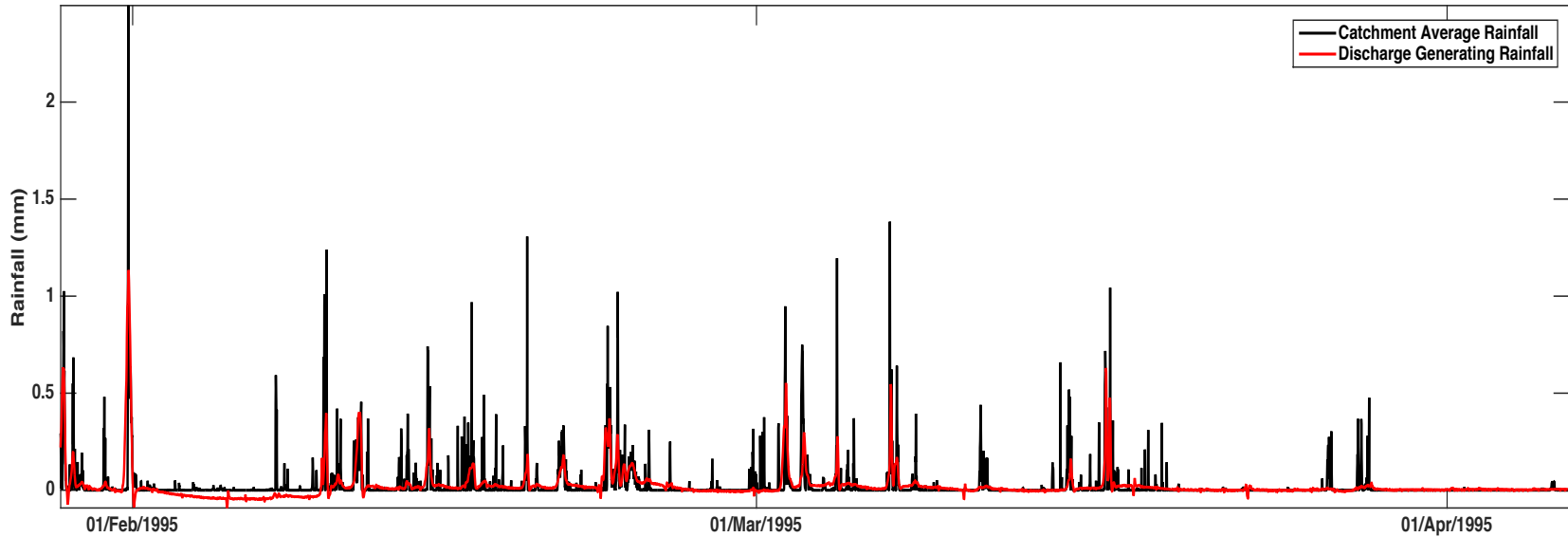


Figure 7-16a - Catchment average and inferred catchment average rainfall during the spring of WY1.

b)  
WY2

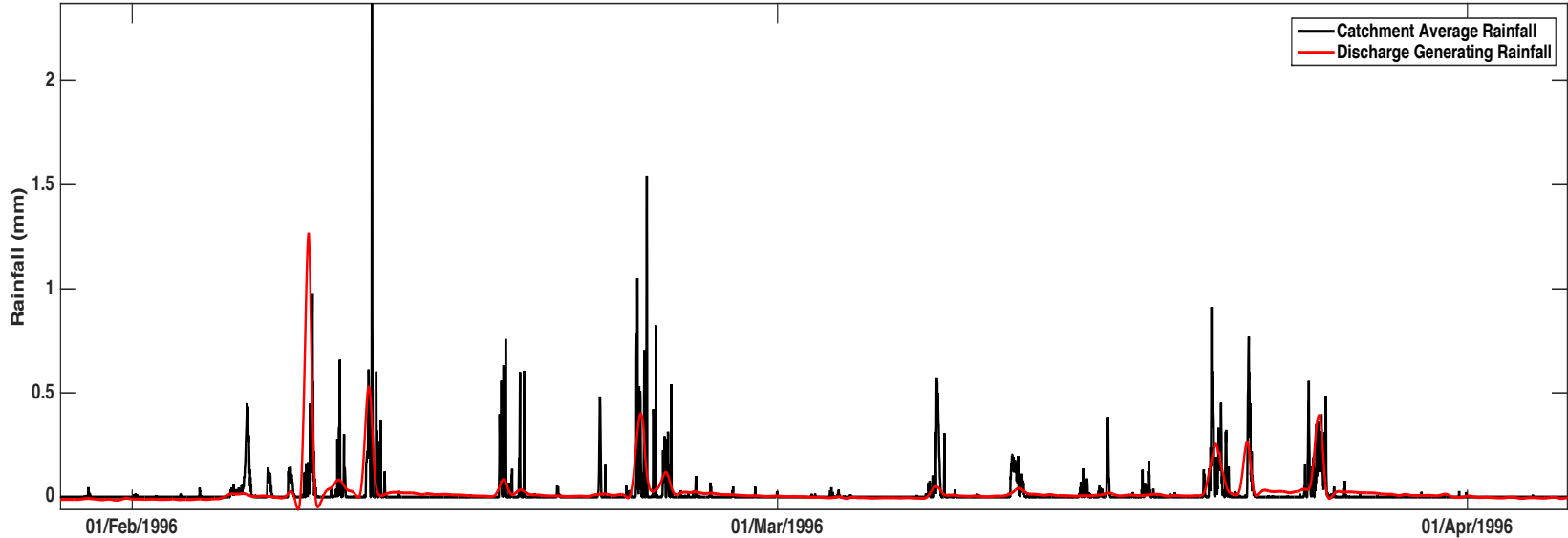


Figure 7-16b - Catchment average and inferred catchment average rainfall during the spring of WY2.

c)  
WY3

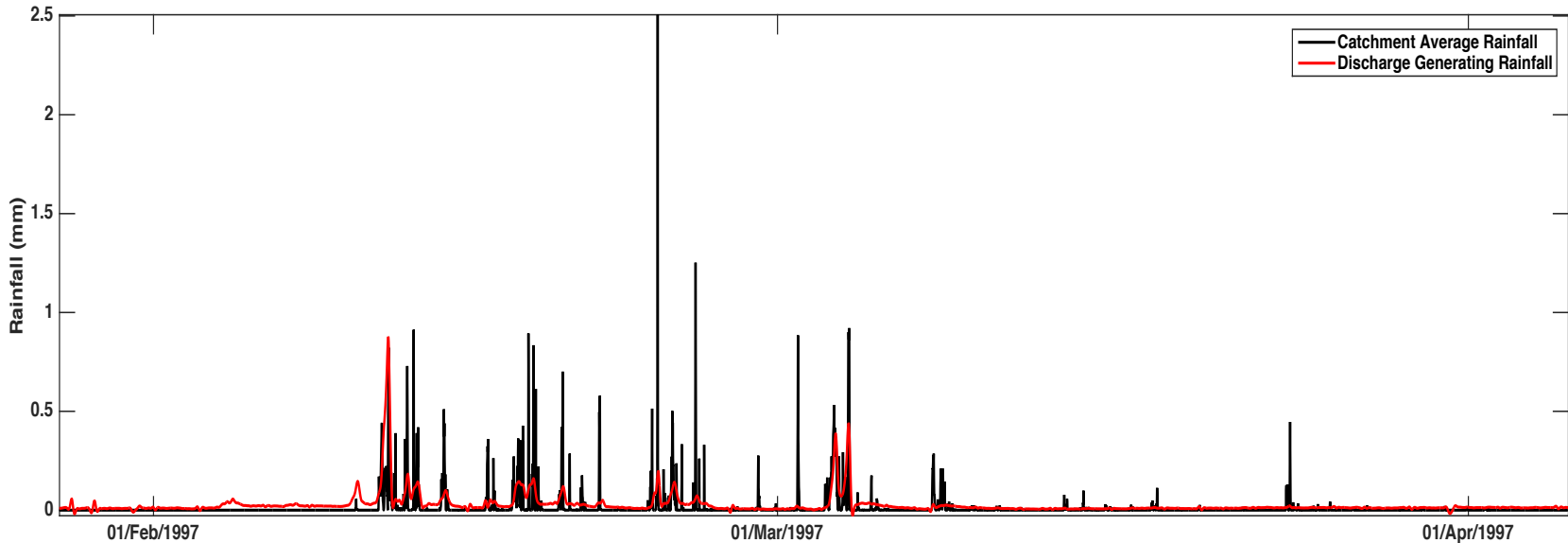


Figure 7-16c - Catchment average and inferred catchment average rainfall during the spring of WY3.

The inversion process extracts the flow generating rainfall signal from the noisy observations because it is based on the catchment outflow. The catchment acts effectively as a low-pass filter and the regularised inversion process likewise filters out the high frequency behaviour of the rainfall process that has either little or no impact on the outflow hydrograph (as illustrated in Figure 7-15) (*c.f.* chapter 2, section 2.7 and chapter 5). The spatial distribution of rainfall will also have an effect. Rainfall measured at a single gauge is generally only part of the rain falling on the catchment. A model fitted to that rainfall will attempt to model the whole catchment based on this highly incomplete information (how incomplete depends on the spatial variation of rainfall, for example, frontal or convective, and of the catchment, for example, low or high elevation, permeable or non-permeable *etc.*). Inversion is based on the outflow from the whole catchment and thus can make use of the information contained in the streamflow as well as the input rainfall. The result is a better estimate of the rainfall driving the discharge than can be obtained from the rainfall alone however it is still not perfect hence the model fit of the hydrograph simulated from DGR often lower than 1.

It can be concluded that DBM modelling and Reverse Hydrology can be used to recognise when the model fitted to the rainfall-flow combination at a gauge is non-representative of the catchment as a whole. This is not to say that the gauge observations are not accurate representations of their own local conditions but that these conditions are not, at this time, representative of the whole catchment. The model fit ( $Rt2$ ) provides a measure of the confidence that can be placed on the gauge in question. It should also be noted that whether a gauge is representative or not varies with time due to the rainfall regime (convective or frontal), the track of the storm and the size and position of internal storm cells. If gauges are consistently found to be non-representative, there is an argument for removing them from the network as they do not adequately represent the conditions in the catchment. Using DGR instead of CAR or SGR can significantly improve the fit of the hydrograph but if the gauge is severely non-representative, not even Reverse Hydrology can extract enough of the DGR from the rainfall signal and the gauge should be rejected.

### 7.13. Summary and Conclusions

Reliance is often on a small number of rain gauges to make inferences about catchment response. The densely instrumented Brue catchment provided a rare opportunity to investigate the importance of spatial variability in the rainfall field and catchment response as measured by the ability of a CT-TF model to replicate the catchment rainfall-runoff transformation measured by model performance ( $R_t^2$ ). Models, with as few parameters as were necessary to capture the system dynamics, were identified between catchment average rainfall (CAR) and catchment outflow and rainfall measured at individual gauges (SGR) and catchment outflow. Model selection was made by maximising  $R_t^2$  and minimising  $YIC$  for models that inverted well using the regularisation technique introduced by Kretzschmar *et al.* (2014) (chapter 4). A rainfall series was inferred from the catchment outflow, producing an estimate of the part of the rainfall spectrum responsible for generating discharge. This has been termed Discharge Generating Rainfall (DGR).

The influence of time-scale was investigated by aggregating the measured 15-minute rainfall data into periods up to 1 day. It was found to have an effect on estimation of various key characteristics of the rainfall field. Aggregation can be thought of as a low-pass filter in the same way as regularisation and the filtering effect of the catchment storage. Spatial and temporal resolution are related, in that they represent the spatio-temporal integration of catchment rainfall.

This paper aimed to show whether matching the spatio-temporal rainfall field is important when generating a streamflow hydrograph given the uncertainty inherent in the modelling process. Uncertainty may be introduced by both spatial and temporal variability in the rainfall field. Various studies have shown that rainfall variability decreases as sampling interval increases (Shaghagian and Abedini, 2013) and this was found to be true at sub-daily scale. The shape of the rainfall distribution changes significantly as aggregation increases as characterized by the first four statistical moments (Figure 7-6). Key characteristics were found to decrease with aggregation tending towards an asymptotic value at 24 hrs. Maximum rainfall intensity decreases with aggregation because the rainfall is spread over a longer period.

The effect of rainfall variability was measured by comparing the performance of models of the CAR or SGR combinations with the catchment outflow. If the model fitted to the CAR performs well, then the CAR is representative of the catchment as a whole and the gauge network is performing well, for that time period, and all the SGR series used to estimate CAR are likely to be representative. If the model fitted to CAR performs less well, the network is not performing as well and further investigation is required. Performance of different parts of the network can be investigated by modelling each SGR series individually. Any gauges showing a poor performance are not representative of the catchment as a whole, on average, during the period in question. Different parts of the catchment may be driving the outflow at different times and SGR may contribute to the CAR without being representative of the whole catchment at that time. It is also possible that although single gauges are misinformative, pairs or sets of gauges may be able to work together to represent the whole catchment better. This is worth future study. The dominant processes operating in a catchment change with time and will be dependent on the rainfall regime and storm patterns as well as catchment conditions. Any gauges showing a consistently poor performance may be inappropriately sited and consideration should be given to removing or repositioning (network optimization).

The Reverse Hydrology approach is able to extract the part of the rainfall necessary for generating the catchment discharge from the broad rainfall spectrum. The high frequency part of the rainfall spectrum can be disregarded when generating a streamflow hydrograph. This is a form of spectral decomposition which will be utilised in chapter 8 to generate a rainfall series that can be used to extend or fill a gap in a rainfall record assuming a streamflow record exists.

Generating a hydrograph from the complete rainfall spectrum using a forward model results in a hydrograph with features (mostly peaks) not visible in the observed hydrograph. Using DGR to generate a hydrograph results in a 'cleaned-up' version that matches the observed hydrograph well. The process is not perfect despite the apparent circular logic because the inversion method is not perfect. The spatial distribution of rainfall also has an effect because the model is fitted based on incomplete information due to variations in the rainfall field and the catchment characteristics. The inversion process enables the information contained in the catchment outflow, which relates to

the whole catchment, to be utilized. In most cases, DGR inferred from the rainfall from a single gauge can give a better estimate of the outflow hydrograph than CAR however, if the information contained in the rainfall-streamflow combination is extremely misinformative, then not even Reverse Hydrology can recover enough information to generate a reliable hydrograph.

It can be concluded that the spatio-temporal rainfall field is important when generating a streamflow hydrograph. How well the catchment can be modelled is dependent on the 'representativeness' of the rainfall (CAR or SGR) of the catchment as a whole, which can change with time due to changes in rainfall characteristics or catchment conditions. DBM modelling can provide a means of assessing how representative a particular gauge or gauge combination is. If DGR, inferred from the catchment outflow is used, further knowledge of the spatio-temporal structure of the rainfall may not be required to get a good estimate of the outflow hydrograph.

Each catchment is unique but common principles apply (McMillan *et al.*, 2014). The methodology presented here should be extended to catchments of different sizes and rainfall regimes with varying density of rain gauge networks. It might be useful to relate patterns of model fit to weather patterns, for example, Lamb weather types (Lamb, 1972) which may be useful when designing gauge networks. A method for generating rainfall using the spectral properties of the rainfall series is being developed and is the subject of chapter 8 and could also be used to fill gaps in rainfall records.

## Appendix A1 – Best fit models to SGR

Table A 1 - structure of best fit models identified for the observations at each of the 23 rain gauges used in the study. Model fits shown  $R^2$  between simulated and observed hydrographs and hydrographs simulated from inferred rainfall (DGR). Model structure is given as a triad (defined in Equation 2-2).

Gauge	WY1			WY2			WY3		
	Model	Rt2	IRt2	Model	Rt2	IRt2	Model	Rt2	IRt2
ALFO	[2225]0.55	0.902	1.000	[2234]0.7	0.810	0.990	[2220]0.6	0.754	0.956
BATC	[2226]0.65	0.873	1.000	[2232]0.6	0.809	0.988	[2227]0.65	0.632	0.967
CAST	[2225]0.55	0.873	1.000	[2234]0.7	0.817	0.990	[2220]0.65	0.828	0.999
COGL	[2225]0.6	0.871	1.000	[2233]0.6	0.838	0.990	[2230]0.6	0.701	0.971
CRAB	[2226]0.65	0.916	1.000	[2234]0.65	0.828	0.990	[2226]0.55	0.815	1.000
CRAW	[2225]0.6	0.883	1.000	[2235]0.55	0.823	0.993	[2228]0.55	0.786	1.000
DITC	[2225]0.6	0.909	1.000	[2234]0.65	0.806	0.990	[2227]0.55	0.810	1.000
EVER	[2226]0.65	0.883	1.000	[2240]0.75	0.747	0.995	[2228]0.55	0.680	1.000
FLAG	[2225]0.65	0.874	1.000	[2234]0.65	0.833	0.990	[2227]0.6	0.801	1.000
FRAN	[2226]0.55	0.901	1.000	[2234]0.65	0.835	0.990	[2220]0.55	0.811	1.000
GLAD	[2226]0.65	0.883	1.000	[2233]0.55	0.806	0.990	[2228]0.6	0.702	0.968
GODM	[2226]0.6	0.874	1.000	[2234]0.65	0.832	0.990	[2227]0.5	0.808	0.999
GOOD	[2224]0.65	0.893	1.000	[2233]0.6	0.839	0.990	[2228]0.65	0.786	1.000
JACO	[2225]0.6	0.901	1.000	[2234]0.7	0.816	0.991	[2220]0.6	0.843	1.000
KILK	[2225]0.55	0.884	1.000	[2233]0.65	0.804	0.987	[2220]0.55	0.689	0.967
KNAP	[2225]0.65	0.868	1.000	[2235]0.7	0.814	0.991	[2220]0.6	0.644	0.966
KNOW	[2226]0.6	0.882	1.000	[2234]0.6	0.818	0.992	[2220]0.5	0.741	0.971
MILT	[2226]0.65	0.886	1.000	[2233]0.65	0.839	0.989	[2228]0.55	0.712	0.963
MOWO	[2225]0.6	0.895	1.000	[2234]0.65	0.833	0.991	[2226]0.55	0.825	1.000
PITC	[2226]0.6	0.885	1.000	[2234]0.7	0.835	0.990	[2227]0.5	0.804	1.000
SPRI	[2225]0.6	0.907	1.000	[2240]0.75	0.722	0.995	[2228]0.55	0.794	1.000
WADD	[2225]0.6	0.863	1.000	[2234]0.7	0.819	0.990	[2227]0.5	0.797	0.999
WHAD	[2225]0.65	0.891	1.000	[2233]0.65	0.831	0.989	[2220]0.65	0.764	1.000





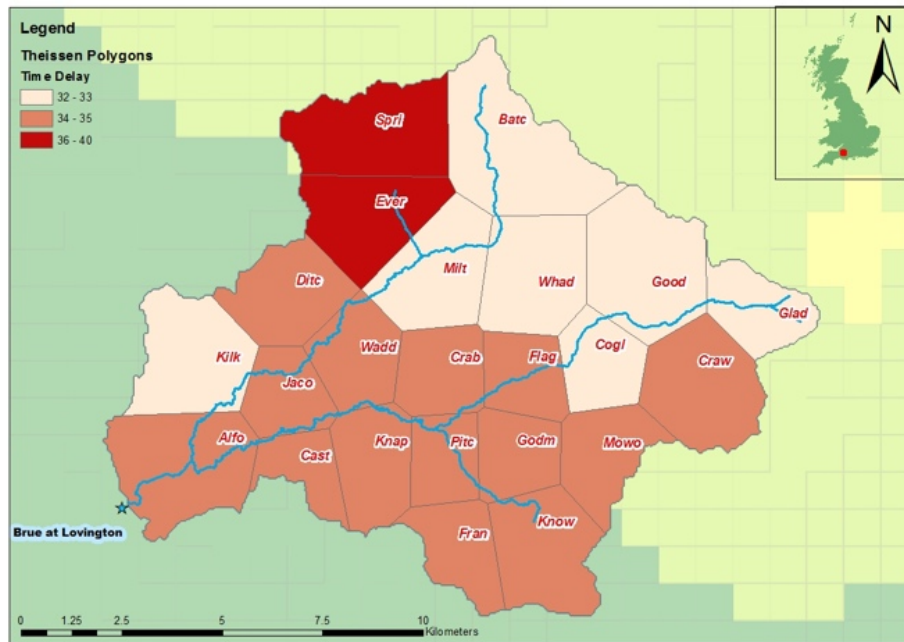


Figure A2-2a WY2 – Time –delay is shorter, further from the catchment outlet with 2 exceptions which lie on the permeable band. There appears to be no significant correlation with rainfall amounts (see Figure 7-12b)

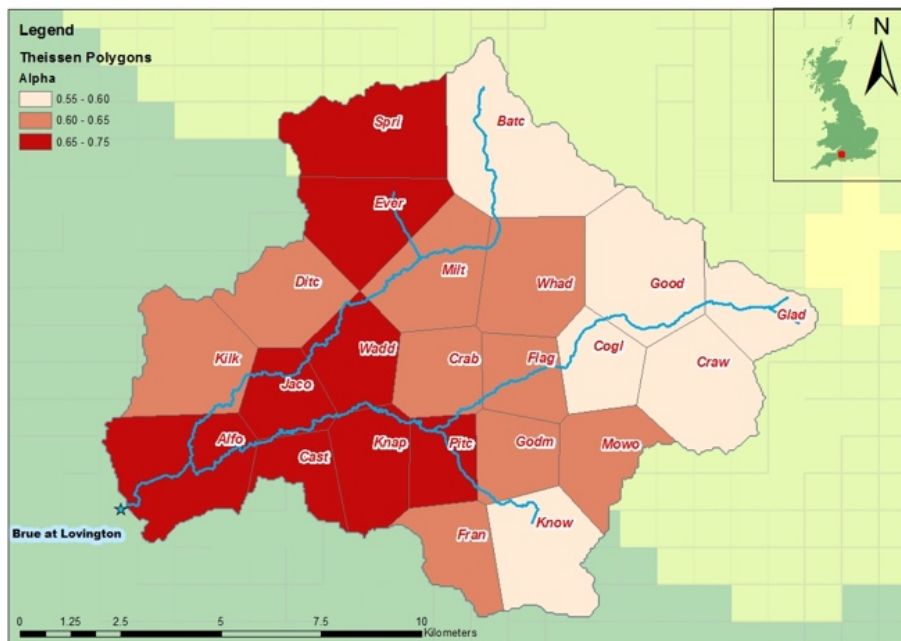


Figure A2-2b WY2 – The pattern of non-linearity is the reverse of WY1 with lowest being furthest from the catchment outlet.

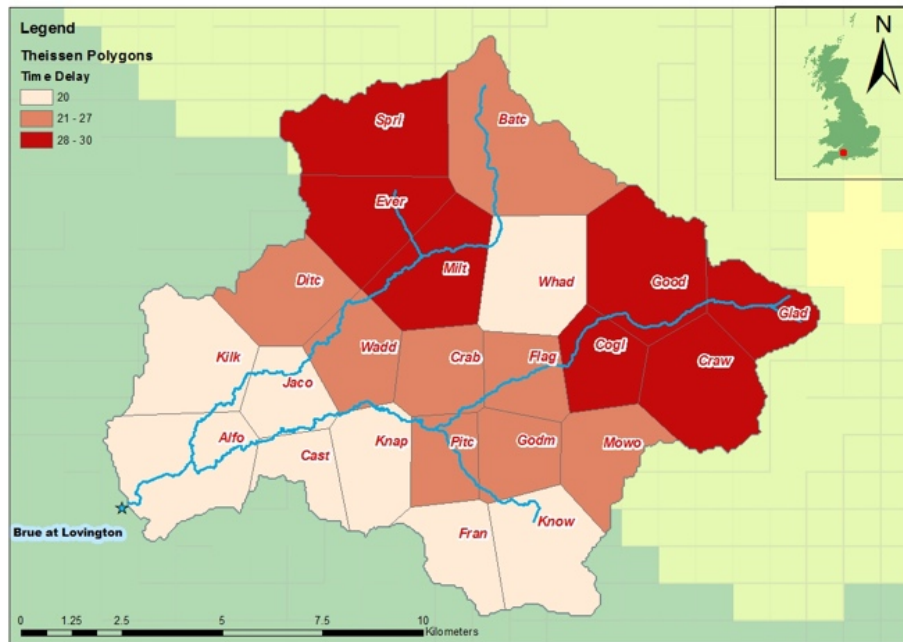


Figure A2-3a WY3 – Time delay generally decreases towards catchment outlet – with two exceptions. Rainfall generally follows the same pattern (see Figure 7-12c).

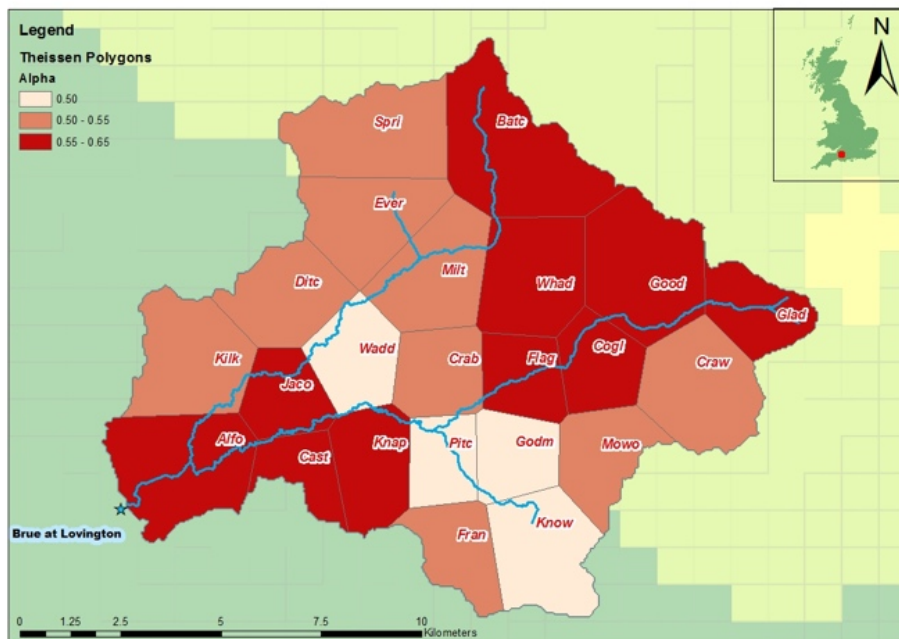


Figure A2-3b WY3 – No distinct pattern is visible in the non-linearity. Rainfall generally decreases towards the outlet (see Figure 7-12c) occurring in much more defined bursts than in other years (see Figure 7-4) resulting in several distinct flow events unrelated to the seasons (see Figure 7-5).

## **Appendix B – Cross-validation plots**

Cross-validation plots showing hydrographs simulated from observed rainfall using models fitted to each year to simulate the flow in each of the other years

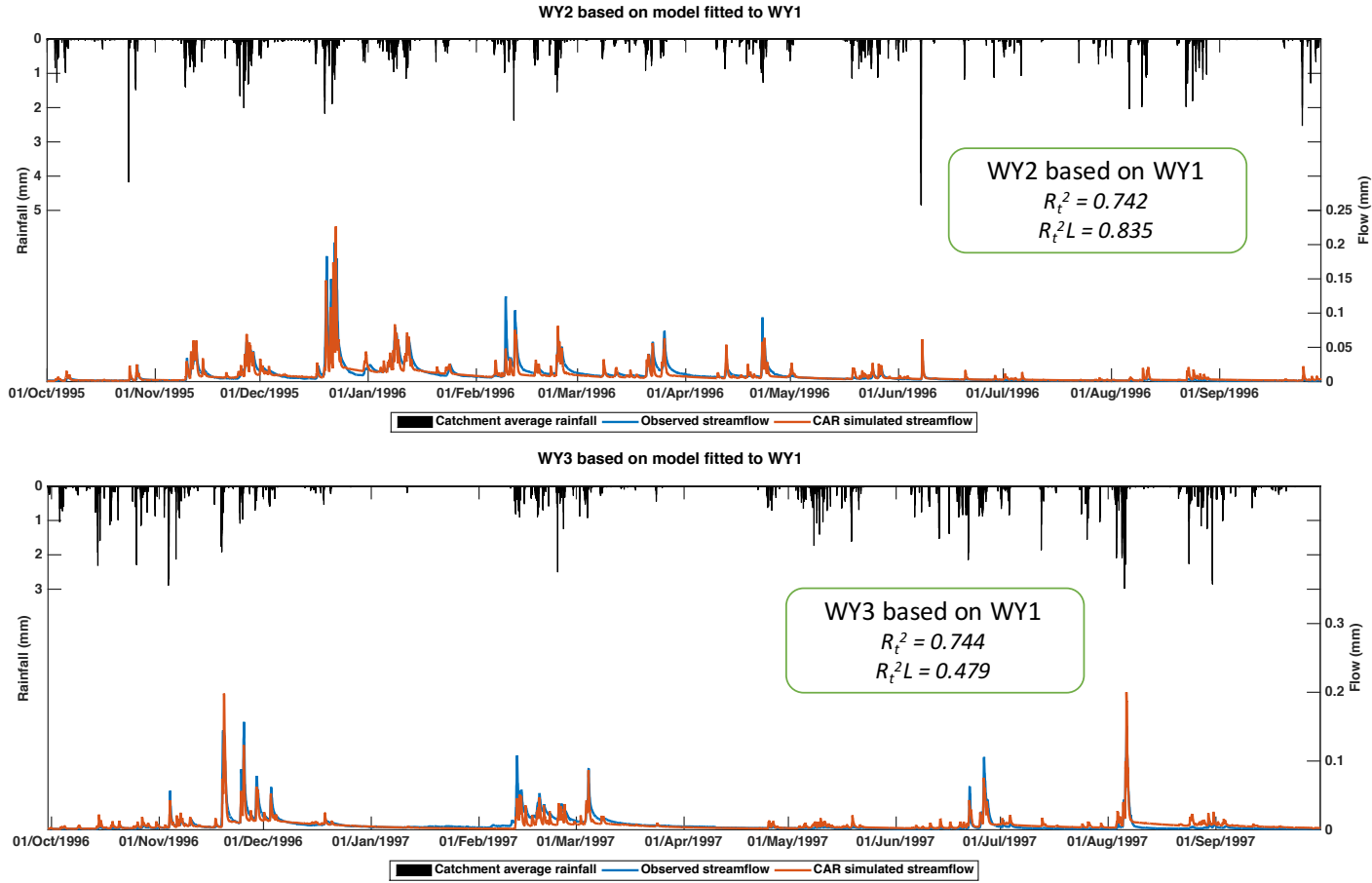


Figure B - 1: Cross-validation plots for WY2 and WY3 based on the model identified for WY1. The  $R_t^2$  fits are acceptable in both cases indicating the model for WY1 is a reasonable average model for the whole period. In WY3 the recessions are better reproduced than by the best-fit model for WY3 (Figure 7-9)

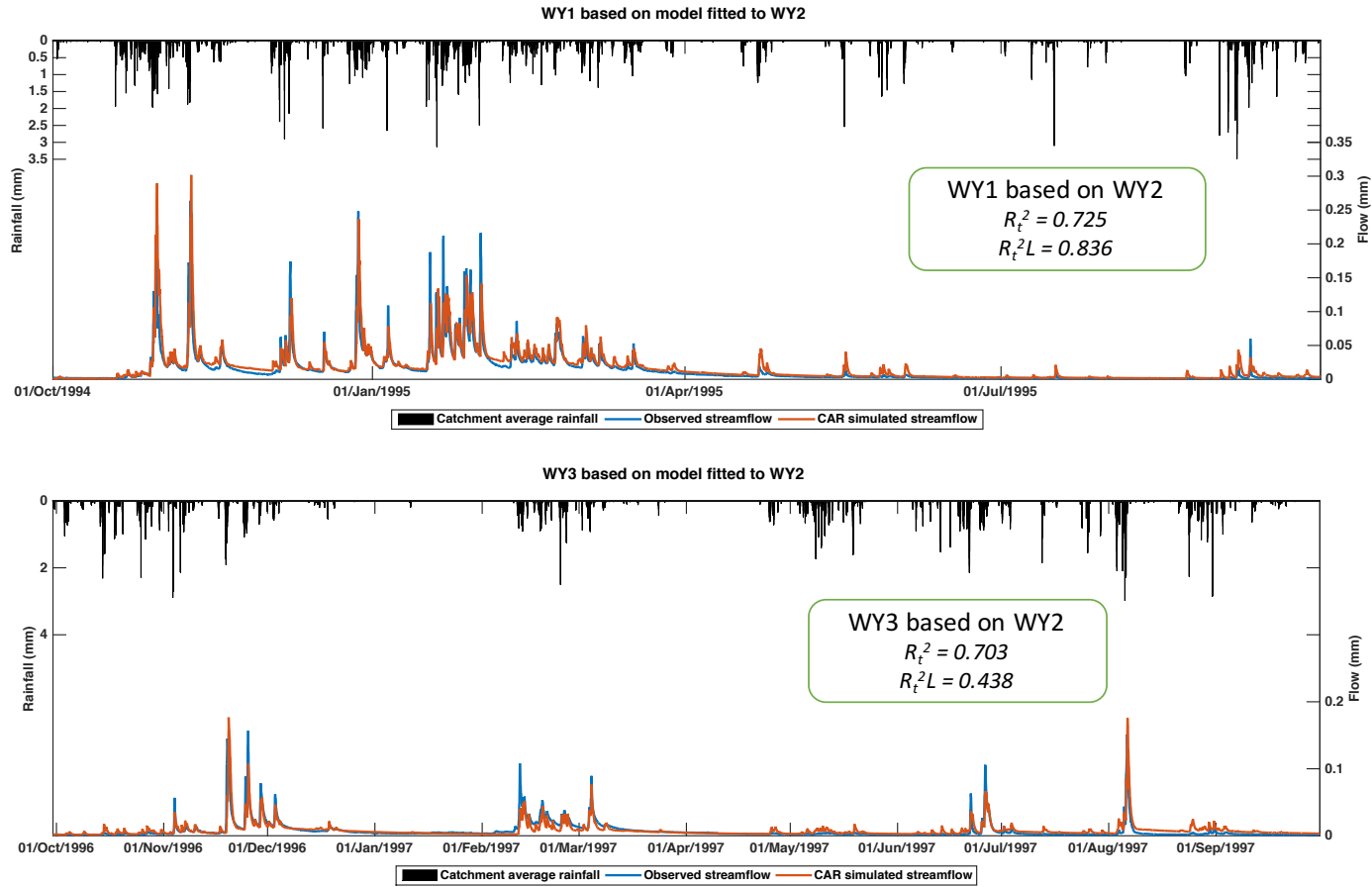


Figure B - 2: Cross-validation plots for WY1 and WY3 based on the model identified for WY2. The  $R_t^2$  fits are acceptable in both cases indicating the model for WY2 is a reasonable average model for the whole period. In WY3 the recessions are better reproduced than by the best-fit model for WY3 (Figure 7-9)

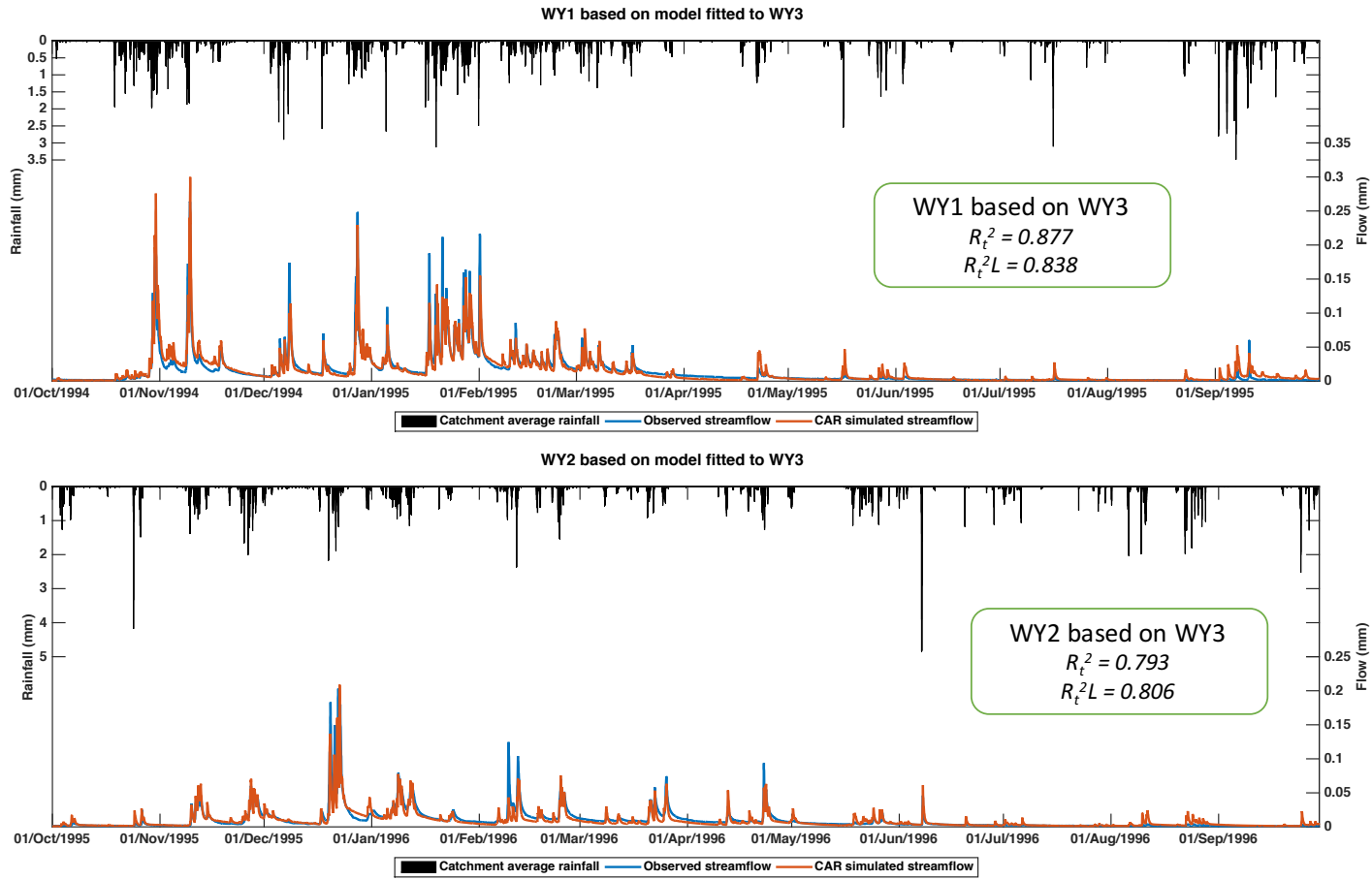


Figure B - 3: Cross-validation plots for WY1 and WY2 based on the model identified for WY3. The  $R_t^2$  and  $R_t^2L$  fits are acceptable in both cases indicating the model for WY3 is a reasonable average model for the whole period over the whole performance range even though the recessions fit poorly in WY3. (Figure 7-9)

## Appendix C – Event based patterns

### Example rainfall events

Three short rainfall events were chosen as examples for further investigation of the effect of rainfall patterns on the representativeness of rain gauges. The summer event is a short-lived convective event that affects the whole catchment as the storm passes over (3D plot in Table C-1). Most of the rainfall is concentrated on the east side of the catchment (darkest coloured polygons). Both the autumn and winter events are more wide-spread (possibly frontal rainfall) that affects the whole catchment but has heavier cells within the overall pattern. The autumn rainfall is heaviest at the south-eastern edge of the catchment and the winter rainfall on the higher ground to the north-east.

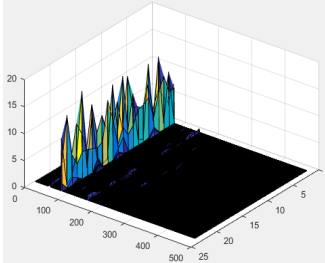
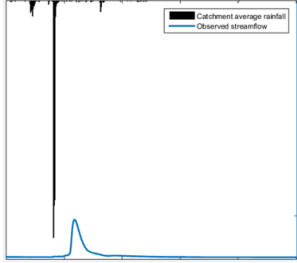
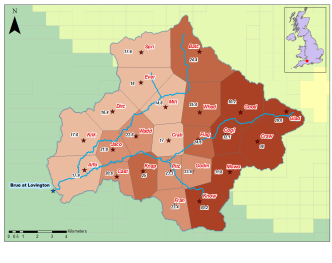
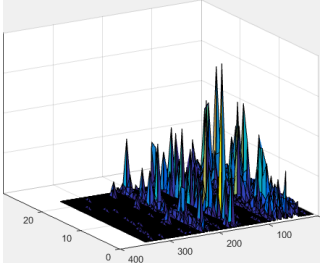
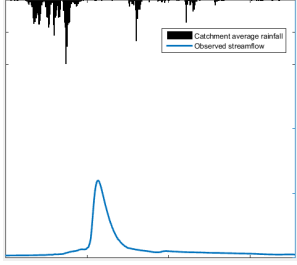
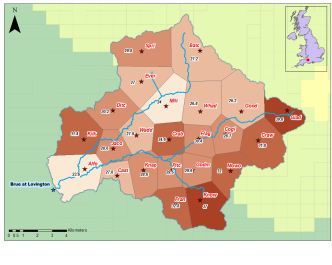
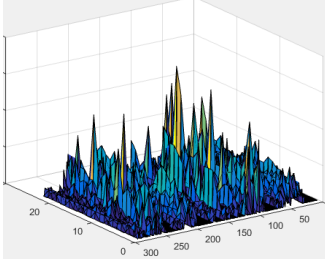
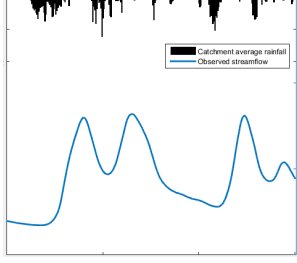
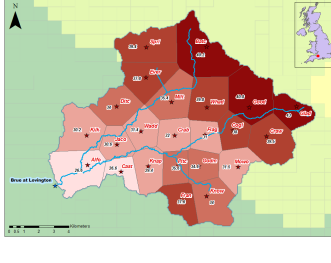
These examples are used to illustrate how DBM modelling and reverse hydrology can be used to identify and compensate for non-representative gauges when estimating CAR. Spatial variability in the rainfall field due to causes such as storm size, direction of movement and topographic effects mean that each ‘event’ is unique and that the contribution of the rainfall at each gauge to the catchment average as well as how representative it is of the catchment as a whole will vary from storm to storm. This is illustrated by looking at the rainfall distribution over three diverse events and the reliability of a sample of gauges. The characteristics of the selected storms are shown in Table C-1.

The first stage is to identify the model that best fits the event CAR (ECAR) and event observed outflow (EQobs). The fit of this model will provide a measure of the reliability of the estimate of the ECAR. Model fits and hydrographs for the events described in Table C-1 are shown in Figure C-1. Both summer and autumn events show simulated hydrographs that display a reasonable approximation to the observed hydrograph. They show some peaks not present in the observed outflow hydrograph due to rain at some gauges which is included in the ECAR but has no effect on the outflow. The Autumn event does not fit well and it can be assumed that several gauges are supplying misinformation, that is, adding significant amounts of rain to ECAR that is not affecting the outflow or some significant rainfall has missed the gauges but affected the outflow. Misinformative measurements do not fit the model well but may still provide



substantial useful information about which areas of the catchment are actively generating flow. Figure C-1 also shows the hydrographs generated from the DGR inferred by inverting the ECAR model. In all cases, these hydrographs are a much better fit to the observed hydrograph than the hydrograph directly modelled using ECAR but, in the case of the Autumn event, the improvement is only slight. It is likely that so much disinformation is being supplied that it is not possible to accurately extract the DGR for this event.

*Table C-1 – descriptions of the three example events used to illustrate the DBM/ Reverse Hydrology method of identifying misinformative gauges. The three storms can be seen to have very different characteristics a) is a short-lived summer convective cell that passes mostly over the eastern side of the catchment. Storm b) is a more widespread over the catchment with the heaviest rain to the northeast. Storm c) is a widespread event with a heavier core falling mostly on the northern side of the catchment but with a few southern gauges measuring more rain.*

Description	Date	Spatial distribution	Catchment rainfall and Observed flow	Distribution of event rainfall totals (darker colour = more rain)
a) Summer event (SED4)	2/8/1994 — 7/8/1994			
b) Autumn event (SS5)	9/9/1995 — 13/9/1995			
c) Winter event (JANS)	26/1/1995 — 29/1/1995			

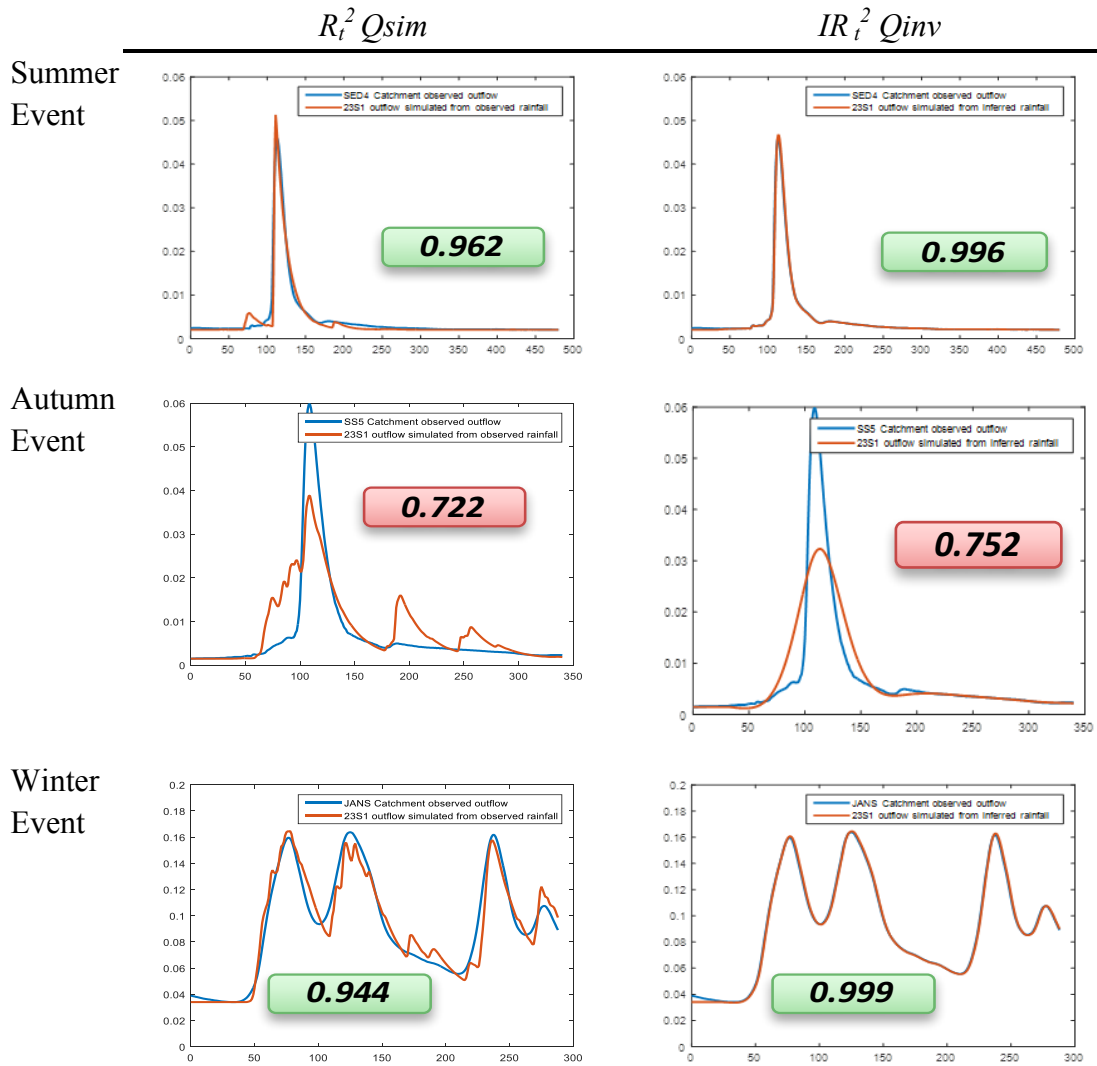


Figure C-1 – Comparison of model fits and hydrographs generated from ECAR (which could be an average of several gauges or an estimate from one gauge) and DGR for the same gauge or gauge-set . It can be seen that although for both the summer and autumn events the catchment average generates a good approximation of the observed hydrograph, it shows some peaks not present in the observed outflow hydrograph due to rain at gauges which are included in the ECAR but having no effect on the outflow. The Autumn event does not fit at all well and it can be assumed that several gauges are supplying misinformation, that is, adding significant amounts of rain to ECAR whilst not affecting the outflow.

The next stage is to examine the fit of models to the rainfall measured at each individual gauge throughout the event (ESGR). Four gauges spread round the edge of the catchment are shown as examples in Table C-2. Their locations can be seen in Figure 7-2. Gauge fits are colour coded as shown in Table 7-4. The relationship between the fit of the ECAR model and models fitted to SGR can be clearly seen by examining Table C-2. The summer event shows a very good fit to ECAR and all the gauges also

show good fits which are only slightly improved by using DGR implying that all gauges are representative of the catchment as a whole. In the case of the winter event that fits slightly less well than the summer event, one of the example gauges fits not as well implying that it (and maybe others) are supplying disinformation. Using the DGR to generate the hydrograph results in a significant improvement for all gauges. The observed hydrograph of the autumn event is not well reproduced by the hydrograph simulated from ECAR. The reason for this is clear from the fits of the sample gauges. Two (or more) fit poorly and are significantly non-representative whilst even the well-fitting gauges are on the low side of acceptable. Even using the DGR to simulate the hydrographs is not enough to render two of the gauges acceptable and they should not be used.

*Table C-2 – Model fits for a selection of gauges for each of the example events. The hydrograph generated from ECAR for the summer event shows a good fit to the Qobs as do each of the sample gauges. The Qinv hydrograph shows an improved fit. The Qsim hydrograph for the winter event shows a slightly less good fit and one of the individual sample gauges shows less good fit. The autumn event shows a poor fit to ECAR. Two of the sample gauges show a poor fit that is only partly resolved by using the DGR.*

Gauge	Summer Event		Autumn Event		Winter Event	
	$R_t^2$	$IR_t^2$	$R_t^2$	$IR_t^2$	$R_t^2$	$IR_t^2$
	<i>Qsim</i>	<i>Qinv</i>	<i>Qsim</i>	<i>Qinv</i>	<i>Qsim</i>	<i>Qinv</i>
Kilk	0.958	0.995	0.647	0.718	0.905	0.998
Batc	0.957	0.997	0.645	0.704	0.954	0.999
Craw	0.965	0.996	0.881	0.998	0.934	0.999
Fran	0.961	0.996	0.863	0.998	0.738	0.913

It can be concluded from this exercise that DBM modelling and Reverse Hydrology can be used to recognise when gauges which, whilst providing useful information to the CAR, are not significantly involved in flow generation, and identify any that can be might be disregarded for flow generation. This is not to say that the gauge observations are not accurate representations of their own local conditions but that these conditions are not, at this time, representative of the flow generation characteristics of the catchment as a whole. The model fit ( $R_t^2$ ) provides a measure of the confidence that can be placed on the gauge in question. Using DGR instead of CAR or SGR can significantly improve the fit of the hydrograph but if the gauge is severely non-representative, not even Reverse Hydrology can extract enough of the DGR from the

rainfall signal and the gauge should be rejected. It should also be noted that whether a gauge is representative or not varies with time due to the rainfall regime (convective or frontal) and the track of the storm and the size and position of internal storm cells.

## Chapter 8 In-filling and extending a rainfall record using Reverse Hydrology and Spectral Decomposition

Kretzschmar, A., Tych, W., Beven, K.J. and Chappell N.A.  
Lancaster Environment Centre

### Abstract

Long rainfall and flow records are required for design purposes, for example, the design of flood protection schemes. The method proposed here utilises Reverse Hydrology and Spectral Decomposition to either extend the rainfall record, or fill a gap in that record caused, for example, by failure of a rain gauge, with a realistic rainfall series that will generate the correct hydrograph. It is assumed that a flow record exists over the gap in the rainfall. A model is built using a calibration section of the record by first identifying a parsimonious continuous time transfer function model between rainfall and flow then inverting it, using the *RegDer* method of Kretzschmar *et al.* (2014), to obtain an estimate of the Discharge Generating Rainfall (DGR). The distribution of residuals between the DGR and observed rainfall is estimated. A uniformly distributed random number generator is used to construct a simulated, uncorrelated residual series with the estimated distribution. Correlation structure is introduced using an AR model based on the observed residual series. The high frequency simulated residual series and low frequency DGR are then combined and a threshold value applied to maintain the proportion of non-rain time periods in the record and the amount rescaled to match the volume of the observed rainfall. The transfer function *RegDer* model can then be used to estimate DGR from the flow over the missing section and the a possible rainfall sequence constructed by combining the high frequency simulated residual series with the low frequency DGR. The result is a series that looks realistic, has the correct residual structure and is capable of generating the correct hydrograph. The same methodology might be used to extend a rainfall record where a flow record exists but a rainfall record does not.

## 8.1. Introduction

Flooding is one of the most common natural hazards affecting thousands of people worldwide each year and there is evidence to suggest it will get worse due to climate change (Huntington, 2006). There have been improvements in rainfall measuring techniques in recent years with the introduction of telemetry, rainfall radar and remote sensing however much rainfall data still comes from point gauges often at hourly or even daily intervals (Garcia-Pintado *et al*, 2009). Flood forecasts are often based on models that are simplified representations of the processes acting within a catchment. Their main input is usually rainfall which is highly variable in both space and time. The rainfall field is damped (smoothed) by the catchment storage and area as it becomes streamflow. Uncertainty is introduced from many sources including the model structure and parameters, observation errors in both the inputs and outputs, lack of knowledge of the processes at work at the scale of interest and other sources some of which are known about and some which are not (Beven, 2016).

Long rainfall records are required as input to rainfall-runoff models used for generating the long streamflow series needed for planning purposes. Many methods of stochastic rainfall generation have been proposed and may be used to extend existing short records. A method using Data-Based Mechanistic (DBM) modelling and Reverse Hydrology (Kretzschmar *et al.*, 2014, 2015 and chapter 7) that may be used to in-fill and extend existing records is proposed in this paper. Reverse hydrology allows an estimate of the rainfall required to generate discharge given a forward model derived from rain gauge inputs. A system model is identified linking rainfall and discharge then run backwards, that is, streamflow is used to infer the rainfall that has generated it using an inverted model (Kretzschmar *et al.*, 2014). The integrative dynamics of the process mean that it is not feasible to simply fit a model ‘in reverse’ (that is, use streamflow as the model input and rainfall as the output).

## 8.2. Review

Long series of rainfall data may be required for simulation studies (Marien and Vandewiele, 1986) for uses such as design of flood defences, reservoirs and sewerage systems, landslide modelling, soil erosion and sediment transport, water quality including monitoring disperse pollution, vulnerability to desertification and

downscaling of global and regional climate change scenarios (Onof *et al.*, 2000, Burton *et al.*, 2008, Baigorria and Jones, 2010, Engida and Esteves, 2011). If rainfall records of the required length and/or resolution do not exist then modelling must be applied to make good this deficiency. Onof *et al.* (2000) defined 4 groups of approaches to rainfall generation: complex process-based, multi-scale stochastic including multi-fractal cascades, statistical models that use the observed rainfall characteristics and point-process stochastic models, for example, Bartlett-Lewis and Neyman-Scott cluster models. Cameron *et al.* (2000) categorise stochastic rainfall models used for continuous simulation as profile based or pulse based. Profile based models use statistical distributions to characterise mean intensity and inter-event arrival time. Depths generated are split into components of the required resolution via a profile or mass curve. Pulse based models use the same process but also use a statistical distribution to represent the characteristics of rain-cells found randomly within a rainstorm, for example, Neyman-Scott (for details *c.f.* references in Cameron *et al.*, 2000). They state that pulse models are good at representing the inter-event arrival times but are not so good as profile based models at recreating extremes.

Many of the same techniques used to generate rainfall may also be used to in-fill gaps in rainfall records. Most work on in-filling focuses on spatial interpolation at daily or longer timescales, however Dirks *et al.* (1998) compared Thiessen polygon (TP), Inverse Distance Weighting (IDW), areal mean and Kriging methods at temporal scales from hourly to yearly and found that all methods produced comparable results for 13 rain-gauges in a 35 km<sup>2</sup> catchment on Norfolk Island. Ahrens (2006) reported that using a statistical rather than geographical distance between gauges resulted in a more robust rainfall estimate especially in mountainous terrain. A method for preserving the statistical properties of the time series utilising multiple linear regression, that avoided over-estimation of the number of wet days and under-estimation of high-intensity events, was proposed by Simolo *et al.* (2010). They stated that daily methods are complicated by the space-time variability. Several studies have compared traditional techniques with geospatial methods such as Kriging and Kriging with local means (for example, Mair and Fares, 2011) and suggest that geospatial methods can produce better estimates as they account for spatial correlation however they require large amounts of data and access to suitable software. Other methods used include Artificial Neural Networks (Nkuna and Odiyo, 2011), Gaussian copulas (Bardossy and Pegram, 2013),

multi-variate linear regression using 10 nearest neighbours (Serrano-Notivoli, 2016) and incorporation of radar and remote sensing data (Brocca *et al*, 2013; 2014). Teegavarapu (2014) provided a comparison of many methods with associated references. He states that spatial interpolation generally under-estimates high extremes and over-estimates low and fails when there is precipitation at neighbouring gauges but not at the base gauge or conversely when there is rain at the base gauge but not the surrounding ones. This last limitation may be at least partially addressed by the method presented here because it utilises information about rainfall over the whole catchment extracted from the streamflow not just from rainfall. The suggested method can also infill at a much higher resolution than many of the existing techniques assuming some high resolution records exist.

In this paper, a composite point-process stochastic model, utilising sub-daily rainfall and flow records, based on combining low frequency Discharge Generating Rainfall, representing the catchment dynamics, with high frequency behaviour of the residuals, which has no impact on discharge generation. The model may be used to fill gaps in rainfall records or extend existing records where flow records exist but rainfall records do not. In future, it may be possible to extend this concept to deriving a ‘DGR generator’ that could be used to generate longer series and extremes when rainfall records are not available. The smooth profile of the DGR, carrying only the information required to generate discharge, should make it easier to transfer rainfall estimates from one catchment to another, leading to reduction in the uncertainty due to no high frequency signal being present, when predicting in ungauged basins (PUB).

### **8.3. Aim of the paper**

The aim of this paper is to introduce a method for constructing a rainfall sequence by combining Discharge Generating Rainfall (DGR) (introduced in Chapter 7) and simulated residuals – an application of spectral decomposition and reverse hydrology that may be used to extend existing sub-daily rainfall records where runoff records exist and rainfall records do not. The same process may be used to infill gaps in rainfall records.



## 8.4. Discharge Generating Rainfall

Estimating the characteristics of the Discharge Generating Rainfall (DGR) - the rainfall responsible for producing the hydrograph (introduced in Chapter 7) allows simulation of synthetic rainfall series that may be used in many applications including input to flood forecasting models or infilling gaps in rainfall records that could be caused by equipment failure, for example, due to freezing or blockage of rain-gauges. The dynamic part of the discharge generation process is described by linear, time invariant dynamics, modelled using a continuous time transfer function model (Kretzschmar *et al.*, 2014). The rainfall-runoff non-linearity is modelled using a Hammerstein memoryless input non-linearity (*c.f.* Young and Beven (1994) and Beven (2012), for the hydrology perspective, also Wills *et al.*, (2013) for a general system perspective) as shown in Figure 8-1. This method uses a hybrid dynamical modelling approach (Young *et al.*, 2006; Laurain *et al.*, 2008) combining a continuous time model and a discrete time error model to produce a realistic rainfall series. The method is similar to that described by Liu and Munson (1982). They proposed a method for generating a random sequence with a specified marginal distribution and auto-covariance using white Gaussian noise as input to a linear filter followed by a zero-memory non-linearity chosen so that the distribution is reproduced and the auto-covariance approximated.

Systems analysis techniques, implemented using the Captain toolbox in Matlab (Taylor *et al.*, 2007), were used to identify a continuous time (CT) transfer function model using high-resolution rainfall and streamflow data to capture the dynamics of the catchment. The model (or models) thus identified can be inverted using the regularisation process (*RegDer*) presented in Kretzschmar *et al.* (2014). The output from the *RegDer* process is an inferred rainfall series that is an estimate of Discharge Generating Rainfall (DGR). DGR is not the same as CAR which includes the broad rainfall spectrum whereas the DGR is an estimate of the part of the rainfall spectrum (the lower frequencies) that generates flow.

DGR can be negative. Comparison of rainfall and flow plots (*c.f.* Figure 8-7) shows how this can be explained in terms of catchment behaviour and rainfall spatial distribution. Negative DGR often occurs during a recession because the flow is driven by the catchment (that is, flow comes from catchment storage) not the rainfall

(Montesarchio *et al.*, 2015). Small negative spikes may also occur when the inversion process compensates because it has stopped raining in one part of the catchment and not another, but the flow is still increasing. Negative periods of rainfall are a product of the inversion and do not impede its use as a tool for generating catchment outflow, in fact they are an important part of the mechanism. The proportion of negative DGR will vary over time depending on catchment conditions and the rainfall distribution.

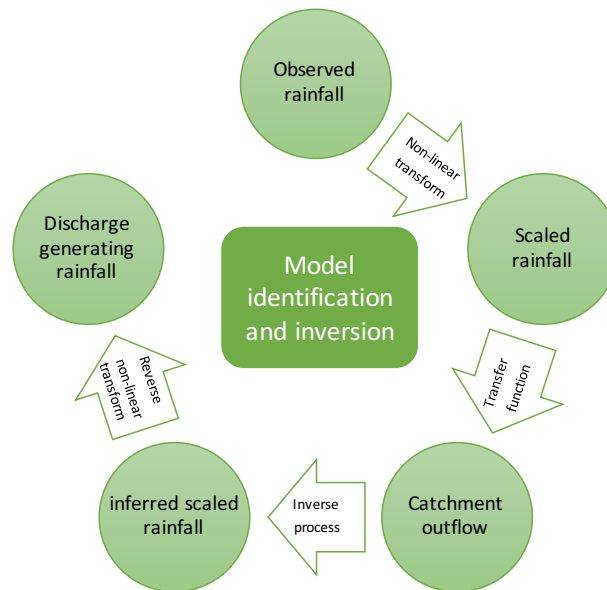


Figure 8-1 - Model identification and inversion workflow showing the off-line linear transformation.

A CT formulation is used because it enables a wide range of catchment dynamics to be modelled, also the parameters have a direct physical interpretation that is independent of the sampling rate (Young, 2010). Inverting processes which have been integrated in both time and space means that the inversion is badly posed. Applying the regularisation technique makes inversion possible without the amplification of the noise present in the data (Kretzschmar *et al.*, 2014). Other approaches may be found in the referenced literature (Croke, 2006, 2010; Kirchner, 2009; Andrews *et al.*, 2010; Young and Sumislawska, 2012; Brocca *et al.*, 2013, 2014; Kretzschmar *et al.*, 2014, 2015, 2016). Kretzschmar *et al.* (2014) showed that the regularisation process produced a rainfall profile that sacrificed time resolution in favour of numerical stability, the result of the damping effect of the catchment in both space and time. They showed that this rainfall sequence resulted in modelled flow sequences that fitted the observed streamflow data more closely than flow modelled using the observed rainfall, implying

that the dynamics of the catchment were being effectively captured. This was recognised to be the rainfall responsible for generating the discharge (chapter 7).

### **8.5. Data source – Brue Experimental Catchment, South-west England**

This study utilises rainfall and runoff data from the Brue catchment in South-west England where 23 of the available 49 rain gauges (see section 7.5) were used to estimate catchment average rainfall using the Thiessen Polygon method (Shaw *et al.*, 2011). There is an elevation change of approximately 300 m from south-west to north-east across the catchment. The catchment can largely be split into impermeable low-land to the west (mostly mudstone and siltstone), higher land to the east where the limestone ridge is permeable, and the far east of the catchment which is largely impermeable (mostly mudstone with siltstone or sandstone) – see Figure 8-2. Land use is mostly pasture with some woodland on the elevated eastern side. The Brue research catchment was set up in 1993 as part of a Natural Environment Research Council (NERC) special topic research programme – the Hydrological Radar Experiment (HYREX) (Wood *et al.*, 2000). It ran for three years but the data has been extensively used in many subsequent research projects (for example, Wood *et al.*, 2000; Moore *et al.*, 2000; Bell and Moore, 2000; Villarini and Krajewski, 2008; Villarini *et al.*, 2008).

Rainfall and flow data sampled at 15 minute intervals at 23 rain gauges and a single flow gauge at the catchment outlet for the period October 1994 to September 1997 (3 years) were used in this analysis. The density of the gauge network (1 gauge per 5.9 km<sup>2</sup>) is enough to give good estimate of the true catchment rainfall (CAR).

### **8.6. Model fitting and hydrograph generation**

Models were fitted, using DBM modelling techniques, as described in Kretzschmar *et al.* (2014), to a ‘observed rainfall series’ (ORS) and the observed catchment outflow (Qobs). ORS may be an estimate of CAR or rainfall from a single gauge or a set of gauges. Model fit was measured using a combination of the Nash-Sutcliffe efficiency (NSE or  $R_t^2$ ) and the Young Information Criterion (YIC; Young, 1984), an objective measure combining model fit with a measure of over-parameterisation. The primary criterion was the performance of the inversion technique – also measured using  $R_t^2$

(Nash –Sutcliffe efficiency) – here defined as  $IR_t^2$  to distinguish it from the fit of the forward model.

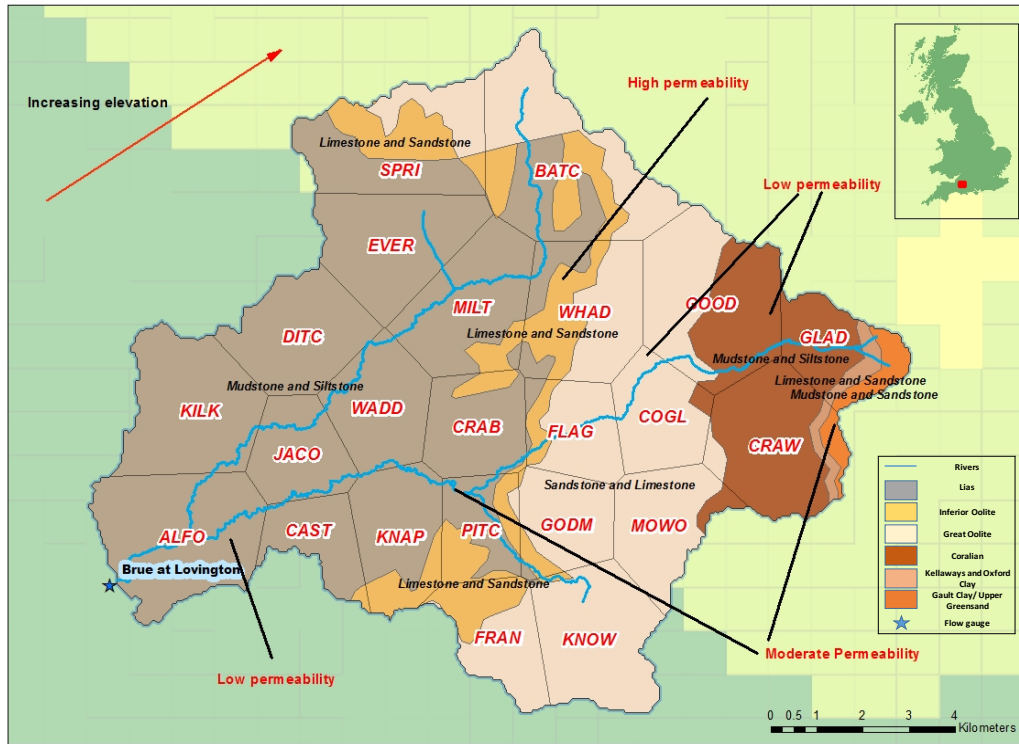


Figure 8-2 - Brue catchment showing location of 23 gauges used in the study and the underlying geology. (used elsewhere but included here for clarity)

$R_t^2$  is given by:

$$R_t^2 = 1 - \frac{\sum_{i=1}^n (O_i - P_i)^2}{\sum_{i=1}^n (O_i - \bar{O})^2} \quad (\text{Equation 8-1})$$

where  $O_i$  are the observed values and  $P_i$  the predicted values and  $\bar{O}$  is the average of  $O_i$ . and  $YIC$  is given by:

$$YIC = \ln \frac{\sigma_r^2}{\sigma_o^2} + \ln \{NEVN\} \quad (\text{Equation 8-2})$$

where  $\sigma_r^2$  and  $\sigma_o^2$  are the variances of the residual and observed series respectively and NEVN (the normalised error variance norm) is given by:

$$NEVN = \frac{1}{np} \sum_{i=1}^{np} \frac{\sigma_r^2 P_{ii}}{a_i^2} \quad (\text{Equation 8-3})$$

where  $np$  = the number of parameters,  $P_{ii}$  is the  $i^{th}$  diagonal element of the parameter covariance matrix and  $a_i^2$  is the square of the  $i^{th}$  parameter. The first term measures how well the model fits the data and the second the efficiency of its parameterisation. A

large negative value indicates a good fit with lowest number of parameters necessary to capture the system dynamics. *YIC* can be interpreted as a compromise between model fit and model complexity (Young *et al.*, 1996).

Additional information on the performance of a model may be obtained by calculating  $R_t^2$  calculated from a log transform of the data ( $R_t^2L$ ).  $R_t^2$  gives extra weight to the peak flows because it is calculated using the square of the differences between the observed and simulated data (see Equation 8-1). Taking logs flattens out the higher values whilst having little effect on the lower ones (Krause *et al.*, 2005) giving more weight to the lower values. A combination of  $R_t^2$  and  $R_t^2L$  may be used to assess how well a model performs across the whole range of the hydrograph. The inferred rainfall sequence is much smoother usually with lower peaks than the observed sequence and has a lower time resolution. Kretzschmar *et al.* (2015; 2016) have shown that the inferred rainfall series captures the dynamics of the catchment, in both space and time, despite the loss of resolution. The inversion process extracts the Discharge Generating Rainfall or DGR (signal) from the measured rainfall with its broad-spectrum – *c.f.* chapter 7. An example comparing DGR with the corresponding ORS is shown in Figure 8-4.

The inversion process extracts the flow generating rainfall signal from the broad spectrum of observations because it makes use of information contained in the catchment outflow. The catchment acts effectively as a low-pass filter and the regularised inversion process likewise filters out the high frequency behaviour that has little impact on the outflow hydrograph.

### **8.7. Modelling realistic rainfall series by spectral decomposition**

Long rainfall sequences are often needed for design purposes. Reverse hydrology can be used as a method for generating rainfall sequences that reproduce the low frequency characteristics of the catchment and the high frequency characteristics that are a result of climatic factors, including the spatio-temporal distribution, that affect hydrograph characteristics such as the rising limb, time-to-peak and peak magnitude (Montesarchio *et al.*, 2015). The high frequencies can be modelled using statistical methods based on the structure of the residuals between the DGR and the ORS. Combining the high and low frequencies produces a synthetic rainfall series that generates the right hydrograph

and maintains the correlation structure of the residuals (Figure 8.3). Long series of daily rainfall are often available but the methodology employed here could generate rainfall at a much higher resolution – dependent on a short series of rainfall and flow being available at a higher resolution long enough to identify a stable model. The method used is similar to that used by Liu and Munson (1982) (*c.f.* section 8.4).

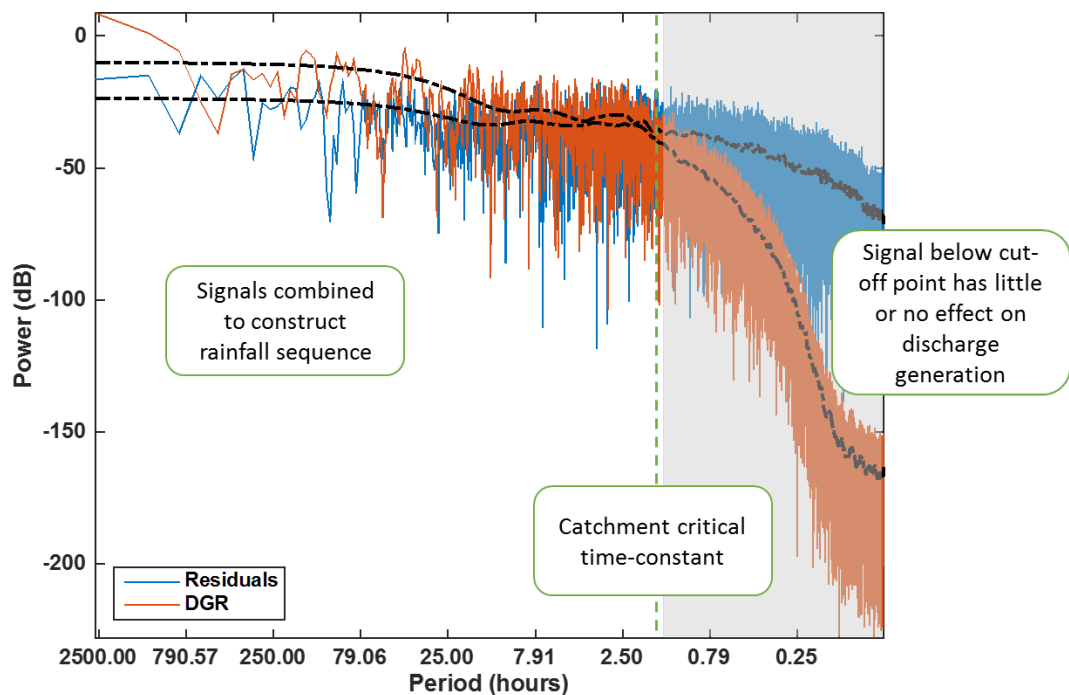


Figure 8-3 - Frequency plots of the DGR and the residual series CAR-DGR. DGR mirrors the flow and drops sharply at the frequency of the critical time constant of the catchment. All frequencies below the cut-off point – where the amplitude of the DGR has dropped by 6 dB – are low power and have no significant effect on discharge generation (shaded area) as these parts of the signal are filtered-off by the catchment dynamics.

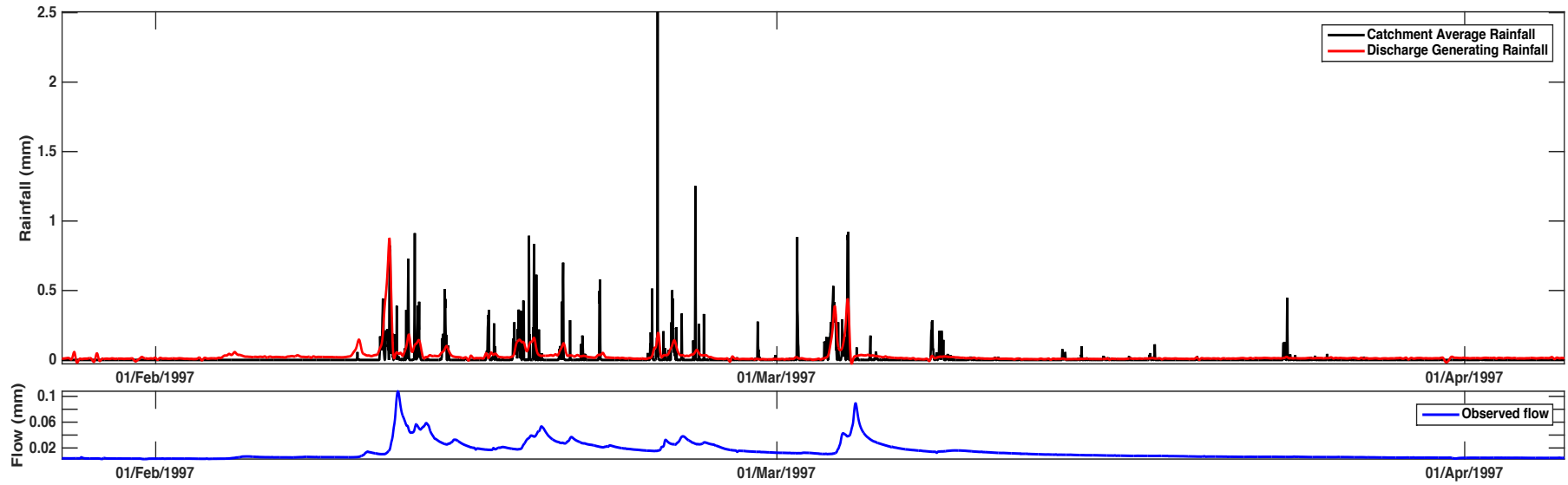


Figure 8-4 – Comparison of CAR and DGR for a short section of record. DGR mirrors the flow but it is also obvious that the same amount of rain does not always generate the same amount of flow – non-linearity – due probably to the state of the catchment.

Figure 8-5 shows the basic method for constructing a rainfall sequence using reverse hydrology to infer the low-frequencies and residual correlation structure to generate the high frequencies. The reconstructed rainfall sequence should look like rainfall, is based on the correlation structure of the residuals and can generate the correct hydrograph. A hybrid dynamic model (Young, 2006) is built by modelling the low frequency DGR using an inverted continuous time TF model (Kretzschmar *et al.*, 2014, 2015) and a DT error model based on the auto-correlation structure of the residuals between CAR and DGR. An example of rainfall reconstruction based on WY1 follows. Once the model for reconstruction has been built, it can be used to generate new rainfall series for catchments that have long flow records but only short rainfall records or for filling gaps in rainfall records.

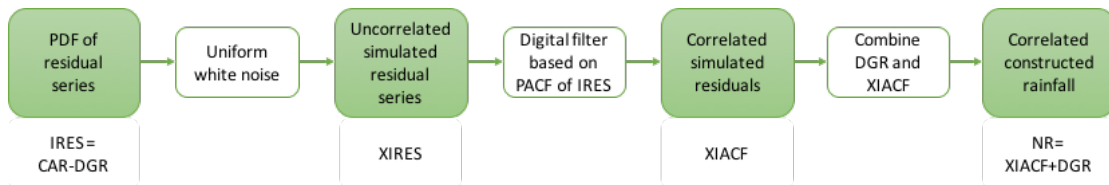


Figure 8-5 – The basic method for rainfall generation by spectral decomposition. Reverse hydrology is used to generate the low frequency band part of the rainfall signal related to the catchment hydrograph response (DGR), and analysis of the residuals (CAR-DGR) is used to build a model of the high frequency part of the rainfall spectrum with the same distribution as the modelled residual series. A digital filter is constructed based on the AR structure of the residual series. After some manipulation, the resulting rainfall sequence looks like rainfall, has a similar temporal and frequency structure to the observed rainfall.

## 8.8. Building the hybrid rainfall model

The following example is based on WY1 (October 1994 – September 1995). The CAR in this example is calculated using all available gauges, so is the best estimate obtainable; however if only a single gauge is available, this must be assumed to be the best estimate of CAR. Residuals between catchment average rainfall (CAR) and inferred rainfall (DGR) using the best identified model between CAR (or its estimate) and catchment outflow (Qobs) are calculated to give a residual series (IRES) as shown in equation 8-4. CAR and flow modelled from CAR are shown in Figure 8-6. Performance of the constructed rainfall sequence is assessed by comparison with the observed rainfall and the modelled flow using the  $R_t^2$  and  $R_t^2L$  as metrics (*c.f.* section 8.6).



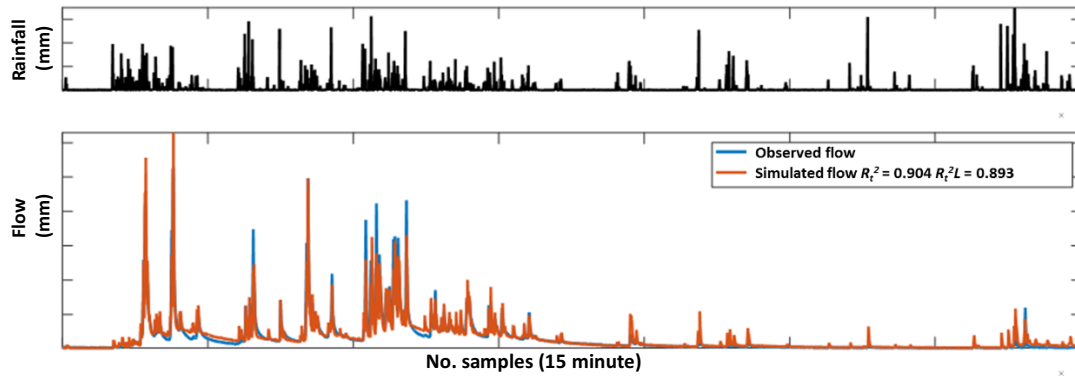


Figure 8-6 – The rainfall construction model is based on the rainfall and flow series for WY1. Flow modelled using the best available estimate of CAR and the best-fit model is compared to the observed hydrograph.  $R^2$  of 0.904 suggests that the peaks and high flows are well matched but the  $R^2L$  is lower suggesting that recessions are slightly less well captured. This is the benchmark with which to compare the performance of the constructed rainfall series for the same period.

DGR and IRES are shown in Figure 8-7 where IRES is given by:

$$IRES = CAR - DGR \quad (\text{Equation 8-4})$$

The method is based on combining the high and low frequency parts of the signal into a realistic rainfall series. DGR has a lower resolution than the original sampled rainfall (Kretzschmar *et al.*, 2015) due to the filtering effect of the catchment processes (the low frequency part of the rainfall signal) and is estimated using the regularisation process presented by Kretzschmar *et al.*, (2014; 2015). The residuals between the CAR and DGR are an estimate of the high frequency part of the signal that is a result of the rainfall which does not affect the outflow (*c.f.* Figure 8-4). Figure 8-3 shows the DGR and residuals in the frequency domain and Figure 8-7 shows the same series in the time domain. Negative DGR, a result of the non-homogeneity of the rainfall field, is discussed in section 8.4. An estimated realisation of the high-frequency part of the signal is simulated using the method described here.

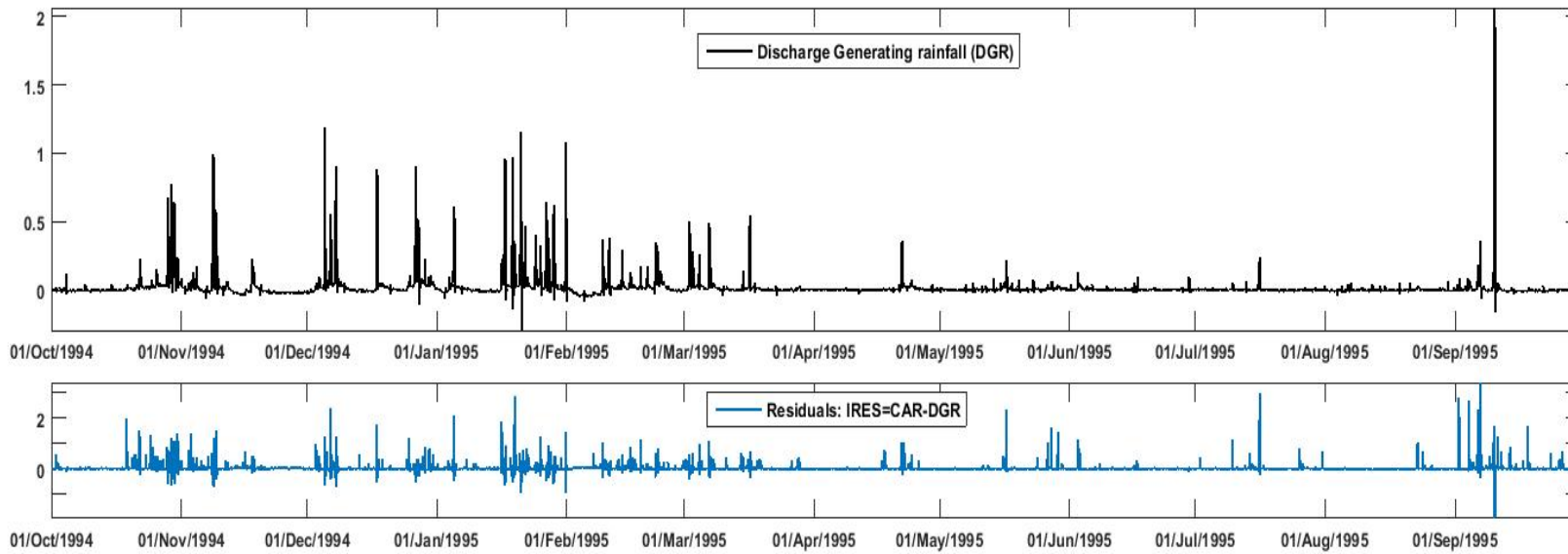


Figure 8-7 – Time domain plots of Discharge Generating Rainfall (DGR (mm)) ( top plot), an estimate of the low frequency part of the signal. and the residual difference CAR-DGR (lower plot), an estimate of the high frequency part of the rainfall signal, for WY1.

An Auto-Regressive (AR) model of the auto-correlation structure of the residual series (IRES), based on its significant partial auto-correlation, is built and has the form (assuming  $m$  significant lags):

$$y_k = \frac{1 - \sum_{i=1}^m a_i z^{-i}}{1 - a_1 z^{-1} + \dots - a_m z^{-m}} e_u \quad (\text{Equation 8-5})$$

where  $a_i$  are the first  $m$  significant auto-correlation coefficients of IRES and  $e_u$  is white noise. The auto-correlation structure of IRES is shown in Figure 8-8.

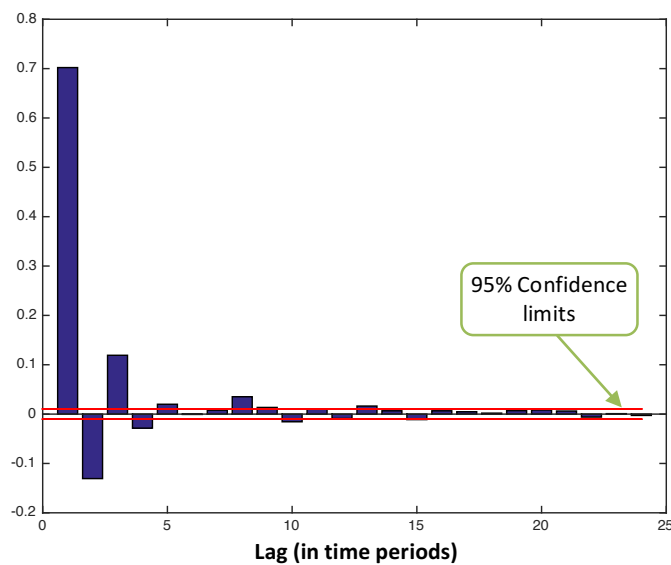


Figure 8-8 – the auto-correlation structure of the residual series, IRES. The 95% confidence limits are shown in red. In this example, 13 correlation coefficients should be included to reproduce the correlation structure.

The residual PDF is estimated from IRES then a sequence of uniform random numbers generated to represent their probability of occurrence and transformed using the PDF of IRES, to obtain an uncorrelated pseudo residual series (XIRES) with the same distribution. One possible comparison of the real (IRES) and synthetic (XIRES) series is shown in Figure 8-9. It can be seen from the plots that the distribution of synthetic residuals has a similar shape to the observed but is spread out more around zero. The auto-correlation structure is approximated by filtering using the DT model constructed from the auto-correlation to give a series of correlated, simulated residuals (XIACF). The generated residual series should now have a similar distribution to IRES. Comparison of the distributions of XIACF and IRES are shown in Figure 8-10.

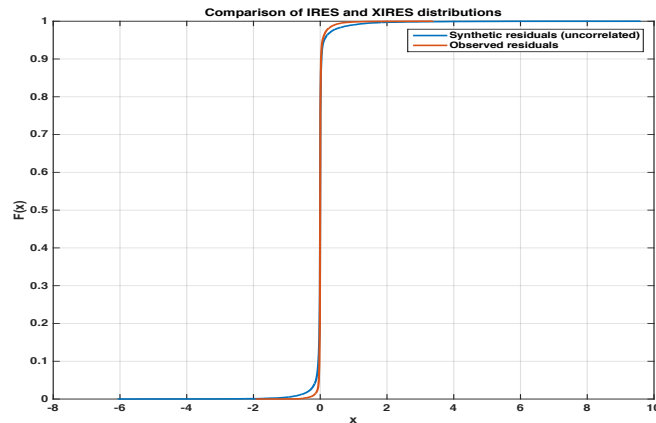


Figure 8-9: Comparison of the distributions of calibration residuals (IRES) and simulated residuals (XIRES).

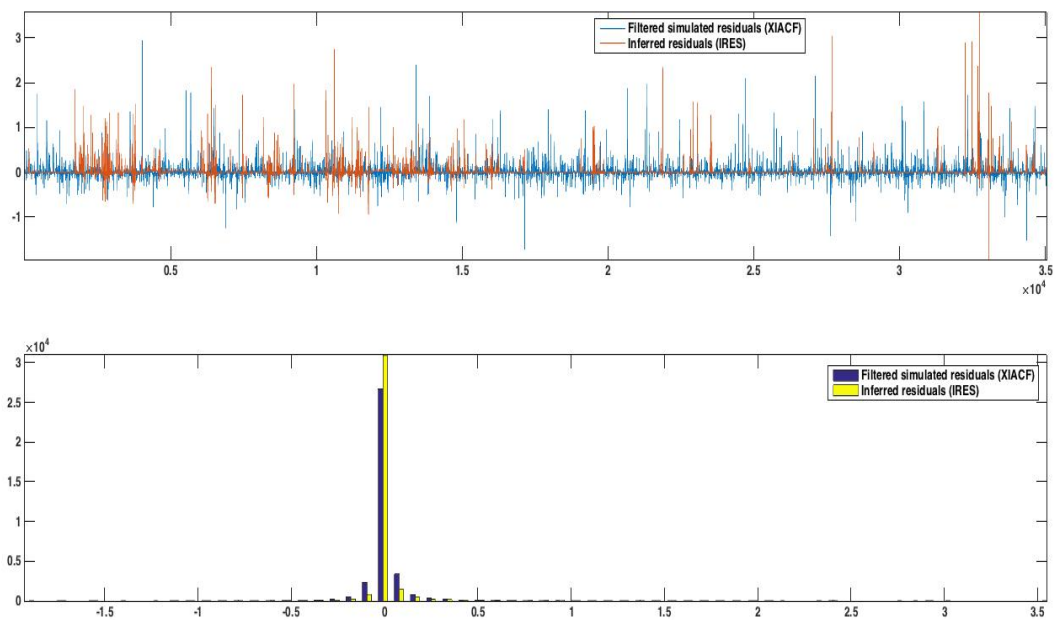


Figure 8-10 – comparison of the series of simulated residuals (XIACF – blue line and blue bars) and base residuals (IRES – red line and yellow bars) shows them to have similar distributions

The new rainfall series is constructed by combining the low frequency DGR and the generated high frequency residuals-like series to give a new rainfall series (NR):

$$NR = DGR + XIACF \quad (\text{Equation 8-6})$$

when  $DGR > 0$  and 0 at other times. DGR is the discharge generating rainfall series and XIACF the simulated pseudo-residuals. In this example, 12.6% of the DGR is negative. Although there are some large negative values (for example, in January and February 1995), these are short periods only. The majority are very small and close to zero. The

reason for these negative values is discussed in section 8.4. In order to reduce the number of negative ordinates generated by equation 8-6, DGR can be truncated, that is negatives removed, and then rescaled to preserve the mass balance. The updated equation becomes:

$$NR = \left( \frac{\sum CAR}{\sum DGR_T} * DGR \right) + XIACF \quad (\text{Equation 8-6a})$$

where  $DGR_T$  is the truncated DGR series. XIACF is not added to zero values of rescaled series.

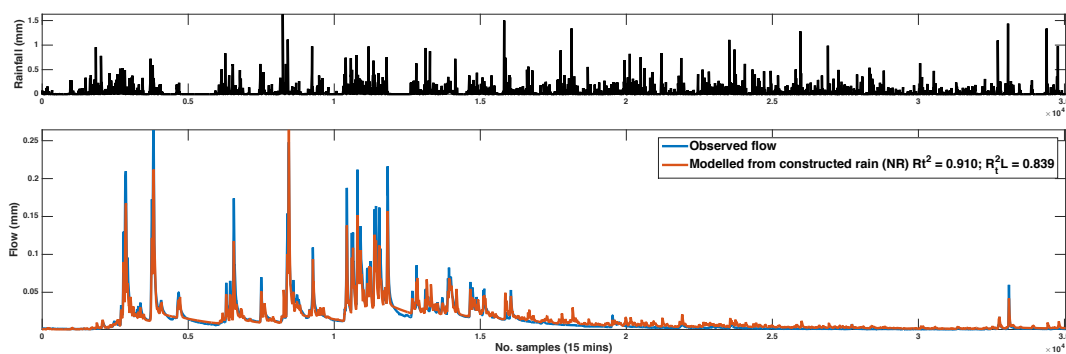


Figure 8-11 – the top plot shows the series  $NR = \left( \frac{\sum CAR}{\sum DGR_T} * DGR \right) + XIACF$  (Equation 8-6a). The bottom plot compares hydrographs generated from this series with the observed hydrograph.

The resultant series (NR) in Figure 8-11 may still contain some negative ordinates and small amounts of rain in many more time periods than in the original series. The hydrograph generated from this rainfall series shows a similar fit to that generated from observed rainfall (0.904). This is not surprising as the new series is based on the DGR with noise added. A frequency domain plot comparing CAR and NR is shown in Figure 8-12. Above the cut-off point the traces are very similar, below, where rainfall has little influence on flow, the traces start to diverge but here rainfall could take almost any value. A threshold value of rainfall ( $>0$ ) can be used to constrain negative and very small values to 0 (NRC). The threshold value can be manually adjusted until the proportion of zeros in NRC matches the proportion in CAR. Some typical values are shown in Table 8-1. Truncation and rescaling of the series in this way may result in a bias being introduced into the generated series. This is discussed in section 8.11.

*Table 8-1 – Proportion of zero rainfall periods in CAR is 0.81. Adjusting the threshold value and setting all values in NR less than the threshold to 0 allows the proportion of zero rainfall periods in the constructed sequence to be matched with CAR. (Due to the stochastic nature of the process, the exact figures will vary with every realisation)*

Threshold value	NRC
0.0	0.559
0.01	0.667
0.032	0.810

Constraining the rainfall series results in a change in the total rainfall so it must be rescaled to match CAR in order to compensate (NRCV). At this point, the runoff coefficient (RC) is also calculated because, during periods of missing rainfall, CAR will not be available so a consistent ratio between the proportion of rainfall converted into discharge is assumed. The RC is given by:

$$RC = \frac{\sum Q_{obs}}{\sum CAR} \quad (\text{Equation 8-7})$$

Constraining and rescaling the rainfall series should have little effect on its ability to generate a realistic hydrograph because the changes will only be reflected in the high frequency part of the spectrum that, due to catchment dynamics, has little effect on flow generation however some bias may be introduced. The frequency spectra of NRCV and CAR are shown in Figure 8-13 and show greater divergence than in Figure 8-12.

Comparing frequency spectra confirms that the auto-correlation structure is being preserved (duality of ACF and frequency spectrum). The series must also be compared in the time domain as equivalence in the frequency domain is necessary but not sufficient to ensure a match. Generated hydrographs are compared in Figure 8-14. Comparing the  $R_t^2$  and  $R_t^2L$  values with the hydrograph generated from CAR indicates that NRCV generates a hydrograph closer to the observed than using CAR alone because it is based on the DGR, the part of the rainfall necessary for generating flow. The ability of NRCV to generate an acceptable hydrograph is confirmed by Figure 8-15 where discharge generated from pure DGR is plotted against discharge generated from NRCV. Correlation between the flow series is 0.968 showing that the ‘noise’ added to the DGR does not affect its efficacy when generating a realistic flow series.

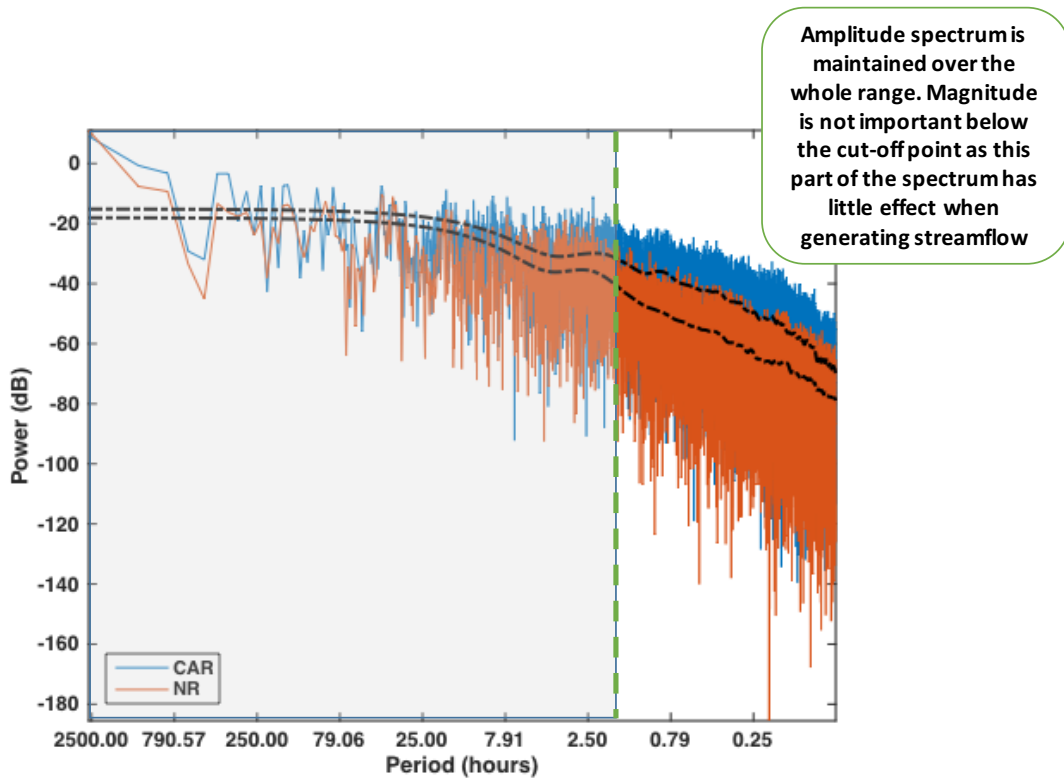


Figure 8-12 – Frequency spectra of NR (new rainfall sequence) and CAR are very similar in the area of interest showing that the auto-correlation structure has been maintained.

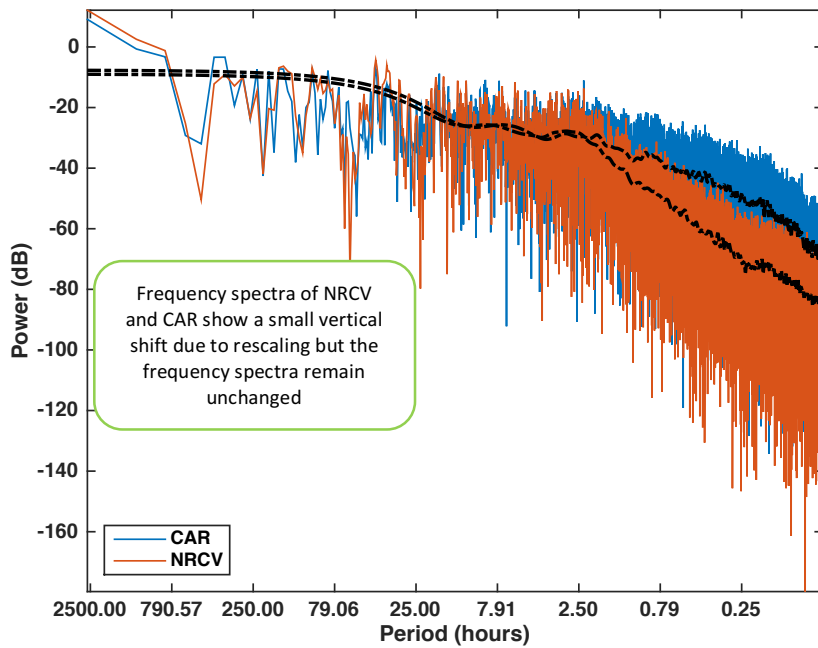


Figure 8-13 - Frequency spectra of CAR and NRCV. The spectra show a slight vertical shift as a result of the rescaling of the rainfall series but the frequency patterns remain unchanged.

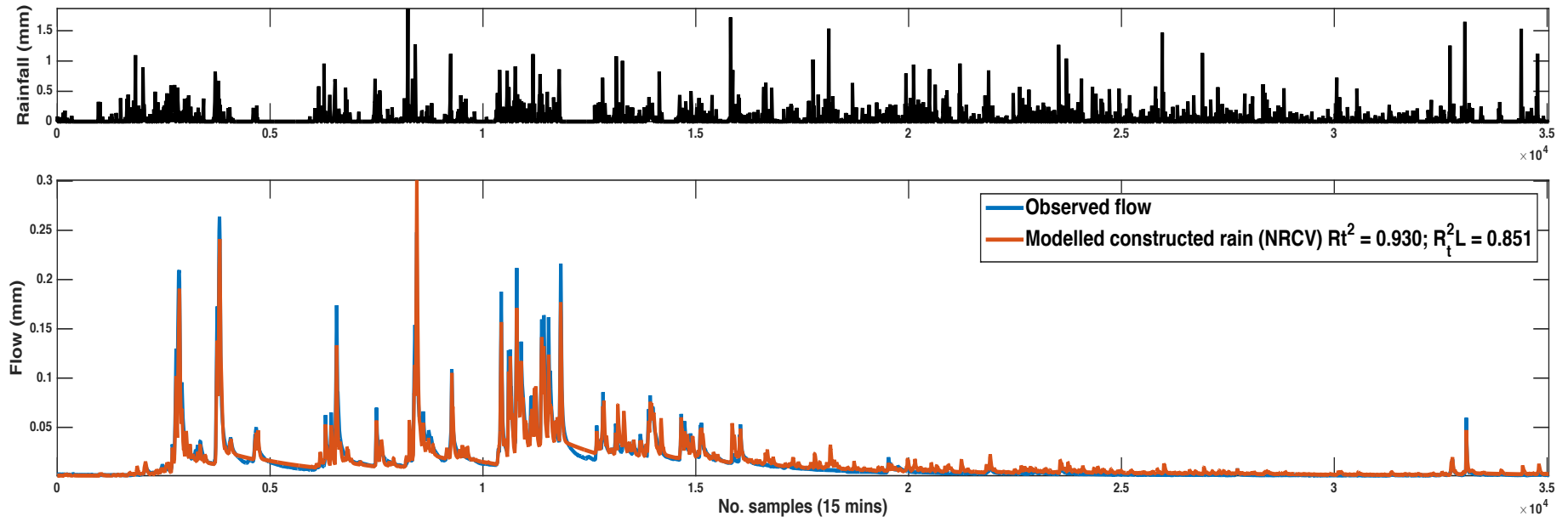


Figure 8-14 – Hydrograph generated from constructed rainfall series NRCV compared with the observed hydrograph. An  $R_t^2$  of 0.930 is better than the hydrograph generated from observed rainfall. The  $R_t^2L$  value confirms that fit is good over the whole flow range.



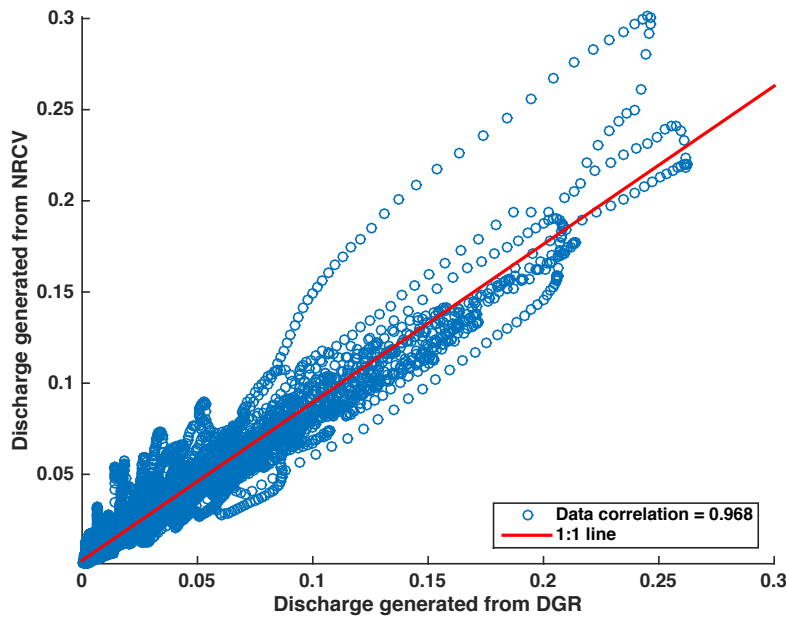


Figure 8-15: Discharge generated from pure DGR plotted against discharge generated from a constructed rainfall series (correlation coefficient = 0.968) showing that the constructed series does generate the correct hydrograph.

Examination of the statistics of the constructed rainfall series (NRCV) in Table 8-2 show that most match CAR reasonably well, it should be noted that this is only one possible series of rainfall that could be generated and further investigation is required to validate the methodology presented (see discussion in section 8.11).

Table 8-2 - characteristics of the series at the stages of building the rainfall model. Many of the statistics are well matched but notable exceptions are Standard deviation and maximum intensity indicating that for this particular reconstruction extreme values are not well represented.

	Hydrograph fit		Mean	Standard deviation	Proportion zero/negative	Maximum Intensity	Total Volume
	Rt2	Rt2L					
CAR	0.904	0.872	0.027	0.129	0.809	13.97	929.2
DGR	0.999	0.991	0.025	0.091	0.269	9.10	867.9
NR	0.910	0.839	0.029	0.131	0.559	9.02	1024.2
NRC	0.899	0.880	0.023	0.077	0.810	6.52	811.4
NRCV	0.930	0.851	0.027	0.089	0.810	7.46	929.2

The hydrograph fit ( $R_i^2=0.930$ ) compares favourably with the CAR hydrograph fit ( $R_i^2=0.904$ ) however the forward hydrograph has the same issues as any other – peaks where none are observed (due to spatial variability of observed rainfall). The model used to fit the hydrograph was the model identified between the observed rainfall (CAR) and observed catchment outflow (Qobs). A model fitted uniquely to the new rainfall sequence might give a better fit. Further refinement of the process may be required however examination of the hydrographs shown in Figure 8-16 derived from the DGR inferred from each rainfall series show the same fit confirming that, although the rainfall sequences look very different, the discharge generating characteristics are preserved. Once the model has been constructed and verified, it can be used to generate further rainfall series as long as flow records exist for the catchment.

DGR extracted from the flow captures the essential flow generating dynamics and, if used to generate flow, results in a reduction in uncertainty however it does not ‘look’ like rain. Whether this is an issue depends on the purpose of the exercise. If flow is to be simulated then only the DGR is required and once the DBM model has been established, the rainfall input could be directly filtered to generate DGR. Adding back some of the high frequencies present in the broader rainfall spectrum produces a synthetic sequence that ‘looks’ more like rainfall, has the essential characteristics of the observed rainfall and generates a correct hydrograph. The pseudo-rainfall series at high frequencies are generated using random numbers so many sequences fulfilling these criteria are possible. Multiple realisations will be examined in the following section.

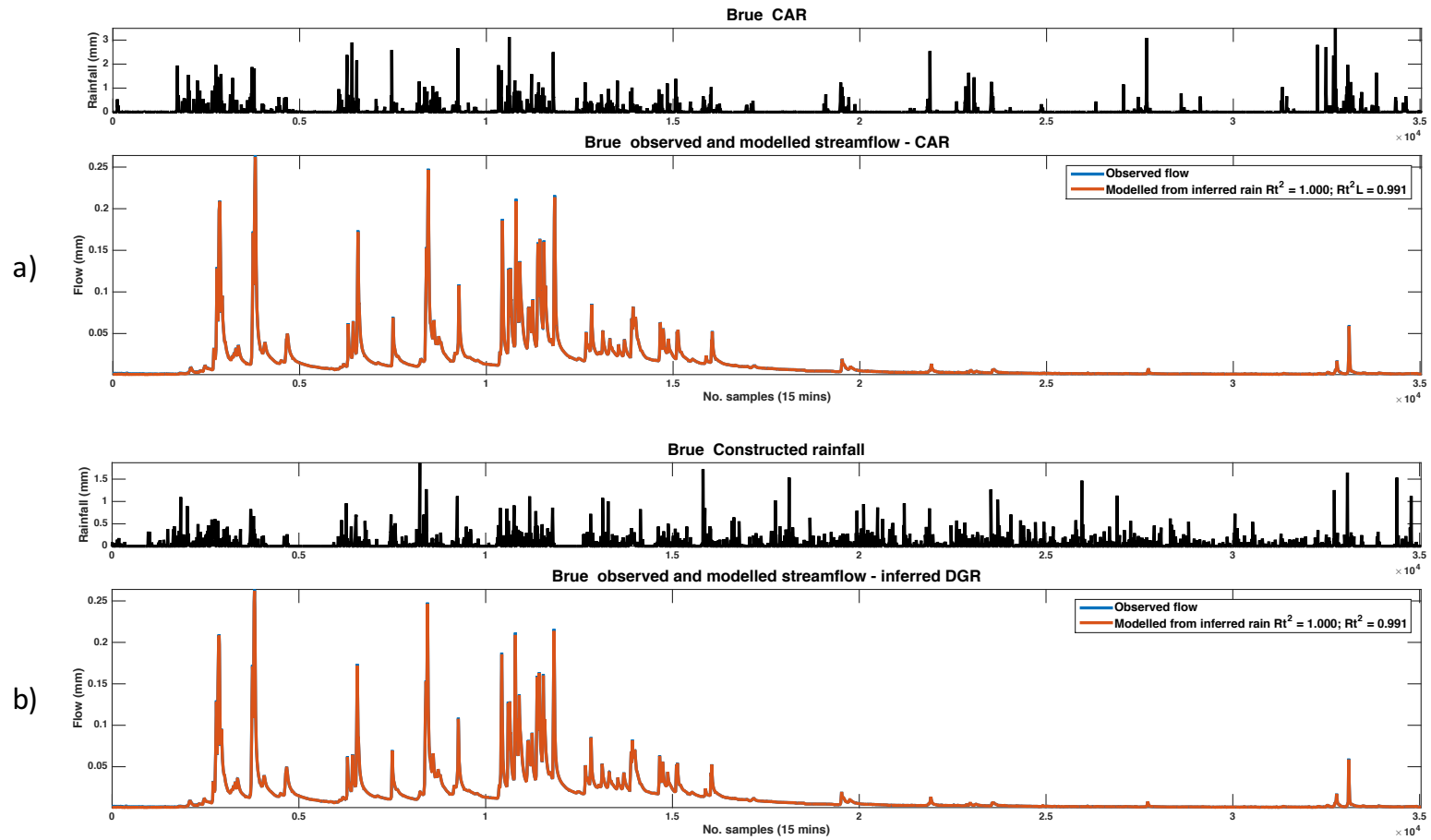


Figure 8-16 – comparison of hydrographs generated from the DGR inferred from the CAR and DGR inferred from NRCV. The fits are almost identical confirming that although the rainfall pattern is different, the discharge generating characteristics have been preserved.

## 8.9. Multiple realisations

The example presented in the previous section is based on one possible realisation of a constructed rainfall series. The generation of the high frequency part of the rainfall spectrum uses a random number generator so it is very straight forward to generate multiple series. An example plot showing 50 possible rainfall realisations is shown in Figure 8-17. Enlargements of two sections are shown in Figure 8-18. The top plot in Figure 8-18 shows a period where rainfall is actively affecting the flow. Where there is significant impact visible, the rainfall traces all tend to follow similar paths (top plot), however where there is a long recession and any rainfall is not affecting flow, possibly due to wetting-up of the catchment after a dry period, random amounts of rainfall are generated. Rainfall can be any amount at this time because it has little impact on the flow.

Hydrographs plotted from each of the 50 simulated rainfall series are shown in Figure 8-19. The hydrographs generally fit well where there is activity in the flow, enabling good estimates of the DGR to be made, and less well where there are low flows and recessions. The hydrographs fits, ranging from 0.892 to 0.951 are plotted (blue circles) in Figure 8-20. Lines indicating the fit of the hydrograph simulated from the observed rainfall (red dashes) and the average of the 50 rainfall realisations (solid red line) are also shown. Most of the constructed rainfall series generate hydrographs that fit better than the hydrograph from observed rainfall indicating that the construction method produces a series that could be used to extend or in-fill existing data. However, the hydrograph generated from the average of 50 series is a much better fit suggesting that using the average of several realisations may generate a more robust series. The following section which demonstrates how a gap in a rainfall record might be filled will utilise the average constructed rainfall series.

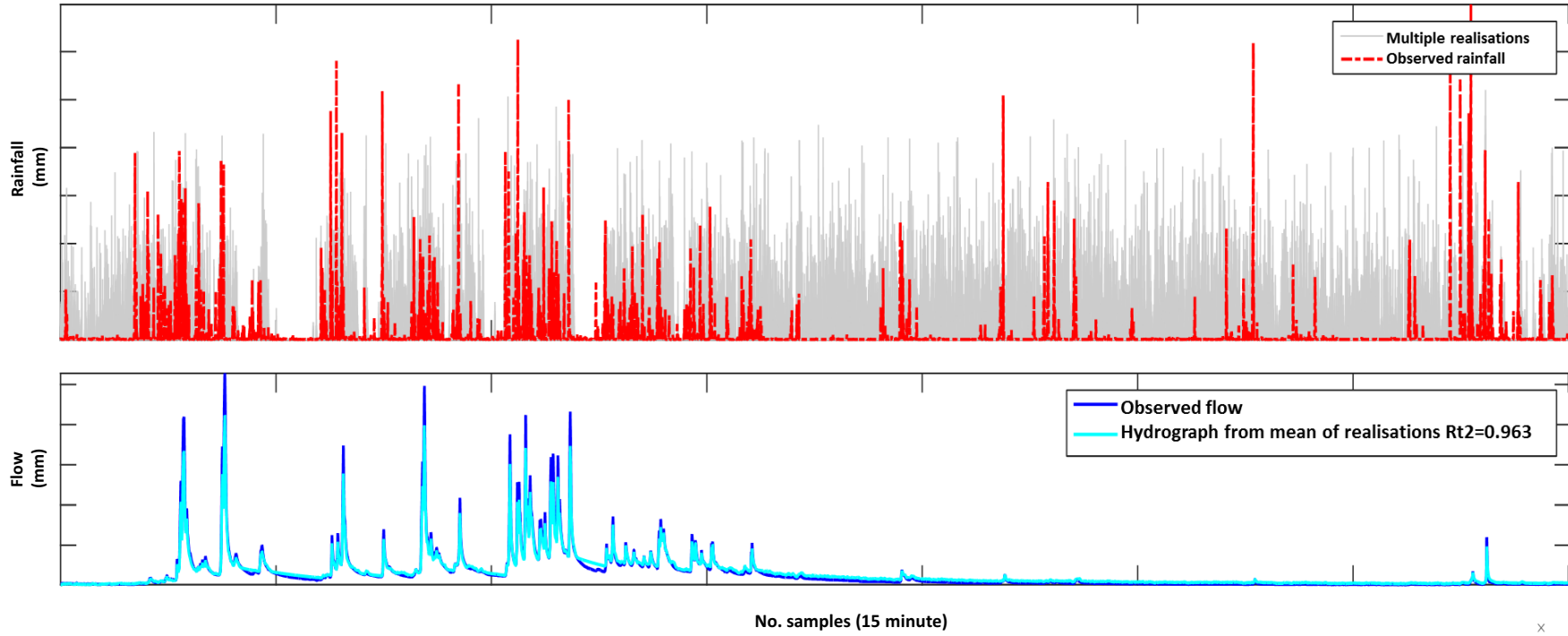


Figure 8-17 - 50 possible rainfall realisations (grey bars) compared with the observed rainfall series (red dotted bars) and the observed flow (blue line, bottom plot) and hydrograph generated from the mean of 50 realisations (light blue line in bottom plot).  $R_t^2$  between observed flow and simulated hydrograph is 0.963. Enlarged section of the plot are shown in Figure 8.18

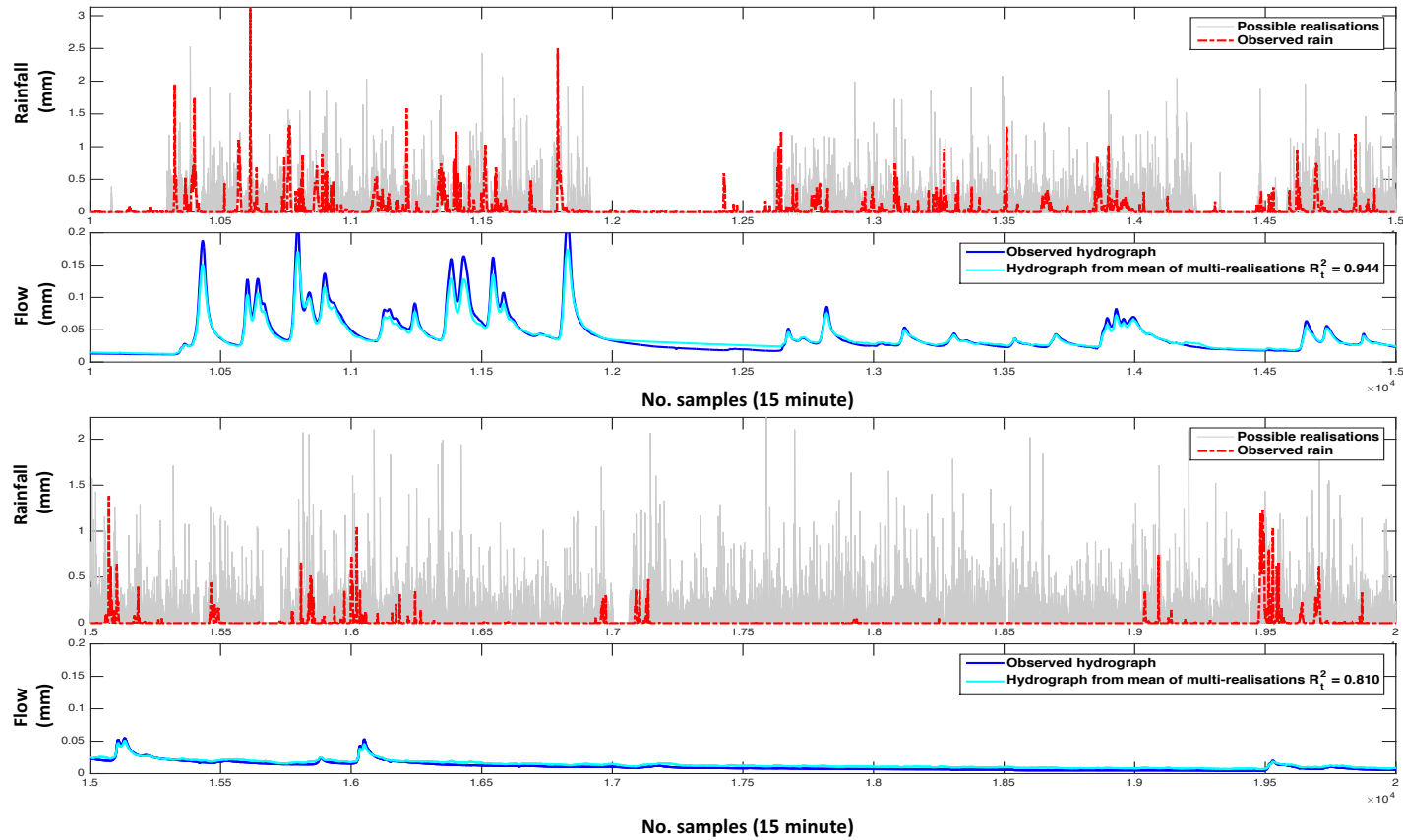


Figure 8-18 - Enlargements of two sections of Figure 8-17. The top plot shows a section where the flow is active and the bottom plot a long slow recession. Usually where flow is active, all the realisations follow similar patterns, where there is little activity and a long recession, rainfall is having little or no effect on the flow so any random amount of rainfall can be generated. The observed hydrograph is shown in blue and the hydrograph simulated from the mean of the rainfall realisations in light blue. The  $R^2$  values are 0.944 for the section with active flow and 0.810 for the recession plot indicating that the process works best where there is active flow.

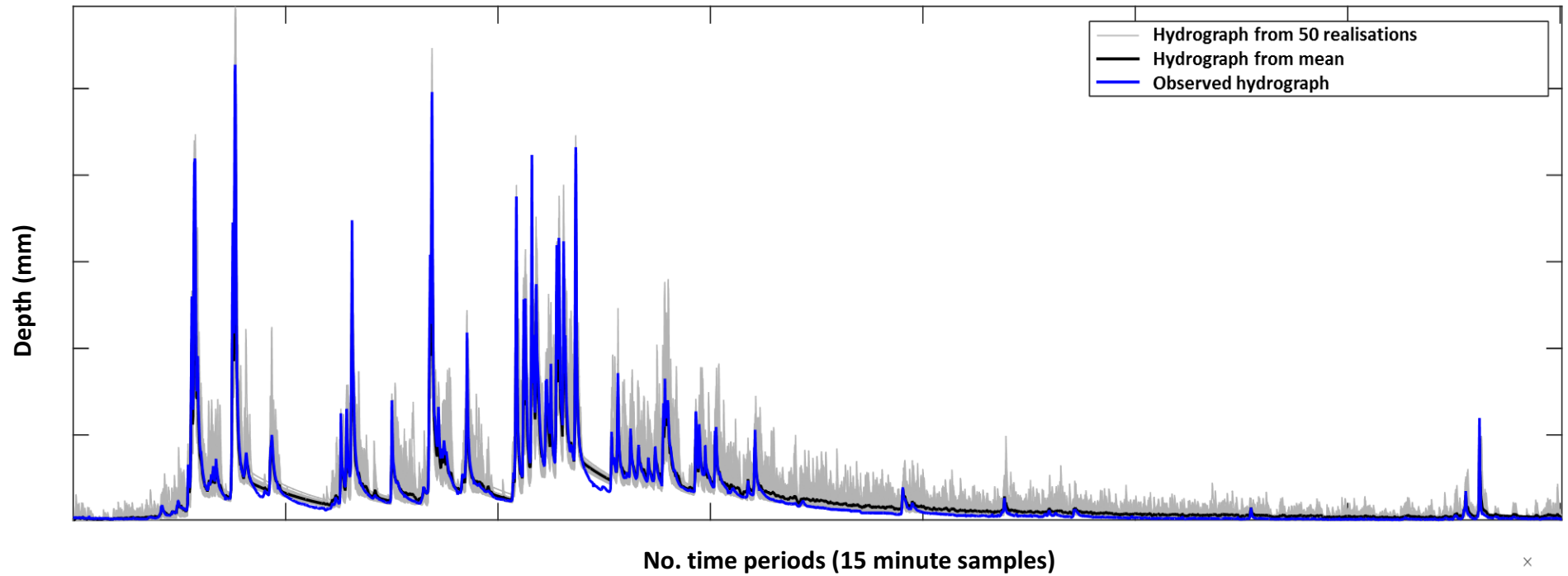


Figure 8-19: Hydrographs simulated from 50 rainfall realisations (grey lines). The hydrograph simulated from the mean of the 50 rainfall realisations is plotted in black and the observed hydrograph in blue

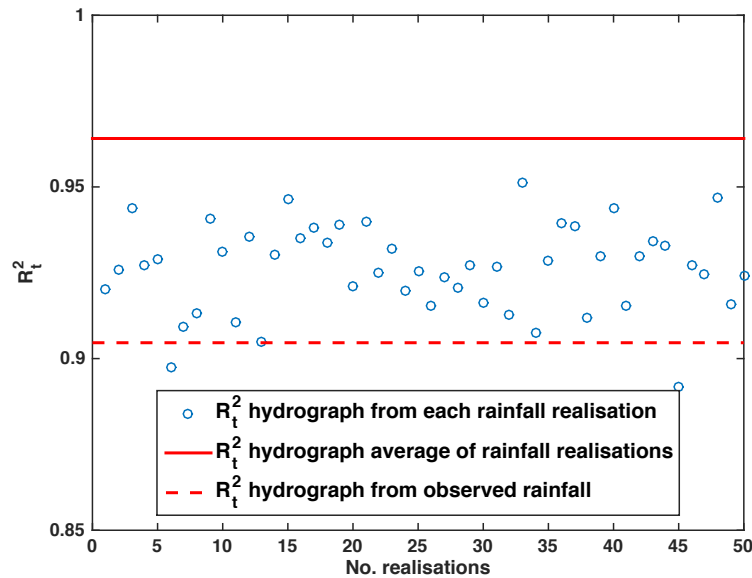


Figure 8-20:  $R_t^2$  values for the hydrographs plotted from each rainfall realisation (blue circles). Also shown, for comparison, are the  $R_t^2$  values for hydrographs simulated from the observed rainfall and the average of the rainfall realisations

### 8.10. Gap filling

One application of this method is in-filling missing data where flow records exist but rainfall does not. A model must be fitted to an existing set of rainfall and runoff data - preferably from a similar flow regime to the missing section of data though this does not guarantee similarity due to potential variation in antecedent conditions. Once a model is identified, multiple realisations can be generated and an average series calculated. The following procedure outlines the proposed method.

To fill a gap in the rainfall record for which flow data exists (Figure 8-21), fit a model to a section of data before (or after) the gap, invert it and generate the DGR. In this example, an artificial gap has been created so that the modelled rainfall series can be compared directly with the observed rainfall. The calibration period and 'gap' are labelled on the plot in Figure 8-21.



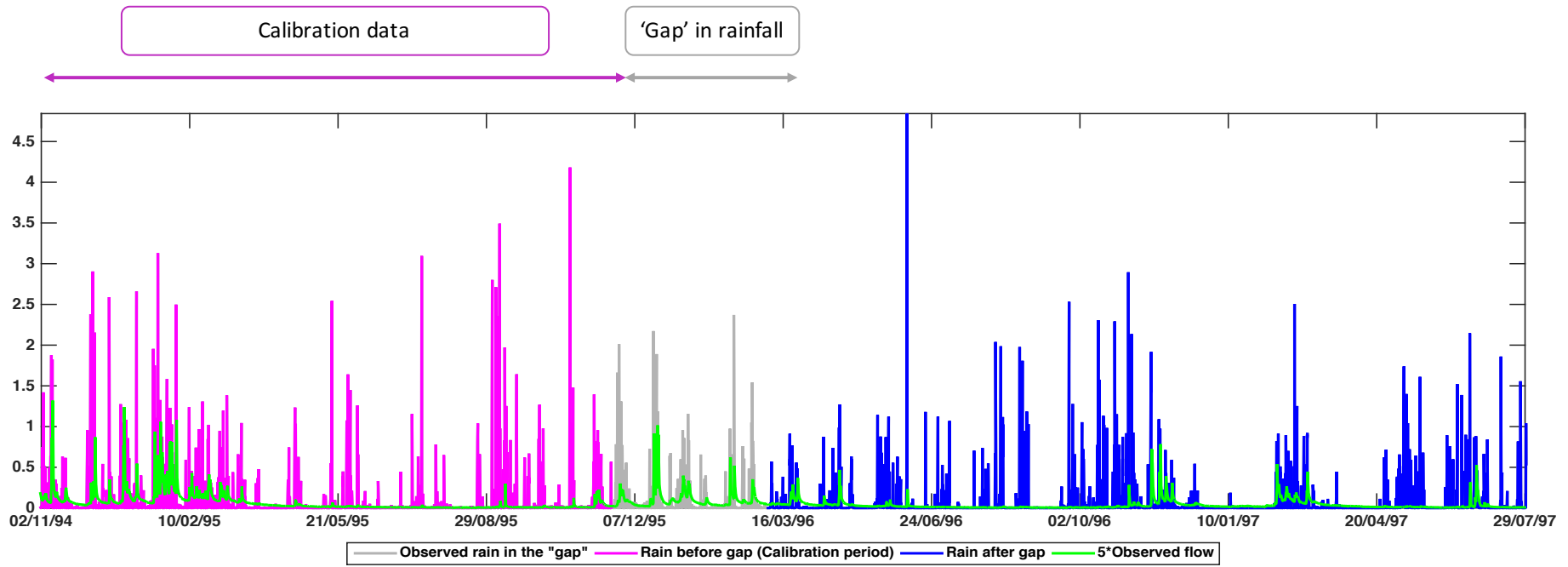


Figure 8-21 – Observed rainfall and flow time-series with a gap in the rainfall (WY1-WY3). The observed rainfall over the gap is shown for comparison with the generated rainfall.

The process outlined in sections 8.8 and 8.9 is used to build a model that can be used to construct rainfall over the gap. A TF model is identified for the calibration rainfall series, multiple realisations estimated and an average series derived. Figure 8-22 shows hyetograph and hydrograph plots of the observed rainfall and simulated streamflow during the calibration period (top plots). The bottom plots show the same plots based on modelled rainfall for the same period. This model will be used as the basis for constructing a rainfall series to fill the gap. Figure 8-23 is a plot of observed rainfall with the gap in-filled by the DGR generated using the flow over the gap and the model fitted to the calibration period.

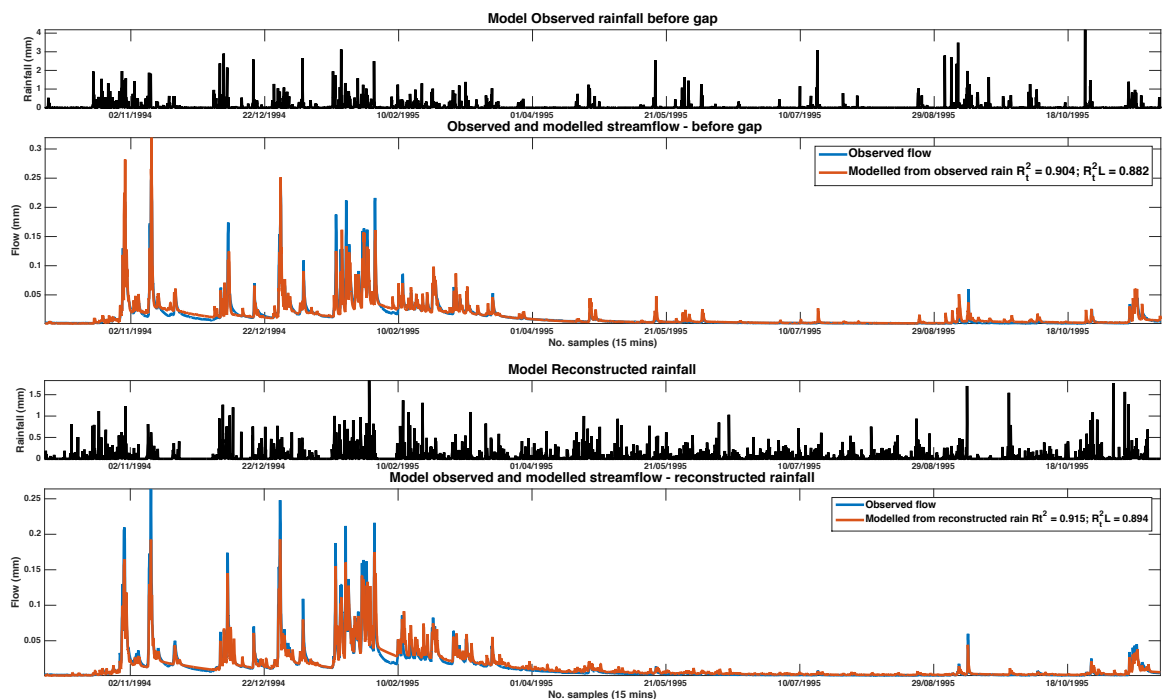


Figure 8-22: Hydrographs modelled from observed rainfall in the calibration period (top plot) and from reconstructed the rainfall model (bottom plot)

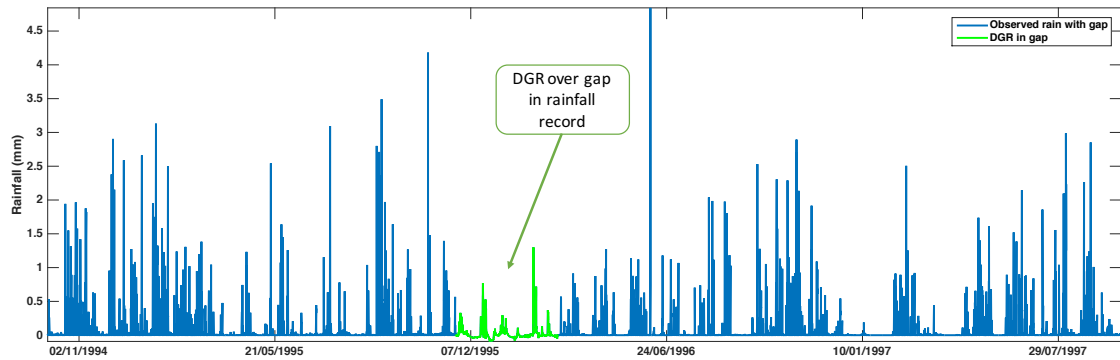


Figure 8-23 – Gap in WY2 (length 10000 time periods) in-filled by DGR generated from flow and model fitted to calibration time-series. The calibration series is effectively WY1.

The rainfall construction model developed from the rainfall and flow in the calibration period was used to generate the high frequency part of the rainfall spectrum which was combined with the DGR to produce a realistic rainfall sequence to fill the gap in the record. Figure 8-24 shows the in-filled rainfall plotted on top of the observed rainfall (top plot) for comparison and as it would be if the observed rain did not exist (lower plot). The in-fill is less variable than the observed rain in this example but is not so different as to be obviously simulated. Hydrographs were plotted using the in-fill rainfall and the of the whole record with the gap filled. They are shown in Figure 8-25. Note that as the high frequency simulated residuals are generated randomly, many sequences, some more acceptable than others, can be generated.

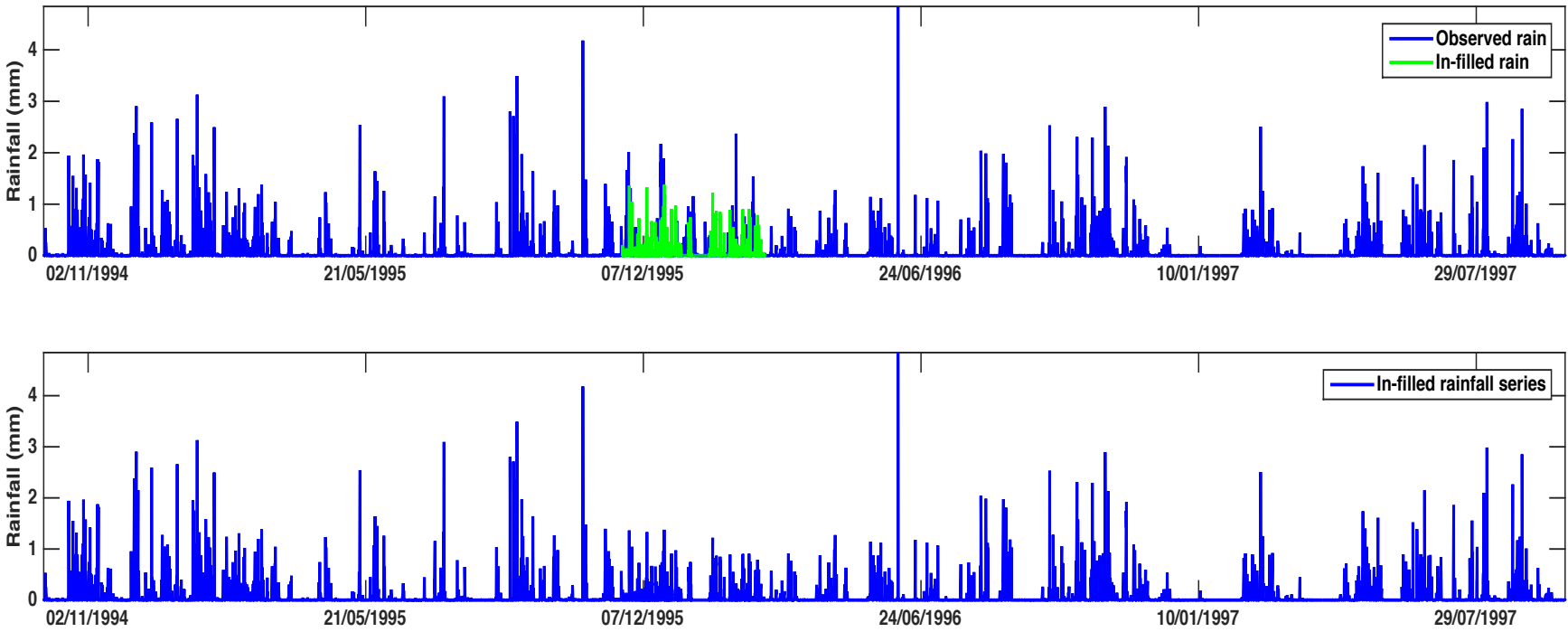


Figure 8-24 - Top plot shows the observed rainfall with the in-fill over plotted. The bottom plot shows just the in-filled series.

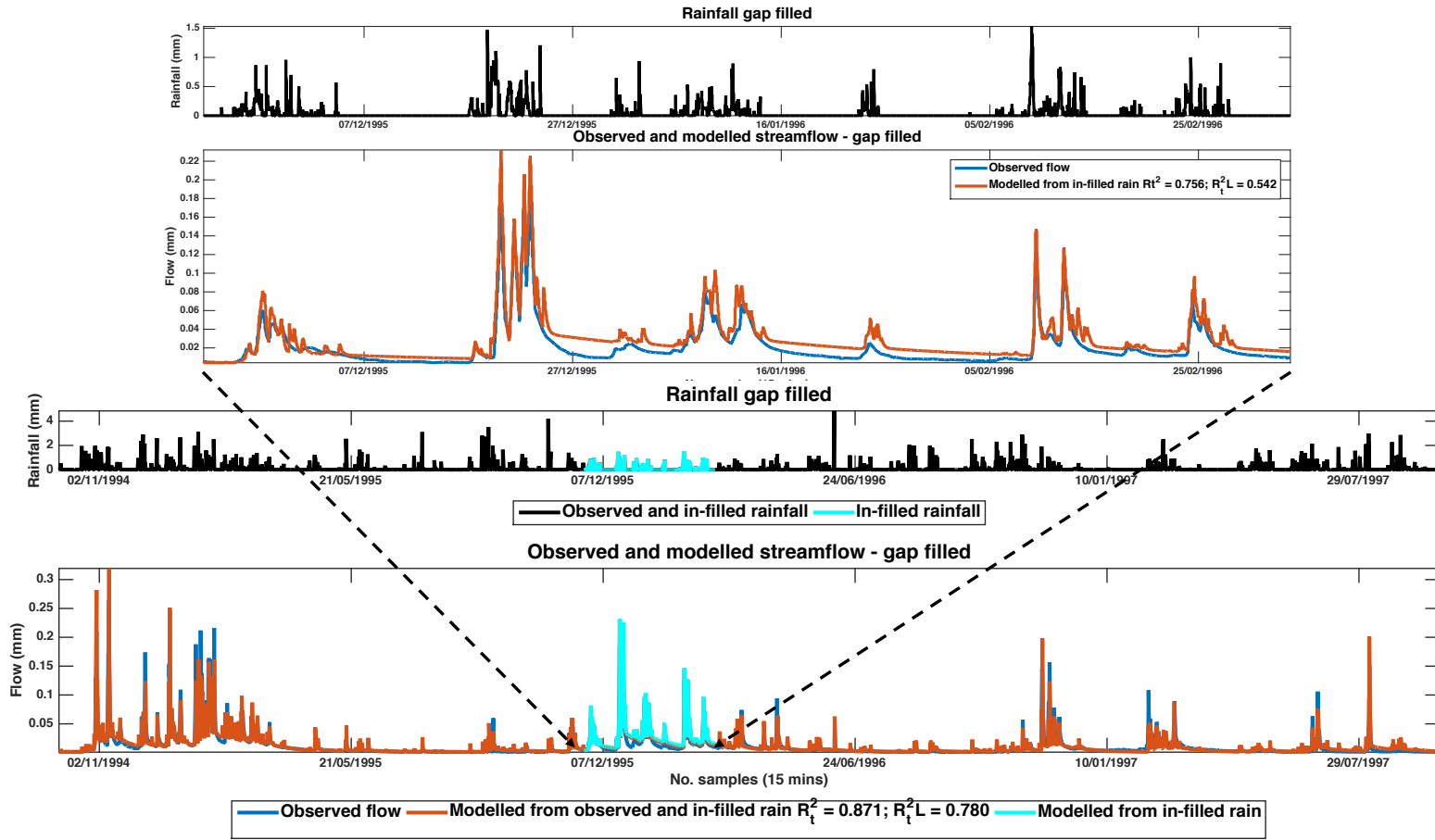


Figure 8-25 - Hyetograph of in-filled rain and the hydrograph generated from it over the gap (top plots) and the hyetograph and hydrograph for the full record with the gap filled.

### 8.11. Discussion

By using a section of record that has observed rainfall and simulating a gap in the record it is possible to compare the resulting ‘in-fill’ with the observed sequence directly. Figure 8-24 shows ‘before’ and ‘after’ plots of the ‘gap’ in the rainfall.

*Table 8-3 - Basic statistics for the whole record - Observed rainfall, no gap and observed rainfall with a ‘gap’ filled. Also shown, for comparison, are the same statistics for the observed rain over the period of the ‘gap’ and for the constructed rain used to fill the gap.*

	Mean	Standard Deviation	Lag-1 ACF	Proportion zeroes	Maximum	Total
Observed Rain	0.023	0.118	0.768	0.826	4.8	2412
Observed rain with filled gap	0.024	0.119	0.782	0.826	4.8	2541
Observed rain gap only	0.027	0.112	0.751	0.770	2.2	272
Gap filler rain	0.040	0.122	0.904	0.809	1.5	401

Table 8-3 shows basic before and after statistics for the whole record and the ‘gap’. With respect to the whole record, filling the gap has not significantly changed the overall statistics although there has been an increase in the total amount of rainfall (approx.. 5%). When looking at the gap only, there are obvious variations in the statistics, significantly, the mean has increased significantly from 0.027 to 0.040 (48%), the standard deviation has increased and the maximum decreased whilst the lag-1 auto-correlation coefficient is much greater even though there is a higher proportion of zero rain. This suggests that a wet time period is more likely to be followed by a wet time period and a dry time period by another dry time period causing rain to ‘clump’ more than in the observed record (see Figure 8-26).

The systematic positive bias in the statistics of the gap-filler rain is likely to be due to the truncation method used to maintain the proportion of zero rain (*c.f.* Table 8-3 and Figure 8-25). An alternative method of combining the high and low frequency parts of the rainfall spectrum using relative rather than absolute magnitudes, has been suggested and will be followed up in further work. This adjustment to the method should reduce the occurrence of unrealistic negative rainfall and also improve the current under-estimation of the magnitude of extreme events. The hydrograph over the gap period

(top plot in Figure 8-25) shows a reasonable fit to the peaks but over-estimates the recessions due to the bias introduced by the truncation process and the ‘less rain more often’ rainfall pattern evident over the period. Despite the presence of the bias, the overall rainfall statistics are maintained well because the variation is in the high frequencies which are filtered out by the catchment dynamics and play little or no part in discharge generation.

*Table 8-4 - Negative DGR as a percentage of total DGR at each stage of the gap filling routine. High values may indicate that the calibration model is not a good representation of the gap in the record.*

	Negative DGR
Observed record	20.2%
Calibration period	14.8%
Gap in record	63.7%
Gap filler	64.6%
Record with gap filled	23.3%

Table 8-4 lists the percentage of the DGR that is negative at each stage of the gap filling process. A model is fitted to the calibration period then used to fill a gap in the record. The high percentage of negative DGR may suggest that the model fitted to the calibration period is not a good representation the processes operating in the gap period. This may indicate that a more representative calibration period should be chosen.

The method presented here is a first attempt at using a combined spectral decomposition approach to construct a rainfall sequence from the low frequency Discharge Generating Rainfall (Kretzschmar *et al*, 2014, 2015, 2016) and the high frequency residual structure. In order to build a model that allows a rainfall sequence to be constructed by combining low-frequency DGR with high frequency simulated residuals, certain assumptions must be made when comparing the calibration period with the simulation period (gap in a record or record extension):

1. The catchment dynamics model used to generate the DGR in the calibration period is also representative in the simulation period
2. The distribution of the residual series must be the same in both periods
3. The auto-correlation structure does not change
4. The proportion of no-rainfall time periods is the same in both periods

5. The proportion of rainfall converted into flow (Runoff Coefficient) is constant between periods

Estimation of DGR is based on the best fit CT transfer function model and is dependent on the time-series used for calibration. It is the only model available but may not apply to the 'gap' or to the rest of the record. The model's ability to characterise the rainfall-runoff dynamics will depend on the choice of calibration period (whether it is representative of the whole record and of the period of the gap) and the stationarity of the time-series. If an in-fill series is not acceptable, a different section of record, more representative of the gap period, could be used for calibration. The distribution of residuals is also dependent on the DGR and will be affected by the choice of initial model.

Sampling from the residual distribution is by random selection from the residual PDF and assumes a representative PDF has been estimated. As sampling is carried out randomly, multiple residual series resulting in multiple rainfall realisations can be generated as demonstrated in section 8.9. If one realisation is not acceptable, then another can be tried or an average taken of many realisations. Where flow is active, rainfall realisations will all show similar patterns however where there is little flow activity, the rainfall could show any pattern as it is not having an effect on the flow and patterns will vary from realization to realization. This could account for the patterns of hydrograph fit shown in figure 8-20. The exact high frequency patterns that are filtered off by the catchment dynamics are not important, as long as they generate the same discharge. The auto-correlation structure of the residual series is applied to the randomly generated uncorrelated series. The resulting set of correlated residuals assumes a stationary correlation structure.

The proportion of no-rain time periods is maintained between the calibration and model periods by applying a threshold value below which all rainfall is set to zero. This eliminates any negative periods resulting from the combination of DGR and the simulated residual series but introduces a bias. This threshold may be adjusted to ensure the proportion of no-rain periods remains constant. The application of the threshold has implications for the rainfall total which must be rescaled to match the total rain in the calibration period. An alternative combination method which may reduce the



occurrence of negative values will be explored in future work. When using the model to extend a record or fill a gap, the observed rainfall total would not be available so the Runoff Coefficient (Equation 8-7) must be used to adjust the rainfall volume. It is assumed that the proportion of rain converted to flow remains constant from one period to another.

However, taking these assumptions into account, the method has promise. The rainfall sequence used to fill the gap in the above example fits into the whole record without changing the overall statistics significantly (Table 8-3) and generates a reasonable approximation to the observed hydrograph (Figure 8-19) with an acceptable  $R_i^2$  value of 0.871. The method could be used not just to fill gaps in a rainfall record but also to extend a record where flow records exist and rainfall records do not.

## 8.12. Conclusions

This paper aimed to show that a realistic rainfall sequence could be constructed by using a spectral decomposition approach. To achieve this, Reverse Hydrology was used to extract the low frequency Discharge Generating Rainfall (DGR) from the broad frequency rainfall spectrum. A continuous time transfer function relating CAR to catchment outflow, inverted using the method described by Kretzschmar *et al.* (2014), acts as a low-pass filter in the same way as the catchment thus the resulting DGR corresponds to the low frequency part of the rainfall spectrum. The high frequency part, driven by climate, is not involved in discharge generation and can be disregarded when generating a streamflow hydrograph. However, when attempting to construct a realistic rainfall sequence, these frequencies must be included. The method presented here aims to construct a realistic rainfall series from a flow time series that should retain the correlation structure of the residual series and generates the correct hydrograph.

To use the spectral decomposition approach to generate a long rainfall sequence, a flow record of the required length beyond the calibration regime is required. The assumptions stated in Section 8.11 mean that the method should be used with care. The methodology shown is a first attempt at building a rainfall series by this method. Results are promising however the simulated sequence under-estimates the extremes and contains a positive bias as a result of the method resulting in over-estimation of low

flows (echoing the work of Simolo *et al*, 2010). Further work is required to refine the method and address the issue of negative rainfall.

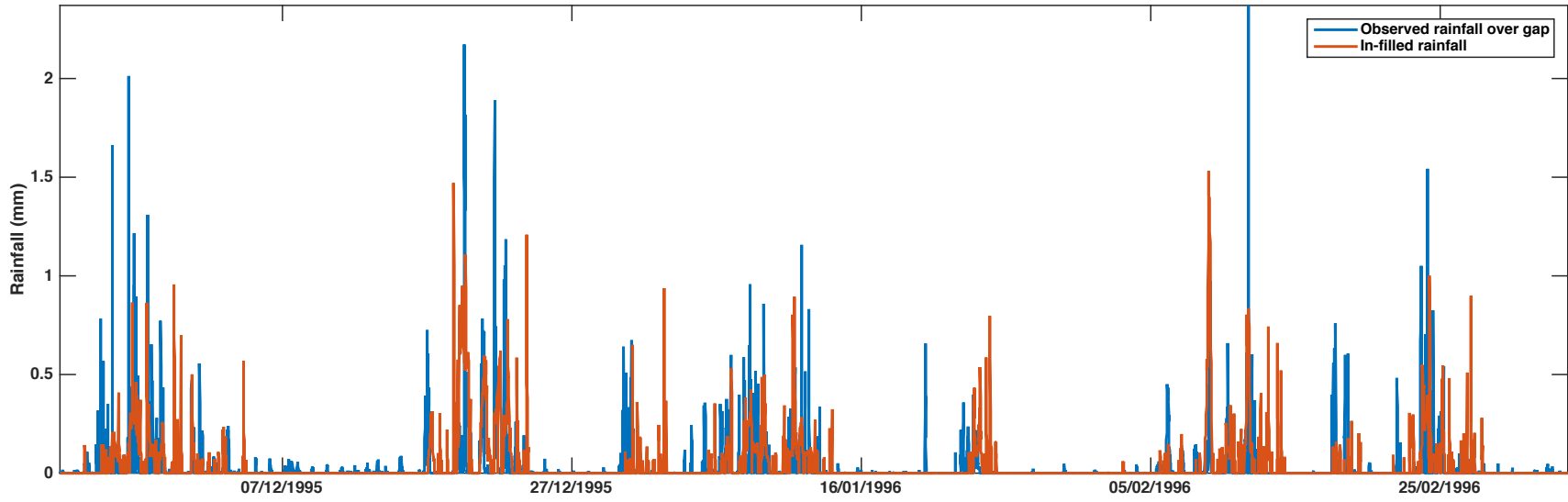


Figure 8-26 - Hyetograph of the observed rainfall over the 'gap' and the simulated series used to in-fill. Similar patterns of rainfall can be observed although the spread of the simulated rain is not as great as the observed

## Chapter 9 Summary and conclusions

### 9.1 Summary of key findings

A **novel method** for inversion of CT transfer function models (objective 1.i) utilising regularised derivatives (*RegDer*) was developed and presented (Kretzschmar *et al.*, 2014). The method was compared with the direct inverse (*InvTF*) and tested on two catchments with very different rainfall regimes and flow pathways (objective 1.ii). Both methods produced synthetic rainfall time-series that were able to simulate almost all of the dynamics in the streamflow time-series for both catchments, assessed by comparing hydrographs simulated using the inferred rainfall with the observed hydrograph and a range of metrics (chapter 4). The filtering effect of the *RegDer* method, which mirrors the low-pass spatio-temporal filtering action of catchment storage, generates a low frequency inferred rainfall sequence without the high-frequency noise generated by other methods such as the *InvTF* method (objective 1.iii). This high frequency noise is an artefact of some methods, due to direct differencing of the discharge series, and would cause it to fail the criteria for DBM modelling. It does not contribute to the discharge and, thus, is not identifiable so there exist an infinite number of rainfall sequences able to generate the same discharge (objectives 1.iii and 2.ii). The smoothing introduced by the new *RegDer* method, however, does not mask the dominant dynamics of the catchment (chapter 5, Kretzschmar *et al.*, 2015).

The alternative method amplifies high frequencies present in the rainfall record that are filtered out by the regularisation process in the *RegDer* method. Critically, the slightly smoothed rainfall series produced by *RegDer* is capable of simulating observed streamflow better than the original rainfall data (objective 1.iii). This highlights that some high frequency dynamics in rainfall may not be pertinent for streamflow generation, even for some flashy tropical catchments. The resolution of the derived rainfall was estimated in the time domain by aggregation and in the frequency domain by comparing amplitude spectra (objective 1.iii). The degree of smoothing produced by the *RegDer* method is dependent on the dominant dynamic mode and hence the degree of storage in the catchment (objective 1.iv). The greater the storage (for example, presence of an aquifer) the more the *RegDer* method smooths the rainfall. Resolution

is also affected by the rainfall regime, for example, whether convective or frontal rain is dominant (Chappell *et al.*, 2017b), and by how well the original model fits (chapter 5).

Chapter 6 introduces the effects of spatial variation (objective 1.iv). A rainfall field varies in both space and time and a catchment integrates spatially as well as temporally as rainfall is converted into flow. A single rain gauge or a sparse network of gauges is often used to sample the highly variable rainfall field leading to uncertainties in the estimation of the true catchment rainfall (objective 2.i). Use of data from a single rain gauge to derive the *RegDer* rainfall series usually produces a better model of streamflow than models based on observations from a dense network of gauges integrated with the Thiessen Polygon method.

Models based on observed rainfall from an individual rain gauge typically provided good simulations in WY1, but often poor in WY3. It is likely that changes in the dominance of the hydrometric regime between years made individual rain gauge records sensitive to these changes (objectives 1.iv, 2.i). This sensitivity was reduced by using the *RegDer* rainfall from individual gauges (chapter 7). It is clear from the maps in Figure 7-12 that, although the total rain varies from year to year, the average pattern is similar with increased rainfall on the higher ground and lowest near the catchment outlet. This average pattern masks the detail displayed in the sample event maps presented in Appendix C. Table C-1 shows how the dominance of a gauge varies on an event basis. The rainfall total demonstrates the importance of a gauge with respect to the estimation of CAR whilst the fit of the model indicates its importance as a driver of catchment discharge for that time period (objective 2.i).

In Chapter 8, the *RegDer* method was utilised to in-fill gaps in the rainfall record (objective 2.ii). For periods with observed rainfall and streamflow, the *RegDer* series was derived. The *RegDer* parameters were then used to derive *RegDer* rainfall estimates for the periods lacking rainfall observations (objective 2.iii). By utilizing the statistical properties of the *RegDer* modelling for periods with rainfall and streamflow observations, the hydrologically insignificant, high-frequency component of rainfall (normally removed by *RegDer*) could be estimated and combined with the *RegDer* series for the period with no rainfall observations. This gives records with similar

spectral properties to the observed rainfall where records are present (objectives 2.ii; 2.iii). The synthetic data created for the period with no rainfall observations was then merged with those from periods with rainfall observations to give a complete record.

## 9.2 Conclusions

The novel method of inferring rainfall from flow using regularisation, presented here, extracts the low frequency Discharge Generating Rainfall from the broad-spectrum rainfall that encapsulates the essential dynamics required to generate streamflow. The higher frequencies are not required for hydrograph generation and can be ignored. Discharge Generating Rainfall (inferred from streamflow using the regularisation process) has a lower temporal resolution than the measured rainfall but this is not a problem as long as the resolution is fine enough to capture the catchment dynamics. The reduction in the resolution of the rainfall is the price paid for the numerical stability of the regularisation process and is a function of the catchment dynamics.

A combined form of spectral decomposition with a causal dynamics model was proposed as a method for generating a sequence of rainfall from the Discharge Generating Rainfall that could be used for extending existing records where streamflow exists but rainfall does not (subject to a short section of record being available to allow a model to be fitted) or for in-filling gaps in rainfall records. The method presented shows promise but is very much a ‘work in progress’.

The conclusions drawn as related to the objectives of the study are:

- 1.i **Develop a new method** for inferring rainfall from sub-hourly streamflow data based on a **novel regularisation technique**
  - A new technique for inferring sub-hourly rainfall from streamflow was developed and presented (Kretzschmar *et al.*, 2014; chapter 4) using robust identification techniques to fit a parsimonious continuous-time transfer function model according to DBM philosophy. Both the new *RegDer* method and the existing *InvTF* method were able to capture the dynamics contained in the streamflow series (chapter 4).

- 1.ii **Evaluate the regularisation technique** by comparison with existing inversion methods utilising data from two catchments with contrasting rainfall characteristics and flow-paths using a range of metrics
- The new *RegDer* method inferred a series with much less high frequency noise than the *InvTF* method especially considering the tropical basin with convective rainfall. The high frequency artefacts present in the *InvTF* series would cause it to fail DBM modelling criteria as it is a product of the method and has no physical explanation (chapter 4).
  - A range of evaluation metrics, including residual analysis, was able to confirm that both the methods (*RegDer* and *InvTF*) produced similar results for the temperate catchment dominated by frontal rain (Blind Beck) whilst *RegDer* is better able to reproduce the characteristics of the convective, tropical Baru catchment. (chapter 4).
- 1.iii Assess the ability of the regularisation technique to capture the **dominant modes** of the rainfall-runoff behaviour using methods of **temporal aggregation and spectral analysis**
- The smoothing of the *RegDer* method can be controlled by adjusting the NVR (Noise Variance Ratio) parameters of the inverse model. Applying smoothing to the *InvTF* output would not achieve the same result. (chapter 4).
  - The integrating effect of the catchment resulting in a damped hydrograph can be seen in both catchments. This was expected for Blind Beck given the presence of deep pathways (aquifers) but not expected for Baru which has shallow pathways. This result highlights the role of even shallow pathways in damping intense rainfall (chapter 4).
- 1.iv Assess the ability of the regularisation technique to capture the **spatio-temporal structure** of catchment rainfall
- The smoothing introduced by the *RegDer* method is on a smaller temporal scale than the dominant catchment dynamics suggesting that the detailed temporal rainfall distribution may not be important when generating streamflow (chapter 4, chapter 5).

- The smoothed inferred rainfall sequence is able to generate the streamflow output as well as if not better than when the observed rainfall is used as model input (chapter 5).
- Temporal aggregation results in lower peaks as the same rainfall is spread over a longer period effectively smoothing the record. The estimated time resolution of the inferred series for both catchments assessed by aggregation and spectral analysis is within the Nyquist safe sampling limits and below the critical catchment time constants indicating that, even though some temporal resolution has been lost as a trade-off for numerical stability, the dominant rainfall-streamflow dynamics are being captured. (chapter 5).
- Increase in sampling time scale (by aggregation) up to periods of one day has an impact on the distribution of key characteristics of the rainfall field. Aggregation in the form of a moving total is a form of low-pass filter in the same way as regularisation so the loss of resolution due to the *RegDer* inversion process is also likely to have an effect on the distributions of statistics (chapter 7).

#### 2.i **Quantify local rainfall records** that are **misinformative** for flood modelling

- The geographical proximity of rain gauges in the Brue catchment mean they are highly correlated so the network was reduced from 49 gauges to 23. The reduced network provides estimates of catchment rainfall within 0.4% of the full network when the Thiessen Polygon averaging method is used. The density of the gauge network means that elevation did not need to be explicitly included however its influence is expected to change from event to event (chapter 6, chapter 7).
- Examination of the rainfall field in space and time shows that it may be raining hard in one place in the catchment whilst it is dry in another. This has implications for the calculation of catchment average rainfall and for assessing which areas of the catchment are driving discharge generation at a given time. The fit of a model, relating rainfall measured at a gauge to catchment outflow, provides a measure of the quality of the information being provided by a particular rainfall series with regard to flow generation as if only that gauge were available to the modeller (chapter 6, chapter 7).



- Rainfall at a single gauge may only represent the processes active in a limited area of the catchment. Reverse Hydrology utilises the information present in the catchment outflow – integrated over the whole catchment – and is therefore likely to be more representative of the whole catchment. The inferred rainfall estimated in this way is termed Discharge Generating Rainfall because it is the part of the rainfall that drives discharge generation. (chapter 7).
  - The fit of a model between rainfall at a single gauge and catchment outflow varies across the catchment indicating that the distribution of rainfall (and catchment characteristics) is important when generating streamflow hydrographs. Rainfall at a single gauge only provides partial information on the rainfall pattern however the streamflow is a result of all the rainfall and contains information about the whole catchment. Inferring rainfall from streamflow (DGR) may mean that further information about the spatio-temporal distribution of rainfall may not be required and uncertainty in the simulated hydrograph may be reduced (chapter 7).
  - Rainfall from all rain gauges in a network should be included when calculating an estimate of catchment average rainfall because it is just that – an average depth of rainfall over the catchment – however this does not mean that rainfall at all gauges is driving the streamflow generation process as identified by the fit of the models. Any gauge identified as consistently under-performing may be inappropriately sited (chapter 7).
- 2.ii **Quantify the spectral components** of the rainfall signal responsible for flood generation
- The *RegDer* method of inversion infers a rainfall sequence from the streamflow. This sequence was originally thought to be an estimate of catchment average rainfall but has since been recognised to be the rainfall responsible for generating discharge (DGR), the low-frequency part of the rainfall signal. The high frequency part of the signal plays little or no part in the hydrograph generation and can be ignored for this purpose (chapter 7).
  - Negative DGR can be explained in terms of catchment behaviour and rainfall spatial distribution. It often occurs during a recession when flow is driven by the catchment rather than the rainfall. Small negative spikes may

also occur when the inversion process compensates because it has stopped raining in one part of the catchment, but the flow is still increasing. These negative periods of rainfall are a product of the inversion. The proportion of negative DGR varies over time depending on catchment conditions and the rainfall distribution.

- Using inferred rainfall alone generates a hydrograph close to the observed hydrograph however, despite the apparent circularity, the process is not perfect, for example, the regularised derivative method is only an approximation, model identification is not perfect and the information content of the rainfall and streamflow data may not be complete (chapter 7).

2.iii **Develop a new technique** for in-filling and extending rainfall records based on a combination of **regularisation and spectral decomposition**

DGR generating rainfall has a lower resolution than the observed rainfall. It carries all the information required to generate a streamflow hydrograph very similar to the observed hydrograph. It does not look like real rainfall. In order to produce a realistic rainfall series which generates the correct hydrograph, the high-frequency part of the spectrum, simulated from the observed residuals, must be combined with the low-frequency DGR. This will not affect the capability of the (synthetic) rainfall series to generate a realistic hydrograph because the high frequencies play little or no part in flow generation. The resulting series should look realistic, have a similar residual structure to the original series and generate the correct hydrograph (chapter 8) The resulting series should look realistic, have a similar residual structure to the original series and generate the correct hydrograph (Chapter 8) however the current method introduces a bias into the simulated rainfall series due to the added high frequency component which mimics the correlation structure and distribution of actual residuals (where CAR is available).

### 9.3 Suggestions for further work

- The *RegDer* method has been tested against one other method of inverting a (DT) transfer function. Other methods exist (*c.f.* literature referenced in chapter 4). A further systems analysis based method that could be followed up is the feedback method suggested by Young and Sumislawska (2012). All testing has been carried out on relatively small test catchments so it is

suggested that this be expanded to larger catchments with a wide range of characteristics and rainfall regimes to see if the same conclusions hold true at all scales. Including catchments where snowmelt is a significant factor would link with the work of Hernegger *et al.*, (2014) on alpine catchments.

- Refinement of the rainfall generation model to improve its streamflow generation capabilities and reduce the tendency to introduce a bias.
- Significant assumptions (listed in section 8.11) are required to use the gap-filling routine based on spectral decomposition and reverse hydrology. Reducing and refining these assumptions may result in a more robust generator better able to reproduce the variability in the rainfall, perhaps by using a different base distribution to select from the residual distribution (for example in order to capture the tails of the distribution better).
- There is scope to follow up on the method for assessing the ‘representativeness’ of a gauge by extending to assess the performance of pairs (or more) sets of gauges. This methodology could also be used to refine gauge networks and determine good sites for locating rain gauges dependent on the prevailing weather conditions. Should different gauges be used dependent on the conditions, perhaps by relating to the Lamb weather types?
- The Thiessen Polygon method used here weights rain gauge contribution to the average by the area they are assumed to represent. This area is geometric only and has no relationship with the underlying catchment characteristics (or weather conditions) that drive discharge generation. There is scope for developing a new method of catchment average calculation based on which gauges drive the discharge (Sugawara (1992) suggests that gauges should be weighted by meteorological conditions) and their underlying characteristics.
- Spectral analysis could be used to develop a measure of information content, possibly entropy based, that could be used to aid in model assessment and selection.

- The reduction in resolution due to the *RegDer* method could be investigated as a down-scaling technique for relating Regional Climate Models to local conditions. The reduced resolution sequences, may also be easier to transfer from one location to another with implications for prediction in ungauged basins (PUB).

## References

- Abbott, M.B., Bathurst, J.C., Cunge, J.A., O'Connell, P.E., & Rasmussen, J., (1986) *An introduction to the European Hydrological System — Systeme Hydrologique Europeen, "SHE", 1: History and philosophy of a physically-based, distributed modelling system*. Journal of Hydrology, 87(1), 45-59.
- Adhikary, S.K., Yilmaz, A.G. & Muttill N. (2015) *Optimal design of rain gauge network in the Middle Yarra River catchment*. Hydrological Processes, 29(11), 2582-2599.
- Ahrens, B., (2006) *Distance in spatial interpolation of daily rain gauge data*. Hydrol Earth Syst Sci 10:197–208
- Ajami, K., Gupta, H., Wagener, T. & Sorooshian, S., (2004) *Calibration of a semi-distributed hydrologic model for streamflow estimation along a river system*. Journal of Hydrology, 298(1), 112-135.
- Alexandrov, G.A., Ames, D., Bellocchi, G., Bruen, M., Crout, N., Erechtkhoukova, M., Hildebrandt, A., Hoffman, F., Jackisch, C., Khaiteer, P., Mannina, G., Matsunaga, T., Purucker, S.T., Rivington, M. & Samaniego, L., (2011) *Technical assessment and evaluation of environmental models and software: Letter to the Editor*, Environmental Modelling and Software, Vol. 26 (3), 328-336.
- Anctil, F., Lauzon, N., Andréassian, V., Oudin, L. & Perrin, C., (2006) *Improvement of rainfall-runoff forecasts through mean areal rainfall optimization*. Journal of Hydrology, 328(3), 717-725.
- Anderssen R. & Bloomfield, P., (1974) *Numerical Differentiation Procedures for Non-Exact Data*, Numerische Mathematik, 22, 57-182.
- Andréassian V., Perrin, C., Michel, C., Usart-Sanchez, I. & Lavabre, J., (2001) *Impact of imperfect rainfall knowledge on the efficiency and the parameters of watershed models*. Journal of Hydrology, 250 (1), 206-223.
- Andrews, F., Croke, B. & Jakeman, A., (2011) *An open software environment for hydrological model assessment and development*. Environmental Modelling & Software, 26 (10),1171-1185.
- Andrews, F., Croke, B. & Jeanes, K., (2010) *Robust estimation of the total unit hydrograph*. In: 2010 International Congress on Environmental Modelling and Software Modelling for Environment's Sake. Ottawa, Canada.
- Anquetin, S., Braud, I., Vannier, O., Viallet, P., Boudevillain, B., Creutin, J-D. & Manus, C., (2010) *Sensitivity of the hydrological response to the variability of rainfall fields and soils for the Gard 2002 flash-flood event*. Journal of Hydrology, 394(1-2), 134-147.
- Antsaklis, P., (1978) *Stable Proper Nth-Order Inverses*. IEEE Transactions on Automatic Control, 23(6), 1104-1106.

- Arnaud, P., Bouvier, C., Cisneros, L. & Dominguez R., (2002) *Influence of rainfall spatial variability on flood prediction*. Journal of Hydrology, 260(1), 216-230.
- Baigorria, G. A. & Jones, J.W., (2010) *GiST: A stochastic model for generating spatially and temporally correlated daily rainfall data*. Journal of Climate, 23(22), 5990-6008.
- Bardossy, A. & Das, T., (2008). *Influence of Rainfall Observation Network on Model Calibration and Application*. Hydrology and Earth System Sciences, 12(1), 77-89.
- Bárdossy, A. & Pegram, G., (2013) *Interpolation of precipitation under topographic influence at different time scales*. Water Resources Research, 49(8), 4545-4565.
- Bell, V.A. & Moore, R.J., (2000) *The sensitivity of catchment runoff models to rainfall data at different spatial scales*. Hydrology & Earth System Sciences, 4, 653-667, doi:10.5194/hess-4-653-2000.
- Bennett, N.D., Croke, B.F.W., Guariso, G., Guillaume, J.H.A., Hamilton, S.H., Jakeman, A.J., Marsili-Libelli, S., Newham, L.T.H., Norton, J.P., Perrin, C., Pierce, S.A., Robson, B., Seppelt, R., Voinov, A.A., Fath, B.D. & Andreassian, V., (2013) *Characterising performance of environmental models*. Environmental Modelling & Software 40: 1-20.
- Beven, K.J., (1989) *Changing ideas in hydrology — The case of physically-based models*. Journal of Hydrology, 105(1), 157-172.
- Beven, K.J., (2006) *A manifesto for the equifinality thesis*. Journal of Hydrology, 320, 18-36.
- Beven, K.J., (2009) *Environmental modelling: An uncertain future?: An introduction to techniques for uncertainty estimation in environmental prediction*. London: Routledge.
- Beven, K.J., (2012a) *Rainfall-Runoff Modelling - the Primer*, second ed. John Wiley and Sons, Chichester, England.
- Beven, K. J., (2012b) *Causal models as multiple working hypotheses about environmental processes*, Comptes Rendus Geoscience, Académie de Sciences, Paris, 344: 77–88.
- Beven, K.J., (2016) *Facets of uncertainty: epistemic uncertainty, non-stationarity, likelihood, hypothesis testing, and communication*. Hydrological Sciences Journal, 61:9,1652-1665, DOI: 10.1080/02626667.2015.1031761.
- Beven, K. J., and Germann, P., (1982) *Macropores and water flow in soils*. Water Resources Research, 18(5), 1311-1325.
- Beven, K.J. & Hornberger, G.M., (1982) *Assessing the effect of spatial pattern of precipitation in modelling streamflow hydrographs*. Water Resources Bulletin, 18(5), 823-829.

- Beven, K.J. & Lamb R., (2014) *The uncertainty cascade in model fusion*. In: Riddick, A. T. Kessler, H. & Giles, J.R.A., (eds) *Integrated Environmental Modelling to Solve Real World Problems: Methods, Vision and Challenges*. Geological Society, London, Special Publications, 408, <http://dx.doi.org/10.1144/SP408.3>.
- Beven, K.J. & Smith, P.J., (2015) *Concepts of Information Content and Likelihood in Parameter Calibration for Hydrological Simulation Models*, ASCE Journal of Hydrologic Engineering, DOI: 10.1061/(ASCE)HE.1943-5584.0000991.
- Beven, K. & Westerberg, I., (2011) *On red herrings and real herrings: disinformation and information in hydrological inference*. *Hydrological Processes*, 25: 1676–1680. doi: 10.1002/hyp.7963.
- Beven, K. & Young, P., (2013) *A guide to good practice in modeling semantics for authors and referee.*, *Water Resources Research*, 49, doi:10.1002/wrcr.20393.
- Bhattacharyya, S., (1978) *Observer design for linear systems with unknown input*. In: *IEEE Transactions on Automatic Control*, Vol. 23, no. 3, 483-484.
- Bidin, K. & Chappell, N., (2003) *First evidence of a structured and dynamic spatial pattern of rainfall within a small humid tropical catchment*. *Hydrology & Earth System Sciences*, 7 (2), 245-253.
- Bidin, K. & Chappell, N., (2006) *Characteristics of rain events at an inland locality in North-eastern Borneo, Malaysia*. *Hydrological Processes*, 20 (18), 3835-3850.
- Bloomfield, P., (1976) *Fourier Analysis of Time Series: An Introduction*, John Wiley & Sons, New York.
- Blöschl, G., Sivapalan, M., Wagener, T., Viglione, A. & Savenije, H., (Editors), (2013) *Runoff prediction in ungauged basins: synthesis across processes, places and scales*. Cambridge University Press.
- Bonnell, M. and Gilmour, D. A., (1978) *The development of overland flow in a tropical rainforest catchment*. *J. Hydrol.*, 39, 365-382.
- Boorman, D., (1989) *A new approach to Unit Hydrograph Modelling*. PhD Lancaster.
- Box, G.E.P., (1976) *Science and Statistics*, *Journal of the American Statistical Association*, 71: 791–799, doi:10.1080/01621459.1976.10480949.
- Box, G.E.P., Jenkins, G.M. & Reinsel, G.C., (2008) *Time Series Analysis: Forecasting and Control*, 4th Edition.
- Bradley, A., Peters-Lidard, C., Nelson, B., Smith, J. & Young, C., (2002) *Raingauge network design using nexrad precipitation estimates 1*. *JAWRA Journal of the American Water Resources Association*, 38(5), 1393-1407.
- Bras, R.L. & Rodríguez-Iturbe, I., (1976) *Rainfall network design for runoff prediction*, *Water Resources Research*, 12(6), 1197–1208, doi:10.1029/WR012i006p01197.

- British Geological Survey (BGS), (2017) *UK Soil Observatory Viewer* <http://www.bgs.ac.uk/data/services/soilwms.html> Retrieved 28/6/2017.
- Brocca, L., Moramarco, T., Melone, F. & Wagner, W., (2013) *A new method for rainfall estimation through soil moisture observations*. *Geophysical Research Letters*, 40(5), 853-858.
- Brocca, L., Ciabatta, L., Massari, C., Moramarco, T., Hahn, S., Hasenauer, S., Kidd, R., Dorigo, W., Wagner, W. & Levizzani, V., (2014) *Soil as a natural rain gauge: Estimating global rainfall from satellite soil moisture data*. *Journal of Geophysical Research: Atmospheres*, 119(9), 5128-5141.
- Brutsaert, W., (2005) *Hydrology: An introduction*. Cambridge; New York: Cambridge University Press.
- Bryson, A. E. & Ho, Y.-C., (1969) *Applied Optimal Control: Optimization, Estimation, and Control*. Routledge, London.
- Buchholz, J. J. & von Grünhagen, W., (2004) *Inversion Impossible?* Technical Report, University of Applied Sciences, Bremen, September 2004.
- Bunting, B. T., (1961) *The role of seepage moisture in soil formation, slope development and stream initiation*, *American Journal of Science*, 259, 503-518
- Burton, A., Kilsby, C.G., Fowler, H.J., Cowpertwait, P.S.P. & O'Connell, P.E., (2008) *RainSim: A spatial-temporal stochastic rainfall modelling system*. *Environmental Modelling and Software*, 23(12), 1356-1369.
- Cameron, D., Beven, K. & Tawn, J., (2000) *An evaluation of three stochastic rainfall models*. *Journal of Hydrology*, 228(1), 130-149.
- Chandler, R.E. & Wheeler, H.S., (2002) *Analysis of rainfall variability using generalized linear models: A case study from the west of Ireland*, *Water Resources Research*, 38(10), 1192, doi:10.1029/2001WR000906.
- Chandler, R.E., Isham, V.S., Wheeler, H.S., Onof, C.J., Leith, N., Frost, A.J. and Second, M.L., (2006) *Spatial-temporal rainfall modelling with climate change scenarios*. London: University College London.
- Chapman, T.G., (1996) *Common unit-graphs for sets of runoff events: Part 2. Comparisons and inferences for rainfall loss models*. *Hydrological Processes*, 10:783-792.
- Chappell, N., Franks, S. & Larenus, J., (1998) *Multi-scale permeability estimation for a tropical catchment*. *Hydrological Processes*, 12 (9), 1507-1523.
- Chappell, N.A., Bonell, M., Barnes, C. & Tych, W., (2012) *Tropical Cyclone Effects on Rapid Runoff Responses: Quantifying with New Continuous-Time Transfer Function Models*. In: Webb, A.A., Bonell, M., Bren, L., Lane, P.N.J., Mcguire, D., Neary, D.G., Nettles, J., Scott, D.F., Stednick, J. & Wang, Y. (eds.) *Revisiting Experimental Catchment Studies in Forest Hydrology: Proceedings of a Workshop Held During the Xxv IUGG General Assembly in Melbourne, June-*



- July 2011. Wallingford: International Association of Hydrological Sciences (IAHS).
- Chappell, N.A., Douglas, I., Hanapi, J.M. & Tych, W. (2004) *Sources of suspended sediment within a tropical catchment recovering from selective logging*. Hydrological Processes, 18: 685–701. doi:10.1002/hyp.1263.
- Chappell, N.A., Jones, T.D., & Tych, W., (2017a). *Sampling frequency for water quality variables in streams: Systems analysis to quantify minimum monitoring rates*. Water Research, 123, 49-57.
- Chappell, N.A., Jones, T.D., Tych, W. & Krishnaswamy, J., (2017b) *Role of rainstorm intensity underestimated by data-derived flood models: emerging global evidence from subsurface-dominated watersheds*. Environmental Modelling and Software, 88: 1-9.
- Chappell, N.A., McKenna, P., Bidin, K., Douglas, I. & Walsh, R.P.D., (1999) *Parsimonious modelling of water and suspended-sediment flux from nested catchments affected by selective tropical forestry*. Philosophical Transactions, Royal Society, London, Series B: Biological Sciences, 354, 1831–1846.
- Chappell, N.A., Tych, W., Chotai, A., Bidin, K., Sinun, W. & Chiew, T.H., (2006) *Barumodel: combined data based mechanistic models of runoff response in a managed rainforest catchment*. Forest Ecology & Management, 224 (1), 58-80.
- Chappell, N.A., Sherlock, M., Bidin, K., Macdonald, R., Najman, Y., Davies, G., Sawada, H., Araki, M., LaFrankie, J.V. & Shimizu, A., (2007) *Runoff Processes in Southeast Asia: Role of Soil, Regolith and Rock Type*. In: Forest Environments in the Mekong River Basin: With a Focus on the Mekong River, Springer.
- CHASM, 2016,  
<http://www.ncl.ac.uk/ceg/research/water/catchmenthydrology/#overview>  
 (accessed 4/6/2017).
- Choi, H.T. & Beven, K.J., (2007) *Multi-period and multi-criteria model conditioning to reduce prediction uncertainty in distributed rainfall-runoff modelling within GLUE framework*. Journal of Hydrology, vol 332, no. 3-4, 316-336. DOI: 10.1016/j.jhydrol.2006.07.012.
- Clark, M.P. & Kavetski, D., (2010) *Ancient numerical demons of conceptual hydrological modeling: 1. Fidelity and efficiency of time stepping schemes*, Water Resources Research, 46, W10510, doi:10.1029/2009WR008894.
- Cole, S. J., Moore, R. J., (2008) Hydrological modelling using raingauge- and radar-based estimators of areal rainfall, Journal of Hydrology, Volume 358, Issues 3–4, 2008, Pages 159-181, ISSN 0022-1694.
- Croke, B., (2006) *A technique for deriving an average event unit hydrograph from streamflow - only data for ephemeral quick-flow-dominant catchments*. Advances in Water Resources, 29 (4), 493-502.

- Croke, B., (2010) *Exploring changes in catchment response characteristics: application of a generic filter for estimating the effective rainfall and unit hydrograph from an observed streamflow time-series*, Proceedings, British Hydrological Society International Conference: Role of Hydrology in Managing Consequences of a Changing Global Environment, July 19-23 2010, Newcastle University, Newcastle upon Tyne, UK (ISBN 1 903741 17 3), 494-499.
- Croke, B. & Jakeman, A.J., (2004) *A catchment moisture deficit module for the IHACRES rainfall-runoff model*. Environmental Modelling and Software, 19(1), 1-5.
- Cuchi, J., Chinarro, D., Villarroel, J., Antonio Cuchi, D. & Luis Villarroel, J., (2014) *Linear system techniques applied to the Fuenmayor Karst Spring, Huesca (Spain)*. Environmental Earth Sciences, 71(3), 1049-1060.
- Cunha, L., Mandapaka, P., Krajewski, W., Mantilla, R. & Bradley, A., (2012) *Impact of Radar-Rainfall Error Structure on Estimated Flood Magnitude across Scales: An Investigation Based on a Parsimonious Distributed Hydrological Model*. Water Resources Research, 48.
- Dadu, K.S. & Deka, P.C., (2016) *Applications of Wavelet Transform Technique in Hydrology—A Brief Review* In: Urban Hydrology, Watershed Management and Socio-Economic Aspects, Springer International Publishing.
- Dai, Q., Han, D., Rico-Ramirez, M.A., Zhuo, L., Nanding, N. & Islam, T., (2015) *Radar rainfall uncertainty modelling influenced by wind*. Hydrological Processes, 29: 1704–1716. doi: 10.1002/hyp.10292.
- Dale, M., (2005) *Impact of climate change on UK flooding and future predictions* . Proceedings of the ICE - Water Management, 158(4), 135-140.
- De Brabanter, K., De Brabanter, J. & De Moor, B., (2011) *Nonparametric Derivative Estimation*. Proceedings of the 23rd Benelux Conference on Artificial Intelligence.
- De Campos Velho, H., Ramos, F., Chalhoub, E., Stephany, S., Carvalho, J. & De Sousa, F., (2007) *Inverse problems in space science and technology*. Inverse Problems in Science and Engineering, 15(4), 359-372.
- De Roo, A., Wesseling, C., Van Deursen, W., Brooks, S. M., & McDonnell, R. A., (2000) *Physically based river basin modelling within a GIS: The LISFLOOD model*. Hydrological Processes, 14(11-12), 1981-1992.
- Dettinger, M., (2011) *Climate Change, Atmospheric Rivers, and Floods in California – A Multimodel Analysis of Storm Frequency and Magnitude Changes*. Journal of the American Water Resources Association (JAWRA) 47(3):514-523.
- Devaney, A.J., (2012) *Mathematical Foundations of Imaging, Tomography and Wavefield Inversion*, Cambridge University Press.

- Dirks, K.N., Hay, J.E., Harris, D., (1998) *High-resolution studies of rainfall on Norfolk Island part II: interpolation of rainfall data*. J Hydrol 208(3–4):187–193
- Dokuchaev, N., (2016) *Near-ideal causal smoothing filters for the real sequences*. Signal Processing, 118, 285-293.
- Duband, D., Obled, C. & Rodriguez, J-Y., (1993) *Unit hydrograph revisited: an alternative approach to UH and effective precipitation identification*, Journal of Hydrology, 150, 115-149.
- Dunne, T., (1978) *Field studies of hillslope flow processes* In: Kirby, M.J. (ed.) Hillslope Hydrology, John Wiley and Sons, pp 227-294
- Dunne, T. and Black, R. D., (1970) *An experimental investigation of runoff production in permeable soils*. Water Res. Res., 6,478-490.
- Eagleson, P., (1967) *Optimum Density of Rainfall Networks*. Water Resources Research, 3(4), 1021.
- Engida, A.N. & Esteves, M., (2011) *Characterization and disaggregation of daily rainfall in the Upper Blue Nile Basin in Ethiopia*. Journal of Hydrology, 399(3), 226-234.
- Emmanuel, A., Leblois, E., Janey, N. & Payraastre, O., (2015) *Influence of rainfall spatial variability on rainfall–runoff modelling: Benefit of a simulation approach?* Journal of Hydrology, 531, 337-348.
- Evans, J.P. & Jakeman, A.J., (1998) *Development of a simple, catchment scale, rainfall-evapotranspiration-runoff model*. Environmental Modelling and Software 13, 385–393.
- Faurès, J.-M., Goodrich, D.C., Woolhiser D.A. & Sorooshian, S., (1995) *Impact of small-scale spatial rainfall variability on runoff modeling*. Journal of Hydrology, 173(1), 309-326.
- Fleming, S., Marsh Lavenue, A., Aly, A., Adams, A., Beven, K. & Feyen, J., (2002) *Practical applications of spectral analysis to hydrologic time series*. Hydrological Processes, 16(2), 565-574.
- Flügel, W., (1995) *Delineating hydrological response units by geographical information system analyses for regional hydrological modelling using PRMS/MMS in the drainage basin of the River Bröl, Germany*. Hydrological Processes, 9(3-4), 423-436.
- Fujihara, Y., Simonovic, S., Topaloglu, F., Tanaka, K. & Watanabe, T., (2008) *An inverse modelling approach to assess the impacts of climate change in the Seyhan River Basin, Turkey*. Hydrological Sciences Journal, 53 (6), 1121-1136.
- García-Pintado, J., Barberá, G. G., Erena, M. and Castillo, V. M., (2009), *Rainfall estimation by rain gauge-radar combination: A concurrent multiplicative-additive approach*, Water Resour. Res., 45, W01415, doi:[10.1029/2008WR007011](https://doi.org/10.1029/2008WR007011).

- Goodrich, D.C., Faurès, J.-M., Woolhiser, D.A., Lane, L.J. & Sorooshian, S., (1995) *Measurement and analysis of small-scale convective storm rainfall variability*. Journal of Hydrology, 173(1), 283-308.
- Greer, T., Douglas, I., Bidin, K., Sinun, W. & Suhaimi, J., (1995) *Monitoring geomorphological disturbance and recovery in commercially logged tropical forest, Sabah, East Malaysia, and implications for management*. Singapore Journal of Tropical Geography, 16(1), 1-21.
- Günther, T., Rücker, C. & Spitzer, K., (2006) *Three-dimensional modelling and inversion of dc resistivity data incorporating topography – II. Inversion*. Geophysical Journal International, 166(2), 506-517.
- Gupta, H.V., Kling, H., Yilmaz, K.K. & Martinez, G.F., (2009) *Decomposition of the mean squared error and NSE performance criteria: Implications for improving hydrological modelling*. Journal of Hydrology, 377(1), 80-91.
- Henn, B., Clark, M.P., Kavetski, D. & Lundquist, J.D., (2015) *Estimating mountain basin-mean precipitation from streamflow using Bayesian inference*. Water Resources Research, 51, 8012– 8033, doi:10.1002/2014WR016736.
- Hewlett, J. D. and Hibbert, A. R., (1963) *Moisture and energy conditions within a sloping soil mass during drainage*. J. Geophys. Res., 68, 1081-1087
- Hino, M., (1986) *Improvements in the Inverse Estimation of Effective Rainfall from Runoff*. Journal of Hydrology, 83(1-2), 137-147.
- Hirabayashi, Y., Mahendran, R., Koirala, S., Konoshima, L., Yamazaki, D., Watanabe, S., Kim, H. & Kanae, S., (2013) *Global flood risk under climate change*, Nature Climate Change, 3, 816-821.
- Hjelmfelt, A., (1981) *Overland Flow from Time-Distributed Rainfall*. Journal of the Hydraulics Division-Asce, 107(2), 227-238.
- Holman-Dodds, J.K., Bradley, A.A. & Sturdevant-Rees, P.L., (1999) *Effect of temporal sampling of precipitation on hydrologic model calibration*, Journal of Geophysical Research, Vol. 104, No. D16, Pages 19,645-19,654.
- Hornberger, G.M., Beven, K.J., Cosby, B.J. and Sappington, D.E., (1985) *Shenandoah Watershed Study: Calibration of a topography-based, variable contributing area hydrological model to a small forested catchment*. Water Resour. Res., 21: 1841-1850.
- Horton, R. E. (1933). *Drainage-basin characteristics*. Trans. Amel: Geophys. Un., 13, 350-361.
- Hudson, J.A., Crane S.B. & Blackie J.R., (1997) *The Plynlimon water balance 1969-1995: The impact of forest and moorland vegetation on evaporation and streamflow in upland catchments*. Hydrology and Earth System Sciences, 1(3), 409-427.

- Huntington, T., (2006) *Evidence for intensification of the global water cycle: Review and synthesis*. Journal of Hydrology, 319(1), 83-95.
- Hursh, C. R., (1936) *Storm water and absorption*. Trans. Amel: Geophys. Un., 17,301-302.
- Ibbitt, R.P. and O'Donnell, T., (1971) *Designing conceptual catchment models for automatic fitting methods*. IASH Publ., 101: 461-475.
- Jakeman, A.J. and Hornberger, G.M., (1993) *How much complexity is warranted in a rainfall-runoff model?* Water Resources Research, 29(8), 2637-2649.
- Jakeman, A.J., Littlewood, I.G., Whitehead, P.G., (1990) *Computation of the instantaneous unit hydrograph and identifiable component flows with application to two small upland catchments*. Journal of Hydrology 117, 275-300.
- Jakeman, A. & Young, P., (1984) *Recursive Filtering and Smoothing Procedures for the Inversion of Ill-Posed Causal Problems*. Utilitas Mathematica, 25(MAY), 351-376.
- JBAtrust, (2016) *Flooding after Storm Desmond*, PERC, <http://www.jbatrust.org/wp-content/uploads/2016/08/flooding-after-storm-desmond-PUBLISHED-24-August-2016.pdf> Retrieved 4/5/2017.
- Kalman, R.E., (1960) *A New Approach to Linear Filtering and Prediction Problems*. Transactions of the ASME – Journal of Basic Engineering, (82 (Series D)), 35-45.
- Kavetski, D. & Clark, M.P. (2010) *Ancient numerical daemons of conceptual hydrological modelling: 2. Impact of time stepping schemes on model analysis and prediction*. Water Resources Research, 46, W10511, doi:10.1029/2009WR008896.
- Kavetski, D., Fenicia, F., & Clark, M., (2011) *Impact of temporal data resolution on parameter inference and model identification in conceptual hydrological modeling: Insights from an experimental catchment*. Water Resources Research, 47(5)
- Kendall, A.D. & Hyndman, D.W., (2007) *Examining watershed processes using spectral analysis methods including the scaled-windowed fourier transform*, in Subsurface Hydrology Data Integration for Properties and Processes. Geophysical Monograph Series, Vol. 171, edited by Hyndman, D.W., Day-Lewis, F.D., & Singha, K., 183200, AGU, Washington, D.C.
- Kirchner J., (2003) *A double paradox in catchment hydrology and geochemistry*. Hydrological Processes 17: 871– 874.
- Kirchner, J., (2006) *Getting the right answers for the right reasons: Linking measurements, analyses, and models to advance the science of hydrology*. Water Resources Research, 42(3).

- Kirchner, J., (2009) *Catchments as simple dynamical systems: catchment characterization, rainfall-runoff modelling, and doing hydrology backward*. Water Resources Research, 45.
- Kirchner, J.W., Feng, X. & Neal, C., (2000) *Fractal stream chemistry and its implications for contaminant transport in catchments*. Nature, 403(6769), 524-527.
- Krajewski, W.F., Lakshmi, V., Georgakakos, K.P. & Jain, S.C., (1991) *A Monte Carlo study of rainfall sampling effect on a distributed catchment model*. Water Resources Research, 27 (1), 119-128.
- Krause, P., Bäse, D. & Boyle, F., (2005) *Comparison of different efficiency criteria for hydrological model assessment*. Advances in Geosciences, 5, 89-97.
- Kretzschmar, A., Tych, W. & Chappell, N.A., (2014) *Reversing hydrology: Estimation of sub-hourly rainfall time-series from streamflow*. Environmental Modelling & Software 60: 290-301.
- Kretzschmar, A., Tych, W., Chappell, N.A. & Beven, K.J., (2015) *Reversing hydrology: quantifying the temporal aggregation effect of catchment rainfall estimation using sub-hourly data*. Hydrology Research, Jun. 2016, 47 (3) 630-645; DOI: 10.2166/nh.2015.076.
- Kretzschmar, A., Tych, W., Chappell, N. & Beven, K., (2016) *What Really Happens at the End of the Rainbow? – Paying the Price for Reducing Uncertainty (Using Reverse Hydrology Models)*. Procedia Engineering, Volume 154, Pages 1333-1340, ISSN 1877-7058, <http://dx.doi.org/10.1016/j.proeng.2016.07.485>.
- Krier, R., Matgen, P., Goergen, K., Pfister, L., Hoffmann, L., Kirchner, J.W., Uhlenbrook, S. & Savenije, H.H.G., (2012) *Inferring catchment precipitation by doing hydrology backward: a test in 24 small and mesoscale catchments in Luxembourg*. Water Resources Research, 48, W10525.
- Kundzewicz, Z., Kanae, S., Seneviratne, S., Handmer, J., Nicholls, N., Peduzzi, P. & Sherstyukov, B., (2014) *Flood risk and climate change: Global and regional perspectives*. Hydrological Sciences Journal, 1-28.
- Lamb, H.H., (1972) *British Isles weather types and a register of daily sequence of circulation patterns, 1861-1971*. Geophysical Memoir, Vol. 116, HMSO, London, 85.
- Laurain, V., Gilson, M., Garnier, H. & Young, P.C., (2008) *Refined instrumental variable methods for identification of Hammerstein continuous-time Box–Jenkins models*. 47th IEEE Conference on Decision and Control, CDC'08, Dec 2008, Cancun, Mexico. 210-216, 2008.
- Laurenson, E.M. & O'Donnell, T., (1969) *Data error effects on unit hydrograph derivation*. Journal of Hydraulic Engineering, ASCE (HY6), 1899-1917.

- Lavers, D.A., Allan, R.P., Wood, E.F., Villarini, G., Brayshaw, D.J. & Wade, A.J., (2011) *Winter floods in Britain are connected to atmospheric rivers*. Geophysical Research Letters, Vol. 38.
- Lebel, T., Bastin, G., Obled, C. & Creutin, J.D., (1987) *On the accuracy of areal rainfall estimation: A case study*. Water Resources Research, 23(11), 2123–2134, doi:10.1029/WR023i011p02123.
- Lees, M.J., (2000) Data-based mechanistic modelling and forecasting of hydrological systems, Journal of Hydro-informatics, 02.1
- Leedal, D.T., (2006) *Sequential decision-making in climate change mitigation: a control systems perspective*. Unpublished PhD thesis, Lancaster.
- Legates, D.R. & McCabe, G.J. (1999) *Evaluating the use of “goodness-of-fit” Measures in hydrologic and hydro-climatic model validation*. Water Resources Research, 35(1), 233-241.
- Linsley, R. K., (1967) *The relation between rainfall and runoff*, J. Hydrol. 5, 297–371
- Littlewood, I. G., (2007) *Rainfall–streamflow models for ungauged basins: uncertainty due to modelling time step*. In: Uncertainties in the ‘Monitoring–Conceptualisation–Modelling’ Sequence of Catchment Research (Proc. Eleventh Biennial Conference of the Euro-mediterranean Network of Experimental and Representative Basins) (L. Pfister & L. Hoffmann, eds), 149–155. Paris: UNESCO Tech. Doc. in Hydrology Series 81.
- Littlewood, I.G. & Croke, B.F.W., (2008) *Data time-step dependency of conceptual rainfall–streamflow model parameters: an empirical study with implications for regionalisation*. Hydrological Sciences Journal, 53:4, 685-695, DOI: 10.1623/hysj.53.4.685.
- Littlewood, I. & Croke, B., (2013) *Effects of data time-step on the accuracy of calibrated rainfall-streamflow model parameters: practical aspects of uncertainty reduction*. Hydrology Research, 44 (3), 430-440.
- Littlewood, I.G., Young, P.C. & Croke, B.F.W., (2010) *Preliminary comparison of two methods for identifying rainfall–streamflow model parameters insensitive to data time-step: the Wye at Cefn Brwyn, Plynlimon, Wales*. In: Proceedings of the Third International Symposium (British Hydrological Society, 19–23 July 2010, Newcastle University, UK).
- Liu, B. & Munson, D., (1982) *Generation of a random sequence having a jointly specified marginal distribution and auto-covariance*. Acoustics, Speech and Signal Processing, IEEE Transactions on, 30(6), 973-983.
- Ljung, L., (1999) *System identification. Theory for the user*. Prentice Hall, Upper Saddle River, 2<sup>nd</sup> edition.
- Lowdermilk, W. C., (1934) *The role of vegetation in erosion control and water conservation*. J. Forest., 32,529-536.

- Luo, J., Kui Y., & Jing B., (2005) *Savitzky–Golay smoothing and differentiation filter for even number data*. *Signal Processing* 85.7 (2005): 1429-1434.
- Mair, A., Fares, A., (2011) *Comparison of rainfall interpolation methods in a mountainous region of a tropical island*. *J Hydrol Eng* 16(4):371–383
- Maquin, D., Gaddouna, B. & Ragot, J., (1994) *Estimation of unknown inputs in linear systems*. *American Control Conference*, 1994, 1, 1195-1197.
- Marien, J.L. & Vandewiele, G.L., (1986) *A Point Rainfall Generator with Internal Storm Structure*. *Water Resources Research*, 22(4), 475-482.
- Mayes, W.M., Walsh, C.L., Bathurst, J.C., Kilsby, C.G., Quinn, R.F., Wilkinson, M.E., Daugherty, A.J. & Connell, P.E., (2006) *Monitoring a flood event in a densely instrumented catchment, the Upper Eden, Cumbria, UK*. *Water & Environment Journal*, 20 (4), 217-226.
- Mazzoleni, M., Verlaan, M., Alfonso, L., Monego, M., Norbiato, D., Ferri, M. & Solomatine, D.P., (2017) *Can assimilation of crowdsourced data in hydrological modelling improve flood prediction?* *Hydrological Earth System Sciences*, 21, 839-861, <https://doi.org/10.5194/hess-21-839-2017>.
- McDonnell, J., (2003) *Where does water go when it rains? Moving beyond the variable source area concept of rainfall-runoff response*. *Hydrological Processes*, 17(9), 1869-1875.
- McMillan, H., Gueguen, M., Grimon, E., Woods, R., Clark, M. & Rupp, D., (2014) *Spatial variability of hydrological processes and model structure diagnostics in a 50 km<sup>2</sup> catchment*. *Hydrological Processes*, 28(18), 4896-4913.
- Merz, B., Hall, J., Disse, M. & Schumann, A., (2010) *Fluvial flood risk management in a changing world*. *Natural Hazards and Earth System Sciences*, 10(3), 509-527.
- Met. Office, (2010) *The British Rainfall Network in 2010*, Tim Allott <https://www.rmets.org/sites/default/files/pdf/presentation/20100417-allott.pdf> Retrieved 27/6/2017.
- Michaud, J. & Sorooshian, S., (1994a) *Comparison of simple versus complex distributed runoff models on a mid-sized semiarid watershed*. *Water Resources Research*, 30(3), 593-605.
- Michaud, J. & Sorooshian, S., (1994b) *Effect of rainfall-sampling errors on simulations of desert flash floods*. *Water Resources Research*, 30(10), 2765-2775.
- Milly, P.C.D., Wetherald, R.T., Dunne, K.A. & Delworth T.L., (2002) *Increasing risk of great floods in a changing climate*. *Nature*, vol. 415, 514-517.
- Minshall, N. E., (1960) *Predicting storm runoff on small experimental watersheds*, *ASCE Journal of the Hydraulics Division*, 86 (HY8): 17-38



- Montanari, A., & Toth, E., (2007) *Calibration of hydrological models in the spectral domain: An opportunity for scarcely gauged basins?* Water Resources Research, 43, W05434, doi:10.1029/2006WR005184.
- Montesarchio, V., Orlando, D., Del Bove, D., Napolitano, F. & Magnaldi, S., (2015) *Evaluation of optimal rain gauge network density for rainfall-runoff modelling.* AIP Conference Proceedings, 1648(1), Proceedings Of The International Conference On Numerical Analysis And Applied Mathematics 2014 (Icnaam-2014), Rhodes, Greece (22–28 September 2014).
- Moore, R., Jones, D., Cox, V. & Isham, V., (2000) *Design of the HYREX raingauge network.* Hydrology and Earth System Sciences, 4(4), 523-530.
- Moran, P.A.P., (1950) *Notes on continuous stochastic phenomena.* Biometrika, 37(1/2), 17– 23. <https://doi.org/10.2307/2332142>.
- Moriasi, D.N., Arnold, J.G., Van Liew, M.W., Bingner, R.L., Harmel, R.D. & Veith, T.L., (2007) *Model Evaluation Guidelines for Systematic Quantification of Accuracy in Watershed Simulations.* Transactions of the ASABE, 50, 885-900. <http://dx.doi.org/10.13031/2013.23153>.
- Moussaoui, S., Brie, D. & Richard, A., (2005) *Regularization Aspects in Continuous-Time Model Identification.* Automatica, 41(2), 197–208.
- Naoum, S. & Tsanis, I.K., (2004) *A Multiple Linear Regression GIS Module Using Spatial Variables to Model Orographic Rainfall.* Journal of Hydroinformatics, Vol. 6, 2004, 39-56.
- National River Flow Archive NERC (CEH), (2012) <http://nrfa.ceh.ac.uk/data/station/spatial/52010> Accessed 21/3/2016.
- Neumaier, A., (1998) *Solving Ill-Conditioned and Singular Linear Systems: A Tutorial on Regularization.* SIAM Review.
- Nijssen, B. & Lettenmaier, D., (2004) *Effect of precipitation sampling error on simulated hydrological fluxes and states: Anticipating the Global Precipitation Measurement satellites.* Journal Geophysical Research, 109, D02103, doi:10.1029/2003JD003497.
- Nkuna, T.R. & Odiyo, J.O., (2011). *Filling of missing rainfall data in Luvuvhu River catchment using artificial neural networks.* Physics and Chemistry of the Earth, 36(14), 830-835.
- Norton, J.P., (2009) *An Introduction to Identification.* Dover Publications.
- O'Sullivan, F., (1986) *A Statistical Perspective on Ill-Posed Inverse Problems.* Statistical Science, 1(4), 502-518.
- Obled, C., Wendling, J. & Beven, K., (1994) *The sensitivity of hydrological models to spatial rainfall patterns - an evaluation using observed data.* Journal of Hydrology, 159 (1-4), 305-333.

- Ockenden, M.C., (2010) *Identification of catchment runoff processes as a basis for defining water quality protection zones*. Unpublished PhD thesis, Lancaster.
- Ockenden, M.C. & Chappell, N.A., (2011) *Identification of the dominant runoff pathways from data-based mechanistic modelling of nested catchments in temperate UK*. *Journal of Hydrology*, 402 (1), 71-79.
- Ockenden, M.C., Chappell, N.A. & Neal, C., (2014) *Quantifying the differential contributions of deep groundwater to streamflow in nested basins, using both water quality characteristics and water balance*. *Hydrological Research*, 45, 200-212.
- Ogden, F. & Julien, P., (1994) *Runoff Model Sensitivity to Radar Resolution*. *Journal of Hydrology*, 158(1-2), 1-18.
- Olivera, F. & Maidment, D., (1999) *Geographical information systems (GIS)- based spatially distributed model for runoff routing*. *Water Resources Research*, 35, 1155-1164.
- Onof, C., Chandler, R., Kakou, A., Northrop, P., Wheeler, H. & Isham, V., (2000) *Rainfall modelling using Poisson-cluster processes: A review of developments*. *Stochastic Environmental Research and Risk Assessment*, 14(6), 384-411.
- Oreskes, N. & Belitz, K., (2001) *Philosophical issues in model assessment*. In: Anderson, M.G., Bates, P.D., *Model Validation - Perspectives in Hydrological Science*, Chichester, John Wiley and Sons.
- Ormerod, S. & Durance, I., (2009) *Restoration and recovery from acidification in upland Welsh streams over 25 years*. *Journal of Applied Ecology*, 46 (1), 164-174.
- Pan, M. & Wood, E., (2013) *Inverse streamflow routing*. *Hydrology and Earth System Sciences*, 17(11), 4577-4588.
- Pasquier, P. & Marquotte, D., (2006) *Steady- and transient-state inversion in hydrogeology by successive flux estimation*. *Advances in Water Resources*, 29(12), 1934-1952.
- Pessoa, M., Bras, R. & Williams, E., (1993) *Use of weather radar for flood forecasting in the Sieve River basin: A sensitivity analysis*. *Journal of Applied Meteorology*, 32(3), 462-475.
- Pollock, M., Quinn, P., Dutton, M. & Wilkinson, M., (2014) *The problems of rain gauge measurement undercatch: an inconvenient truth*. *Geophysical Research Abstracts*, vol 16, EGU2014-11643.
- Ratto, M., Young, P.C., Romanowicz, R., Pappenberger, F., Saltelli, A. & Pagano, A. (2007) *Uncertainty, sensitivity analysis and the role of data based mechanistic modeling in hydrology*. *Hydrology and Earth System Sciences*, 11(4), 1249-1266.

- Reynard, N.S. & Stewart, E.J., (1993) *The derivation of design rainfall profiles for upland areas of the UK*. Meteorological Magazine, 122, 116-123.
- Ritter, A. & Muñoz-Carpena, R., (2013) *Performance evaluation of hydrological models: Statistical significance for reducing subjectivity in goodness-of-fit assessments*. Journal of Hydrology, 480, 33-45.
- Royal Society (2017) *13. How does climate change affect the strength and frequency of floods, droughts, hurricanes, and tornadoes?* <https://royalsociety.org/topics-policy/projects/climate-change-evidence-causes/question-13/> Retrieved 4/5/2017.
- Rusjan, S. & Mikoš, M., (2015) *A catchment as a simple dynamical system: Characterization by the streamflow component approach*. Journal of Hydrology, Volume 527, August 2015, Pages 794-808.
- Schaefli, B., Gupta, H., Ohta, T., Ueno, K., Hiyama, T., Tanaka, K., Tanaka, K. & Kuraji, K., (2007) *Do Nash values have value?* Hydrological Processes, 21(15), 2075-2080.
- Segond, M.-L., Wheater, H.S. & Onof, C., (2007) *The significance of spatial rainfall representation for flood runoff estimation: A numerical evaluation based on the Lee catchment, UK*. Journal of Hydrology, 347(1), 116-131.
- Seibert, J., (2001) *On the need for benchmarks in hydrological modelling*. Hydrological Processes, 15(6), 1063-1064.
- Serrano-Notivol, R., De Luis, M., & Beguería, S., (2017). *An R package for daily precipitation climate series reconstruction*. Environmental Modelling and Software, 89, 190-195.
- Seyfried, M.S. & Wilcox, B.P. (1995) *Scale and the Nature of Spatial Variability: Field Examples Having Implications for Hydrologic Modeling*. Water Resources Research, 01/1995, Vol.31(1), 173-184.
- Shaghaghian, M.R. & Abedini, M.J., (2013) *Rain gauge network design using coupled geostatistical and multivariate techniques*. Scientia Iranica, 20(2), 259-269.
- Shah, S., O'Connell, P. & Hosking, J., (1996) *Modelling the effects of spatial variability in rainfall on catchment response. 2. Experiments with distributed and lumped models*. Journal of Hydrology, 175(1-4):89-111.
- Sharma, M.L. and Luxmoore, R.J., (1979) *Soil spatial variability and its consequences on simulated water balance*. Water Resour. Res., 15: 1567-1573.
- Shaw, E.M., Beven, K.J., Chappell, N.A. & Lamb, R., (2011) *Hydrology in practice*. 4th edn, Spon Press (Taylor and Francis), London.
- Sherman, L.K., (1932) *Streamflow from Rainfall by the Unit-graph Method*. Engineering News Record, 108: 501-505.

- Simolo, C., Brunetti, M., Maugeri, M., Nanni, T., (2010) *Improving estimation of missing values in daily precipitation series by a probability density function-preserving approach*. Int J Climatol 30(10):1564–1576
- Singh, V., (1997) *Effect of spatial and temporal variability in rainfall and watershed characteristics on stream flow hydrograph*. Hydrological Processes, 11(12), 1649-1669.
- Sklash, M. G., Beven, K. J., Gilman, K. and Darling, W. G. (1996) *Isotope studies of pipeflow at plynlimon, Wales, UK*. Hydrol. Process., 10: 921–944.
- Skøien, J. O., Blöschl, G. and Western, A. W. (2003) *Characteristic space scales and timescales in hydrology*, Water Resour. Res., 39(10), 1304, doi:10.1029/2002WR001736
- Smith, M.B., Koren, V.I., Zhang, Z., Reed, S.M., Pan, J.-J. & Moreda, F., (2004) *Runoff response to spatial variability in precipitation: An analysis of observed data*. Journal of Hydrology, 298(1), 267-286.
- Somerset Wildlife Trust, (2017) *Somerset Levels and Moors*, <http://www.somersetwildlife.org/levelsandmoors>, Accessed 6/6/2017.
- Sugawara, M., (1992) *On the weights of precipitation stations* in: Advances in Theoretical Hydrology: A Tribute to James Dooge. Edited by J.P. O'Kane, Elsevier, 1992.
- Surkan, A., (1974) *Simulation of storm velocity effects on flow from distributed channel networks*. Water Resources Research, 10(6), 1149-1160.
- Szolgayová, E., Arlt, J., Blöschl, G. & Szolgay, J., (2014) *Wavelet based deseasonalization for modelling and forecasting of daily streamflow series considering long range dependence*. Journal of Hydrology and Hydromechanics, 62 (1). 24-32. ISSN 0042-790X.
- Shankar, U., Pearson, C. P., Nikora, V. I., & Ibbitt, R. P., (2002) *Heterogeneity in catchment properties: A case study of Grey and Buller catchments, New Zealand*. Hydrology and Earth System Sciences, 6(2), 167-184.
- Tarantola, A., (2005) *Inverse Problem Theory and Methods for Model Parameter Estimation*: Society for Industrial and Applied Mathematics.
- Taylor, C.J., Pedregal, D.J., Young, P.C. & Tych, W., (2007) *Environmental time series analysis and forecasting with the Captain toolbox*. Environmental Modelling & Software, 22 (6), 797-814.
- Teegavarapu, R.S.V., (2014) *Statistical corrections of spatially interpolated missing precipitation data estimates*. Hydrol Process 28:3789–3808
- Teuling, A.J., Lehner, I., Kirchner, J.W. & Seneviratne, S.I., (2010) *Catchments as simple dynamical systems: experience from a Swiss pre-alpine catchment*. Water Resources Research, 46 (10).

- Todini E., (2007) *Hydrological catchment modelling: past, present and future*. Hydrological Earth System Sciences, 11 (1) 468–482.
- Troutman, B.M., (1982) An analysis of input errors in precipitation-runoff models using regression with errors in the independent variables. *Water Resources Research*, August 1982, Vol.18(4), 947-964.
- Troutman, B.M., (1983) *Runoff prediction errors and bias in parameter estimation induced by spatial variability of precipitation*. *Water Resources Research*, 19(3), 791-810.
- Tych, W., Pedregal, D.J., Young, P.C. & Davies, J., (2002) *An Unobserved Component Model for Multi-Rate Forecasting of Telephone Call Demand: The Design of a Forecasting Support System*. *International Journal of Forecasting*, 18(4), 673-695.
- Vieux, B.E., Cui, Z., & Gaur, A., (2004). *Evaluation of a physics-based distributed hydrologic model for flood forecasting*. *Journal of Hydrology*, 298(1), 155-177.
- Villarini, G., & Krajewski, W.F., (2008) *Empirically-based modeling of spatial sampling uncertainties associated with rainfall measurements by rain gauges*. *Advances in Water Resources*, 31(7), 1015-1023.
- Villarini, G., Mandapaka, P., Krajewski, W. & Moore, R., (2008) *Rainfall and sampling uncertainties: A rain gauge perspective*. *Journal of Geophysical Research: Atmospheres*, 113(D11).
- Vinogradov, Y., Semenova, O., & Vinogradova, T., (2011) *An approach to the scaling problem in hydrological modelling: The deterministic modelling hydrological system*. *Hydrological Processes*, 25(7), 1055-1073.
- Wagener, T., Wheeler, H.S. & Gupta, H.V., (2004) *Rainfall-runoff modelling in gauged and ungauged catchments*. London: Imperial College Press.
- Walsh, R.P.D., Bidin, K., Blake, W.H., Chappell, N.A., Clarke, M.A., Douglas, I., Ghazali, R., Sayer, A.M., Suhaimi, J., Tych, W. & Annammala, K.V., (2011) *Long-term responses of rainforest erosional systems at different spatial scales to selective logging and climatic change*. *Philosophical Transactions, Royal Society, B: Biological Sciences*, (2011) 366, 3340–3353 doi:10.1098/rstb.2011.0054.
- Wang, W. & Henriksen, R., (1994) *Generalized predictive control of nonlinear systems of the Hammerstein form*. *Modeling, Identification and Control*, 15(4), 253-262.
- Weyman, D. R., (1970) *Throughflow on hillslopes and its relation to the stream hydrograph*. *Bull. Intern. Assoc. Sci. Hydrology*, 15 (3), 25-26.
- Wheeler, H.S., Isham, V.S., Chandler, R.E., Onof, C.J. & Stewart, E.J., (2006) *Improved methods for national spatial-temporal rainfall and evaporation modelling for BSM*. R&D Technical Report F2105/TR, DEFRA, London.

- Whipkey, R. Z., (1965) *Subsurface stormflow from forested slopes*. Bull. Intern. Assoc. Sci. Hydrology, 10 (3), 74-85.
- Whitehead, P.G., Young, P.C. & Hornberger, G., (1979) *A systems model of flow and water quality in the Bedford Ouse river system - I. Streamflow modelling*. Water Research, 13, 1155-1169.
- Wickert, M., (2013) *Signals and Systems for Dummies*. 1st Edition, John Wiley & Sons.
- Wilby, R., Beven, K. & Reynard, N., (2008) *Climate change and fluvial flood risk in the UK: More of the same?* Hydrological Processes, 22(14), 2511-2523.
- Wilderer, P. A. (ed.), (2011) *Treatise on Water Science*, Elsevier Science, Hackensack, N.J.
- Wills, A., Schön, T.B., Ljung, L. & Ninness, B., (2013) *Identification of Hammerstein–Wiener models*. Automatica, Volume 49, Issue 1, January 2013, Pages 70–81.
- Wood, S., Jones, D. & Moore, R., (2000) *Accuracy of rainfall measurement for scales or hydrological interest*. Hydrology and Earth System Sciences, 4(4), 531-543.
- Xu, C., & Singh, V. (1998). *A Review on Monthly Water Balance Models for Water Resources Investigations*. Water Resources Management, 12(1), 20-50.
- Yang F. & Wilde R., (1988) *Observer for linear systems with unknown inputs*. IEEE Trans. on Automatic Control, 33 (7), p. 677-681.
- Ye, W., Bates, B.C., Viney, N.R., Sivapalan, M. & Jakeman, A.J., (1997) *Performance of conceptual rainfall-runoff models in low-yielding ephemeral catchments*. Water Resources Research 33, 153–166.
- Yeh, H.C., Chen, Y.C., Chiang, W. & Chen, R.H., (2011) *Entropy and Kriging approach to rainfall network design*. Paddy and Water Environment, Vol. 9, 343-355.
- Young, P.C., (1974) *Recursive approaches to time-series analysis*, Bulletin of the Institute of Mathematics and its Applications, 10 209-224.
- Young, P.C., (1984) *Recursive estimation and time-series analysis*. Springer-Verlag, Berlin.
- Young, P.C., (1993) *Concise encyclopedia of environmental systems*. Pergamon Press Ltd, Headington Hill Hall, Oxford.
- Young, P., (1998) *Data-based mechanistic modelling of environmental, ecological, economic and engineering systems*. Environmental Modelling and Software, 13(2), 105-122.
- Young, P.C., (1999) *Data-based mechanistic modelling. Generalised Sensitivity and Dominant Mode Analysis*, Computer Physics Communications, 117 (1-2), 113-129.

- Young, P.C., (2001) *Data-based mechanistic modelling and validation of rainfall-flow processes*. In: M. G. Anderson and P.D. Bates (Eds.), *Model Validation: Perspectives in Hydrological Science*. Chichester: J. Wiley, 117-161.
- Young, P.C., (2003) *Top-down and data-based mechanistic modelling of rainfall-flow dynamics at the catchment scale*. *Hydrological Processes*, 17, 2195-2217.
- Young, P.C., (2006) *Data-Based Mechanistic Modelling and River Flow Forecasting*. 14th IFAC Symposium on System Identification, Newcastle, Australia, 756-761.
- Young, P.C., (2010) *The estimation of continuous-time rainfall-flow models for flood risk management*. In: *Proceedings of the Third International Symposium (British Hydrological Society, 19–23 July 2010, Newcastle University, UK)*.
- Young, P.C., (2011) *Recursive estimation and time-series analysis: An introduction for the student and practitioner*. New York: Springer.
- Young, P.C. & Beck, M.B., (1974) *The modelling and control of water quality in a river system*. *Automatica*, 10 (5) 455-468.
- Young, P.C. & Beven, K.J., (1994) *Data-based mechanistic modelling and the rainfall-flow non-linearity*. *Environmetrics*, 5, 335-363.
- Young, P. & Garnier, H., (2006) *Identification and estimation of continuous-time, databased mechanistic (DBM) models for environmental systems*. *Environmental Modelling & Software*, 21 (8), 1055-1072.
- Young, P.C. & Jakeman, A., (1980) *Refined Instrumental Variable Methods of Recursive Time-Series Analysis Part III. Extensions*. *International Journal of Control*, 31(4), 741-764.
- Young, P.C. & Lees, M.J., (1993) *The active mixing volume: a new concept in modelling environmental systems*. In: Barnett, V. & Feridun, T.K. (Eds), *Statistics for the Environment*. J. Wiley, Chichester, 3:44.
- Young, P.C. & Romanowicz, R.J., (2004) *PUB and data-based mechanistic modelling: the importance of parsimonious continuous-time models*. In: *Proceedings of the iEMSs 2004 international congress: complexity and integrated resources management*. International Environmental Modelling and Software Soc., Osnabruech, Germany, 214-224.
- Young, P.C. & Sumińska, M.A., (2012) *Control systems approach to input estimation with hydrological applications*. In: 16th IFAC Symposium on System Identification. July 2012, Brussels, Belgium, 1043-1048.
- Young, P.C., Chotai, A. & Beven, K., (2004) *Data-based mechanistic modelling and the simplification of environmental systems*. In: Wainwright, J. & Mulligan, M., (2004) *Environmental modelling: Finding simplicity in complexity*. Chichester, West Sussex, England; Hoboken, NJ: John Wiley & Son.

- Young, P., Garnier, H., & Gilson, M., (2006) *An optimal instrumental variable approach for identifying hybrid continuous-time box-jenkins models*. IFAC Proceedings Volumes, 39(1), 225-230.
- Young, P., Parkinson, S. & Lees, M., (1996) *Simplicity out of complexity in environmental modelling: Occam's razor revisited*. Journal of Applied Statistics, 23(2-3), 165-210.
- Young, P.C., Pedregal, D.J. & Tych, W., (1999) *Dynamic harmonic regression*. Journal of Forecasting, 18 (6), 369-394.
- Younger, P., Freer, J. & Beven, K., (2009) *Detecting the effects of spatial variability of rainfall on hydrological modelling within an uncertainty analysis framework*. Hydrological Processes, 23(14), 1988-2003.
- Yu, B., Ciesiolka, C., Rose, C. & Coughlan, K., (1997) *Note on Sampling Errors in the Rainfall and Runoff Data Collected Using Tipping Bucket Technology*. Transactions of the ASAE, 40(5), 1305-1309.
- Zadeh, L.A. & Desoer, C.A., (1963) *Linear system theory: the state space approach*. McGraw-Hill.
- Zhang J. & Han D., (2017) *Assessment of rainfall spatial variability and its influence on runoff modelling - A case study in the Brue catchment, UK*. Hydrological Processes. <https://doi.org/10.1002/hyp.11250>.
- Zoccatelli, D., Borga, M., Zanon, F., Antonescu, B. & Stancalie, G., (2010) *Which rainfall spatial information for flash flood response modelling? A numerical investigation based on data from the Carpathian range, Romania*. Journal of Hydrology, 394(1-2), 148-161.